Copyright

By

Brian Allen Schnittker

2008

Allowable Compressive Stress at Prestress Transfer

by

Brian Allen Schnittker, B.S. ARE

Thesis

Presented to the Faculty of the Graduate School of

The University of Texas at Austin

in Partial Fulfillment

of the Requirements

for the Degree of

Master of Science in Engineering

The University of Texas at Austin

December 2008

Allowable Compressive Stress at Prestress Transfer

APPROVED BY
SUPERVISING COMMITTEE:

Oguzhan Bayrak, Supervisor

John E. Breen

Acknowledgements

The research presented in this thesis was funded by the Texas Department of Transportation. I would like to acknowledge the project director, Jeff Cotham, for his help and contributions to this study. I would also like to thank Jason Tucker and Graham Bettis of TxDOT for their continuous support. In addition, I would like to thank the precast/prestressed fabricators who generously donated several of the specimens tested in this study.

To Dr. Bayrak; your guidance and gracious support throughout the duration of this research made this project possible and to Dr. Breen; your suggestions and insight are greatly appreciated.

I would like to thank all of the people at the Ferguson Structural Engineering Laboratory who aided in Project 5197. Specifically, the work by fellow graduate students Chris Heckmann and Alejandro Avendano were greatly appreciated. Additionally, the guidance and kind assistance of David Birrcher helped to make this project a reality. I am also very grateful to the laboratory staff: Blake Stasney, Dennis Fillip, Andrew Valentine, Eric Schell, Barbara Howard, and Jessica Hanten for their support throughout the duration of this project.

I would also like to thank the many prestressed fabricators who helped in the extensive fabrication of all the girders tested in this study. Specifically, the efforts of Gavin Koepp, Chris Leonard, Gil Heldenfels, Burson Patton, Jorge Hinojosa, and David Malaer are greatly appreciated.

To my family and Katie, thank you so much for your continuous love and support. It has shaped me into the person I am today.

Allowable Compressive Stress at Prestress Transfer

Brian Allen Schnittker, M.S.E.

The University of Texas at Austin, 2008

SUPERVISOR: Oguzhan Bayrak

Increasing the maximum compressive stress at prestress transfer from the current limit of $0.6f'_{ci}$ in the AASHTO-LRFD Bridge Design Specifications has been the subject of several research investigations in the last decade. There are many potential benefits of increasing this limit including increased span lengths, a reduction in harped or debonded strands, and a faster turnaround time for beams in prestressed beds. In 2004, The Texas Department of Transportation initiated Project 5197 to investigate the feasibility of increasing this allowable compressive stress limit. Initially, the live load performance of 36 specimens was evaluated by Birrcher and Bayrak (TxDOT Report 5197-1, 2007). Based on the recommendations from their research, further testing on additional section types and different concrete mixture designs was performed. This thesis presents the subsequent research conducted based on recommendations of Birrcher and Bayrak (2007).

In this portion of TxDOT Project 5197, 45 Type-C beams and 10 4B28 box beams were tested to experimentally determine their cracking load. The maximum compressive stress at prestress transfer of all 55 specimens ranged from $0.56f'_{ci}$ to $0.76f'_{ci}$. The Type-C beams were produced in four different fabrication plants using conventionally consolidated concrete. The 10 4B28 box beams were produced in two fabrication plants using concrete mixture designs of both self consolidating concrete as well as conventional concrete. For all specimens, measured cracking loads were compared to predicted cracking loads. The data from the 45 Type-C beams and 10 box beams were added to the 36 beams investigated by Birrcher and Bayrak (2007) to compile a comprehensive set of data from 91 specimens.

An appropriate maximum compressive stress limit was determined from the ability to accurately predict the load at which cracking occurred. As the maximum compressive stress at prestress transfer was increased, a decline in cracking load prediction accuracy was observed. For the specimens subjected to high compressive stresses at release (greater than $0.65f'_{ci}$), the concrete in the pre-compressed tensile zone was subjected to the non-linear inelastic range causing microcracking to occur. This non-linear behavior (due to microcracking) was unaccounted for in prestress losses or standard design equations (P/A±Mc/I). Based on the analysis of the results, an increase of the allowable compressive stress limit at prestress transfer to $0.65f'_{ci}$ is justified. Additionally, the use of self consolidating concrete with a maximum compressive stress of $0.65f'_{ci}$ is not recommended.

Table of Contents

CHAPTER 1 Introduction 1

1.1 Allowable Compressive Stress at Prestress Transfer 1

1.2 Scope of Research 5

1.3 Chapter Outline 6

CHAPTER 2 Literature Review 8

2.1 Overview 8

2.2 Historical Background of Allowable Compressive Stress at Release 9

2.2.1 Allowable Stresses in Reinforced Concrete 9

2.2.2 Compressive Stresses at Release in Prestressed Concrete 10

2.2.3 Recent Research and Discussion 11

2.2.3.1 PCI Standard Design Practice 1996, 1997, and 2003 11

2.2.3.2 Russell and Pang, 1997 12

2.2.3.3 Huo and Tadros, 1997 12

2.2.3.4 Noppakunwijai, Tadros, Ma and Mast, 2001 13

2.2.3.5 Castro, Kreger, Bayrak, Breen, and Wood, 2004 13

2.2.3.6 Hale and Russell, 2006 14

2.2.3.7 Dolan and Krohn, 2007 15

2.2.3.8 Birrcher and Bayrak, 2007 16

2.2.3.9 Summary of Recent Research 17

2.3 Mechanical Properties and Behavior of High Strength Concrete 18

2.3.1 Mechanical Properties of High Strength Concrete at Early Ages 19

2.3.1.1 Khan, Cook, and Mitchell, 1995 20

2.3.2 Response to Uniaxial Loading and Quantifying Internal Damage 21

2.3.2.1 Richart, Brandtzaeg, and Brown, 1929 22

2.3.2.2 Hsu, Slate, Sturman, and Winter, 1963 23

2.3.2.3 Ngab, Slate, and Nilson, 1981 24

2.3.2.4 Smadi, Slate, and Nilson, 1985 and 1987 24

2.3.2.5 Delibes Liniers, 1987 25
2.3.2.6 Gettu, Aguando, and Oliveira, 1996 26
2.4 Properties of Self-Consolidating Concrete 27
2.4.1 D'Ambrosia, Lange, and Brinks, 2005 30
2.4.2 Ozyildirim, and Lane, 2003, and Ozyildirim, 2005 33
2.4.3 Ozyildirim and Davis, 2007 35
2.4.4 Gross, Yost, and Gaynor, 2007 38
2.4.5 Ruiz, Staton, Do, and Hale, 2007 42
2.4.6 Burgueño and Bendert, 2007 46
2.4.7 Naito, Parent, and Brunn, 2006 52
2.5 Methods to Analyze Prestress Loss 54
2.5.1 NCHRP Report 496 Detailed Prestress Loss Method 56
2.5.2 AASHTO-LRFD Refined Loss of Prestress Estimate – Interim Edition 2008 60
2.6 Summary 63
CHAPTER 3 Test Specimens 64
3.1 Overview 64
3.2 Design and Fabrication of TxDOT Type-C Beams 64
3.2.1 Design of Series 1 Beams 66
3.2.2 Design of Series 2 Beams 70
3.2.3 Fabrication of Type-C Girders 72
3.2.3.1 Production of Girders: Fabricator A 73
3.2.3.2 Production of Girders: Fabricator B 77
3.2.3.3 Production of Girders: Fabricator C 81
3.2.3.4 Production of Girders: Fabricator D 83
3.2.4 Shipment and Storage of Type C Girders 86
3.3 Design and Fabrication of TxDOT Box Beams 86
3.3.1 Design of TxDOT Box Beams 89
3.3.2 Production of Box Beams: Fabricator E 92

3.3.3 Shipment and Storage of Box Beams 95
3.4 Summary 96
CHAPTER 4 Test Setup 98
4.1 Overview 98
4.2 Testing of Full-Scale Type-C Girders 99
4.2.1 Load Protocol 99
4.2.2 Test Setup 101
4.2.3 Instrumentation and Data Acquisition 105
4.3 Testing of Full-Scale 4B28 Box Beams 108
4.3.1 Load Protocol 108
4.3.2 Test Setup 109
4.3.3 Instrumentation and Data Acquisition 114
4.4 Summary 115
CHAPTER 5 Analysis of Experimental Results 116
5.1 Overview 116
5.2 Results of Type-C Beam Tests 117
5.2.1 Measured Cracking Loads 117
5.2.2 Predicted Cracking Loads 124
5.2.2.1 NCHRP Report 496 Method 126
5.2.2.2 AASHTO-LRFD 2008 Method 133
5.3 Results of Box Beam Tests 137
5.3.1 Measured Cracking Loads 138
5.3.2 Predicted Cracking Loads 142
5.3.2.1 NCHRP Report 496 Method 144
5.3.2.2 AASHTO-LRFD 2008 Method 148
5.4 Observations on Self Consolidating Concrete 150
5.4.1 Fabrication of Box Beam Girders 151
5.4.2 Top Flange Cracking at Release 154
5.4.3 Modulus of Elasiticty 155

5.4.4 Camber 158
5.4.5 Cracking Load 160
5.4.6 Summary of Observations on Self Consolidating Concrete 164
5.5 Summary 164
CHAPTER 6 Summary, Conclusions, and Recommendations 166
6.1 Summary of Experimental Program 166
6.2 Conclusions and Recommendations 168
6.3 Recommendations for Future Work 169
APPENDIX A 170
APPENDIX B 190
APPENDIX C 211
APPENDIX D 213
BIBLIOGRAPHY 219
VITA 225

List of Tables

Table 2-1 Development of Allowable Stresses in Reinforced Concrete *10*
Table 2-2 Summary of Recent Work Regarding Compressive Stress at Release *18*
Table 2-3 Concrete mixture proportions (D'Ambrosia, 2005) *31*
Table 2-4 Hardened Concrete Tests and Specifications *33*
Table 2-5 Hardened Properties of Instrumented Bridge Beams (Ozyildirim and Davis, 2007) *37*
Table 2-6 Concrete Mixture Proportions per cubic yard (Gross et al., 2007) *39*
Table 2-7 Concrete Mixture Designs (Ruiz et al., 2007) *43*
Table 2-8 Concrete Mixture Proportions (Burgueño and Bendert, 2007) *47*
Table 2-9 NCHRP Report 496 Material Properties Equations (Tadros et al., 2003) *57*
Table 2-10 NCHRP Report 496 Equations for Prestress Loss (Tadros et al., 2003) *59*
Table 2-11 AASHTO-LRFD Equations for Material Properties (AASHTO, 2008) *60*
Table 2-12 AASHTO-LRFD Equations for Prestress Loss (AASHTO 2008) *62*
Table 3-1 Type-C Beam Fabrication Details *65*
Table 3-2 Section Properties of a TxDOT Type-C Beam *66*
Table 3-3 Calculated maximum compressive stresses at prestress transfer: Series 1 Beams *69*
Table 3-4 Calculated maximum compressive stresses at prestress transfer: Series 2 Beams *72*
Table 3-5 Concrete Mixture Design used by Fabricator A (per cubic yard) *74*
Table 3-6 Beam Production Details: Fabricator A *77*
Table 3-7 Concrete Mixture Design used by Fabricator B (per cubic yard) *78*
Table 3-8 Beam Production Details: Fabricator B *80*
Table 3-9 Concrete Mixture Design used by Fabricator C (per cubic yard) *82*
Table 3-10 Beam Production Details: Fabricator C *83*
Table 3-11 Concrete Mixture Design used by Fabricator D (per cubic yard) *84*
Table 3-12 Beam Production Details: Fabricator D *85*
Table 3-13 Box Beam Design Details *89*
Table 3-14 Section Properties of a TxDOT 4B28 Box Beam *89*
Table 3-15 Concrete Mix Designs used by Fabricator E (per cubic yard) *92*
Table 3-16 Beam Production Details: Fabricator E *95*
Table 5-1 Measured Cracking Loads for Series 1 Type-C Beams *122*
Table 5-2 Measured Cracking Loads for Series 2 Type-C Beams *123*
Table 5-3 Calculated K_1 values *128*
Table 5-4 Box Beam Design Details *138*
Table 5-5 Measured Cracking Loads for 4B28 Box Beam Specimens *142*
Table 5-6 Calculated K_1 values for Box Beam test specimens *146*

List of Figures

Figure 1-1 TxDOT Project 5197.....3
Figure 2-1 Compressive Stress at Transfer used by PCI survey respondents (adopted from Dolan and Krohn, 2007).....15
Figure 2-2 Theoretical stress vs. strain response for various concrete strengths.....19
Figure 2-3 Stress-Strain behavior for a 10,000-psi concrete at early ages (Khan et al., 1995 adopted from Birrcher and Bayrak, 2007).....21
Figure 2-4 Depiction of three stages discussed by Richart et al. 1929, adopted from Birrcher, 2007.....22
Figure 2-5 Tensile strength loss as a function of compressive stress for various compression times and general curing conditions (Delibes Liniers, 1987)......26
Figure 2-6 Typical volume fraction for different types of concrete (adopted from Bonen, 2005)......29
Figure 2-7 Total Shrinkage of 3 x 3 x 24.5-inch Specimens (D'Ambrosia et al., 2005).....32
Figure 2-8 Slump Flow Test (TxDOT Research Study 5197).....34
Figure 2-9 Schematic Diagram of a U-Tube (U-Box) Test (Khayat et al., 2004).....35
Figure 2-10 Beam Cross section and strain gauge locations (adopted from Gross et al., 2007).....39
Figure 2-11 Measured prestress loss versus time for SCC beams and HSC beams, respectively (Gross et al., 2007).....41
Figure 2-12 Beam Cross Section Details (adopted from Ruiz et al., 2007).....44
Figure 2-13 Measured prestress loss versus beam age (Ruiz et al., 2007).....45
Figure 2-14 Box Beam Cross Section (Burgueño and Bendert, 2007).....48
Figure 2-15 Full Scale Beam Test Setups (Burgueño and Bendert, 2007).....49
Figure 2-16 Plan view with beam layout of M-50/US-127 bridge (Burgueño and Bendert, 2007).....50
Figure 2-17 Strain monitoring at beam bottom flange at mid-span section (Burgueño and Bendert, 2007).....51
Figure 2-18 Bulb-tee beam cross section (Naito et al., 2006).....53
Figure 2-19 Stress in strands vs. time for a Prestressed Girder (Tadros et al., 2003).....55
Figure 3-1 Strand Pattern: Series 1 Specimens.....67
Figure 3-2 Type-C Beam Harped Strands.....67
Figure 3-3 Typical Harping for Fabricator C.....68
Figure 3-4 Typical Harping for Fabricator D (photographs courtesy of David Birrcher).....68
Figure 3-5 Schematic Drawing of Type-C Beam.....70
Figure 3-6 Strand Pattern: Series 2 Beams.....71
Figure 3-7 Live end of prestressing line (Fabricator A).....75
Figure 3-8 Altered Shear Reinforcement.....79
Figure 3-9 Lifting a Type C Girder at FSEL.....86
Figure 3-10 Box Beam Void Geometry.....88

Figure 3-11 Box Beam Centerline Strand Pattern *90*
Figure 3-12 Debonding pattern for Box Beams (Not to scale) *91*
Figure 3-13 Debonded strands prior to concrete placement *91*
Figure 3-14 Lifting a Box Beam at FSEL *96*
Figure 4-1 Series 1 Beam Loading Protocol *100*
Figure 4-2 Series 2 Beam Loading Protocol *101*
Figure 4-3 Type-C Beam Test Setup (Not to Scale) *102*
Figure 4-4 Picture of a Type-C Beam Flexural Test Setup *102*
Figure 4-5 Midspan Region of a Type-C Beam Test *104*
Figure 4-6 Type C-Beam Roller Support and Pin Support, respectively *104*
Figure 4-7 Linear Potentiometers Located at Midspan *106*
Figure 4-8 Linear Potentiometer Located at a Support (Type-C Beam) *106*
Figure 4-9 Crack Documentation using a Crack Comparator Card *107*
Figure 4-10 Box Beam Loading Protocol *109*
Figure 4-11 Box Beam Loading Apparatus *110*
Figure 4-12 Box Beam Roller Support and Pin Support, respectively *111*
Figure 4-13 Pinned connection with 10-inch long top plate *112*
Figure 4-14 Box Beam Test Setup (Not to Scale) *113*
Figure 4-15 Picture of Box Beam Flexural Test Setup *113*
Figure 4-16 Linear Potentiometers Located at Midspan *114*
Figure 4-17 Linear Potentiometer Located at a Support (Box Beam) *115*
Figure 5-1 Applied Load versus Midspan Deflection for Specimen CA-60-3 ..... *119*
Figure 5-2 Applied Load versus Midspan Deflection for Specimen CC-70-2 ..... *119*
Figure 5-3 Visually observed cracking load for Series 1 Beam CA-60-1 ..... *120*
Figure 5-4 Visually observed cracking load for Series 2 Beam CD-65-5 ..... *121*
Figure 5-5 Typical crack pattern at maximum applied load for Type-C Beam tests *121*
Figure 5-6 Type-C Beam Specimens: Applied Load, Shear Force, and Bending Moment Diagrams *125*
Figure 5-7 Estimated initial slope of load deflection plot to calculate the apparent modulus of elasticity for CB-70-1 ..... *128*
Figure 5-8 Comparison of measured and predicted cracking loads using NCHRP 496 losses *132*
Figure 5-9 Comparison of measured and predicted cracking loads using AASHTO-LRFD 2008 losses *136*
Figure 5-10 Applied Load versus Midspan Deflection for Specimen BB-03 (Conventional Concrete) *139*
Figure 5-11 Applied Load versus Midspan Deflection for Specimen BB-10 (SCC) *140*
Figure 5-12 Visually observed cracking load for specimen BB-10 ..... *141*
Figure 5-13 4B28 Box Beams: Applied Load, Shear Force, and Bending Moment Diagrams *143*
Figure 5-14 Estimated initial slope of load deflection plot to calculate the apparent modulus of elasticity for BB-05 ..... *145*

Figure 5-15 Comparison of measured and predicted cracking loads using NCHRP 496 losses *147*
Figure 5-16 Comparison of measured and predicted cracking loads using AASHTO-LRFD 2008 losses *149*
Figure 5-17 Sample of honeycombing in box beam BB-06 ..... *151*
Figure 5-18 Sample of honeycombing in box beam BB-07 ..... *152*
Figure 5-19 Repaired Honeycombing of box beam BB-06 ..... *153*
Figure 5-20 Repaired Honeycombing of box beam BB-07 ..... *153*
Figure 5-21 Typical flexural tension cracking in the top flange of test specimens *154*
Figure 5-22 Typical flexural tension cracking in the top flange of test specimens *155*
Figure 5-23 Load versus midspan deflection for box beams fabricated with concrete containing hard river gravel course aggregate *156*
Figure 5-24 Load versus midspan deflection for box beams fabricated with concrete containing limestone coarse aggregate *157*
Figure 5-25 Camber measurement at midspan for box beam BB-05 (West face) *158*
Figure 5-26 Measured Camber in box beams fabricated with concrete containing hard river gravel coarse aggregate *159*
Figure 5-27 Measured camber in box beams fabricated with concrete containing limestone coarse aggregate *159*
Figure 5-28 Visually observed cracks of beam BB-04 and BB-08 respectively at an applied load of 200-kips *161*
Figure 5-29 Visually observed cracks of beam BB-01 and BB-06 respectively at an applied load of 180-kips *163*
Figure A-1 Sample Shop Drawing for Series 1 Type-C Beam *171*
Figure A-2 Sample Shop Drawing for Series 2 Type-C Beam *172*
Figure A-3 Sample Stress Calculations at Prestress Release for beam CA-70-1 (Series 1) *174*
Figure A-4 Sample Stress Calculations at Prestress Release for beam CC-70-1 (Series 2) *175*
Figure A-5 Prestress Loss/Cracking Load Calculations according to the NCHRP 496 procedure for Specimen CC-70-2, page 1 of 3 ..... *176*
Figure A-6 Prestress Loss/Cracking Load Calculations according to the NCHRP 496 procedure for Specimen CC-70-2, page 2 of 3 ..... *178*
Figure A-7 Prestress Loss/Cracking Load Calculations according to the NCHRP 496 procedure for Specimen CC-70-2, page 3 of 3 ..... *178*
Figure A-8 Prestress Loss/Cracking Load Calculations according to the AASHTO-LRFD Interim 2008 procedure for Specimen CC-70-2, page 1 of 3 ..... *179*
Figure A-9 Prestress Loss/Cracking Load Calculations according to the AASHTO-LRFD Interim 2008 procedure for Specimen CC-70-2, page 2 of 3 ..... *180*
Figure A-10 Prestress Loss/Cracking Load Calculations according to the AASHTO-LRFD Interim 2008 procedure for Specimen CC-70-2, page 3 of 3 ..... *181*
Figure A-11 Sample Box Beam Shop Drawing for specimen BB-01 ..... *182*
Figure A-12 Sample Stress Calculations at Prestress Release for beam BB-01 ..... *183*

Figure A-13 Prestress Loss/Cracking Load Calculations according to the NCHRP 496 procedure for Specimen BB-01, page 1 of 3 ..... *184*
Figure A-14 Prestress Loss/Cracking Load Calculations according to the NCHRP 496 procedure for Specimen BB-01, page 2 of 3 ..... *185*
Figure A-15 Prestress Loss/Cracking Load Calculations according to the NCHRP 496 procedure for Specimen BB-01, page 3 of 3 ..... *186*
Figure A-16 Prestress Loss/Cracking Load Calculations according to the AASHTO-LRFD Interim 2008 procedure for Specimen BB-01, page 1 of 3 ..... *187*
Figure A-17 Prestress Loss/Cracking Load Calculations according to the AASHTO-LRFD Interim 2008 procedure for Specimen BB-01, page 2 of 3 ..... *188*
Figure A-18 Prestress Loss/Cracking Load Calculations according to the AASHTO-LRFD Interim 2008 procedure for Specimen BB-01, page 3 of 3 ..... *189*
Figure C-1 Static Flexural Test Information *212*
Figure D-1 Bursting crack map key for box beams *214*

CHAPTER 1
Introduction

1.1 ALLOWABLE COMPRESSIVE STRESS AT PRESTRESS TRANSFER

The maximum allowable compressive stress limit at prestress transfer was first introduced by the American Association of State Highway and Transportation Officials (AASHTO) in the 1961 Bridge Design Specifications. Shortly thereafter, the American Concrete Institute (ACI) adopted a maximum allowable compressive stress limit at prestress transfer in the 1963 Building Design Specifications (ACI 318-63). This maximum allowable compressive stress at prestress transfer was presented in both documents as a fraction of the compressive strength of concrete. The limits prescribed by AASHTO in 1961 have not changed since their inception. In the current AASHTO-LRFD (Interim 2008) Bridge Design Specifications, the requirement concerning the allowable release stress is as follows:

> *The compressive stress limit for pretensioned and post-tensioned concrete components, including segmentally constructed bridges, shall be* $0.60f'_{ci}$ (AASHTO LRFD 2008).

In the ACI 318 Building Code Requirements, the original allowable maximum compressive stress at prestress transfer was adopted in 1963 as $0.60f'_{ci}$. This limit remained in ACI 318 until 2008 when the provision was modified to address the allowable compressive stress at the ends of simply supported members. The current code provision regarding this limit in ACI 318-08 is as follows:

> *Stresses in concrete immediately after prestress transfer (before time-dependent prestress losses): (a) Extreme fiber stress in compression except as permitted in (b) shall not exceed* $0.60f'_{ci}$. *(b) Extreme fiber stress in compression at ends of simply supported members shall not exceed* $0.70f'_{ci}$... (ACI 318, 2008).

In the past several years, there has been significant interest in increasing the allowable limit of $0.60f'_{ci}$. Relaxing the maximum allowable release stress limit has many potential benefits to the fabrication and design of prestressed girders. Some of these benefits include:

- A decrease in the cycle time of precast facilities
- A reduction in the number of harped strands in a given beam
- A decrease in the number of debonded strands (leading to improved durability and shear performance)
- A longer span length due to an increased number of prestressing strands in a given cross-section
- The removal of "unnecessary" conservatism in current practice

Because of these potential benefits, many research projects have been conducted to determine the effects of increasing the allowable limit. One of these research projects was funded by the Texas Department of Transportation (TxDOT) and conducted at the Ferguson Structural Engineering Laboratory at University of Texas at Austin. This project, denoted as Project 5197, was funded to investigate the effects of increasing the allowable stress limit in prestressed girders. TxDOT project 5197 has been ongoing since 2004 and has been conducted in two phases. Figure 1-1 displays a visual representation of the 2 phases of TxDOT Project 5197.

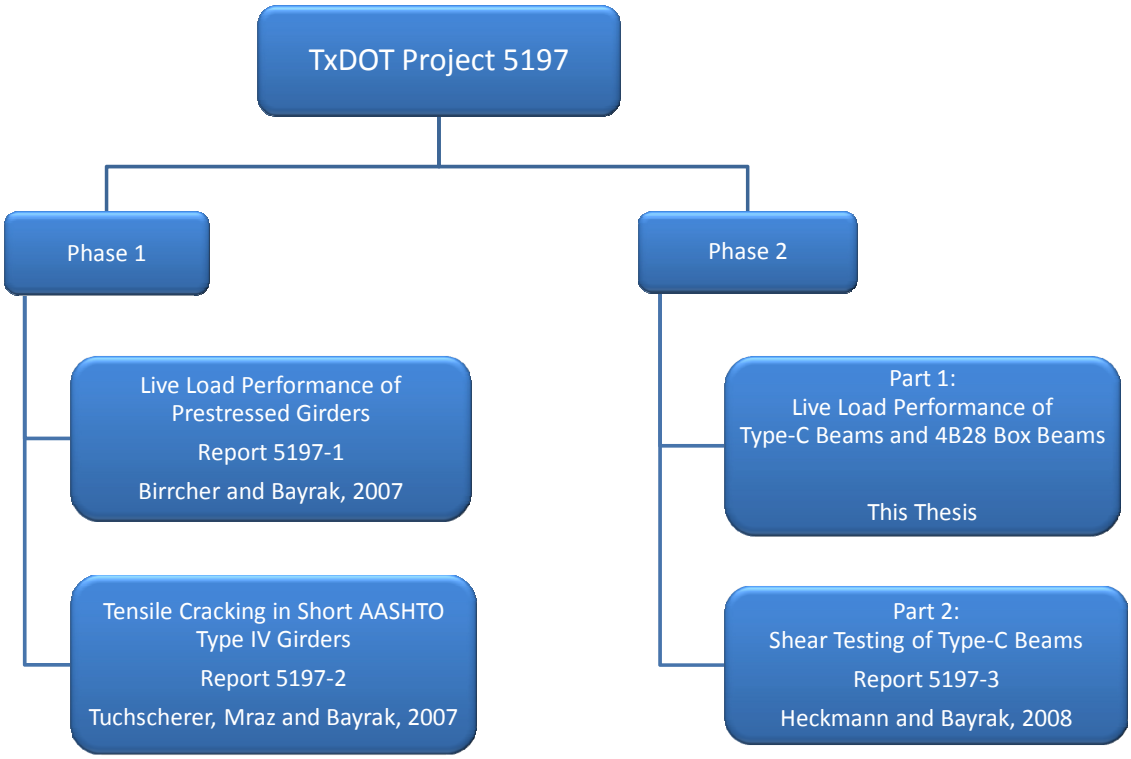

Figure 1-1 TxDOT Project 5197

Phase 1 of TxDOT Project 5197 consisted of two parts:

- The live load evaluation of prestressed concrete beams subjected to compressive stresses at release beyond the allowable limit of $0.60f'_{ci}$ (Birrcher and Bayrak, 2007).
- The investigation of tensile cracking in short AASHTO Type IV girders (Tuchschererer, Mraz, and Bayrak, 2007).

Birrcher and Bayrak experimentally evaluated thirty-six beams of which twenty-four were scaled rectangular, tee, and inverted tee beams and the other twelve were full-scale TxDOT Type-A specimens (28-inch deep I beams). All thirty-six specimens were loaded statically to determine their cracking load. These experimentally measured cracking loads were compared to analytically predicted cracking loads using established methods to calculate prestress losses. Based on the experimentally measured cracking loads, the accuracy of all the predicted cracking loads were determined. For each

specimen, the accuracy of the cracking load was plotted against the maximum compressive stress at prestress transfer. Upon analysis of the data, Birrcher and Bayrak observed an unconservative decrease in cracking load prediction accuracy in specimens subjected to maximum compressive stresses (at prestress transfer) of $0.65f'_{ci}$ or higher. Before endorsing a new allowable compressive stress limit at prestress transfer, Birrcher and Bayrak recommended additional testing on different section types and concrete mixture designs. This recommendation is the basis for the work presented in this thesis.

In addition to the static testing, four of the scaled specimens were tested under fatigue loads and an initial camber database was compiled with information from 223 pretensioned girders. The work completed by Birrcher and Bayrak (2007) is summarized in TxDOT report 5197-1.

Tuchscherer, Mraz, and Bayrak (2007) investigated the tension cracking observed at prestress transfer in short AASHTO Type IV girders. Tuchscherer et al. cast and tested several short AASHTO Type IV girders in an effort to determine an appropriate tensile stress limit in order to eliminate the observed cracking in short Type IV girders. The research by Tuchscherer et al. does not directly pertain to the research presented in this thesis, but is available in TxDOT report 5197-2.

Phase 2 of TxDOT Project 5197 was also completed in two parts:

- Evaluation of the shear performance of Type-C beams stressed beyond the allowable limit (Heckmann and Bayrak, 2008).
- The live load performance of Type-C beams and 4B28 box beams (This Thesis).

Heckmann and Bayrak investigated the impact of increasing the allowable compressive stress limit on the shear capacity of 18 full scale Type-C beam specimens (40-inch deep I beams). In essence, the project evaluated the feasibility of allowing $0.70f'_{ci}$ in the end regions of prestressed Type-C girders. The information from part 2 of phase 2 of TxDOT project 5197 is available in TxDOT report 5197-3.

The live load performance of Type-C girders and 4B28 box beams (28-inch deep by 48-inch wide box beams) is the focus of this thesis and discussed further in section 1.2.

1.2 SCOPE OF RESEARCH

In part 1 of phase 2 of TxDOT Project 5197, experimental research was conducted based on the recommendation from Birrcher and Bayrak (2007). A thorough literature review was conducted along with experimental testing on fifty five full scale beams stressed beyond the allowable limit of $0.60f'_{ci}$. In the literature review, the historical background of the allowable release stress was presented along with recent research regarding the increase of the allowable compressive stress limit. In addition, the early age properties of high strength concrete, the properties of self consolidating concrete (SCC), and the two procedures used to estimate prestress loss in the test specimens were discussed.

The experimental program consisted of the static testing of forty-five Type-C beams and the proof testing of ten 4B28 box beams in flexure. In order to achieve a range of representative data, four different fabricators produced the forty five Type-C beams. The use of several fabricators incorporated different materials and concrete mixture designs from around the state of Texas. Upon completion of the forty five Type-C flexural tests, ten 4B28 box beams were fabricated with a target maximum compressive stress at release of $0.66f'_{ci}$ in order to perform proof testing on a compressive stress limit that seemed adequate for the Type-C beams. Four different concrete mixture designs were used to fabricate the ten box beams. Conventional concrete mixtures containing limestone and hard river gravel coarse aggregate were used as well as SCC mixtures containing limestone and hard river gravel coarse aggregate. The use of several different mixture designs along with fifty-five flexural tests provided a complete range of data to recommend an appropriate maximum allowable compressive stress at prestress transfer.

1.3 CHAPTER OUTLINE

In Chapter 2 a thorough literature review on four topics concerning the effects of increasing the allowable compressive stress limit at prestress release is presented. First, the historical background of the allowable stress limit along with recent research pertaining to its increase is presented. Next, the properties and behavior of high strength concrete used in prestressed applications is discussed. The information on high strength concrete provides insight into the behavior of the precompressed tensile zone of the test specimens. Third, the material properties and behavior of self consolidating concrete (SCC) in relation to conventional concrete are presented. The information presented on SCC is pertinent to understanding the behavior of the five box beams cast using SCC. Finally, the two methods used to estimate prestress losses in the test specimens are presented. These two procedures include the NCHRP 496 Detailed Prestress Loss Method (Tadros et al., 2003) and the AASHTO LRFD Interim 2008 Refined Loss of Prestress Estimate (AASHTO, 2008).

In Chapter 3, the fifty-five specimens tested in flexure are described. Forty-five specimens were TxDOT Type-C girders and were fabricated in four different precast plants in the state of Texas. The maximum compressive stress in the Type-C beams ranged from $0.56f'_{ci}$ to $0.76f'_{ci}$. The remaining ten specimens were TxDOT 4B28 box beams and were fabricated by a single fabricator at two different fabrication plants. The maximum compressive stress at prestress transfer for the box beams ranged from $0.64f'_{ci}$ to $0.66f'_{ci}$. Chapter 3 provides the details of the design and fabrication of all fifty five girders as well as the process of storing and shipping the beams to the Ferguson Structural Engineering Laboratory.

In Chapter 4, the experimental setup for all fifty-five test specimens is described. The load protocol, test setup, instrumentation, and data acquisition setup for both Type-C beam flexural tests as well as 4B28 box beam flexural tests is documented. All fifty five test specimens were subjected to statically determinate four point loading with a five foot constant moment region in the center of the beam.

In Chapter 5, the results and analysis of all fifty five flexural beam tests are presented. The experimentally measured cracking load of each Type-C beam and 4B28 box beam specimen was compared to loads predicted using standard design calculations ($P/A \pm Mc/I$). These plots were then used to determine an appropriate allowable compressive stress at release. In addition, observations from five box beams fabricated with SCC are presented.

Finally in Chapter 6, the conclusions from part 1 of phase 2 of TxDOT project 5197 are presented along with a recommendation of increasing the allowable compressive stress at prestress transfer. In addition, recommendations for future research are discussed.

CHAPTER 2
Literature Review

2.1 OVERVIEW

This literature review covers four main topics related to the effects of increasing the allowable compressive stress limit at prestress release. First, the historical background of establishing the current allowable stress limit, as well as recent research for relaxing this stress limit is presented in Section 2.2. In order to evaluate the adequacy of the current code limit, it is important to understand the origin of the maximum compressive stress limit at prestress transfer as well as the recent research pertaining to increasing that maximum stress limit.

Next, in section 2.3, the properties and behavior of high strength concrete used in prestressed applications are presented. The information presented in this section is pertinent to the behavior of the pre-compressed tensile zone of prestressed girders and therefore, the cracking load of the test specimens. Section 2.3 includes an analysis of the properties and behavior of high strength concrete as compared to those of normal strength concrete. More specifically, the early age strength gain, material properties, response to uniaxial load, and techniques to quantify internal damage are presented.

Third, the properties of self-consolidating concrete (SCC) are compared with those of conventional high strength concrete in Section 2.4. In TxDOT Project 5197, five prestressed 4B28 box girders were fabricated using SCC. An understanding of the material properties and behavior of SCC is needed to effectively evaluate the structural performance of the beams cast with SCC. Section 2.4 contains relevant research pertaining to SCC mixture design, mechanical properties of SCC, and behavior of both small-scale and full-scale girders cast with SCC.

Finally, the two methods used to estimate prestress losses in the test specimens are discussed in Section 2.5. In order to comparatively study the experimentally

observed cracking loads among test specimens, time-dependent methods of estimating prestress losses were needed. The methods described in this section provided a consistent and unbiased means for cracking load prediction of the test specimens.

It should be noted that TxDOT Report 5197-1 (2007) contains a thorough literature review regarding similar topics. As such, any information that has already been presented in the previous report (Birrcher and Bayrak, 2007) will be presented here only in summary for the sake of brevity.

2.2 HISTORICAL BACKGROUND OF ALLOWABLE COMPRESSIVE STRESS AT RELEASE

In the development of standards and codes for reinforced and prestressed concrete, the concept of allowable stresses has changed significantly over time. In the following sections, the evolution of allowable stresses for reinforced concrete and prestressed concrete are presented. Additionally, recent research involving the potential relaxation of the current code limit for allowable compressive stress at prestress transfer is presented.

2.2.1 Allowable Stresses in Reinforced Concrete

In the early 20th century, a need for code provisions for reinforced concrete was becoming apparent. In order to provide some guidance for engineers, allowable stresses were established for various stress conditions. The National Association of Cement Users (NACU) in 1910 issued the first document to gain official standing in the United States titled "*Standard Building Regulations for the Use of Reinforced Concrete*" (Winter 1982). In this publication, the allowable fiber stress for flexural compression was $0.325f'_c$. Over time, several joint committees along with the American Concrete Institute (ACI) changed these allowable stress limits for reinforced concrete. Table 2-1 presents the development of allowable stresses during the 1900s.

Table 2-1 Development of Allowable Stresses in Reinforced Concrete

Year	Document Name	Institution	Allowable Release Stress
1910	Standard Building Regulations for Reinforced Concrete	NACU	0.325 f'_c for flexural Compression
1916	First Joint Committee Report on Concrete and Reinforced Concrete	1st Joint Committee on Concrete and Reinforced Concrete	0.475 f'_c for fiber stress in compression adjacent to supports of continuous members. 0.375 f'_c everywhere else
1924	Second Joint Committee Report on Concrete and Reinforced Concrete	2nd Joint Committee on Concrete and Reinforced Concrete	0.45 f'_c for fiber stress in compression adjacent to supports of continuous members. 0.4 f'_c everywhere else
1936	ACI 501-36	ACI	0.45 f'_c for fiber stress in compression adjacent to supports of continuous members. 0.4 f'_c everywhere else
1941	ACI 318-41	ACI	0.45 f'_c anywhere along a member

After 1941, the allowable stress limit of 0.45f'_c remained until ACI accepted *Ultimate Strength Design* as the fundamental design approach for reinforced concrete. When this was officially adopted in 1971, there was no need for allowable stresses in traditional reinforced concrete. However, allowable compression limits in prestressed concrete still existed.

2.2.2 Compressive Stresses at Release in Prestressed Concrete

In 1942, the American Concrete Institute formed the first committee on prestressed concrete. This committee investigated design procedures and recommended research for this new use of concrete (Hawkins, 1981). The committee expanded over the next several years to form the joint ACI-ASCE Committee 323 (later 423) on Prestressed Concrete. During this same time period, the Bureau of Public Roads was also developing design recommendations for prestressed concrete. Both entities produced separate documents that specified an allowable stress in compression at prestress transfer of 0.6f'_{ci} for prestressed members and 0.55f'_{ci} for post-tensioned members.

No explicit reasoning for these values was provided. Several authorities on prestressed concrete disagreed over the proper amount of compressive stress that should be allowable at release. Many felt uncertain about specifying such a high stress level, but others felt justified based on empirical practice in the prestressed concrete industry.

In 1961, shortly after these documents were circulated, the American Association of State Highway and Transportation Officials' (AASHTO) Standard Specifications for Highway Bridges adopted a maximum allowable stress of 0.6 f'_{ci} for prestressed concrete and 0.55 f'_{ci} for post-tensioned concrete. Later in 1963, ACI Committee 318 accepted 0.6 f'_{ci} for all prestressed and post-tensioned construction. These allowable stresses remained unchanged in ACI 318 until very recently and are discussed in section 2.2.3.9.

2.2.3 Recent Research and Discussion

There has been significant interest in recent years in the possibility of relaxing the current allowable compressive stress limit at prestress transfer of 0.6f'_{ci}. There are many potential benefits of relaxing this limit including a faster production schedule for fabricators and producers, the reduction of harped or debonded strands in prestressed concrete beams, and the increase in the number of prestressing strands in a given section, therefore increasing load-carrying capacity. The following sections document the research conducted on this issue and discussion regarding this release limit. As indicated earlier, any information previously presented in TxDOT Report 5197-1 (2007) is presented here only in summary.

2.2.3.1 PCI Standard Design Practice 1996, 1997, and 2003

PCI Standard Design Practice is a document developed by the Prestressed Concrete Institute (PCI) in an effort to remedy the instances where "*ACI provisions are either ambiguous or in conflict with industry practice*" (Raths, 2007). The PCI Standard Design Practice was first published in 1996 and amended in 1997 and 2003. All three editions of the document suggest that the current ACI limitation of 0.6f'_{ci} is too conservative. Citing common practice and industry experience, the 2003 edition of PCI Standard Design practice endorses a maximum allowable compressive stress at release of 0.7f'_{ci}.

2.2.3.2 Russell and Pang, 1997

Russell and Pang conducted experimental work on 432 concrete cylinders to investigate the effect of sustained compressive stress on overall concrete strength. In this study, cylinders were loaded to sustained stress levels of $0.6f'_{ci}$, $0.7f'_{ci}$, or $0.8f'_{ci}$ for varying durations. Each cylinder had a companion "control" cylinder that was not loaded. Upon completion of the specified load duration, the cylinders were tested in compression to failure. During this testing, four of the cylinders loaded to $0.8f'_{ci}$ failed prematurely under the applied compressive stress. Russell and Pang claimed that their research indicated the possibility of relaxing the allowable compressive stress limit to $0.7f'_{ci}$. However, they suggested that further research be conducted before making such a change.

The conclusion from Russell and Pang's work was only based on a few cylinders which failed prematurely. For those cylinders loaded to $0.8f'_{ci}$ which did not fail prematurely, no significant reduction in strength was noticed. Therefore, analyzing the compressive strength of concrete alone may not be the best means of investigating internal damage in concrete.

2.2.3.3 Huo and Tadros, 1997

Huo and Tadros investigated the effects of early release with the analysis of an 18-inch by 18-inch concentrically prestressed concrete member. Using standard material properties, the researchers ran a linear elastic analysis as well as a separate, iterative non-linear analysis to determine how many strands it would take to crush the concrete upon prestress transfer. Using an f'_{ci} of 3500 psi, the linear elastic method required 45, ½-inch diameter 270 ksi low-relaxation strands. For the non-linear analysis, they assumed that concrete failed when it reached an ultimate strain of 0.003, not when it reached an ultimate stress. Accounting for this fact in their analyses, the non-linear method required 62, ½-inch diameter 270 ksi low-relaxation strands. Huo and Tadros made several observations in this study. First, they showed that both the linear method and the non-linear method provide similar results up to the limitation of $0.6f'_{ci}$. Beyond this, the

linear method began to underestimate the number of strands required to fail the section. Also, Huo and Tadros made the distinction that a prestressed concrete member differs from a member subjected to external forces because of an internal "self-relieving mechanism" which causes the stress in the strands to decrease over time. Huo and Tadros were not able to make any "definitive recommendations" and recommended further investigation of many other factors such as creep and shrinkage before relaxing the $0.6f'_{ci}$ compressive stress limit.

2.2.3.4 Noppakunwijai, Tadros, Ma and Mast, 2001

This research advocated the use of a strength design approach in order to evaluate an appropriate compressive stress at prestress transfer. In this study, the allowable compressive stress at prestress transfer was analyzed as a strength limit state rather than a serviceability limit state. Using a standard PCI rectangular section, the release strength required by ACI 318, PCI, and the proposed strength design method were compared. Additionally, two inverted tee specimens with compressive stresses at release of $0.79f'_{ci}$ and $0.84f'_{ci}$ were fabricated and monitored for approximately 100 days. During this time, the researchers were able to predict the change in concrete strain due to shrinkage and creep with reasonable accuracy. Additionally, the initial and long-term camber of the inverted tees was predicted with reasonable accuracy. The authors observed that increased stresses at release cause increased amounts of prestress loss, therefore reducing the stress on the section.

At the conclusion of this research, the authors recommended the complete elimination of the allowable compression stress limits in favor of their proposed strength design method.

2.2.3.5 Castro, Kreger, Bayrak, Breen, and Wood, 2004

This project, also referred to as TxDOT project 4086, investigated the effect of increasing the allowable compressive stress at prestress release. For this study, 30 pretensioned girders were fabricated with compressive stresses at release ranging from

0.46f'_{ci} to 0.91f'_{ci}. The short and long-term camber for these girders was recorded for all specimens and compared to predicted values. Castro et al. (2004) made several observations from this study. First, camber growth increased with higher levels of compressive stress at prestress transfer. Also, the camber at ten days was more accurately predicted for beams meeting the ACI 318 code provisions than beams subjected to higher release stresses. This result indicated the negative impact of subjecting a beam to a higher compressive stress at release. Ultimately, Castro et al. (2004) recommended that increasing the release stress was acceptable "*as long as the long-term camber was adequately predicted*" (Castro 2004). The results from Castro's work indicated a need for more research and recommended investigating the live load performance of girders stressed above the current allowable limit. This recommendation initiated TxDOT project 5197, the subject of this thesis.

2.2.3.6 Hale and Russell, 2006

Hale and Russell investigated the accuracy of prestress losses in concrete bridge girders stressed above the code allowed limit of 0.6f'_{ci}. For their experimental testing, four I-girders were cast with compressive stresses at release ranging from 0.57f'_{ci} to 0.82f'_{ci}. Prestress losses were measured from concrete surface strains in each of the four girders for one year. All measured prestress losses were accurately predicted within reasonable limits by the available methods used in the research. Additionally, Hale and Russell (2006) observed that the ratio of prestress loss to compressive stress at release was approximately the same for all four bridge girders. Based on this proportionality of prestress loss and compressive stress at release, the authors recommended an increase in the allowable release stress from 0.6f'_{ci} to 0.7f'_{ci}.

It is important to note that although they only recommended increasing the code limitation to 0.7f'_{ci}, their reasoning would justify an increase in the allowable stress limit to 0.82f'_{ci}. Additionally, nonlinear behavior of the prestressed girders was taken into account to accurately estimate deformations at prestress transfer. This practice is not common in prestressed concrete design.

2.2.3.7 Dolan and Krohn, 2007

The investigation by Dolan and Krohn consisted of a thorough literature review on compressive stresses at prestress transfer and a survey of the professional and producer members of PCI. This work was done in an effort to "*determine the current states of research and practice regarding compression transfer stress of prestressed concrete members*" (Dolan and Krohn 2007). The electronic survey was completed by 61 respondents. Of those respondents, 36 stated that they "*routinely use compression transfer stresses above 0.6f'$_{ci}$*" (Dolan and Krohn 2007). Figure 2-1 displays the magnitude of compression transfer stresses used by respondents of the electronic survey.

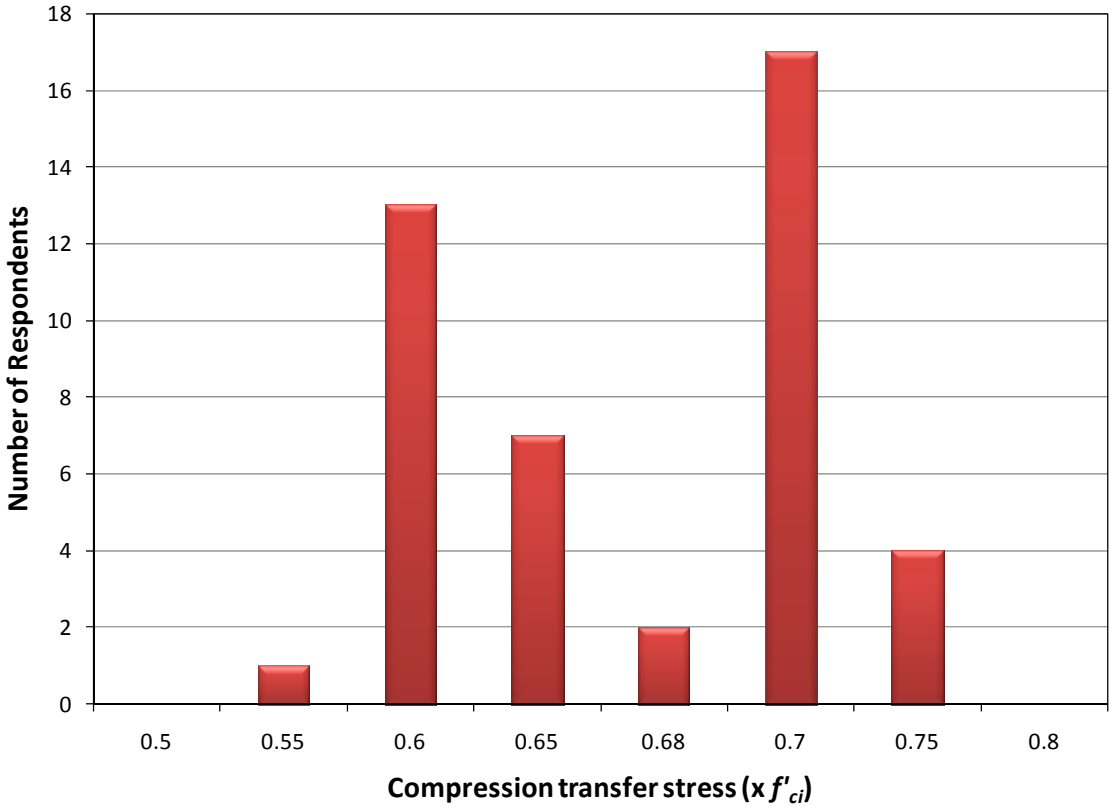

Figure 2-1 Compressive Stress at Transfer used by PCI survey respondents (adopted from Dolan and Krohn, 2007)

Also during the survey, respondents were given the opportunity to identify any problems associated with the use of an increased allowable stress at prestress transfer.

Some problems such as excessive camber or concrete splitting at the ends of the members were noticed and reported. However, a large majority of the respondents noted no problems with using high stresses at release. After evaluating the surveys and investigating literature, Dolan and Krohn concluded that producers have many years of experience in fabricating prestressed concrete beams using compression stresses at release greater than $0.6f'_{ci}$ with minimal problems. Therefore, they recommended that ACI 318 should raise the allowable compressive stress at prestress transfer to $0.7f'_{ci}$. In addition, they recommended that the PCI equations for prestress loss and camber be reviewed and revised for this increased transfer stress.

2.2.3.8 Birrcher and Bayrak, 2007

Following the research of Castro et al. (2004), TxDOT project 5197 was initiated to evaluate the live load performance of prestressed concrete girders stressed beyond the allowable limit. This research study involved the static live load testing of 24 scaled girders from Castro et al. and 12 full-scale TxDOT standard A-beams and the fatigue testing of 4 beams from Castro et al.

The static live load tests were used to experimentally determine the cracking load of the test specimens. These experimentally determined cracking loads were then compared to analytically predicted cracking loads. The following three methods were used to analytically determine cracking loads: PCI Design Handbook Loss of Prestress Estimate (PCI, 2004), the NCHRP Report 496 Detailed Prestress Loss Method (Tadros et al., 2003), and the AASHTO LRFD Refined Loss of Prestress Estimate (AASHTO, Interim 2005).

During the static tests, the specimens were subjected to four-point loading creating a constant moment region at the center of the beam. While testing the specimens, loading was stopped several times to mark cracks as well as document crack widths and crack propagation. All test specimens were loaded until significant cracking was observed. Upon completion of these static tests, the accuracy of the predicted cracking load was plotted against the maximum compressive stress at release. These plots

are displayed in Chapter 1 and Chapter 5 of this thesis. From these plots, Birrcher and Bayrak observed an unconservative drop in cracking load accuracy with beams subjected to a maximum compressive stress higher than $0.65f'_{ci}$.

The results from this work indicate that "*an increase of the allowable compressive stress to* $0.65f'_{ci}$ *was justified*" (Birrcher and Bayrak, 2007). Although Birrcher and Bayrak did believe an increase to $0.65f'_{ci}$ was justified, they recommended further testing of beams with different shapes, different fabricators, and different concrete mixture designs. The recommendations from Birrcher and Bayrak are the basis for the research presented in this thesis. The complete documentation of their research is located in a Center for Transportation Research (CTR) report under TxDOT Project 5197-1.

2.2.3.9 Summary of Recent Research

Table 2-2 provides a summary of the recent research regarding compressive stresses at prestress transfer. Much of the research in recent years has supported changing the allowable release factor to $0.7f'_{ci}$ with only a few concerns about girder performance. Therefore, in 2008, ACI 318 adopted a new allowable compressive stress limit of $0.7\,f'_{ci}$ at the ends of prestressed members citing, "*research in the precast, prestressed concrete industry practice*" (ACI 2008). ACI maintained the limit of $0.6\,f'_{ci}$ at midspan. However, the Interim 2008 Edition of the American Association of State Highway and Transportation Officials (AASHTO-LRFD) Bridge Design Specification maintained the allowable compressive stress at transfer of $0.6f'_{ci}$ everywhere. These limitations are current as of the date of this report.

Table 2-2 Summary of Recent Work Regarding Compressive Stress at Release

Researchers	Year	Focus of Research (In regard to Compressive Stress at Release)	Scope of Experimental Work
Russell and Pang	1997	Compressive Strength	432 cylinders
Huo and Tadros	1997	Nonlinear Behavior	None
Noppakunwijai et al.	2001	Creep, Shrinkage, Camber, etc.	2 IT girders
Castro et al.	2004	Camber	30 Rect., IT, T girders
Hale and Russell	2006	Effective Prestressing Force	4 I-Beams
Dolan and Krohn	2007	Current State of the Industry	None
Birrcher and Bayrak	2007	Live Load Performance	12 Full Scale I-Beams 24 Scaled girders

2.3 MECHANICAL PROPERTIES AND BEHAVIOR OF HIGH STRENGTH CONCRETE

In order to produce beams efficiently, it has been common practice to use high-strength concrete (HSC) to fabricate prestressed concrete girders. Research on this topic has shown that high strength concrete has substantially different mechanical properties than normal strength concrete. Figure 2-2 displays the theoretical stress-strain responses for several concrete strengths. This figure was generated with expressions for stress and strain developed by Thorenfeldt, Tomaszewicz, and Jensen (1987) found in Chapter 3 of the Collins and Mitchell text, *Prestressed Concrete Structures* (1997). As shown in Figure 2-2, the ascending and descending branches of the stress-strain curves become much more linear as the concrete strength increases. Figure 2-2 also illustrates that the response of low strength concrete is substantially different from that of high strength concrete. In addition to stress-strain behavior, the magnitude of shrinkage and creep differs between normal strength and high strength concrete. It is for these reasons that equations specific to high strength concrete have been developed to calculate the modulus of elasticity, shrinkage strains, creep strains, and other mechanical properties.

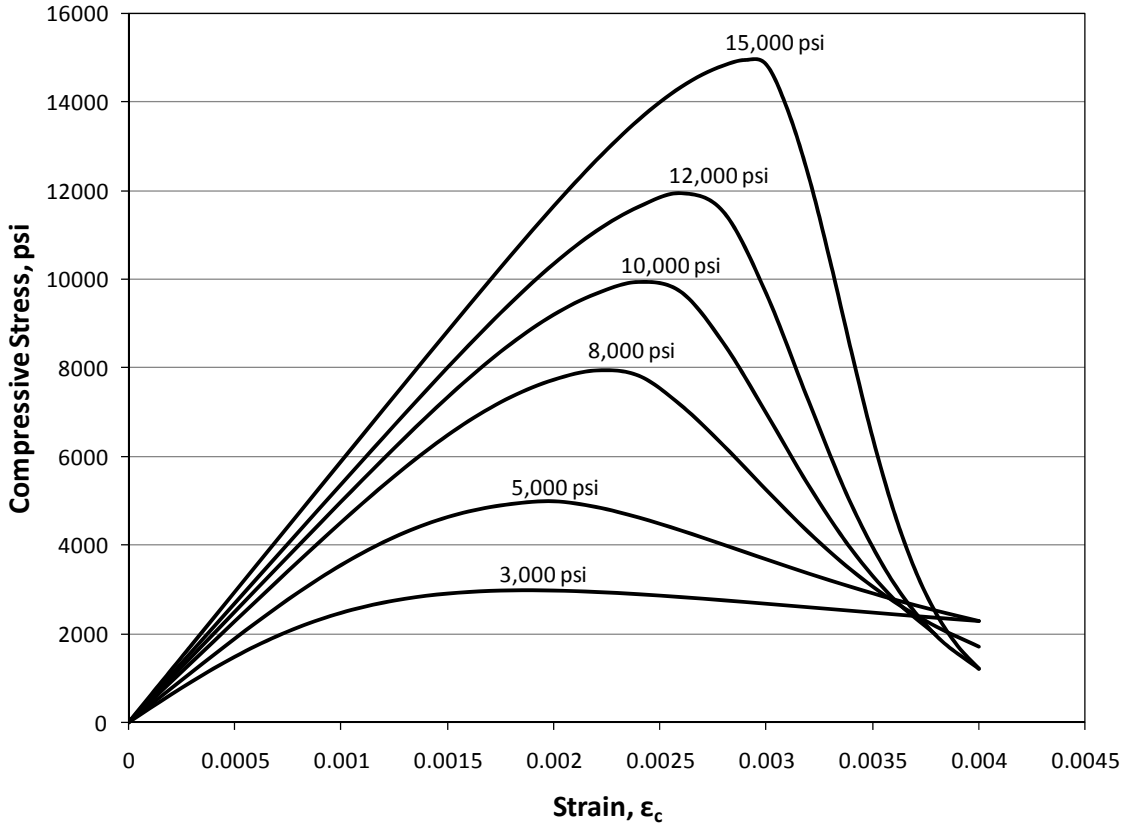

Figure 2-2 Theoretical stress vs. strain response for various concrete strengths

This section details the high strength concrete research on early age mechanical properties, response to uniaxial loading, and methods to measure internal damage. A clear understanding of the material properties and behavior of high strength concrete is needed to evaluate the behavior of the pre-compressed tensile zone of prestressed concrete bridge girders.

2.3.1 Mechanical Properties of High Strength Concrete at Early Ages

In the prestressed concrete beam fabrication industry, high strength concrete is often loaded to large stresses at early ages (less than 24 hours after casting). Therefore, it is important to study and understand the early age strength and behavior of high strength concrete. The 28-day properties of high strength concretes have been extensively researched, but few investigations have focused on the properties of high strength

concrete at younger ages. The following section highlights work on the early age mechanical properties of high strength concrete.

2.3.1.1 Khan, Cook, and Mitchell, 1995

This research study includes an investigation of the stress-strain behavior of three different types of concrete: Low Strength Concrete, LSC, at 4000 psi (30 MPa), Normal Strength Concrete, NSC, at10,000 psi (70 MPa) and High Strength Concrete, HSC, at 14,500 psi (100 MPa). Concrete cylinders were batched and tested in compression during the first 72 hours after batching in order to investigate the concrete strength with temperature rise, stress-strain behavior at early ages, and influence of curing conditions on compressive strength and elastic modulus. The researchers concluded that for all three types of concrete (LSC, NSC, HSC) there is, "*a significant difference in the shape of the compressive stress-strain response at a very early age*" (Khan et al., 1995). Figure 2-3 displays the stress strain behavior of a 10,000 psi (70 MPa) concrete at various ages. It is important to note that the behavior at 16.5 hours is much more nonlinear than at 3 days. As the compressive strength increases, the ascending and descending branches of the stress-strain curve become much more linear.

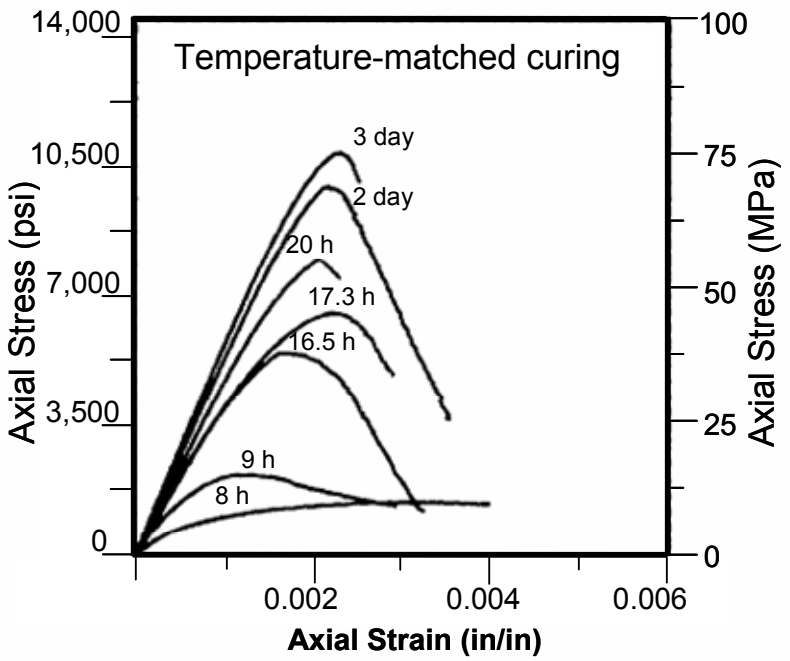

Figure 2-3 Stress-Strain behavior for a 10,000-psi concrete at early ages (Khan et al., 1995 adopted from Birrcher and Bayrak, 2007)

The nonlinearity of concrete at a young age as shown in Figure 2-3 indicates that significant internal damage may occur if the concrete is loaded to high levels of compression during the first 24 hours after casting.

2.3.2 Response to Uniaxial Loading and Quantifying Internal Damage

Concrete is made up of cement paste and aggregates. Both of these materials individually have linear and highly brittle stress strain curves (MacGregor and Wight, 2005). When combined, the stress-strain behavior becomes nonlinear. This nonlinear behavior can be described by the phenomenon of microcracking. Microcracks are tiny internal cracks 1/8-inch to ½-inch in length. Under increasing compressive stresses, the microcracks expand causing nonlinearity and eventually cause failure of concrete in compression. The following research studies document the formation and propagation of this internal damage.

2.3.2.1 Richart, Brandtzaeg, and Brown, 1929

An investigation of the testing of short columns (40-inches tall and 10-inches in diameter) that were either plain concrete or spirally reinforced was presented in this research. These short columns were tested in compression in an effort to understand the "*action of concrete under compressive stresses*" (Richart et al., 1929). Upon testing the plain concrete columns with no reinforcing bars, the researchers deemed it appropriate to divide the concrete response into three stages. In the first stage, the behavior was elastic with stresses and strains proportional to each other. This first stage was observed for at least 25-percent of the ultimate load. The second stage was defined with appreciable deviations from the previous stress-strain proportionality. Finally, the third stage was defined by an abrupt change in lateral deformation of the specimen. During the third stage, the internal structure broke down leading to ultimate failure. This third stage occurred at 75 to 85-percent of the ultimate load. A visual depiction of these three stages is displayed in Figure 2-4.

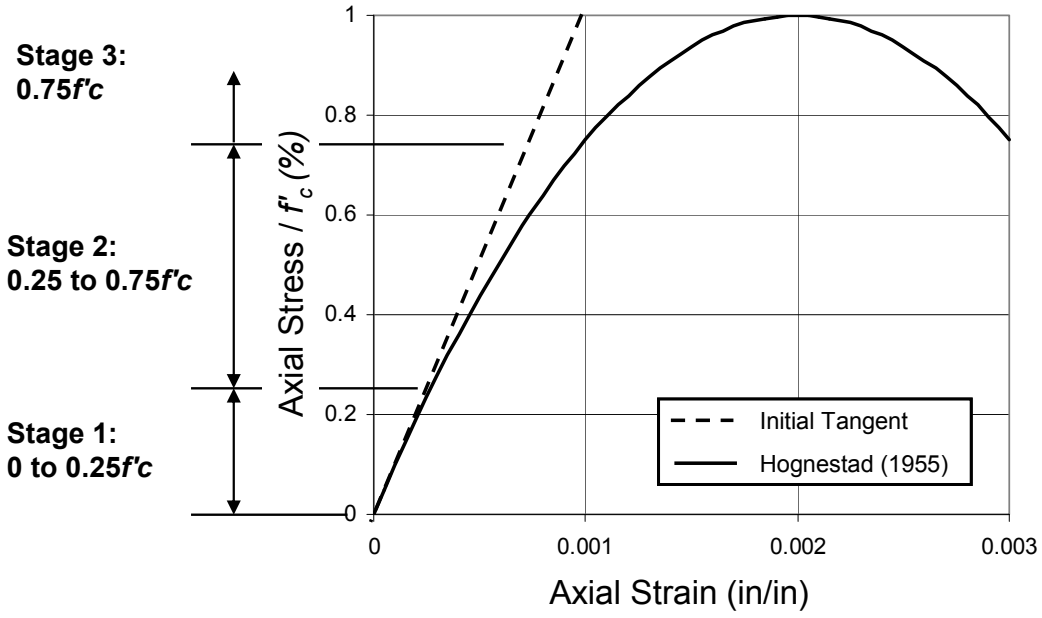

Figure 2-4 Depiction of three stages discussed by Richart et al. 1929, adopted from Birrcher, 2007

Richart et al. concluded that the phenomenon observed in the third stage was due to "*internal splitting or breaking of the continuity of the material*" (Richart et al., 1929). As such, serious damage to the microstructure was observed when concrete was loaded to high stresses (about 75-percent of ultimate strength).

2.3.2.2 Hsu, Slate, Sturman, and Winter, 1963

The type and extent of microcracking in plain concrete cylinders subjected to uniaxial compressive loads was investigated in this research project. Ten representative specimens were examined and reported. The cylinders were loaded to a prescribed amount of strain between 0 and 0.003. After loading, the cylinders were cut with a diamond blade masonry saw and examined under a microscope. Using ink dye to accentuate the cracks, the researchers extensively analyzed the specimens and drew cracking maps. Hsu et al. determined that three types of microcracks exist: bond cracks, mortar cracks, and aggregate cracks. Bond cracks exist at the interface between the aggregate and mortar and are present before loading even begins. After loading is initiated, these bond cracks increase in size and number. As bond cracks propagate, stress in the concrete must redistribute causing cracks within the mortar to develop. Upon reaching 70 to 90-percent of the ultimate load, the mortar cracks increase and bridge between bond cracks to form continuous crack patterns. This formation of continuous crack patterns signifies a "critical" load at which the stress-strain diagram becomes highly non-linear indicating the beginning of the breakdown of the internal structure.

Essentially, Hsu et al. (1963) agreed with the findings of Richart Brandtzaeg and Brown (1929). Both Hsu et al. and Richart et al. indicated critical loads of $0.7P_{ult}$ and $0.75P_{ult}$ respectively where the internal structure of the concrete begins to break down. It is important to note that relatively low strength concrete samples were used in both studies. Even though the compressive strengths investigated by Hsu et al. and Richart et al. were low, the same inelastic behavior exists for normal-strength concrete today (MacGregor, 2005).

2.3.2.3 Ngab, Slate, and Nilson, 1981

Ngab et al. analyzed the microcracking in eighty-four 3.5 x 3.5 x 10-inch specimens of normal strength and high strength concrete subjected to compressive loading. Specimens were tested for different durations at different ages after curing. The applied stress-to-strength ratio of the specimens varied from 0.30 to 0.85. After loading, the specimens were cut with a diamond-blade masonry saw and analyzed. After digitizing, measuring, and mapping the microcracking present in the concrete, the researchers made several observations: First, the amount of microcracking in high strength concrete was significantly less than that of normal strength concrete. Additionally, the amount of microcracking for both high strength and normal strength concrete was found to be a function of the strain imposed on the concrete, regardless of whether the strain was due to short-term loads, sustained loads, or shrinkage.

In addition to analyzing microcracking in concrete, Ngab et al. investigated the creep behavior of these specimens. The researchers concluded that for high strength concrete, the ratio of applied stress and creep deformation was linear until approximately 70-percent of f'_c. Based on these findings, it was concluded that additional creep deformation, and therefore microcracking, could develop at or near loads of 70-percent of f'_c.

2.3.2.4 Smadi, Slate, and Nilson, 1985 and 1987

These two research investigations focused on the sustained loading response of high-strength concrete relative to medium- and low- strength concrete. In this study, high-strength concrete was defined as concrete with compressive strengths between 8500 psi and 10000 psi. All test specimens consisted of 4 x 8-inch cylinders loaded to a specific level of stress ranging from $0.4f'_c$ to $0.95f'_c$. Many specimens loaded to very high values of stress failed under the applied load. Specimens which did not fail were monitored for creep deformation. From this research, Smadi found that high strength concrete achieves 80- to 85-percent of its short term compressive strength when placed under long-term sustained loading. For the specimens that did not fail, Smadi also found

that high strength concrete performed better than medium- and low-strength concrete in regards to creep deformation. Furthermore, creep strain appeared to increase linearly with applied stress until the load reached approximately 70-percent of the ultimate capacity. From that point forward, the creep deformation became nonlinear. Smadi concluded that the "*deviation of creep from linearity with increasing stress is believed to be due to a significant increase in bond cracks along the mortar-aggregate interface*" (Smadi et al., 1987). Smadi et al. also recommended that "*the stresses in HSC can be increased safely up to the creep proportional limit, or up to about 65 percent of ultimate [capacity], without causing significant crack formation*" (Smadi et al., 1987). These results suggest that loading in a range beyond $0.65f'_{ci}$ could cause significant cracking and elevated creep deformation in high strength concrete.

2.3.2.5 Delibes Liniers, 1987

Delibes Liniers investigated the loss of tensile strength in concrete after axial compressive loading. Liniers believed that the internal microcracking in the concrete weakened the tensile strength. The experimental testing involved casting concrete cylinders and loading them in compression to a specified value of their ultimate strength (50-percent to 95-percent) and maintaining the load for a specified period of time. After loading, the cylinders were split in accordance with ASTM C496-71. Delibes Liniers found that tensile strength decreased with increasing compressive stress to strength ratios. Figure 2-5 shows the summarized results from this research investigation.

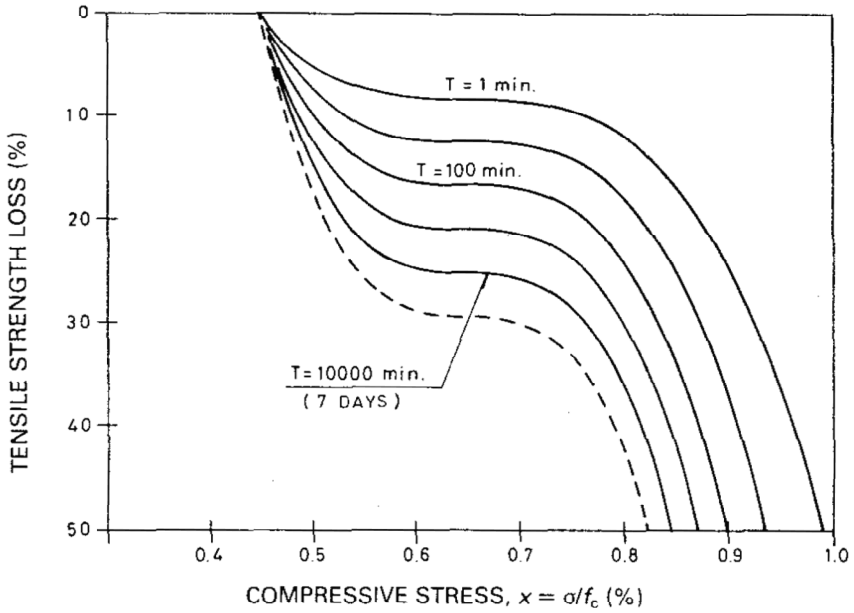

Figure 2-5 Tensile strength loss as a function of compressive stress for various compression times and general curing conditions (Delibes Liniers, 1987).

As shown in Figure 2-5, loading at higher compressive stress-to-strength ratios lead to increased losses in tensile strength. It is important to note that Delibes Liniers found that microcracks typically form parallel to the applied load. Liniers notes that *" 'damage' in a direction perpendicular to the compression was almost negligible"* (Delibes Liniers 1987). This finding is interesting because research by Ngab et al. and Smadi et al. indicated microcracks perpendicular to the applied load.

Ultimately, Delibes Liniers concluded that "*the necessity of limiting compressive stress under 60% of the strength is confirmed*" (Delibes Liniers, 1987). This research showed that tensile strength loss was a reasonable indicator for internal damage and that concrete loaded above 60-percent of its strength could experience tensile strength loss and therefore significant internal damage.

2.3.2.6 Gettu, Aguando, and Oliveira, 1996

Gettu et al. investigated internal damage in concrete induced by monotonic and cyclic compressive loading. In order to evaluate the amount of damage in concrete

specimens, splitting tension tests were performed. For the experimental research, cubes were cast, cured, and subjected to either monotonic or cyclic loads. After loading, the cube was turned 90-degrees about the casting direction and a splitting tension test was performed. This summary only contains the conclusions that were based on the data for the specimens loaded monotonically.

Once the cubes had cured for 28 days, they were loaded to a specified applied stress-to-strength ratio ranging from 0.25 to 0.85. After maintaining the load for fifteen minutes, the specimen was split in tension so that the failure plane was parallel to the previously applied compressive stress. Loading in this fashion was analogous to the testing done by Delibes Liniers (1987). Upon completing this experimental research, Gettu et al. concluded that "*Damage in high-strength concrete due to uniaxial compressive stress is negligible as long as the monotonically applied stress is less than 60 percent of its strength*" (Gettu et al., 1996). In summary, the findings of Gettu et al. (1996) coincide with Delibes Liniers (1987). Both investigations showed that loss in tensile strength provided a good indicator of internal damage. In addition, both research experiments indicated that loading concrete specimens to compressive stresses above 60-percent of their ultimate strength cause internal damage and loss of tensile strength.

2.4 PROPERTIES OF SELF-CONSOLIDATING CONCRETE

In the current research project (TxDOT Project 5197), five box beams were fabricated using self consolidating concrete (SCC). In order to adequately evaluate the behavior of these beams, a thorough understanding of SCC is needed. The following section includes relevant research pertaining to SCC mixture design, mechanical properties of SCC, and behavior of full-scale girders cast with SCC.

Self consolidating concrete (SCC) is a type of concrete that flows freely to fill formwork and requires little to no external vibration. In order to obtain these unique characteristics for use in prestressed concrete, several changes must be made to conventional high strength concrete mixture designs. First, the concrete must become more fluid to adequately fill formwork and congested areas of reinforcing steel without

mechanical vibration. High fluidity in concrete is achieved by using a plasticizing admixture, increasing the water to cementitious materials (w/cm) ratio, using a smaller coarse aggregate size, or a combination of the previous three. By making the concrete more fluid, the mixture is much more likely to segregate during casting, creating a weak and vulnerable layer of cement paste at the top of the vertically cast members. In order to combat segregation, the ratio of fine aggregate to coarse aggregate can be increased, the w/cm ratio can be decreased, and/or a viscosity modifying admixture (VMA) can be used. All of these changes help to suspend the coarse aggregate in the mixture and prevent segregation.

Although the composition of SCC mixtures can vary greatly, two main design methodologies have developed (Bonen, 2005). The first design method is to utilize superplasticizer, low w/cm, and a high amount of fine aggregate. This method is often referred to as the "powder" method because of the relatively large amount of the cementitious materials and fine aggregate in the mixture. The second design method is to incorporate a viscosity modifying admixture. Adding the VMA to the mixture will control the concrete viscosity and therefore reduce the amount of powder needed in the mixture. A visual depiction of the two types of self consolidating concrete as compared to ordinary concrete is displayed in Figure 2-6.

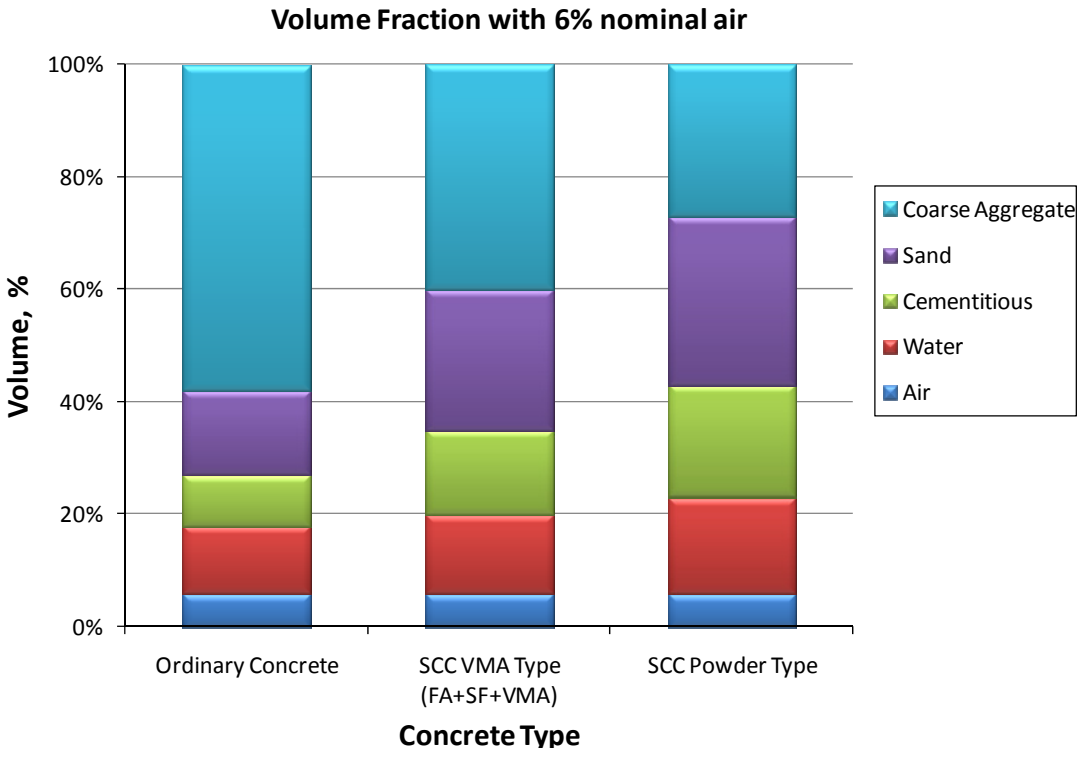

Figure 2-6 Typical volume fraction for different types of concrete (adopted from Bonen, 2005).

The use of self consolidating concrete has many potential benefits for prestressed applications. First, the ability of SCC to flow freely to fill formwork without vibration provides a savings in time and labor. With conventional concrete, the mixture must be properly vibrated by laborers to fill the formwork with layers of concrete free of voids or defects. This can become time-consuming and troublesome in areas of highly congested reinforcing steel or complex geometry. SCC mixtures provide a simpler means of placing concrete. Additionally, due to the fluid nature of the mixture, SCC is less likely to have void-related imperfections such as bug holes, honeycombs, etc. In theory, this provides higher quality concrete requiring less repair.

Although SCC offers many potential benefits to precast beam fabricators, there are some concerns which must be investigated. Because the SCC is very fluid, there is a constant concern regarding segregation. If the mixture does not adequately suspend the

coarse aggregate, then the coarse aggregate will sink, leaving behind weak layers of cement paste and a non-uniform structural material. In addition, D'Ambrosia et al. (2005) has shown that SCC mixtures exhibit high amounts of shrinkage and a lower modulus of elasticity when compared to conventional concrete. Furthermore, the "*raw materials cost of SCC is higher by about 13-30% than that of conventional mixtures with similar mechanical properties*" (Bonen, 2005). This additional cost can be mitigated by the savings from labor and time, but that may not always be the case.

Many departments of transportation around the country have been reluctant to adopt the use of SCC until adequate research assured that the use of SCC would provide acceptable results. The following sections detail recent research relevant to the mechanical properties of SCC and applications of SCC in prestressed concrete.

2.4.1 D'Ambrosia, Lange, and Brinks, 2005

D'Ambrosia et al. investigated the performance of self consolidating concrete at early ages (less than 24 hours). The research team monitored the early age shrinkage, creep, strength gain and modulus of elasticity in an effort to assess the characteristic behavior of SCC. In addition, an effort was made to understand how different mixture design strategies would impact early age properties of hardened concrete.

First, a database of more than 150 SCC mixtures was compiled in an effort to understand SCC mixture proportioning. Upon analysis of the data, the researchers found that SCC mixtures trended toward lower water-to-cementitious material ratios (w/cm) when compared to normal strength concrete. Also, the aggregate content tended to be lower for SCC when compared to typical concrete. Furthermore, SCC mixtures typically had a higher proportion of sand to provide segregation resistance.

After analyzing typical SCC mixtures, four different mixture designs were selected for testing. A conventional high strength mixture design was used as a control and given the designation OPC 1. The proportions for all five mixtures are given in Table 2-3.

Table 2-3 Concrete mixture proportions (D'Ambrosia, 2005)

Material	OPC 1	SCC 1	SCC 2	SCC 3	SCC 4
Portland Cement (lb/yd^3)	726	661	601	685	679
Fly Ash (lb/yd^3)	0	157	325	0	151
Coarse Aggregate: 3/4" maximum (lb/yd^3)	1853	367	1365	1627	579
Coarse Aggregate: 3/8" maximum (lb/yd^3)	0	1075	0	0	1018
Fine Aggregate (lb/yd^3)	1192	1403	1336	1389	1389
Water (lb/yd^3)	290	311	301	278	267
Superplasticizer (fl oz/yd^3)	22	63	29	49	36
VMA (fl oz/yd^3)	0	0	0	22	0
w/cm	0.4	0.38	0.33	0.41	0.34

Specimens from all the mixture designs in Table 2-3 were tested for early age strength, and autogenous and drying shrinkage. To monitor the early age strength gain, two sets of 4 x 8-inch cylinders were subjected to compressive strength tests according to ASTM C39. One set of cylinders was kept in a temperature and humidity controlled environment while the other set was moist cured. In addition, early age indirect tensile strength was measured on the temperature and humidity controlled cylinders in accordance with ASTM C496. Autogenous shrinkage was evaluated with embedded strain gauges on 3 x 3 x 11-inch prisms in a sealed container. The temperature of the specimens was monitored so thermal expansion could be taken into account. To measure restrained and unrestrained drying shrinkage, a uniaxial test method was employed. This involved two companion 3 x 3 x 24.5-inch specimens that were cast and allowed to cure under a plastic sheet for one day. The unrestrained shrinkage specimens were used to monitor free shrinkage measured by using a linear variable differential transducer (LVDT). The restrained shrinkage specimens were placed in a testing machine that applied the necessary tensile force to maintain the specimen's original length.

The compressive strength development testing indicated high early strengths due to the tendency for SCC mixtures to have a low w/cm ratio and high paste content. In order to maintain a similar curing regime, the concrete cylinders tested for tensile

strength were kept in a drying environment with the creep and shrinkage specimens. The results from the tension tests indicated that the tensile strength did not increase very much after three days because the concrete was not given an external source of moisture. This led to the conclusion that the "*lack of external water during curing increased the risk for cracking at early age by limiting strength development*" (D'Ambrosia et al., 2005).

The shrinkage portion of the study indicated that SCC had high amounts of drying shrinkage. The results from the total shrinkage of the concrete prisms are displayed in Figure 2-7.

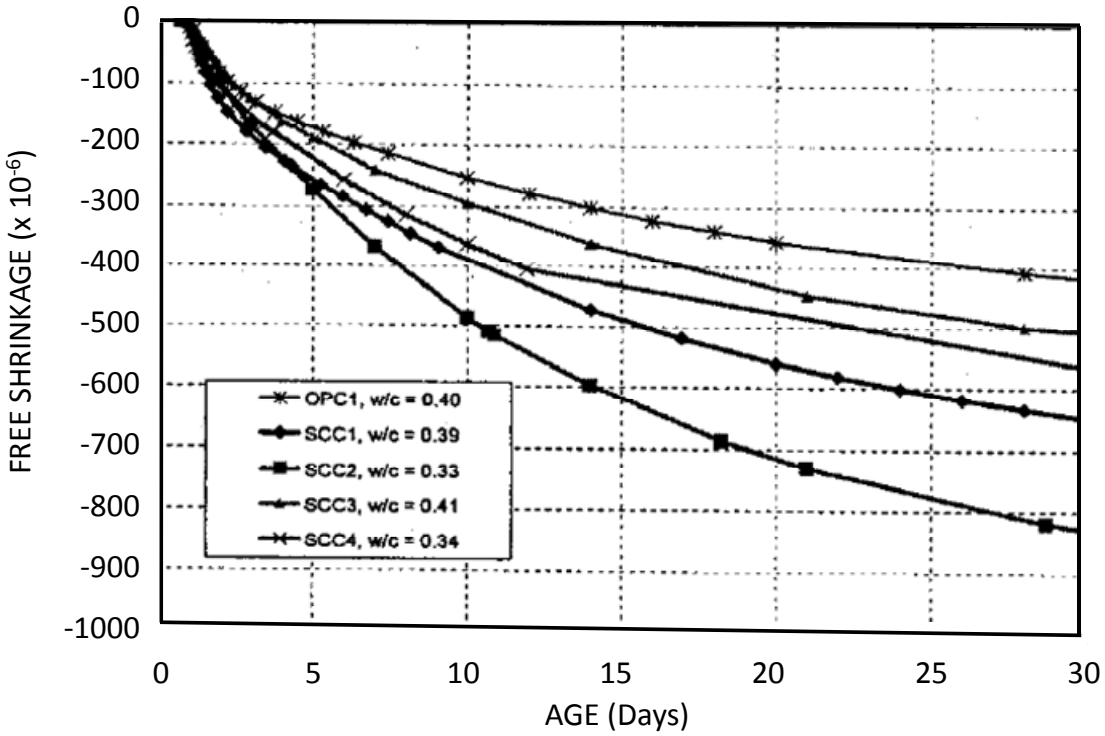

Figure 2-7 Total Shrinkage of 3 x 3 x 24.5-inch Specimens (D'Ambrosia et al., 2005)

As is displayed in Figure 2-7, the drying shrinkage for all four SCC mixtures was noticeably larger than the ordinary concrete mixture. Significant drying shrinkage occurred with SCC when the w/cm ratio was 0.4 or lower. The researchers noted that, "*Low w/cm and high paste content caused a significant amount of autogenous shrinkage,*

which was a major contributor to overall early age shrinkage and subsequent stress development and cracking" (D'Ambrosia et al., 2005).

At the conclusion of their research, the authors recognized a "*potentially high risk for cracking*" and noted that the low w/cm ratios and high cement paste contents found with SCC mixtures generally contributed to a higher early age cracking risk. The researchers also pointed out that SCC typically had a high early strength gain which could mitigate some of this cracking risk. Ultimately, the researchers reported that different methods of mixture proportioning led to SCC materials with similar flow characteristics, but different hardened mechanical properties.

2.4.2 Ozyildirim, and Lane, 2003, and Ozyildirim, 2005

Ozyildirim and Lane documented an investigation on self consolidating concrete conducted by the Virginia Department of Transportation (VDOT). Their research report summarizes the early development and testing of SCC mixtures for use by VDOT. In addition, the report describes the use of SCC in VDOT applications.

In developing suitable SCC mixtures, VDOT prepared fifteen concrete mixtures and tested them for consistency, compressive strength, permeability, drying shrinkage, air voids, and freeze-thaw resistance. All tests performed on the hardened concrete samples and the corresponding specifications are presented in Table 2-4.

Table 2-4 Hardened Concrete Tests and Specifications

Tests	Specification	Age (days)	Size (in)
Compressive Strength	AASHTO T 22	[a]	4 x 8
Permeability	AASHTO T 277	28[b]	2 x 4
Drying Shrinkage	ASTM C 157	28	3 x 3 x 11¼
Freeze-Thaw Analysis	ASTM C 666	[c]	3 x 4 x 16
Air Void Analysis	ASTM C 457	28	4 x 8

[a]At 28 days for lab specimens and 1, 7, and 28 days for plant specimens.
[b]Cured 1 week at 73°F (23°C) and 3 weeks at 100°F (38°C).
[c]Specimens cured 2 weeks moist and air dried 1 week before testing. Test water contained 2% NaCl.

The slump flow and U-tube (or U-box) tests were used to evaluate workability and consistency. Figure 2-8 displays a picture of the slump flow test and Figure 2-9 displays a schematic diagram of the U-tube test. In the slump flow test, concrete is poured into an inverted slump cone. The slump cone is then lifted allowing the concrete to flow out. The diameter of the circular spread of the concrete provides a measure of flow and therefore determines the consistency of the concrete. In the U-tube test, a "U"-shaped testing apparatus is used (Figure 2-9). This apparatus consists of two legs separated by a wall. The wall extends for most of the "U" except at the bottom where the wall is replaced with reinforcing bars. First, a gate is lowered over the reinforcing bars preventing any flow between legs of the "U". Then, concrete is poured to the full height of one leg of the "U". Finally, the gate is removed so the SCC flows through the rebar and rises up the other leg of the "U". The distance that the concrete rises provides a measure of workability.

Figure 2-8 Slump Flow Test (TxDOT Research Study 5197)

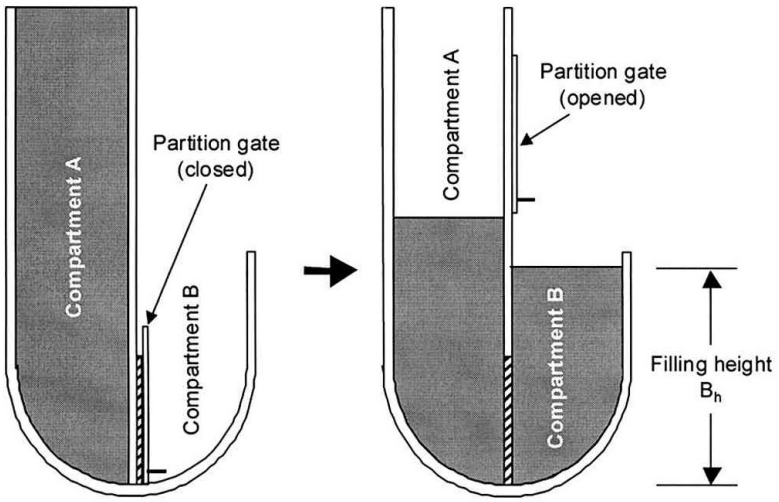

Figure 2-9 Schematic Diagram of a U-Tube (U-Box) Test (Khayat et al., 2004)

During the slump flow and U-tube tests, it was determined that many of the batches had segregation problems and that, "*segregation was an issue that must be watched closely*" (Ozyildirim, 2005). Although many SCC mixture designs did not have adequate flow properties, the researchers reported that some mixtures were "*viable candidates for SCC*" (Ozyildirim, 2005).

In addition to laboratory testing, VDOT had two precast plants batch two different SCC mixtures. These samples were tested in the same manner as the laboratory batches. With the precast plant mixtures, no segregation or bleeding was found and the air contents of the mixtures were within allowable limits. However, shrinkage values of the concrete were greater than the recommended maximum value of 400 microstrain at 28 days. Additionally, a poor air-void system was found within the hardened concrete. These tests results indicated that high shrinkage and poor freeze-thaw resistance can occur with SCC mixtures (Ozyilidirim, 2005).

2.4.3 Ozyildirim and Davis, 2007

This research presented an evaluation of the use of SCC in full-scale bulb-tee beams used in a bridge on Route 33 in Virginia. Ozyildirim and Davis evaluated the

fabrication and placement of SCC concrete and monitored strain and camber over time using vibrating wire gauges (VWG).

Prior to placing SCC beams in an actual bridge, two full-scale specimens were cast and tested for transfer and development length as well as shear and flexural capacity. The test beams' cross section was similar to the cross section of the actual bulb-tee girders in the Route 33 bridge. The beams were 45-inches tall and 60-feet long. Prior to testing, these beams were topped with a conventional concrete slab. In the laboratory, the beams were loaded in four combinations of moment and shear in order to fail the beams in various different modes including flexure, shear, and flexure-shear. No specific information was given in regards to the location of loading, but the researchers reported that, "*a strand development failure was never realized*" and "*the strands were well bonded to the concrete near the beam end, and strand slip was minimal*" (Ozyildirim and Davis, 2007). Furthermore, the experimental testing indicated that "*the tensile capacity of the concrete in the beam web was 5.3 times the square root of the compressive strength"* (Ozyilidirim and Davis, 2007). The value reported for tensile capacity was significantly lower than values typically used in flexural design ($6\sqrt{f'_c}$. or $7.5\sqrt{f'_c}$). In regards to the transfer lengths, the measured values were less than predicted by theoretical calculations. Although this observation was reported, there was no explanation of what theoretical calculations were used and the test method to evaluate the transfer length. The researchers concluded that "*the test beams behaved at least as well as would be expected for normally consolidated concrete beams*" (Ozyildirim and Davis, 2007).

Based on the previous testing of the bulb-tee beams, full scale SCC bridge beams were fabricated and placed in the Pamunkey Bridge on Route 33 in Virginia. For research purposes, eight SCC beams were used to build one of the 49 spans of the bridge. A "control" span of conventional concrete beams was located immediately next the SCC span. Two of SCC beams and two of the conventional concrete beams contained vibrating wire gauges (VWG) to monitor the behavior during service conditions and

thermocouples to monitor the beam temperature while curing. The VWGs were installed near the strands in the top and bottom flanges of the beams during fabrication and the thermocouples were placed at mid-depth in the web. All beams and corresponding test samples were steam cured. Table 2-5 displays the hardened concrete properties of the four instrumented bridge beams evaluated in this study.

Table 2-5 Hardened Properties of Instrumented Bridge Beams (Ozyildirim and Davis, 2007)

Property	Age	B1 (SCC)	B2 (SCC)	B3 (control)	B4 (control)
Compressive Strength (psi)	2 days	7,470	6,650	6,270	5,790
	7 days	9,1790	8,860	7,760	6,960
	28 days	10,110	10,700	7,960	7,610
	1 year	11,230	10,940	9,750	8,730
Elastic Modulus (ksi)	2 days	5.07	4.54	4.99	4.52
	7 days	5.10	5.06	5.45	5.15
	14 days	5.00	5.19	5.69	5.16
	28 days	4.86	5.35	5.26	4.98
	1 year	5.44	5.16	5.80	5.33
Splitting Tensile Strength (psi)	7 days	760	695	715	650
	28 days	820	755	675	565
	1 year	840	895	805	810
Permeability (coulombs)	28 days	869	996	1,011	985
Shrinkage (microstrain)	112 days	295	255	328	320

As is shown in Table 2-5, the SCC batches obtained higher concrete strengths and lower shrinkage values than did the conventional concrete mixtures. However, the elastic modulus values for SCC were equal or lower than that of regular concrete. In addition, camber measurements were recorded for the instrumented beams. The camber in the SCC beams was "*slightly higher than that in the conventional concrete at an early age, but cambers and strains for all beams have been similar in service*" (Ozyildirim and Davis, 2007). The researchers reported that further monitoring of the long-term

shrinkage and creep of these beams was underway and the results would be reported when a sufficient number of seasonal cycles have passed.

After fabrication, monitoring, and testing of these bulb-tee beams, the researchers concluded that "*SCC members can be designed by using the same methods, assumptions, and limiting values as used for normally consolidated concrete*" (Ozyildirim, 2007). However, it was also reported that the mixture proportions of SCC must be carefully monitored because SCC was sensitive to water content. Additionally the researchers reported that, low slump flows (small diameter readings) from the slump flow test leads to concrete which may not self-consolidate. Conversely, high slump flows (large diameter readings) from the slump flow test may lead to segregation problems.

2.4.4 Gross, Yost, and Gaynor, 2007

Gross et al. investigated the time-dependent behavior of prestressed beams cast with self consolidating concrete. In the project, four T-beams were cast using conventional high-strength concrete (HSC) and four separate T-beams were cast with SCC. Each beam was 124-inches long and 5.5-inches deep. Each beam was prestressed with a single 0.208-inch diameter deformed high-strength steel wire located 0.854-inches above the bottom surface of the beam.

To monitor time-dependent behavior, strain gauges were attached to each specimen. One resistance bonded strain gauge (standard foil gauge) was attached to the prestressing strand at midspan prior to stressing. The remaining instrumentation consisted of concrete surface strain gauges applied at midspan at the locations specified in Figure 2-10. The dimensions and strain gauging locations for each of the beams is displayed in Figure 2-10.

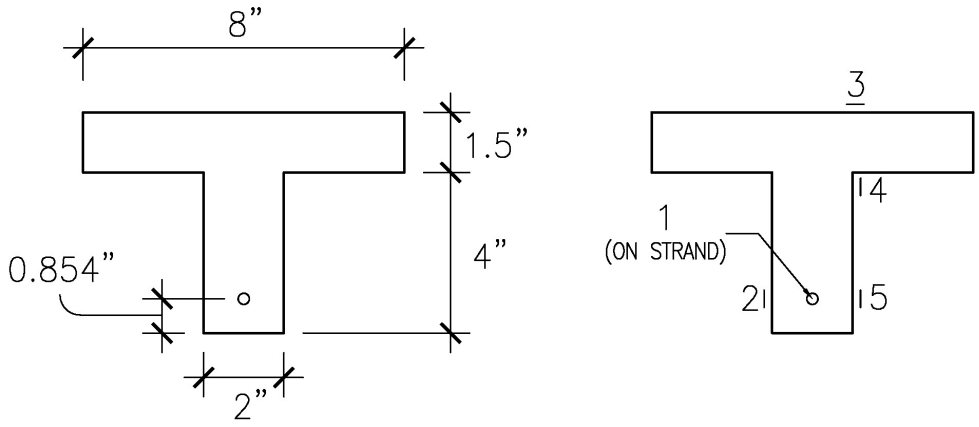

Figure 2-10 Beam Cross section and strain gauge locations (adopted from Gross et al., 2007)

The mixture proportions used in the conventional high-strength concrete (HSC) and self-consolidating concrete (SCC) are included in Table 2-6. Both the SCC and HSC mixtures were designed to reach a 2 day compressive strength of 6000-psi and a 28 day compressive strength of 8000-psi.

Table 2-6 Concrete Mixture Proportions per cubic yard (Gross et al., 2007)

Material	HSC	SCC
Coarse Aggregate	1798 lb	1207 lb
Fine Aggregate	1175 lb	1254 lb
Water	300 lb	370 lb
Type III Cement	726 lb	983 lb
Silica Fume	63 lb	74 lb
High Range Water Reducer	99 oz	180-191 oz
Viscosity Modifying Admixture	0 oz	21 oz
w/cm	0.38	0.35

The eight T-beams in this study were cast in pairs. From each pair, one beam was subjected to a sustained load of 530-pounds at 29 days (Beam B) while the other beam

remained unloaded (Beam A). Thus, four beams (B Beams) were subjected to sustained loads while the remaining four were not loaded (A Beams). Companion 4-x8-inch cylinders were cast with each of the beams in this study. The companion cylinders were used to determine the compressive strength and elastic modulus of the concrete in each specimen. The average 28-day compressive strength of the SCC and HSC mixtures was 8640-psi and 8200-psi respectively. The average measured 28-day modulus of elasticity for the SCC and HSC mixtures was 5140-ksi and 6600-ksi respectively. It is important to note that the 28-day elastic modulus of SCC mixture was significantly lower than that of the HSC mixture.

Using the applied strain gauges, camber and prestress loss were monitored for 300-days. Figure 2-11 displays a plot of measured prestress loss with time for beams cast with SCC and HSC.

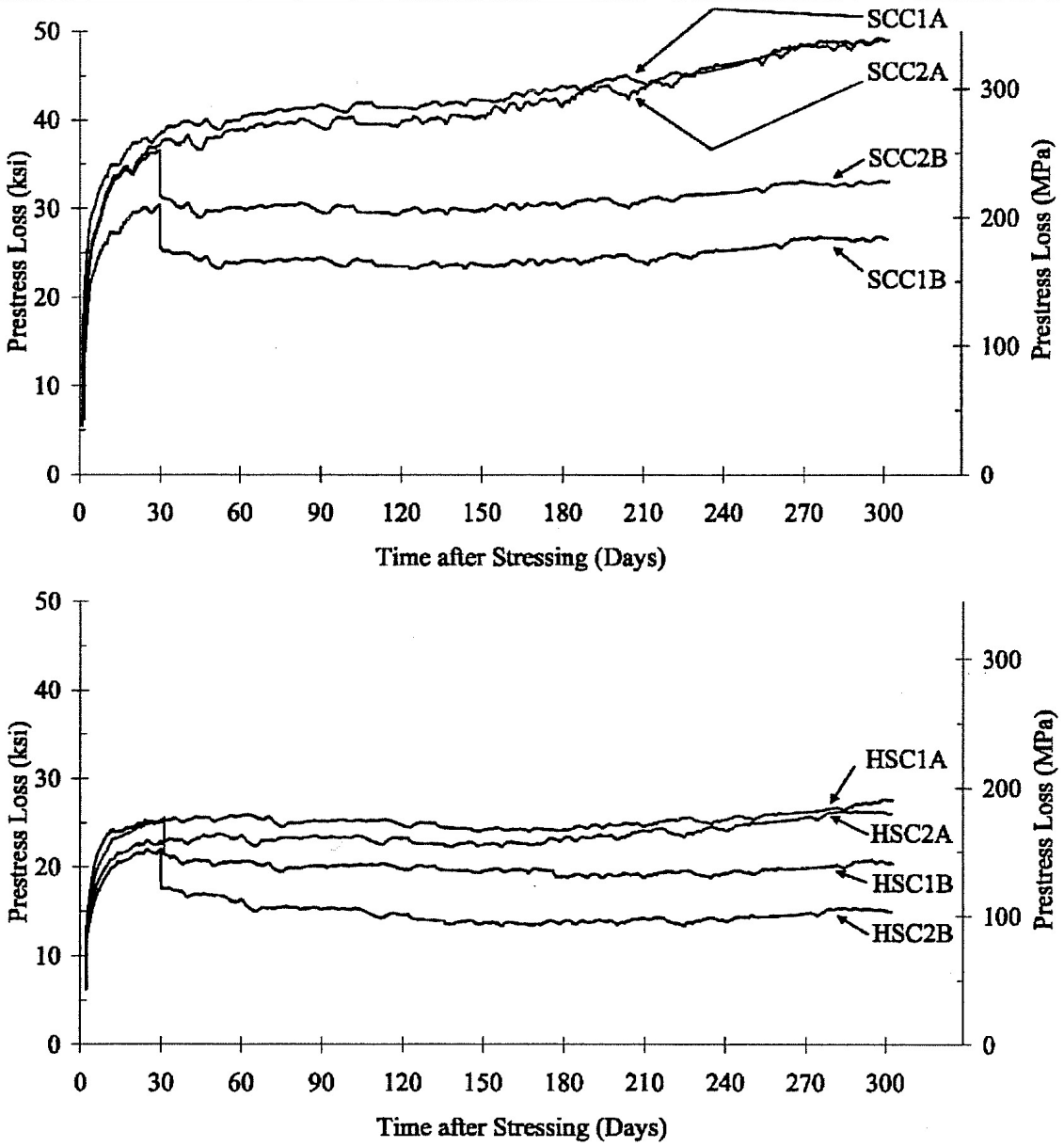

Figure 2-11 Measured prestress loss versus time for SCC beams and HSC beams, respectively (Gross et al., 2007)

As is shown in Figure 2-11, the SCC beams exhibited significantly more prestress losses than did the beams cast with HSC. As was expected, the beams with sustained service loads (B Beams) exhibited less prestress loss due to the elastic gain imposed by

the placement of the dead load. In addition to prestress loss, camber was also measured over the 300-day period. Results of the camber data showed that the beams with SCC exhibited higher cambers than their counterparts cast with HSC.

From these results Gross et al. concluded that, "*Measured prestress losses and net camber after 300 days were significantly higher in the SCC beams as compared to the HSC beams*" (Gross et al., 2007). They conjectured that the higher losses and cambers in SCC beams "*can have a marked impact on the serviceability behavior of self-consolidating concrete prestressed beams*" (Gross et al., 2007). It is important to note that the tests performed by Gross et al. were on a small-scale specimens and may not necessarily represent the response of a full-scale specimen.

2.4.5 Ruiz, Staton, Do, and Hale, 2007

Similar to the experimental research program of Gross et al. (2007), this study provided a comparison of prestress losses in beams cast with SCC to those cast with conventional concrete. In this research program, 20 prestressed beams were cast and prestress losses were measured on 10 beams. Of those 10 beams, 3 were cast with a conventional concrete mixture (HSC), 2 were cast with an SCC mixture containing Type III cement (SCCIII), and 4 were cast with an SCC mixture containing Type I cement (SCCI). All three mixtures were designed to have an initial release strength of 7000-psi and a 28 day strength of 12,000-psi. The actual average release strength (at 24-30 hours) for the HSC and SCC mixtures was 9260-psi and 7760-psi respectively. The actual average 28-day strength for the HSC and SCC mixtures was 12,100-psi and 11,530-psi respectively. The mixture designs for all three types of concretes are included in Table 2-7.

Table 2-7 Concrete Mixture Designs (Ruiz et al., 2007)

Material	SCCI	SCCIII	HSC
Cement (lb/yd^3)	950	808	900
Fly Ash (lb/yd^3)	0	142	0
Coarse Aggregate (lb/yd^3)	1350	1350	1800
Fine Aggregate (lb/yd^3)	1474	1400	1207
Water (lb/yd^3)	285	304	234
w/cm	0.30	0.32	0.26
HRWR1 (fl.oz/cwt)	7.8-14.5[a]	8.0-9.0[a]	9.0-10.5[a]
HRWR2 (fl. oz/cwt)	0-3.0[a]	0	0
VMA (fl. oz/cu. yd)	0-30.4[a]	0-30.4[a]	0

[a] Dosages of admixtures varied due to variations in ambient air temperatures during time of batching for individual mixtures
HRWR= High Range Water Reducer
VMA= Viscosity Modifying Admixture

The beams fabricated in this study were 6.5-inches wide, 12-inches deep and 18-feet long. All specimens were prestressed with two 0.6-inch diameter 270-ksi low-relaxation strands placed 2" away from the bottom of the section. In addition to the prestressing steel, two #6 Grade 60 deformed reinforcing bars were placed at the top of the section. Figure 2-12 depicts the cross sectional details of the specimens (Ruiz et al., 2007).

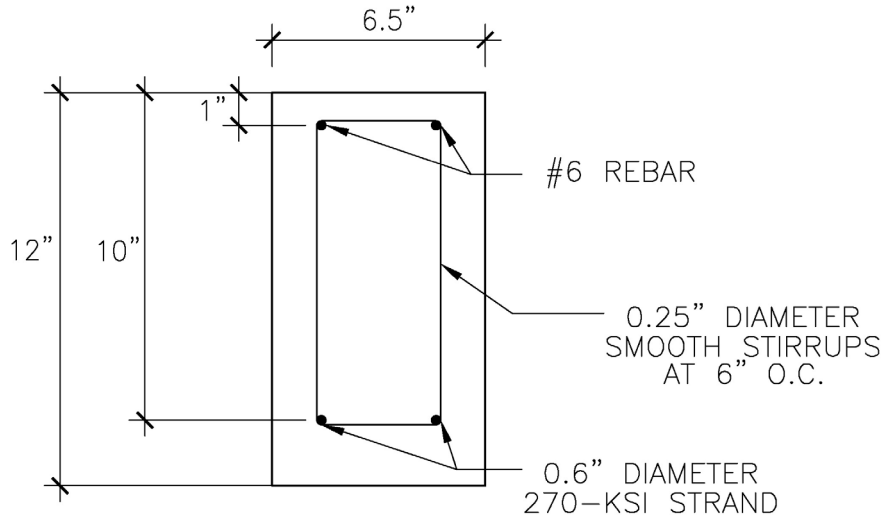

Figure 2-12 Beam Cross Section Details (adopted from Ruiz et al., 2007)

In order to monitor prestress losses with time, vibrating wire gauges were placed at prescribed locations along the beam. Gauge readings were taken prior to release, after release and at 3, 5, 7, 14, and 28 days after release. From that point forward readings were taken monthly and will continue to be taken monthly through 2008, 2009 and perhaps longer. The readings from the strain gauges allowed the researchers to document the prestress loss with time. Figure 2-13 displays a plot of the measured prestress losses in all ten beams fabricated in this study.

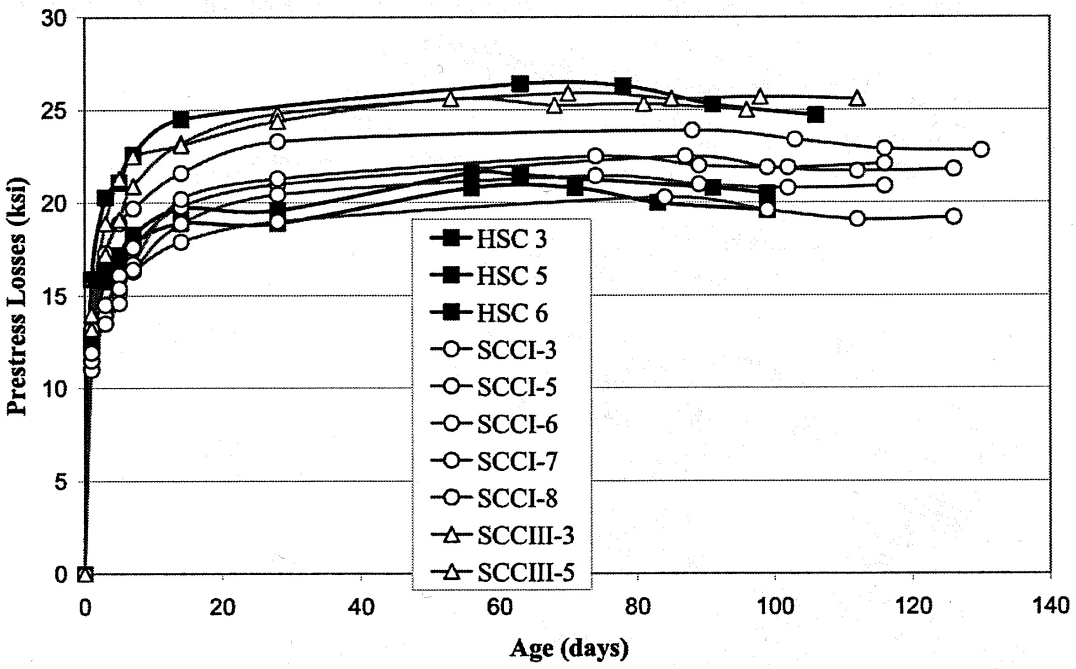

Figure 2-13 Measured prestress loss versus beam age (Ruiz et al., 2007)

As is seen in Figure 2-13, there is no clear separation between prestress losses in HSC mixtures and losses in SCC mixtures. Additionally, there is very little change in prestress loss after 28-days. From this data, the researchers concluded that "*the preliminary results showed little difference in prestress losses between conventional HSC and high strength SCC mixtures*" (Ruiz et al., 2007). In addition, the researchers measured similar amounts of elastic shortening losses between beams with HSC and beams with SCC.

In addition to analyzing data from strain gauges, Ruiz et al. (2007) compared their measured prestress losses to estimated prestress losses calculated using the detailed method of the National Cooperative Highway Research Program (NCHRP) Report 496. The NCHRP Report 496 detailed method is discussed in explicit detail in section 2.5.1 of this thesis. In comparing the measured prestress losses with the losses calculated by the NCHRP 496 method, the researchers found that prestress losses were overestimated by 20% for the beams cast with HSC and 35% for beams cast with SCC. The researchers

reported that "*the [NCHRP 496] equations are more sensitive to increases in release strengths than were the measured losses for the beams in this research program*" (Ruiz et al., 2007). Ruiz et al. mention that if the beams cast with SCC and beams cast with HSC had the same concrete strength at prestress release, the NCHRP 496 report would have calculated very similar amounts of prestress loss. Because the concrete release strength of the SCC mixtures was much lower than that of the HSC mixtures, the NCHRP 496 procedure estimated a greater percentage of prestress loss for the SCC beams.

The findings of Ruiz et al. (2007) seem to contradict the findings of Gross et al. (2007). It is important to note that the testing of Ruiz et al. (2007) is still underway (at the time this thesis was written) and will not be completed until a period of at least one year has elapsed. Furthermore, these two research studies focused on smaller beams that may not necessarily be representative of full-scale member behavior.

2.4.6 Burgueño and Bendert, 2007

During the course of this research project, prestressed box beams were fabricated with SCC and used in a demonstration bridge project in Jackson, Michigan. Prior to the fabrication of the box beams, full-scale flexure and shear tests were performed to ensure adequate performance.

In order to fabricate these prestressed box beams, three separate SCC mixtures were developed along with a standard normally consolidating concrete (NCC) mixture. The three SCC mixtures were proportioned to achieve minimum compressive strengths of 5000-psi at 1 day and 5,500-psi at 28 days. Upon beam fabrication and testing, both the 1 day and 28 day strength requirements were exceeded. Table 2-8 displays the concrete mixture proportions for all four mixture designs.

Table 2-8 Concrete Mixture Proportions (Burgueño and Bendert, 2007)

Material	SCC1	SCC2	SCC3	NCC
Type III Cement (lbs)	700	700	700	564
Sand (lbs)	1591	1513	1320	1354
Coarse Aggregate (oven dry) (lbs)	1350	1350	1450	1883
Water (lbs)	256	285	320	151
Air (target) (%)	6	6	6	6
w/c	0.37	0.41	0.46	0.38
Air Entraining (oz/cwt)	1	1	1	1.9
HRWR (oz/cwt)	15	12	10.7	11.3
VMA (oz/cwt)	1	2	6	0

The full-scale box beams used in this research were 52-feet long with a cross section that was 36-inches wide and 27-inches deep. All prestressing steel in the cross section was 0.6" diameter 270-ksi seven-wire low-relaxation strand. Figure 2-14 includes a drawing of the cross section of the box beams.

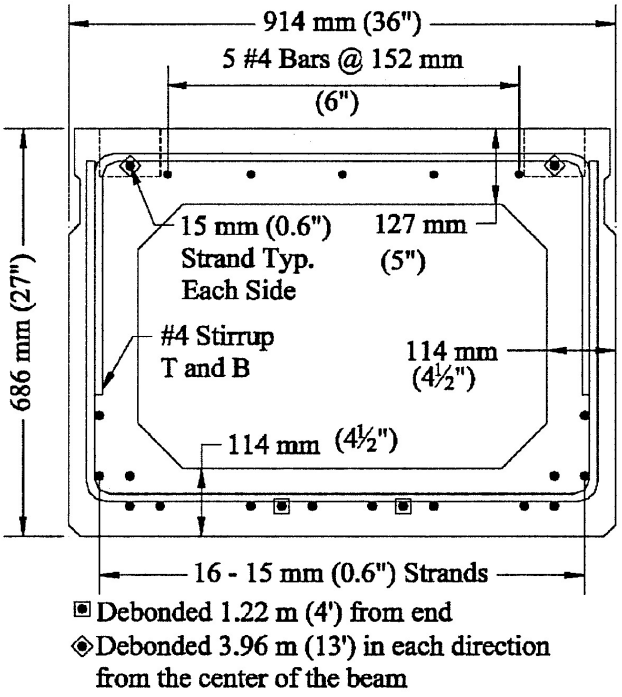

Figure 2-14 Box Beam Cross Section (Burgueño and Bendert, 2007)

In total, 17 beams were fabricated. 8 beams were fabricated with SCC for flexural and shear testing, 6 beams were fabricated with SCC to be used in the bridge, and three substitute beams were produced with NCC in case the performance of the SCC beams was unacceptable. Of the 8 beams fabricated for testing, four were tested in flexure (one beam from each mixture design) and four were tested in shear (also one beam from each mixture design). For the flexural tests, the beams were loaded in four point bending with a span of 50-feet. The two applied loads were spaced 8-feet apart at the center of the beam. For the shear testing, the beams were again loaded in four point bending with loads spaced at 8-feet, but the supports were moved inward to create much smaller shear spans. Schematic diagrams of the flexural and shear test setups are displayed in Figure 2-15.

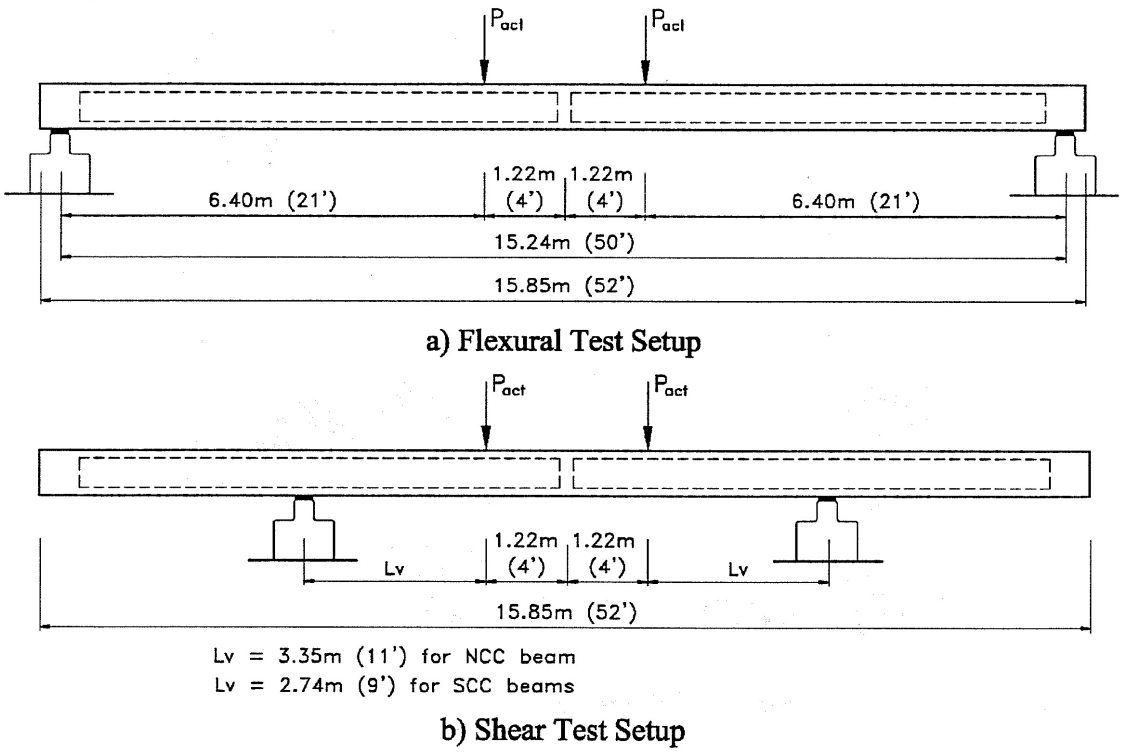

Figure 2-15 Full Scale Beam Test Setups (Burgueño and Bendert, 2007)

For the flexure tests, "*the overall response of all beams was essentially equal*" (Burgueño and Bendert, 2007). In addition, the experimentally determined flexural strengths exceeded design nominal capacities as determined by the simplified approach in the 17th edition of the AASTHO Standard Specifications. The ratio of the experimentally determined flexural strength to the nominal design capacity ranged from 1.1 for the NCC beam to 1.06 for the SCC3 beam. For the shear testing, the response was "*very similar and in all cases the critical sections reached a shear capacity greater than that of the design beam*" (Burgueño and Bendert, 2007). The ratio of the measured shear strength to nominal design strength according to the 17th edition of the AASHTO Standard Specifications ranged from 1.22 for the SCC1 beam to 1.08 for the SCC3 beam.

Due to the favorable results from the flexure and shear testing, the 6 beams cast with SCC were used in the M-50/US-127 bridge of the Grand River in Jackson, Michigan. The beams were oriented in the bridge as shown in Figure 2-16.

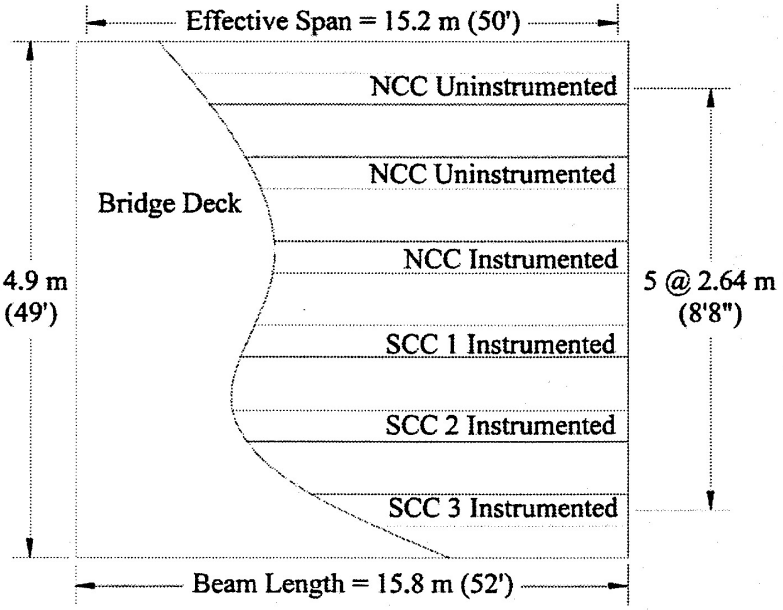

Figure 2-16 Plan view with beam layout of M-50/US-127 bridge (Burgueño and Bendert, 2007)

The four instrumented beams shown in Figure 2-16 were affixed with thermocouples to measure temperature through the cross section as well as vibrating wire gauges. These instruments were placed at midspan and a quarter-point section with a back-up set of instruments located 1-foot away from midspan. Five readings from the strain gauges during construction of the beams:

1. After concrete placement
2. After prestress release
3. After cutting of top strands (shown in Figure 2-14)
4. After the erection, and
5. After deck casting

After these five measurements were taken, the instruments were set up for in-service monitoring. In order to accomplish this objective, the instruments were hooked up to an on-site datalogger from which data could be downloaded on a monthly basis. The continuous monitoring of the gauges and thermocouples began December 21, 2005.

The recorded strain measurements in the bottom flange of the beams at midspan is displayed in Figure 2-17.

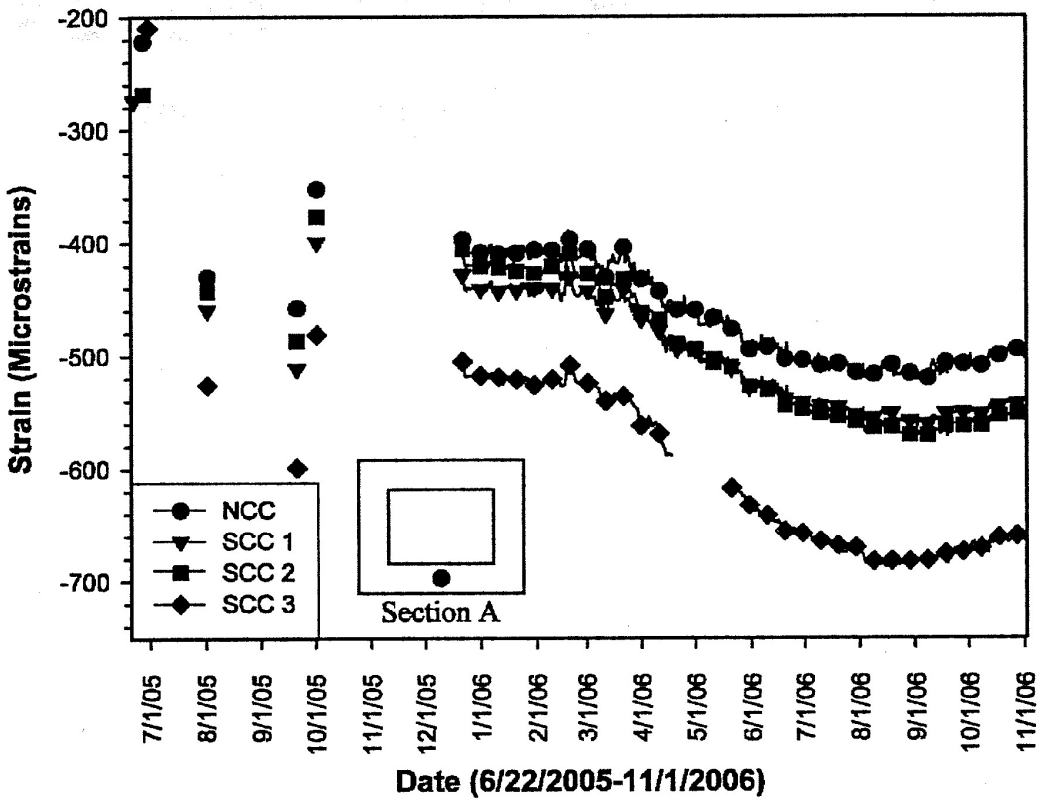

Figure 2-17 Strain monitoring at beam bottom flange at mid-span section (Burgueño and Bendert, 2007)

As is seen in Figure 2-17, the first five data points from each beam are difficult to interpret. However, after the continuous monitoring began in December of 2005, the change of strain with time has been consistent among all four beams. As reported by the authors, "*Investigation on the reasons behind the initial differences and further analyses on the collected data particularly due to temperature effects, is in progress*" (Burgueño and Bendert, 2007). At this point in the research Burgueño and Bendert reached the conclusion that:

> *even though [the] long-term behavior of the SCC prestressed box beams are still to be fully evaluated, their short-term flexural and shear response*

determined through the testing program indicates that the SCC beams safely satisfy their prescribed design requirements"(Burgueño and Bendert, 2007).

2.4.7 Naito, Parent, and Brunn, 2006

Naito et. al (2006) presented the results of their research on the strength gain, creep, shrinkage, stiffness, strand-to-concrete bond quality, and ultimate shear and flexural strength in SCC precast concrete bridge members. In order to accomplish this goal, the research was conducted in two phases. The first phase dealt with material characteristics and the second phase focused on full-scale girder performance.

In the first phase of the research, an SCC mixture and a conventional high early strength (HESC) mixture were designed. The mixtures were designed to reach 6800 psi within 24 hours of placement and a 28 day compressive strength of 8000 psi. Hardened properties of these concretes were monitored throughout the research program. The compressive strength of the two concretes fell within expected values and both were comparable to each other. Additionally, the splitting tension and modulus of rupture as determined by ASTM standard tests were found to be consistent between the two mixtures. The measured elastic modulus for SCC was found to be lower than that for the conventional concrete mixture and the values calculated using ACI 318 provisions. Creep and shrinkage tests were performed on match-cast 6 x 12-inch cylinders. The SCC mixture exhibited greater shrinkage and creep strains than the conventional mixture. After evaluating both mixtures over the course of the research program, it was concluded that, "*early strength-gain properties of the SCC were comparable to those of traditional HESC*" (Naito et al., 2006). Additionally, it was reported that the tensile strength was conservatively higher than the estimates obtained by using ACI 318 expressions and that the direct tension capacity and modulus of rupture between the two concretes were comparable.

In the second phase of the research, Naito et al. (2006) investigated the behavior of full-scale bulb-tee girders cast with SCC. The beams were PennDOT standard beams

and contained 26, ½-inch 270 ksi low-relaxation strands. A visual representation of the girder cross-section is included in Figure 2-18.

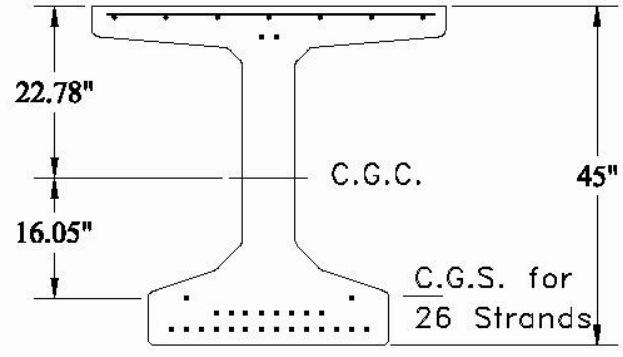

Figure 2-18 Bulb-tee beam cross section (Naito et al., 2006)

In total, four 35-foot long specimens were cast. Two were cast from SCC and the other two were cast from high early strength concrete. After fabrication, the beams were topped with a conventional 8.5-inch thick deck slab. Then, the girders were examined for modulus of elasticity, creep, shrinkage, and transfer length. The modulus of elasticity was measured in three ways: camber, elastic shortening, and elastic response to applied loads. Elastic shortening was measured at prestress transfer with embedded vibrating wire strain gauges at midspan and conventional foil strain gauges affixed to the prestressing strands prior to casting. In addition, surface strains were measured during applied loading and used to calculate the modulus of elasticity. Based on the modulus of elasticity calculation techniques just described, the researchers reported that SCC girders displayed a greater stiffness than the girders fabricated with conventional concrete. This result contradicts the cylinder testing completed by Naito et al. in the first phase of this research project. The authors attributed this contradiction to the fact that the cylinders were moist cured per ASTM standards while the beams were not kept moist after the first 24-hours. In addition to modulus calculations, creep and shrinkage was monitored using the vibrating wire strain gauges embedded in the beam. Naito et al. (2006) reported that the SCC girders experienced less creep and shrinkage than the conventionally cast beams. Furthermore, reduction in prestress force over time due to prestress loss was monitored.

The SCC girders exhibited less prestress loss than the conventional high strength beams for the first 75-days. Finally, the transfer length of the beams was calculated using strain gauge measurements before and after release. Both SCC and conventional concrete beams exhibited similar transfer lengths of 15.7-inches and 15.8-inches respectively. Both of these values were below the transfer length estimate obtained through the use of PCI provisions.

To monitor the structural performance at ultimate, the girders were set up to fail in three different ways: compressive-flexural failure, shear-flexural failure, and tensile-flexural failure. Loading points and support points were adjusted to achieve these different failure conditions. All loads were applied with a 5000 kip test machine at a quasi-static loading rate. In all the tests, no significant strand slip was measured, and all girders exceeded their estimated capacities. Ultimately, the researchers concluded that, "*the studied SCC provides mechanical characteristics that outperform current industry recommendations*" (Naito et al., 2006). In addition, the researchers reported that SCC was a viable material for use in prestressed concrete applications. It is important to note that these conclusions were based on the mixture studied in their research and that the behavior of other SCC mixture designs may need separate investigations.

2.5 METHODS TO ANALYZE PRESTRESS LOSS

In the current research project (TxDOT Project 5197), forty five TxDOT Type-C Beams as well as ten TxDOT 4B28 box beams were tested in flexure to experimentally determine their cracking load. Information on the test specimens is presented in Chapter 3 and the details of the experimental test setup are provided in Chapter 4. In order to compare the observed cracking loads from all fifty-five tests, methods to analytically calculate cracking loads were needed. In order to accurately predict the flexural cracking load for a beam specimen without any bias, two methods were used:

1. The Detailed Prestress Loss Method (Tadros et al., 2003) included in National Cooperative Highway Research Program (NCHRP) Report 496

2. AASHTO-LRFD Refined Loss of Prestress Estimate – 2008 Interim Edition (AASHTO, 2008)

It is important to note that the PCI Design Handbook Loss of Prestress Estimate (PCI, 2004) equations were not used to calculate predicted cracking loads. The PCI equations developed by Zia et al. (1979) do not include time as a variable. Therefore, the PCI equations would provide prestress loss values representative of the total prestress loss that the specimen will experience in its design life. Since the flexural testing of all beam specimens took place within the first two months of casting, the PCI equations would not provide meaningful estimates of test specimen cracking loads.

Both the Detailed Prestress Loss Method (Tadros et al., 2003) and the AASHTO-LRFD Refined Loss of Prestress Estimate (AASHTO, 2008) include refined equations to account for instantaneous elastic shortening loss as well as time dependent losses due to creep and shrinkage of concrete and relaxation of prestressing strands. Figure 2-19 displays the typical loss and gain of prestress over time for a bridge girder. For the purposes of this research, only the elastic shortening loss during prestress transfer and the additional loss due to creep, shrinkage and relaxation before deck placement (at the time of flexure test) is of interest.

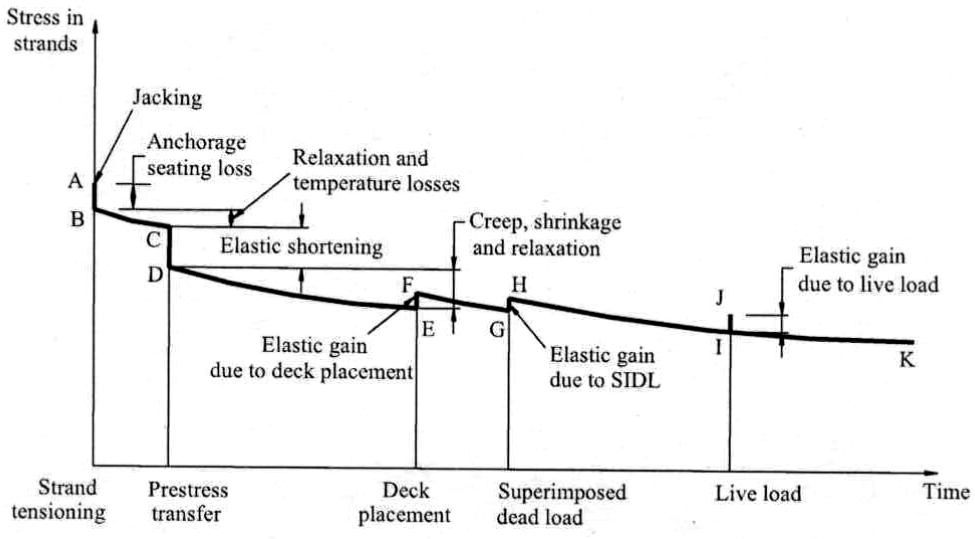

Figure 2-19 Stress in strands vs. time for a Prestressed Girder (Tadros et al., 2003)

Prior to the adoption of the NCHRP 496 procedure into the AASHTO-LRFD specification, some conservative, simplifying assumptions were made to aid the designer. This results in two similar, but somewhat different, procedures. The details of these two procedures to estimate of prestress loss are discussed further in Sections 2.5.1 and 2.5.2. These two procedures will be referred to as the NCHRP 496 method and the AASHTO-LRFD method respectively for the remainder of this document.

2.5.1 NCHRP Report 496 Detailed Prestress Loss Method

In 2003, National Cooperative Highway Research Program (NCHRP) published Report 496: Prestress Losses in Prestensioned High-Strength Concrete Bridge Girders. The report was meant to, "*develop design guidelines for estimating prestress losses in high-strength pretensioned concrete girder bridges*" (Tadros et al., 2003). Tadros et al. evaluated the material properties and prestress loss data from seven full-scale bridge girders from four different states. One of the seven girders was from the Harris County FM 1960 underpass in Texas. Based on this experimental data and other data assembled from a literature search, formulas were developed to accurately evaluate material properties and prestress loss for high-strength concrete bridge girders.

The authors concluded that local material properties significantly affect the losses due to shrinkage and creep, and modulus of elasticity (Tadros et al., 2003). It is for this reason that two correction factors (K factors) were included into the material properties equations for modulus of elasticity, shrinkage and creep (Table 2-9). The first factor, K_1, represents the difference between local average material properties and the national average. The second value, K_2, corrects the equations to provide an upper bound, lower bound, or average value. Table 2-9 displays the material properties equations developed from the NCHRP report.

Table 2-9 NCHRP Report 496 Material Properties Equations (Tadros et al., 2003)

Property	Equation	Variables
Modulus of Elasticity	$E_c = 33{,}000K_1K_2\left(0.140 + \frac{f'_c}{1000}\right)^{1.5}\sqrt{f'_c}$	E_c=Modulus of Elasticity (ksi) K_1=Correction factor corresponding to local material variability K_2=Correction factor corresponding to an upper or lower bound f'_c=Concrete strength at time of interest (ksi)
Shrinkage Strain	$\varepsilon_{sh} = 480 * 10^{-6}\gamma_{sh}K_1K_2$ $\gamma_{sh} = k_{td}k_sk_{hs}k_f$ $k_{td} = \frac{t}{61 - 4f'_{ci} + t}$ $k_s = \frac{1064 - 94\,{}^{V}/_{S}}{735}$ $k_{hs} = 2.00 - 0.0143H$ $k_f = \frac{5}{1 + f'_{ci}}$	ε_{sh}=Concrete shrinkage strain K_1 and K_2=same values as in Modulus Equation k_{td}=Time-development factor k_s=size factor k_{hs}=humidity factor for shrinkage k_f=concrete strength factor V/S=Volume to Surface Area Ratio (in) t=age of concrete after loading (days) H= relative humidity (%)
Creep Coefficient	$\psi(t,t_i) = 1.90\gamma_{cr}K_1K_2$ $\gamma_{cr} = k_{td}k_{la}k_sk_{hc}k_f$ $k_{hc} = 1.56 - 0.008H$ $k_{la} = t_i^{-0.118}$	$\psi(t,t_i)$=Concrete creep coefficient K_1 and K_2=same values as in Modulus Equation k_{td}, k_s, k_f=same as above k_{hc}=humidity factor for creep k_{la}=loading factor t= age of concrete after loading (days) t_i=age of concrete at loading (days)

Refined equations for prestress loss were developed based on the material properties equations from Table 2-9. Tadros et al. (2003) developed equations for the loss of prestress for the entire life of a bridge girder through prestress transfer, deck placement, and service conditions. Since the girders in this research were tested individually without a deck, only the prestress loss equations between prestress transfer and deck placement (time of flexure test) were needed.

The NCHRP 496 equations, given in Table 2-10, represent the state-of-the-art for accurately estimating time-dependent prestress losses. It is important to note that the NCHRP 496 method uses transformed section properties to estimate loss due to elastic

shortening. This loss is implicitly accounted for by using transformed section properties and the initial prestressing force just prior to transfer. Calculating elastic shortening loss in this manner is more cumbersome but does not require iteration or an estimate of the prestress force after transfer. The equations for prestress loss recommended by NCHRP Report 496 are listed in Table 2-10.

Table 2-10 NCHRP Report 496 Equations for Prestress Loss (Tadros et al., 2003)

Prestress Loss	Equations	Variables
Elastic Shortening	$\Delta f_{pES} = \frac{E_p}{E_{ci}} f_{cgp}$ $f_{cgp} = P_i\left(\frac{1}{A_{ti}} + \frac{e^2{}_{pti}}{I_{ti}}\right) - \frac{M_g e_{pti}}{I_{ti}}$	Δf_{pES}= Loss of prestress due to Elastic Shortening f_{cgp}= Concrete stress at steel centroid (ksi) E_p= Modulus of elasticity of prestressing strands (ksi) E_{ci}= Initial modulus of elasticity of concrete (ksi) P_i= Initial prestressing force just prior to transfer (kip) A_{ti}= Area of the transformed section at transfer (in^2) I_{ti}= Moment of Inertia of transformed section at transfer (in^4) e_{pti}= eccentricity of strands of transformed section at transfer (in) M_g= Self weight moment (in-kips)
Shrinkage	$\Delta f_{pSR} = \epsilon_{bit} E_p K_{it}$ $K_{it} = \frac{1}{1 + n_i \rho_n \alpha_n \left(1 + \chi \psi(t_f, t_i)\right)}$ $n_i = \frac{E_p}{E_{ci}}$ $\rho_n = \frac{A_{ps}}{A_n}$ $\alpha_n = \left(1 + \frac{A_n e^2{}_{pn}}{I_n}\right)$ $\chi \approx 0.7$	Δf_{pSR}= Loss of prestress due to shrinkage K_{it}= transformed section age-adjusted effective modulus of elasticity factor ϵ_{bit}= Shrinkage strain from initial loading to time of flexural test n_i= Modular ratio between prestressing steel and concrete ρ_n= tensile reinforcement ratio for initial net section α_n= factor for initial net section properties χ= aging coefficient that accounts for concrete stress variability with time $\psi(t_f, t_i)$= Ultimate creep coefficient A_n= Area of the net section (in^2) I_n= Moment of inertia of the net section (in^4) e_{pn}= eccentricity of strands of net section (in)
Creep	$\Delta f_{pCR} = n_i f_{cgp} \psi(t_t, t_i) K_{it}$	Δf_{pCR}=Loss of prestress due to creep n_i, f_{cgp}, K_{it}=same values as above $\psi(t_t, t_i)$=Creep Coefficient from loading to test (days)
Relaxation	$\Delta f_{pR} = \phi_i L_i K_{it}$ $\phi_i = 1 - \frac{3\left(\Delta f_{pSR} + \Delta f_{pCR}\right)}{f_{po}}$ $L_i = \frac{f_{po}}{45}\left(\frac{f_{po}}{f_{py}} - 0.55\right) log\left(\frac{24t_t + 1}{24t_i + 1}\right)$	Δf_{pR}= Loss of prestress due to relaxation ϕ_i= reduction factor reflecting the decrease in strand prestressing from creep and shrinkage L_i= Intrinsic Relaxation Loss f_{po}= stress in strands just after transfer (ksi) f_{py}= specified yield strength of strands (ksi) t_t= age of concrete at time of test (days) t_i= age of concrete at prestress transfer (days)

2.5.2 AASHTO-LRFD Refined Loss of Prestress Estimate – Interim Edition 2008

The American Association of State Highway and Transportation Officials (AASHTO) publishes the AASHTO-LRFD Bridge Design Specification. This specification is the national standard for bridge design in the United States. The material properties equations in the AASHTO-LRFD (2008) specifications are very similar to those included in NCHRP 496 with a few exceptions. First, the K factors were removed from the shrinkage strain and creep coefficient equations. For the modulus of elasticity calculation, only the K_1 factor was adopted. While the absence of K-factors allows for slightly simpler equations, the method becomes less responsive to local materials. The material properties in section 5.4.2 of the 2008 AASHTO-LRFD Bridge Design Specification are presented in Table 2-11.

Table 2-11 AASHTO-LRFD Equations for Material Properties (AASHTO, 2008)

Property	Equation	Variables
Modulus of Elasticity	$E_c = 33{,}000 K_1 {w_c}^{1.5} \sqrt{{f'}_c}$	E_c=Modulus of Elasticity (ksi) K_1=Correction factor for source of aggregate w_c=unit weight of concrete (kcf) ${f'}_c$=Concrete strength at time of interest (ksi)
Shrinkage Strain	$\varepsilon_{sh} = k_s k_{hs} k_f k_{td} 0.48 * 10^{-3}$ $k_s = 1.45 - 0.13(V/S) \geq 1.0$ $k_{hs} = 2.00 - 0.014H$ $k_f = \frac{5}{1 + {f'}_{ci}}$ $k_{td} = \frac{t}{61 - 4{f'}_{ci} + t}$	ε_{sh}=Concrete shrinkage strain k_{td}=Time-development factor k_s=factor for the effect of V/S ratio k_{hs}=humidity factor for shrinkage k_f=factor for concrete strength V/S=Volume to Surface Area Ratio (in) t=age of concrete after the end of curing (days) H= relative humidity (%)
Creep Coefficient	$\psi(t, t_i) = 1.9 k_s k_{hc} k_f k_{td} {t_i}^{-0.118}$ $k_{hc} = 1.56 - 0.008H$	$\psi(t, t_i)$=Concrete creep coefficient k_{td}, k_s, k_f=same as above k_{hc}=humidity factor for creep t= age of concrete after loading (days) t_i=age of concrete at loading (days)

In addition to providing equations for material properties, the AASHTO-LRFD (2008) specification includes a refined, time-dependent method to calculate prestress losses. As is listed in the commentary in the AASHTO-LRFD (2008) specification, these equations were based on research by Tadros et al., 2003 (*NCHRP Report 496*). Therefore, the equations for elastic shortening, creep, shrinkage, and relaxation are similar to those of the NCHRP 496 method. One important difference lies in the calculation of prestress loss due to elastic shortening. To estimate elastic shortening loss, the AASHTO-LRFD (2008) procedure recommends the use of gross section properties with an estimated force of 90-percent of the prestress force before transfer. Using gross section properties is easier for the design engineer but creates a source of inconsistency between the NCHRP 496 method and the AASHTO-LRFD (2008) method. Additionally, in the AASHTO-LRFD (2008) procedure, the K_{it} factor used in the creep and shrinkage loss equations is based on gross section properties. The NCHRP 496 method, however, uses net section properties to calculate K_{it}. That difference causes a small inconsistency in otherwise identical procedures to calculate losses due to creep and shrinkage. Finally, the AASHTO-LRFD (2008) equation for relaxation loss is a simplified version of the equation presented in the NCHRP 496 method. The AAHSTO-LRFD (2008) specifications in calculating the loss due to steel relaxation provide a simple equation that is easy for designers to use. All the equations for prestress loss in Section 5.9.5 of the AASHTO-LRFD (2008) specification are summarized in Table 2-12

Table 2-12 AASHTO-LRFD Equations for Prestress Loss (AASHTO 2008)

Prestress Loss	Equations	Variables
Elastic Shortening	$\Delta f_{pES} = \frac{E_p}{E_{ct}} f_{cgp}$ $f_{cgp} = 0.9P_i\left(\frac{1}{A_g} + \frac{e^2{}_{pg}}{I_g}\right) - \frac{M_g e_{pg}}{I_g}$	Δf_{pES}= Loss of prestress due to Elastic Shortening f_{cgp}= Concrete stress at steel centroid (ksi) E_p= Modulus of elasticity of prestressing strands (ksi) E_{ct}= Modulus of elasticity of concrete at transfer (ksi) P_i= Initial prestressing force just before transfer (kip) A_g= Area of the gross section (in^2) I_g= Moment of Inertia of gross section (in^4) e_{pg}= eccentricity of strands of gross section (in) M_g= Self weight moment (in-kips)
Shrinkage	$\Delta f_{pSR} = \epsilon_{bit} E_p K_{it}$ $K_{it} = \frac{1}{1 + \frac{E_p}{E_{ci}}\frac{A_{ps}}{A_g}\left(1 + \frac{A_g e^2{}_{pg}}{I_g}\right)\left[1 + 0.7\psi(t_f, t_i)\right]}$	Δf_{pSR}= Loss of prestress due to shrinkage K_{it}= transformed section coefficient ϵ_{bit}= Shrinkage strain from end of curing to time of flexural test E_{ci}=Modulus of elasticity of concrete at transfer (ksi) $\psi(t_f, t_i)$= Ultimate creep coefficient A_g= Area of the gross section (in^2) I_g= Moment of inertia of the gross section (in^4) e_{pg}= eccentricity of strands of gross section (in)
Creep	$\Delta f_{pCR} = \frac{E_p}{E_{ci}} f_{cgp}\psi(t_t, t_i) K_{it}$	Δf_{pCR}=Loss of prestress due to creep n_i, f_{cgp}, K_{it}=same values as above $\psi(t_t, t_i)$=Creep Coefficient from loading to test (days)
Relaxation	$\Delta f_{pR} = \frac{f_{pt}}{K_L}\left(\frac{f_{pt}}{f_{py}} - 0.55\right)$ K_L=30 for low relaxation strands	Δf_{pR}= Loss of prestress due to relaxation f_{pt}= stress in strands just after transfer (ksi) f_{py}= specified yield strength of strands (ksi)

2.6 SUMMARY

Four main topics were covered in this literature review. First a discussion of the history and recent research of the allowable compressive stress at prestress release was presented. This serves as a background for understanding the origin of allowable compressive stresses and documents the research (Table 2-2) pertaining to the increase of the current code limits.

Next, a discussion of the mechanical properties of high strength concrete was analyzed. A thorough discussion on concrete material properties was presented. Additionally, the behavior of high strength concrete subjected to temporary and sustained uniaxial load and methods of quantifying internal damage was documented. An understanding of the response of high strength concrete to axial load provides insight into the behavior of the pre-compressed tensile zone in prestressed concrete girders.

Third, the properties and behavior of self-consolidating concrete (SCC) were presented. Research relating to the hardened properties of SCC as well as the effects of SCC in full-scale bridge beams was presented. Self consolidating concrete has been used in prestressed applications and a thorough understanding of the material is necessary to evaluate the behavior of girders cast with SCC in this research project.

Finally, two methods used to estimate prestress loss in prestressed girders was presented. Both the NCHRP Report 496 detailed prestress loss method and the AASHTO-LRFD (2008) refined loss of prestress method were discussed. These two procedures provide refined, time-dependent estimates of prestress loss and will be used to provide an unbiased and consistent means of estimating the cracking moment.

CHAPTER 3
Test Specimens

3.1 OVERVIEW

For the experimental program in this phase of TxDOT Project 5197, forty five full-scale TxDOT Type-C beams (40-inch deep I-beams) as well as ten full-scale TxDOT 4B28 box beams (28-inch deep by 48-inch wide box beams) were tested in flexure. All specimens were designed to experience a maximum compressive stress at release of $0.60f'_{ci}$ to $0.70f'_{ci}$. The design and production of the forty five Type C beams and ten 4B28 box beams are discussed in sections 3.2 and 3.3 respectively.

3.2 DESIGN AND FABRICATION OF TXDOT TYPE-C BEAMS

In this research study (Phase II of TxDOT Project 5197), forty five TxDOT Type-C beams as well as 10 4B28 box beams were tested in flexure. This section presents a discussion on the design and fabrication of the forty five Type-C beams. Type-C girders are commonly used in Texas bridges and investigating their behavior provided a meaningful basis for understanding of the impact of early prestress transfer. In an effort to gain comprehensive data of prestressed girders produced throughout the state, three different fabricators produced twelve beams and one fabricator produced nine beams, totaling forty five Type-C beams. For the remainder of this report, the four fabricators will remain anonymous and will be simply listed as fabricator A, B, C and D.

In addition to targeting a range of different beam fabrication practices, two main variables were studied in four beam fabrication plants. First, the coarse aggregate used in the mix design for fabricators A and C was limestone whereas fabricators B and D used hard river gravel. This distinction was made in an effort to determine if the coarse aggregate in the concrete would have a significant effect on the live load performance of the girders. The compressive strength of high strength concrete is heavily dependent upon

the strength of the coarse aggregate. Additionally, concrete mixtures using river gravel are typically stiffer than those using limestone (Birrcher and Bayrak, 2007). Varying the coarse aggregate among the beams allowed for the investigation of the role of coarse aggregates in prestress transfer and live load performance. The nominal release strength of the beams was the other primary variable. Beams from fabricator A and B were designed for a nominal release strength of 4000 psi while the beams from fabricator C and D were designed for a nominal release strength of 6000 psi. The beams designed for a nominal release strength of 4000 psi were designated as "Series 1" beams. Likewise, the beams designed for a nominal release strength of 6000 psi were designated as "Series 2" beams. The design release strength was varied in order to reflect TxDOT standard designs while giving a realistic representation of the range of release strengths used in prestressed beam production in Texas. The strand pattern of Series 1 beams and Series 2 beams are discussed in sections 3.2.1 and 3.2.2 respectively. Table 3-1 summarizes the key features of the 45 beams fabricated in four different precast plants.

Table 3-1 Type-C Beam Fabrication Details

Fabricator	Nominal Release Strength	Coarse Aggregate	Beams Produced
A	4000 psi *(Series 1)*	Limestone	12
B	4000 psi *(Series 1)*	Hard River Gravel	9
C	6000 psi *(Series 2)*	Limestone	12
D	6000 psi *(Series 2)*	Hard River Gravel	12

Aside from the strand pattern design, all of the Type-C beams were designed according to AASHTO LRFD Interim Bridge Design Specifications (2008) as shown in the TxDOT standard Type-C drawings. It is important to note here that in addition to the flexural testing described in Chapter 4, the shear strength of 18 Type-C girders was evaluated. The detailed information on the shear testing is reported by Heckmann and Bayrak (2008). After initial shear testing on a couple of test specimens from fabricator A, a modification was made to the shear reinforcement design of these Type-C beams. It

was deemed necessary to reduce the shear reinforcement in order to ensure a shear failure would occur before flexural crushing of the beam. In order to weaken the shear capacity, minimum shear reinforcement was used outside of the bursting regions at the end of the beam. It is important to note that this reduction in shear reinforcement has no impact on the flexural strength or cracking moment of the Type-C beams. It is only presented here for the sake of completeness. This change is discussed in further detail in sections 3.2.3.2, 3.2.3.3, and 3.2.3.4 as well as Heckmann and Bayrak, 2008.

Each full-scale Type-C specimen in this study was 56.5 feet long. Designing and testing these full-scale girders provided results that are not influenced by any potential scaling effects. The cross-sectional dimensions and geometric properties of standard Type-C beams are included in Table 3-2.

Table 3-2 Section Properties of a TxDOT Type-C Beam

Beam Type	y_t (in)	y_b (in)	A (in^2)	I (in^4)	w (lb/ft)
C	22.91	17.09	494.9	82,602	516

In order to effectively evaluate the possibility of increasing the current code limit on compressive stress at release, all Type-C specimens produced were designed such that the maximum compressive stress at prestress transfer was within the range of $0.60f'_{ci}$ to $0.70f'_{ci}$.

3.2.1 Design of Series 1 Beams

The TxDOT standard Type C beam design was modified for this research study. A custom, non-standard strand pattern was used to target a maximum compressive stress at release of $0.60f'_{ci}$ to $0.70f'_{ci}$ at a nominal concrete strength of 4000 psi. The strand pattern used for Series 1 beams is displayed in Figure 3-1.

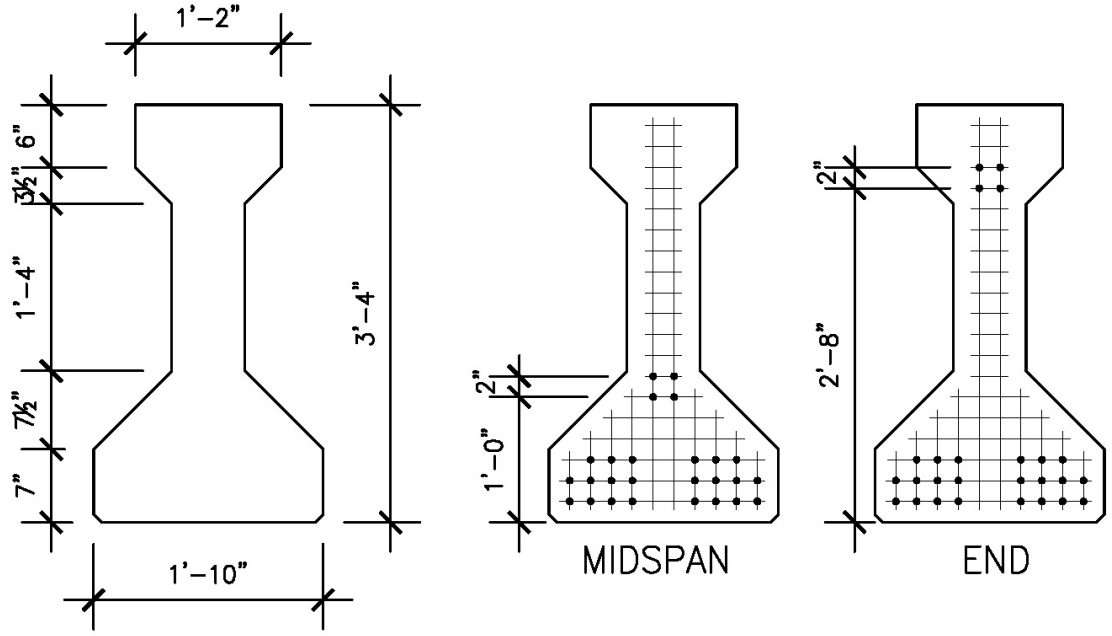

Figure 3-1 Strand Pattern: Series 1 Specimens

The strand pattern used in Series 1 beams consisted of twenty-six, ½" diameter, 270-ksi low relaxation strands, four of which were harped. The harped strands pass through two "hold down" points located five feet from the centerline of the beam. A representation of the beam and the harping points is shown in Figure 3-2.

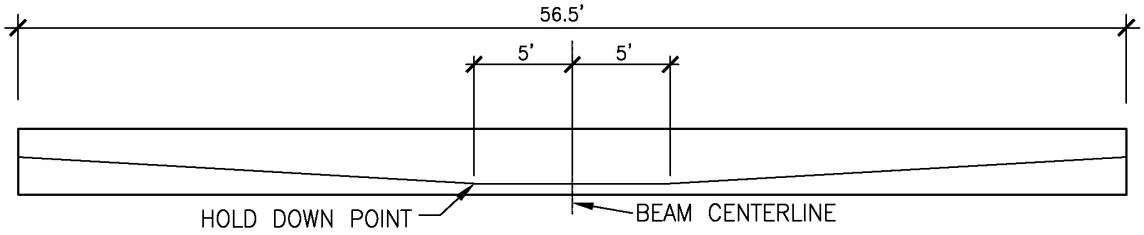

Figure 3-2 Type-C Beam Harped Strands

Fabricators A, B, and C achieved this harping pattern by pulling down on the strands as seen in Figure 3-3. Fabricator D harped the strands by pushing down on them with hollow cylindrical rods as shown in Figure 3-4.

Figure 3-3 Typical Harping for Fabricator C

Figure 3-4 Typical Harping for Fabricator D (photographs courtesy of David Birrcher)

The arrangement of harped strands shown in Figure 3-2 was carefully selected to produce maximum compressive stresses at the bottom surface of the beam at each of the harping points and at the transfer lengths (60 strand diameters from each end of the beam). Using NCHRP K_1 and K_2 factors of 1.0 in material properties equations (Table 2-9 in Chapter 2) for beam design, the strand pattern shown in Figure 3-1 was selected to produce a maximum compressive stress of $0.69f'_{ci}$ when prestress transfer occurred at a concrete compressive strength of 4000 psi. Likewise, the maximum compressive stress was $0.65f'_{ci}$ when prestress transfer occurred at a concrete strength of 4300 psi. Finally, the maximum compressive stress was $0.60f'_{ci}$ when prestress transfer occurred at a concrete compressive strength of 4700 psi.

In addition to the transfer length and harping points, compressive stresses at release were calculated at "critical sections". These critical sections were located 2.5-feet away from the centerline of the beam and represented the end of a 5-foot constant moment region applied to the Type-C beam during flexural testing. This 5-foot constant moment region was also used in the flexural tests by Birrcher and Bayrak (2007) and provided a consistent basis for experimental testing. A complete discussion on the experimental test setup is presented in Chapter 4. The aforementioned critical sections were the locations inside the constant moment region (during the flexure test) that experienced the highest compressive stress at prestress transfer. Table 3-3 displays the calculated stresses at the hold down location, transfer length, and the critical section for Series 1 Beams. Figure 3-5 displays a schematic drawing of the transfer lengths, critical sections, and hold-down points on the Type-C beams.

Table 3-3 Calculated maximum compressive stresses at prestress transfer: Series 1 Beams

	Compressive Stress at Release (% f'_{ci})		
f'_{ci} (psi)	**Critical Section**	**Hold Down Point**	**Transfer Length**
4000	69.0	69.3	69.2
4300	64.5	64.8	64.6
4700	59.4	59.6	59.4

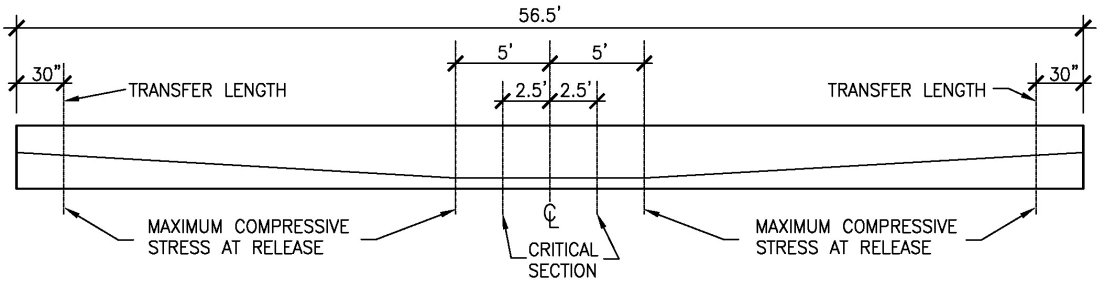

Figure 3-5 Schematic Drawing of Type-C Beam

As seen in Table 3-3, the Series 1 strand pattern adequately produced a range of compressive stress between $0.60f'_{ci}$ and $0.70f'_{ci}$ at a nominal release strength of 4000 psi. Additionally, the tensile stresses did not exceed the tensile stress limit at release ($7.5\sqrt{f'_{ci}}$,with f'_{ci} in psi) anywhere along the beam at any of the targeted release strengths. Therefore, no cracking was observed on the top flange of the beams due to prestress force transfer. A sample shop drawing and release stress calculation of a Series 1 Type-C Beam is included in Appendix A.

3.2.2 Design of Series 2 Beams

In order to obtain a maximum compressive stress at release of $0.60f'_{ci}$ to $0.70f'_{ci}$ at a nominal concrete strength of 6000 psi, the standard Type-C beam strand pattern was altered once again. The strand pattern used for Series 2 beams is displayed in Figure 3-6.

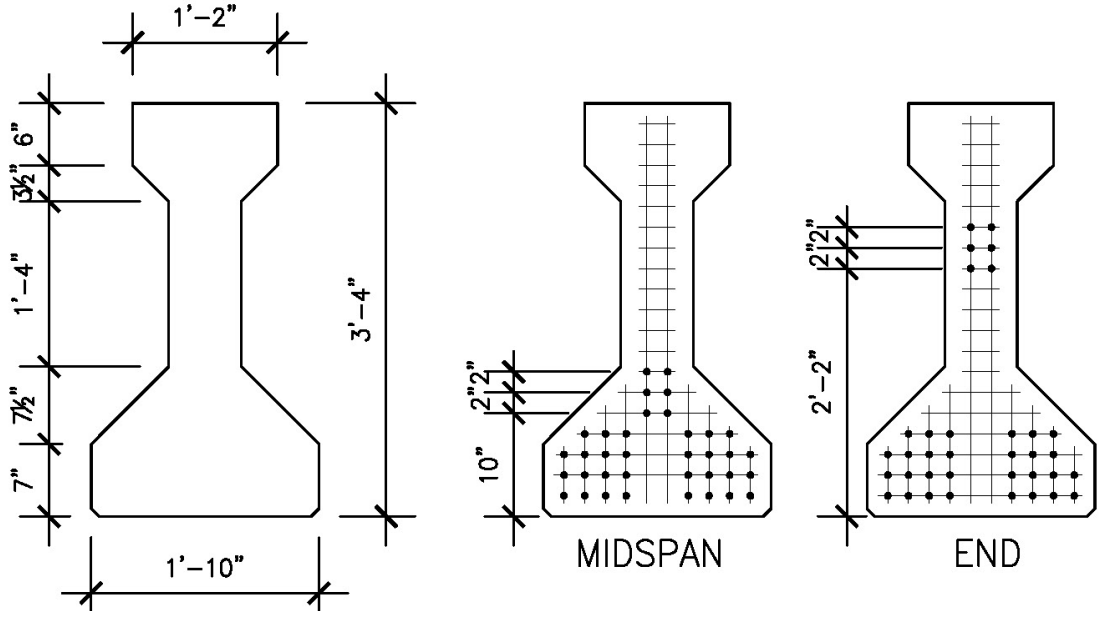

Figure 3-6 Strand Pattern: Series 2 Beams

The Series 2 beams consisted of thirty-six, ½" diameter, 270-ksi low relaxation strands, six of which were harped. The harping, or "hold down" points for the Series 2 beams were identical to those in the Series 1 beams and are shown in Figure 3-2. As with the Series 1 beams, the maximum compressive stress at release occurred at the hold down locations and transfer lengths. Using NCHRP K_1 and K_2 factors of 1.0 in material properties equations for beam design, the strand pattern shown in Figure 3-6 produced a maximum compressive stress at release of $0.70f'_{ci}$ when prestress transfer occurred at a concrete strength of 5400 psi. Likewise, the maximum compressive stress was $0.65f'_{ci}$ when prestress transfer occurred at a concrete strength of 5850 psi. Finally, the maximum compressive stress was $0.60f'_{ci}$ when prestress transfer occurred at a concrete strength of 6400 psi. Table 3-4 displays the calculated stresses at the hold down location, transfer length, and the critical section for Series 2 Beams. All three locations were the same for both Series 1 and Series 2 beams (See Figure 3-5).

Table 3-4 Calculated maximum compressive stresses at prestress transfer: Series 2 Beams

	Compressive Stress at Release (% f'_{ci})		
f'_{ci} (psi)	Critical Section	Hold Down Point	Transfer Length
5400	70.2	70.4	70.0
5850	65.1	65.3	65.0
6400	59.9	60.1	59.7

As with the Series 1 beams, the strand pattern used in Series 2 beams provided a range of compressive stress between $0.60f'_{ci}$ and $0.70f'_{ci}$ at a nominal release strength of 6000 psi. Once again, this strand pattern did not result in tensile stresses in excess of $7.5\sqrt{f'_{ci}}$ (as per TxDOT specifications) anywhere along the beam at any of the target release strengths listed above. Thus, no cracking was observed in the top flanges of the beams upon prestress transfer for Series 2 beams. A sample shop drawing and release stress calculation of a Series 2 Type-C Beam is included in Appendix A.

3.2.3 Fabrication of Type-C Girders

In order to generate a wide range of data representative of prestressed beam fabrication in Texas, four different fabricators produced Type-C beams for this study. Although all fabricators used somewhat different methods and concrete mixtures for beam production, the general process for producing Type-C beams was as follows:

1. Prestressing strands were placed along a beam fabrication line and anchored to a thick steel plate at one end (termed the "Dead End").
2. Strands were tensioned with hydraulic rams to the appropriate jacking force (within a ±2% tolerance) and anchored to a second steel plate at the opposite end of the beam line (termed the "Live End" see Figure 3-7).
3. All mild reinforcing steel was tied in place, and inspected.
4. Steel forms were placed and secured.

5. Concrete was placed using motorized hopper trucks (sidewinders).
6. Beams were covered with wet burlap or waterproof tarps.
7. At an appropriate concrete strength, prestressing strands were released.

The following sections detail the fabrication of all forty five Type-C girders used in this research study. It is important to note that even though the general process for fabricating a Type-C beam was the same, no two fabricators produced Type-C beams with identical methods. It is for this purpose that the details of beam production for each fabricator are documented in the following sections. Also, a copy of the beam fabrication specifications used by each fabricator is included along with the sample shop drawings in Appendix A.

3.2.3.1 Production of Girders: Fabricator A

Fabricator A produced Series 1 girders using limestone as the coarse aggregate. The concrete mixture design used to fabricate these beams complied with class H concrete mixture design (TxDOT specifications) and was representative of the standard mixtures used in prestensioned beam production. The components of the mixture design used by fabricator A are listed in Table 3-5. Because the moisture conditions of the fine and coarse aggregate could vary, the exact mixture proportions for each casting were documented on batch tickets. The batch tickets for fabricator A are included in Appendix B.

Table 3-5 Concrete Mixture Design used by Fabricator A (per cubic yard)

Components	Mixture Design	Source
Water / Cement Ratio	0.37	--
Water	207 lbs	San Marcos Water Co.
Cement	564 lbs	Alamo Type III
Fine Aggregate	1486 lbs	TXI- Green Pit
Coarse Aggregate	1796 lbs	Hanson-Ogden (Limestone)
High-range water-reducing admixture	8 oz/100 lbs	Sika Viscocrete 2100
Retarding admixture	2.4 oz/100 lbs	Sika Plastiment
Theoretical Unit weight	150.11 lbs/ft^3	--

All beams produced by fabricator A met AASHTO-LRFD Interim Design Specifications (2008) and TxDOT Standard Type-C Beam details (ftp://ftp.dot.state.tx.us/pub/txdot-info/cmd/cserve/standard/bridge/ibdstde1.pdf) Of the twelve beams produced by fabricator A, three were targeted for a maximum compressive stress at release of $0.70f'_{ci}$, six were targeted for $0.65f'_{ci}$, and three were targeted for $0.60f'_{ci}$. This fabricator produced the twelve beams in two separate castings of three beams ($0.60f'_{ci}$ and $0.70f'_{ci}$) and one casting of six beams ($0.65f'_{ci}$). In order to successfully monitor the concrete strength gain with time, twenty four cylinders were cast with each beam line. These cylinders were prepared immediately after the final beam in the beam line was cast. The cylinders were temperature match-cured. As part of the match-curing system (Sure Cure) thermocouples were placed in the beams on the casting line to match the curing temperature of the cylinders to the beams on the casting line. This process ensured that the cylinders gained strength in the same environment as the beams. Starting at approximately six hours after casting, two cylinders were tested every hour. The average value of these two cylinder tests was taken as the concrete strength. As the concrete strength neared the targeted release strength, pairs of cylinders were tested at shorter time intervals to document the strength gain. Once the compressive

strength of concrete within 100-200 psi of the targeted release strength, the beam line was released.

Because class H concrete gains strength quickly within the first twenty-four hours, the prestress release process needed to occur quickly to ensure that the prestress force was transferred to the beams at the targeted release strength. Just prior to release, the steel form ties (at the top and bottom of the side forms) were removed and the side formwork was separated from the beams. Large concrete "hold-down" blocks were placed over the beam's hold down points to avoid any cracking due to the dynamic nature of prestress transfer. When the concrete strength reached its targeted value, two workers flame cut the device holding the strands down at harping points. Immediately after that, the stressing plate at the live end of the beam line was retracted toward the beam specimens, gradually transferring the force from all the strands into the beams. A photograph of the live end of a typical beam line is included in Figure 3-7.

Figure 3-7 Live end of prestressing line (Fabricator A)

For all three castings, the entire release process was completed in approximately fifteen minutes. Immediately after release, two additional cylinders were broken. The average strength of the two cylinders before prestress transfer and the two cylinders after prestress transfer yielded the release strength for the last beam cast (youngest) in the line.

To account for the concrete strength gain between the first and last beam on the line in a given casting, linear interpolation was used. For each beam on the line, the time when concrete first entered the formwork was recorded. This time was designated as the "start" time. Additionally, the time when the last batch of concrete was placed was recorded. This was designated the "finish" time. Therefore, every beam on the line had an individual "start" and "finish" time. Using this time lapse data, the concrete strength at release for each individual beam was calculated through interpolation. Table 3-6 displays the maximum compressive stresses induced on the bottom face of the beams at the critical section for Fabricator A.

Table 3-6 Beam Production Details: Fabricator A

Beam Mark	Design Release Strength (psi)	Actual Release Strength (psi)	Maximum Compressive Release Stresses[2]		Date of Cast
			Targeted σ_{BOTTOM}	Actual σ_{BOTTOM}	
CA-70-1	4000	3940	-0.70*f'_{ci}	-0.70*f'_{ci}	9/26/07
CA-70-2	4000	3930	-0.70*f'_{ci}	-0.70*f'_{ci}	9/26/07
CA-70-3	4000	3930	-0.70*f'_{ci}	-0.70*f'_{ci}	9/26/07
CA-65-1	4300	4370	-0.65*f'_{ci}	-0.64*f'_{ci}	10/9/07
CA-65-2	4300	4380	-0.65*f'_{ci}	-0.63*f'_{ci}	10/9/07
CA-65-3	4300	4310	-0.65*f'_{ci}	-0.64*f'_{ci}	10/9/07
CA-65-4	4300	4340	-0.65*f'_{ci}	-0.64*f'_{ci}	10/9/07
CA-65-5	4300	4330	-0.65*f'_{ci}	-0.64*f'_{ci}	10/9/07
CA-65-6	4300	4300	-0.65*f'_{ci}	-0.65*f'_{ci}	10/9/07
CA-60-1	4700	4540[1]	-0.60*f'_{ci}	-0.61*f'_{ci}	10/3/07
CA-60-2	4700	4540[1]	-0.60*f'_{ci}	-0.61*f'_{ci}	10/3/07
CA-60-3	4700	4540[1]	-0.60*f'_{ci}	-0.61*f'_{ci}	10/3/07

[1]Start and finish times for beams in this casting were not recorded

[2]At Critical Section

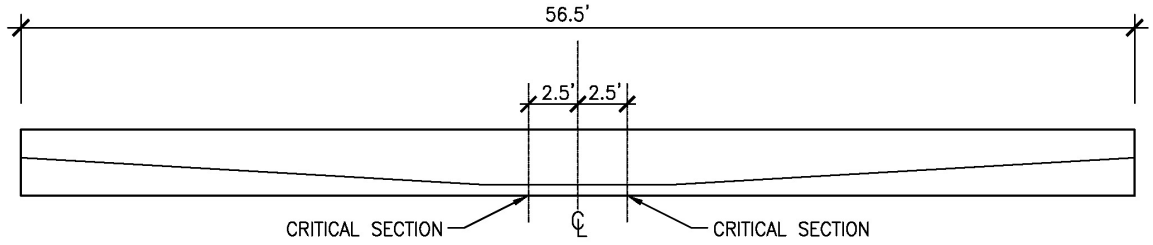

Upon completion of the prestress transfer, the side forms were moved away from the beams and the beams were lifted and transported to storage. Type-C beam shipment and storage is discussed in section 3.2.4

3.2.3.2 Production of Girders: Fabricator B

Fabricator B produced Series 1 girders using river gravel as the coarse aggregate. Representative of common concrete mixture designs used in this plant, the class H

concrete used by Fabricator B contained supplementary cementitious materials (Type F fly ash). The components of the concrete mixture design used by fabricator B are listed in Table 3-7. The batch tickets reflecting the exact mixture proportions for each casting are included in Appendix B.

Table 3-7 Concrete Mixture Design used by Fabricator B (per cubic yard)

Components	Mixture Design	Source
Water / Cement Ratio	0.27	--
Water	223 lbs	Well Water
Cement	658 lbs	Alamo Type III 1a
Fine Aggregate	1191 lbs	Arena
Coarse Aggregate	1789 lbs	Eagle Lake
Supplementary Cementitious Material	165 lbs	Headwaters, Type F Fly Ash
High-range water-reducing admixture	7 oz/100lbs	Sika 2100
Retarding admixture	0.5 oz/100lbs	Plastiment
Theoretical Unit weight	149.11 lbs/ft^3	--

The beams were designed in accordance with the AASHTO-LRFD Interim Specifications (2008) and TxDOT Standard Type-C beam details with one exception. The spacing of the shear reinforcement (R-bars shown in Figure 3-8) was increased to 24 inches outside of the bursting (end) regions of the beam. Figure 3-8 displays this increased stirrup spacing.

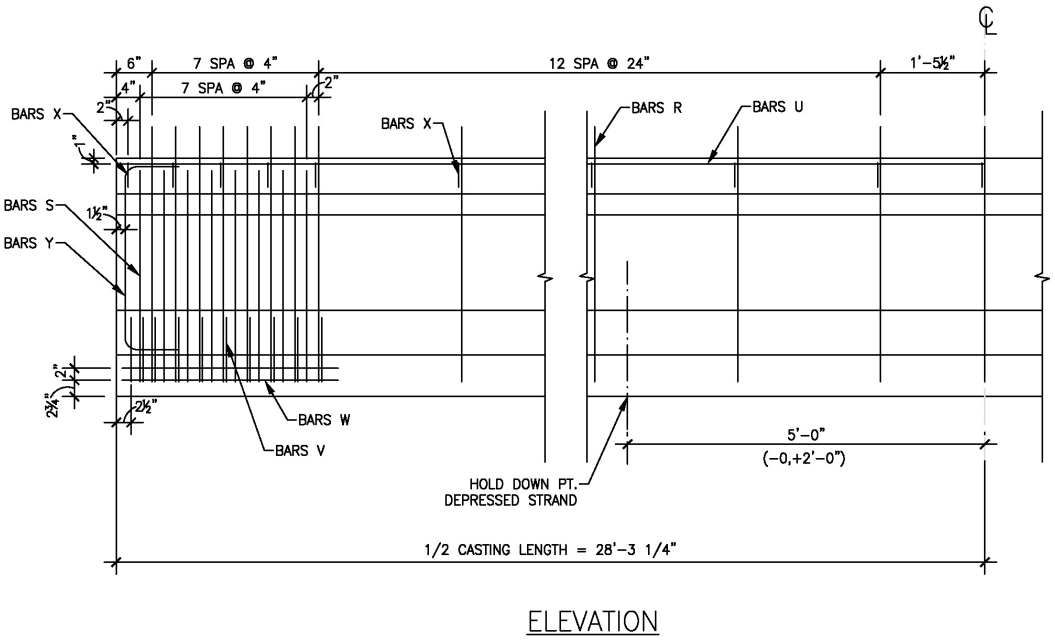

Figure 3-8 Altered Shear Reinforcement

The new shear design with increased spacing of the R-bars meets the AASHTO-LRFD (2008) minimum requirements for shear reinforcement. Further information about the testing of these Type-C girders in shear can be found in Heckmann and Bayrak, 2008.

Fabricator B intended to produce twelve beams, but due to unforeseen complications in construction, only nine beams were acceptable to the research program. Table 3-8 displays all the fabrication information for the beam specimens produced by fabricator B.

Table 3-8 Beam Production Details: Fabricator B

Beam Mark	Design Release Strength (psi)	Actual Release Strength (psi)	Maximum Compressive Release Stresses[1]		Date of Cast
			Targeted σ_{BOTTOM}	Actual σ_{BOTTOM}	
CB-70-1	5400	4540	-0.70*f'_{ci}	-0.62*f'_{ci}	5/6/08
CB-70-2	5400	4360	-0.70*f'_{ci}	-0.64*f'_{ci}	5/6/08
CB-70-3	5400	4180	-0.70*f'_{ci}	-0.67*f'_{ci}	5/6/08
CB-70-4	5400	4030	-0.70*f'_{ci}	-0.69*f'_{ci}	5/6/08
CB-70-5	5400	3880	-0.70*f'_{ci}	-0.72*f'_{ci}	5/6/08
CB-70-6	5400	3680	-0.70*f'_{ci}	-0.76*f'_{ci}	5/6/08
CB-60-1	5850	4820	-0.60*f'_{ci}	-0.59*f'_{ci}	4/23/08
CB-60-2	5850	5010	-0.60*f'_{ci}	-0.56*f'_{ci}	4/23/08
CB-60-3	5850	4620	-0.60*f'_{ci}	-0.61*f'_{ci}	4/23/08

[1]At Critical Section (See Table 3-6)

As seen in Table 3-8, three beams were targeted for a maximum compressive stress at release of 0.65f'_{ci}, while the remaining six beams were targeted for a maximum compressive stress at release of 0.70f'_{ci}. These nine beams were fabricated in two separate castings. To monitor the concrete strength gain with time, fabricator B used a temperature match-curing system similar to that of fabricator A. The match-cured cylinders were tested as necessary until the concrete strength was near the targeted value. In an effort to release quickly, the forms had been removed before the concrete reached its targeted value. When it was time to release, the devices used at the hold down points to harp the strands were flame-cut. Then, the stressing block at the live end of the beam line was retracted to release most of the prestressing force in the strands. Finally, the prestressing strands in-between each beam were flame-cut. For both castings, this process was complete within fifteen minutes.

As with fabricator A, the "start" and "finish" time for each beam was recorded and used to calculate the concrete strength at release for each specimen on the beam line. Because this concrete mixture had a water to cement ratio much lower than fabricators A, C, and D, the concrete gained strength with high variability. For the casting on May 6,

additional cylinders were taken from the very first beam cast. These cylinders from the first beam were tested just before and just after release of the beam line. The average compressive strength of the cylinders just before release and just after release were used to calculate the strength of the first beam on the line at release. Using the strength from the first beam and the last beam, the release strength for each beam on the beam line was calculated through interpolation. This measure was only used to make absolutely sure that accurate values of release strength were documented for this concrete mixture design that was gaining strength at a rapid pace. The concrete strengths at release for the beams produced by fabricator B are displayed in Table 3-8.

Upon completion of the prestress transfer, the beams were lifted off the beam line and placed in storage on-site. Type-C beam shipment and storage is discussed in section 3.2.4

3.2.3.3 Production of Girders: Fabricator C

Fabricator C produced Series 2 girders using limestone coarse aggregate. The concrete mixture design used to fabricate these beams was a class H concrete mixture with limestone aggregate representative of standard mixtures used in TxDOT Type-C beam production. The components of the mixture design used by fabricator C are listed in Table 3-9. The exact mixture proportions adjusted for the moisture content at each casting are included with the batch tickets in Appendix B.

Table 3-9 Concrete Mixture Design used by Fabricator C (per cubic yard)

Components	Mixture Design	Source
Water / Cement Ratio	0.37	--
Water	242 lbs	BCW Well
Cement	658 lbs	Capital Type III
Fine Aggregate	1326 lbs	River Sand Multisources
Coarse Aggregate	1789 lbs	Vulcan 1604 Grade 5
High-range water-reducing admixture	7.5 oz/100 lbs	Sika 2100
Retarding admixture	1 oz/100 lbs	Sika Plastiment
Theoretical Unit weight	148.7 lbs/ft^3	--

Fabricator C produced three beams targeted for a maximum compressive stress at release of 0.70f'_{ci}, six beams at 0.65f'_{ci}, and three beams at 0.60f'_{ci}. For Series 2 beams, this translated into target concrete strengths of 5400 psi, 5850 psi, and 6400 psi respectively. Fabricator C produced the twelve beams in three separate castings of three beams (0.70f'_{ci}), six beams (0.65f'_{ci}), and three beams (0.60f'_{ci}) respectively. To monitor the concrete strength gain, fabricator C made 48 cylinders with each beam line. All cylinders were cured with the beam underneath a waterproof tarp. At the appropriate time, cylinders were removed from underneath the tarp and tested. As with fabricators A, and B, fabricator C tested two cylinders approximately six hours after casting and continued to test cylinders every hour after that. When the concrete strength was within 1000 psi of the target, cylinders were tested at a maximum of every half hour until the target strength was achieved. The results from all three castings by fabricator C are displayed in Table 3-10.

Table 3-10 Beam Production Details: Fabricator C

Beam Mark	Design Release Strength (psi)	Actual Release Strength (psi)	Maximum Compressive Release Stresses[1]		Date of Cast
			Targeted σ_{BOTTOM}	Actual σ_{BOTTOM}	
CC-70-1	5400	5380	-0.70*f'_{ci}	-0.70*f'_{ci}	3/14/08
CC-70-2	5400	5360	-0.70*f'_{ci}	-0.71*f'_{ci}	3/14/08
CC-70-3	5400	5330	-0.70*f'_{ci}	-0.70*f'_{ci}	3/14/08
CC-65-1	5850	5970	-0.65*f'_{ci}	-0.64*f'_{ci}	3/26/08
CC-65-2	5850	6000	-0.65*f'_{ci}	-0.64*f'_{ci}	3/26/08
CC-65-3	5850	6130	-0.65*f'_{ci}	-0.62*f'_{ci}	3/26/08
CC-65-4	5850	6070	-0.65*f'_{ci}	-0.63*f'_{ci}	3/26/08
CC-65-5	5850	6350	-0.65*f'_{ci}	-0.60*f'_{ci}	3/26/08
CC-65-6	5850	6250	-0.65*f'_{ci}	-0.61*f'_{ci}	3/26/08
CC-60-1	6400	6350	-0.60*f'_{ci}	-0.60*f'_{ci}	4/1/08
CC-60-2	6400	6370	-0.60*f'_{ci}	-0.60*f'_{ci}	4/1/08
CC-60-3	6400	6370	-0.60*f'_{ci}	-0.60*f'_{ci}	4/1/08

[1]At Critical Section (See Table 3-6)

To prepare for an expedient release of the beam line, the forms were removed before the concrete strength was near the targeted value in all three castings. Once the concrete strength was within ±100 psi of the target, workers flame-cut the device used at the hold down locations. Immediately after that, the stressing plate at the live end was retracted, transferring the prestressing force into the specimens. Then, the strands between each of the beams were flame-cut to finalize the prestress transfer operation. In all three castings, prestress transfer took place within fifteen minutes. Once the beams were visually inspected, they were lifted off the stressing line and placed in storage until they were shipped to the Ferguson Structural Engineering Laboratory.

3.2.3.4 Production of Girders: Fabricator D

Fabricator D produced Series 2 girders using river gravel as the coarse aggregate. The concrete mixture design used to fabricate these beams was again a class H concrete mixture representative of standard mixtures used in beam production. The components of

the mixture design used by fabricator D are listed in Table 3-11. The exact mixture proportions adjusted for the moisture conditions at each casting are included with the batch tickets in Appendix B.

Table 3-11 Concrete Mixture Design used by Fabricator D (per cubic yard)

Components	Mixture Design	Source
Water / Cement Ratio	0.33	--
Water	196 lbs	City of Victoria
Cement	611 lbs	Alamo Type III
Fine Aggregate	1285 lbs	Fordyce Murphy
Coarse Aggregate:	1990 lbs	Fordyce Murphy
High-range water-reducing admixture	27 oz/100 lbs	Rheobuild 1000
Retarding admixture	3 oz/100lbs	Pozzolith 300R
Theoretical Unit weight	151.19 lbs/ft^3	--

As with fabricators A and C, fabricator D cast three beams targeted at $0.70f'_{ci}$, six beams at $0.65f'_{ci}$, and three beams at $0.60f'_{ci}$. Fabricator D used four separate castings (3 beams per casting) to achieve these different targeted release strengths. In order to monitor the concrete strength gain with time, twenty four cylinders were prepared after the last beam on the beam line was cast. All twenty four cylinders were temperature match-cured. As with the previously mentioned fabricators, cylinders were tested in a structured manner to transfer the prestressing force at a concrete strength very close to the targeted value. The results from all four castings are shown in Table 3-12.

Table 3-12 Beam Production Details: Fabricator D

Beam Mark	Design Release Strength (psi)	Actual Release Strength (psi)	Maximum Compressive Release Stresses[2]		Date of Cast
			Targeted σ_{BOTTOM}	Actual σ_{BOTTOM}	
CD-70-1	5400	5580	-0.70*f'_{ci}	-0.68*f'_{ci}	3/4/08
CD-70-2	5400	5500	-0.70*f'_{ci}	-0.69*f'_{ci}	3/4/08
CD-70-3	5400	5420	-0.70*f'_{ci}	-0.70*f'_{ci}	3/4/08
CD-65-1	5850	5670[1]	-0.65*f'_{ci}	-0.67*f'_{ci}	3/7/08
CD-65-2	5850	5670[1]	-0.65*f'_{ci}	-0.67*f'_{ci}	3/7/08
CD-65-3	5850	5670[1]	-0.65*f'_{ci}	-0.67*f'_{ci}	3/7/08
CD-65-4	5850	5940[1]	-0.65*f'_{ci}	-0.64*f'_{ci}	3/14/08
CD-65-5	5850	5940[1]	-0.65*f'_{ci}	-0.64*f'_{ci}	3/14/08
CD-65-6	5850	5940[1]	-0.65*f'_{ci}	-0.64*f'_{ci}	3/14/08
CD-60-1	6400	6320	-0.60*f'_{ci}	-0.61*f'_{ci}	3/12/08
CD-60-2	6400	6310	-0.60*f'_{ci}	-0.61*f'_{ci}	3/12/08
CD-60-3	6400	6300	-0.60*f'_{ci}	-0.61*f'_{ci}	3/12/08

[1]Strength was not interpolated between beams for this casting

[2]At Critical Section (See Table 3-6)

For two of the castings from this fabricator, the cylinder tests conducted prior to release yielded larger values than those from the tests conducted after prestress transfer. For these casting lines, interpolation using these strength values would mean that the first beam cast on the line would have a slightly smaller compressive strength value than the last beam cast on the line. This result is simply unreasonable. It was deemed appropriate to assume the strength at release for all beams on the casting line was the average strength of the cylinders tested immediately before and after prestress transfer. This is noted in Table 3-12.

As with the previous fabricators, fabricator D took less than 15 minutes to transfer the prestress force to all beams. After inspection, the beams were lifted and stored on-site until delivery to the Ferguson Structural Engineering Lab.

3.2.4 Shipment and Storage of Type C Girders

All Type C girders were stored at their respective fabrication plants until delivery to the Ferguson Structural Engineering Laboratory. Beams were shipped either individually or in pairs on trucks. Upon arrival, each beam was at least seven days old. In the laboratory, a 25 ton crane and a 50 foot twin-girder lifting beam were used to move the specimens off the truck and into the testing setup. The specimen was picked up at lifting points located 5.75' from each end. The crane and lifting beam used to move the C-Beam specimens is shown in Figure 3-9.

Figure 3-9 Lifting a Type C Girder at FSEL

3.3 DESIGN AND FABRICATION OF TXDOT BOX BEAMS

In addition to the forty five C-beam specimens in this study, ten TxDOT 4B28 box beams were tested in flexure. All ten box beams were produced in two different fabrication plants of a single producer designated as fabricator E. All ten beams were

designed for a nominal concrete compressive strength of 4100 psi at prestress transfer using four different concrete mixture designs. The purpose of testing ten box beams fabricated with four different concrete mixture designs was to perform proof-testing on a compressive stress limit at release that seemed adequate for all of the C-beam tests reported in this thesis and other beams previously tested by Birrcher and Bayrak (2007).

In order to obtain comprehensive results, several variables were employed in the fabrication of these beams. First, the coarse aggregate type was varied. Four of the ten box beams were fabricated by using limestone for the coarse aggregate while the remaining six were produced by using hard river gravel. This distinction was made to investigate whether early release was more damaging to limestone concrete mixtures or river gravel concrete mixtures. As well as the coarse aggregate, the type of concrete used to fabricate these beams was varied. Conventional concrete was used to fabricate five beam specimens while five specimens were fabricated by using self-consolidating concrete. There has been significant interest to investigate the properties and behavior of self-consolidating concrete mixtures in prestressed concrete beam production. Varying the type of concrete used in beam production allowed for a comparison between self consolidating concrete and conventional concrete.

In addition to varying the coarse aggregate type and concrete consolidation technique used in fabricating the box beams, various adjustments were made to the standard beam design for a different research objective of investigating shear capacity at skewed ends of box beams (TxDOT Research project 5831). Therefore, all ten beams were fabricated with one square end and one skewed end. Also, the shape of the box beam void was modified in order to investigate the behavior of the concrete end block and its role in transferring shear forces in TxDOT Project 5831. As well as adjusting the void, the shear reinforcement in the beams was reduced to allow for shear failures of the specimens such that shear behavior of the specimens could be studied. Figure 3-10 displays the shape of the box beams and the three different types of voids used in fabrication.

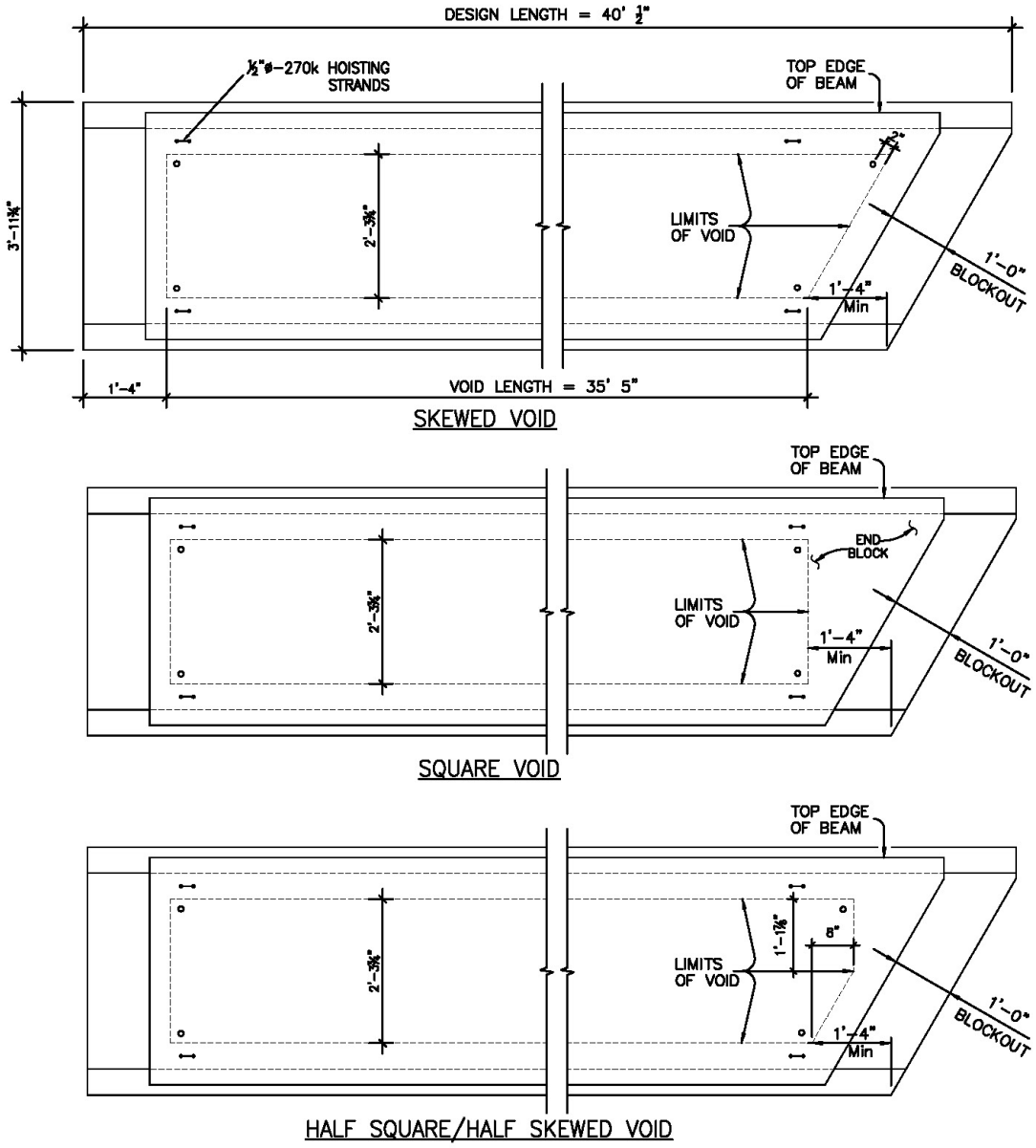

Figure 3-10 Box Beam Void Geometry

All adjustments made to the beams for shear are outside the scope of this research and are not discussed in this thesis. Table 3-13 summarizes all the variables in the design and fabrication of these ten box beam specimens.

Table 3-13 Box Beam Design Details

Beam Mark	Target Release Strength	Concrete Type	Coarse Aggregate Type	Skewed End Void Geometry
BB-01	4100 psi	Conventional	Limestone	30° Skew
BB-02	4100 psi	Conventional	Limestone	Square
BB-03	4100 psi	Conventional	Hard River Gravel	30° Skew
BB-04	4100 psi	Conventional	Hard River Gravel	Square
BB-05	4100 psi	Conventional	Hard River Gravel	Half Square/ Half Skew
BB-06	4100 psi	Self Consolidating	Limestone	30° Skew
BB-07	4100 psi	Self Consolidating	Limestone	Square
BB-08	4100 psi	Self Consolidating	Hard River Gravel	30° Skew
BB-09	4100 psi	Self Consolidating	Hard River Gravel	Square
BB-10	4100 psi	Self Consolidating	Hard River Gravel	Half Square/ Half Skew

Each full-scale box beam was designed to have a length on the long end of 40'-½". The section properties of a standard TxDOT Box Beam are displayed in Table 3-14.

Table 3-14 Section Properties of a TxDOT 4B28 Box Beam

Beam Type	y_t (in)	y_b (in)	A (in^2)	I (in^4)	w (lb/ft)
4B28	14.38	13.62	678.8	68,745	707*
*Does not include the weight of the concrete end blocks					

As indicated earlier, to effectively evaluate the possibility of increasing the current code limit on compressive stress at release, all specimens produced were designed to be released at a nominal strength of 4100 psi such that the maximum compressive stress at release of $0.66f'_{ci}$ at the critical sections of the beam (See Table 3-16).

3.3.1 Design of TxDOT Box Beams

The TxDOT standard box beam strand pattern was altered for this experimental research. A unique, non-standard strand pattern was used to target a maximum

compressive stress at release of $0.66f'_{ci}$ at a nominal concrete strength of 4100 psi. The strand pattern used for all ten box beams is displayed in Figure 3-11.

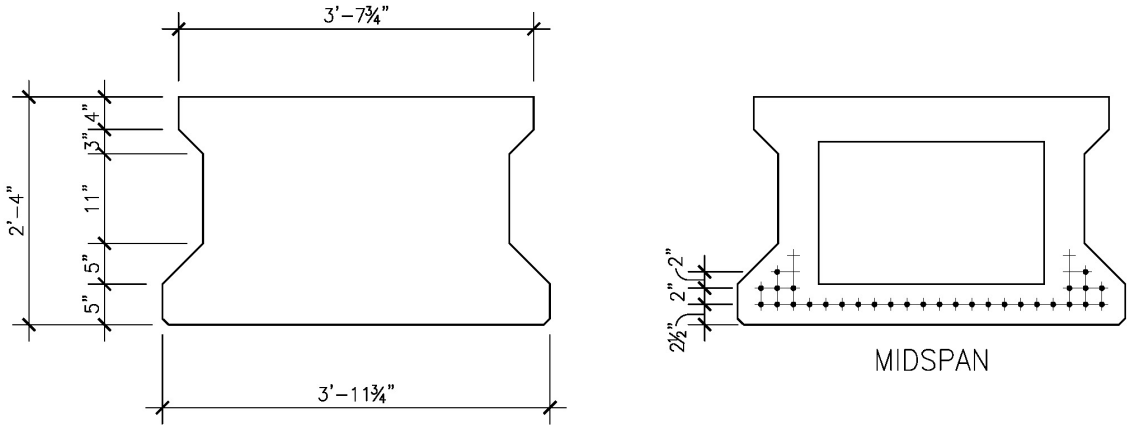

Figure 3-11 Box Beam Centerline Strand Pattern

The strand pattern shown in Figure 3-11 consists of thirty, ½" diameter, 270-ksi low relaxation strands, none of which were harped. Because the box beam geometry does not permit harping strands, strands were debonded along the length of the beam to ensure that the tensile stress induced anywhere along the length of the beam at release was below $7.5\sqrt{f'_{ci}}$. In order to debond prestressing strands, a plastic tubing was placed over the strand and duct-taped. This tubing served as a bond breaker between the concrete and the prestressing strands. In the beams fabricated for this research, four strands were debonded ten feet from each end and four additional strands were debonded at four feet from each end. Figure 3-12 includes the debonding pattern used in all ten box beams. Figure 3-13 displays a picture of the debonded strands prior to concrete placement.

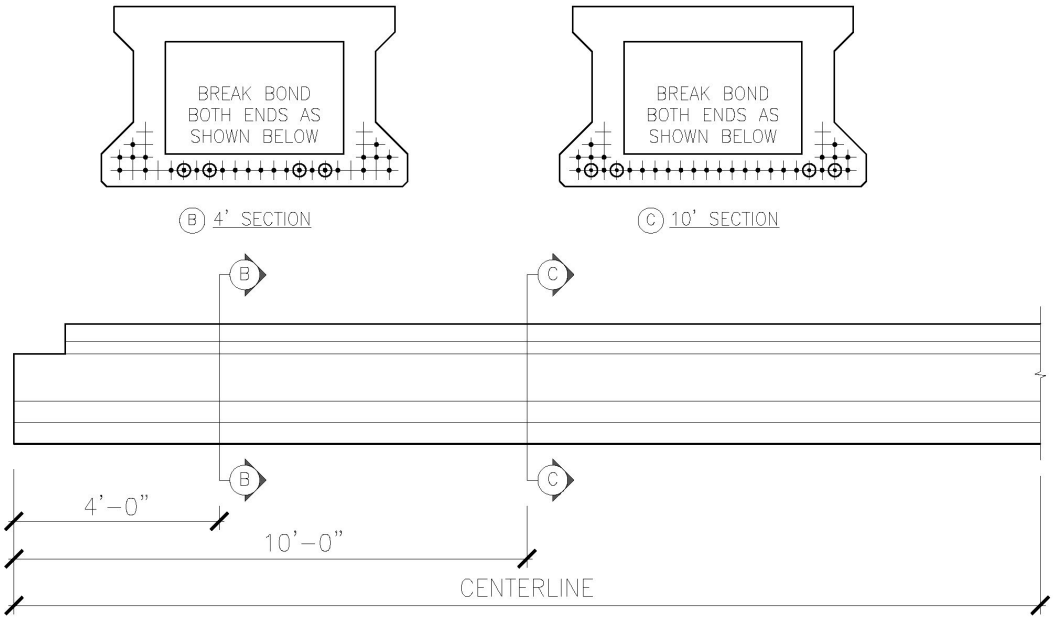

Figure 3-12 Debonding pattern for Box Beams (Not to scale)

Figure 3-13 Debonded strands prior to concrete placement

3.3.2 Production of Box Beams: Fabricator E

A precaster with two separate fabrication plants was used to make all ten box beams tested in this research. Five box beams were produced by using conventional concrete and five were fabricated by using self consolidating concrete. Additionally, four beams contained limestone coarse aggregate while six beams contained river gravel coarse aggregate. This combination of variables resulted in four different concrete mixture designs. While the conventionally consolidating concrete mixture designs were representative of the concrete used in typical production, mixture designs used in self consolidating concrete were developed by fabricator E for their commercial projects and were never before used in TxDOT beams. The components of all four mixture designs used by fabricator E are included in Table 3-15.

Table 3-15 Concrete Mix Designs used by Fabricator E (per cubic yard)

Components	Mix 1	Mix 2	Mix 3	Mix 4
Concrete Type	Conventional	Conventional	SCC	SCC
Coarse Aggregate Type	Limestone	River Gravel	Limestone	River Gravel
Water / Cement Ratio	0.29	0.27	0.355	0.354
Water	229 lbs	222 lbs	240 lbs	246
Type I/II Cement	0 lbs	658 lbs	0 lbs	0 lbs
Type III Cement	599 lbs	0 lbs	545 lbs	560 lbs
Class F Fly Ash	200 lbs	165 lbs	136 lbs	140 lbs
Fine Aggregate	1148 lbs	1033 lbs	1515 lbs*	1498 lbs*
Coarse Aggregate:	1829 lbs	1948 lbs	1530 lbs	1500 lbs
High-range water-reducing admixture	3.1 oz/cwt	6 oz/cwt	5.58 oz/cwt	6 oz/cwt
Retarding admixture	3 oz/cwt	1 oz/cwt	1.5 oz/cwt	1.5 oz/cwt
Theoretical Unit weight	148.33 lb/ft^3	149.11 lb/ft^3	146.9 lb/ft^3	146.1 lb/ft^3
*Fine aggregate blend of river sand and manufactured sand				

In order to fabricate the ten box beams, fabricator E used four separate castings. The box beam casting process consisted of the following:

1. Prestressing strands were placed along the beam fabrication line and anchored to a thick steel plate at one end (termed the "dead" end).
2. Strands were tensioned with hydraulic rams to the appropriate jacking force (within a 2% tolerance) and anchored to another thick steel plate at the opposite end of the beam line (termed the "live" end).
3. All mild reinforcing for the lower half of the box-beam specimen was placed, tied and inspected.
4. Steel side forms were connected to the soffit form and secured.
5. Concrete was poured in the bottom flange of the box beams using motorized hopper trucks (or sidewinders). This casting was termed the "stage 1" concrete placement.
6. A Styrofoam void was placed in the beam specimens and the remaining mild reinforcing in the top half of the beam was expediently placed, tied, and inspected.
7. Concrete was placed in the top flanges and webs of the box beams using motorized hopper trucks. This was termed a "stage 2" concrete placement. While stage 2 concrete placement took place, concrete placed in the bottom flange (Stage 1 concrete placement) was still plastic (i.e. initial set did not take place) as per TxDOT's two-stage monolithic concrete placement specifications.
8. Beams were covered with wet burlap or waterproof tarps.
9. At appropriate concrete strength, prestressing strands were released.

In order to monitor strength gain with time, 36 cylinders were made from the stage 1 pour and 12 cylinders were made from the stage 2 pour. All cylinders were made immediately after the last beam on the line was cast. In addition, 24 of the stage 1 cylinders were conditioned by using a temperature match-curing system.

Because this research is focused on the behavior of the pre-compressed tensile zone of pretensioned girders (i.e. the bottom flange), the prestress transfer was based on the compressive strength of the cylinders from the stage 1 concrete placement.

Approximately six hours after casting, two match-cured cylinders from the stage 1 pour were tested. Thereafter, match-cured cylinders were tested as needed to target the release strength of 4100 psi. When the stage 1 cylinders were within 500 psi of the target value, two stage 2 cylinders were tested. This was done to understand the concrete strength throughout the beam. Once the stage 1 concrete was within 100-200 psi of the target, the prestressing force was transferred.

The prestress transfer operation was completed by retracting the hydraulic rams attached to the thick steel plate at the live end of the prestressing line. In this way, the prestressing strands were detensioned, and therefore the prestressing force was transferred into the specimens. Subsequently, workers flame cut the prestressing strands between the beams, completing the transfer operation. This process took approximately fifteen minutes for each casting. Immediately after prestress transfer, two stage 1 cylinders and two stage 2 cylinders were broken. The cylinder strengths before and after release were averaged to give the concrete strength at release, f'_{ci}.

In order to account for the concrete strength gain between the first and last beams cast on a line, the start time and finish time for each beam was recorded. Using the time-lapse data between the first and last beam cast on the line, the concrete strength at release for each individual beam was calculated through interpolation. The results from the box beam castings are displayed in Table 3-16. As with Fabricator D, when concrete cylinder tests indicated a slight concrete strength decrease during prestress transfer, interpolation was not used to calculate compressive strength. In this situation, the average of the concrete cylinder strengths before and after prestress transfer was taken as the concrete compressive strength at prestress release for all specimens on the beam line. This is noted in Table 3-16. Immediately after fabrication, all box beams were inspected and stored on-site.

Table 3-16 Beam Production Details: Fabricator E

Beam Mark	Design Release Strength (psi)	Actual Release Strength from Stage 1 casting (psi)	Maximum Compressive Release Stresses[2]		Actual Release Strength from Stage 2 casting (psi)	Date of Cast
			Targeted σ_{BOTTOM}	Actual σ_{BOTTOM}		
BB-01	4100	4140	-0.66*f'_{ci}	-0.65*f'_{ci}	3280	8/21/08
BB-02	4100	4070	-0.66*f'_{ci}	-0.66*f'_{ci}	3130	8/21/08
BB-03	4100	4120	-0.66*f'_{ci}	-0.65*f'_{ci}	2320[1]	7/22/08
BB-04	4100	4220	-0.66*f'_{ci}	-0.64*f'_{ci}	2320[1]	7/22/08
BB-05	4100	4170	-0.66*f'_{ci}	-0.64*f'_{ci}	2320[1]	7/22/08
BB-06	4100	4060[1]	-0.66*f'_{ci}	-0.66*f'_{ci}	4050	8/25/08
BB-07	4100	4060[1]	-0.66*f'_{ci}	-0.66*f'_{ci}	3920	8/25/08
BB-08	4100	4040[1]	-0.66*f'_{ci}	-0.66*f'_{ci}	3270[2]	8/26/08
BB-09	4100	4040[1]	-0.66*f'_{ci}	-0.66*f'_{ci}	3270[2]	8/26/08
BB-10	4100	4040[1]	-0.66*f'_{ci}	-0.66*f'_{ci}	3270[2]	8/26/08

[1]Strength was not interpolated between beams

[2]Data from cylinders tested after prestress transfer

[3]At Critical Section`

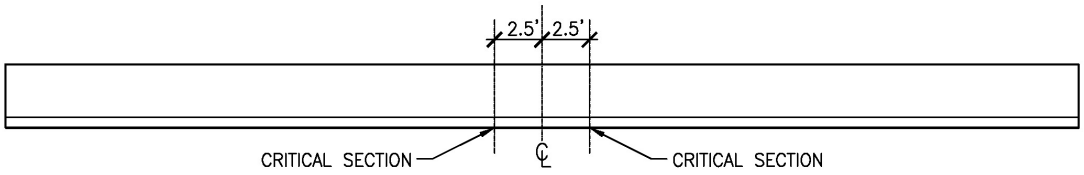

3.3.3 Shipment and Storage of Box Beams

All box beams were stored at the fabrication plant until delivery to the Ferguson Structural Engineering Laboratory. Beams were shipped individually on a truck. Upon arrival, each beam was at least seven days old. In the laboratory, a 25 ton crane and a 50 foot twin-girder lifting beam were used to move the specimens off the truck and into the testing setup. The specimen was picked up at lifting points located 35-feet apart. The crane and lifting beam used to move the box beam specimens is shown in Figure 3-14.

Figure 3-14 Lifting a Box Beam at FSEL

3.4 SUMMARY

Forty-five full-scale Type-C girders and ten full-scale 4B28 box beams were fabricated and tested in this research study. Five different precast plants were utilized to provide a broad sample of beams (i.e. concrete mixture designs and beam fabrication practices) made throughout the state of Texas.

A non-standard strand pattern was created for the Type-C beams in order to achieve a maximum compressive stress at prestress release between $0.6f'_{ci}$ and $0.7f'_{ci}$. The Type-C girders were split into two categories based on nominal release strength. Twenty one girders were designated as Series 1 beams with a nominal release strength of 4000 psi while the remaining twenty four girders were designated as Series 2 beams with a nominal release strength of 6000 psi. In essence, the primary difference between Series 1 and Series 2 beams lies in the cementitious materials content of the mixture designs. In addition, twenty one girders (9 Series 1 beams + 12 Series 2 beams) were produced with

river gravel as the coarse aggregate and twenty four girders (12 Series 1 beams + 12 Series 2 beams) were produced with limestone as the coarse aggregate.

As with the Type-C girders, a non-standard strand pattern was used to target a maximum compressive stress at release of $0.66f'_{ci}$ at a concrete compressive strength of 4100 psi. Previously, scaled test specimens from TxDOT research project 4086 as well as Type-A beams and Type-C beams had performed well when the maximum compressive stress at prestress transfer was kept below $0.65f'_{ci}$. The compressive stress at release for the box beams was held constant in order to verify that a potential increase of the stress limit to $0.65f'_{ci}$ would be acceptable for a variety of concrete mixture designs. The coarse aggregate and concrete type was varied among the ten specimens. Five specimens were produced by using conventional high strength concrete and the remaining five with self consolidating concrete. Additionally, six beams (3 beams with SCC and 3 beams with conventional concrete) contained hard river gravel as the coarse aggregate while four contained limestone as the coarse aggregate (2 beams with SCC and 3 beams with conventional concrete).

All fifty five test specimens were fabricated and tested within sixteen months as part of a modification made to extend TxDOT project 5197. This extension involved a wide-ranging set of concrete mixture designs, and beam fabrication practices used to produce C-Beams and Box-Beams. The fabrication of test specimens was discussed in Chapter 3. The experimental program is discussed in Chapter 4.

CHAPTER 4
Test Setup

4.1 OVERVIEW

The experimental program for part I of phase II of TxDOT project 5197 consisted of the flexural static testing of the following types of beams:

- Full-scale Series 1 Type-C girders (21 tests: 12 beams from Fabricator A + 9 beams from Fabricator B)
- Full-scale Series 2 Type-C girders (24 tests: 12 beams from Fabricator C + 12 beams from Fabricator D)
- Full-scale 4B28 Box Beams (10 tests: 10 beams from Fabricator E)

The full-scale static testing of the Type-C girders described in Section 3.2 was very similar to the full-scale testing on Type-A beams within the previous phase of TxDOT project 5197 (Birrcher and Bayrak 2007). The Type-C beam testing consisted of loading the beams up to approximately 30% above the observed cracking load. The load was applied in a way to produce a constant moment region of five feet at the center of the simply supported beam span. During the tests, the applied load was constantly monitored, and deflection measurements were taken at midspan and at both supports.

The full-scale static testing of the 4B28 Box Beams described in Section 3.3 is similar to that of the Type-C testing. The testing consisted of loading the beams up to approximately 20% above the observed cracking load. Like the Type-C beam tests, the load was applied to produce a five foot constant moment region in the center of the beam. The applied load, midspan deflection and support deflections were constantly monitored during the tests.

In addition to the flexural static testing of the Type-C girders 18 beams were failed in shear following the flexural test. The loading protocol and test setup for the shear testing of TxDOT Project 5197 is described in Heckmann and Bayrak, 2008.

Likewise, all ten 4B28 box beams are scheduled to be tested in shear (TxDOT Project 5831). The results of the box beam shear tests will be reported at a later date and do not appear in this thesis and are considered to be beyond the scope of this research.

The flexural static testing of Type-C girders and 4B28 Box beams are discussed in Sections 4.2 and 4.3 respectively.

4.2 TESTING OF FULL-SCALE TYPE-C GIRDERS

Static flexural testing of forty five TxDOT Type-C girders was performed to experimentally evaluate their cracking load. The loading protocol, test setup, and instrumentation and data acquisition used in these tests are described in the following sections.

4.2.1 Load Protocol

All Type-C Girders were loaded up to approximately 30% above their observed cracking load. The typical load protocol for all Type-C beams was to load steadily with brief pauses to approximately 85% of the predicted cracking load. At this point, loading was suspended to visually inspect the beams for cracking. Then, the beam was loaded by increments of 2 to 5 kips with intermittent pauses to inspect the beam. During testing, all visually observed cracks were marked on the beam and crack widths were measured using a crack comparator card. Once the load exceeded the observed cracking load by approximately 10%, loading proceeded by increments of 10 to 20-kips. Within the last load stage, cracks were marked and crack widths were measured. After this point, the beam was completely unloaded. Pictures were taken during all loading breaks to document the crack propagation during testing.

For typical static tests of Series 1 beams, loading began steadily with brief pauses up to 90-kips. At 90-kips the beam was visually inspected for cracks. After 90 kips, the load was increased to 100-kips and the beam was again visually inspected. After this load level, the beam was loaded in small increments of 2 to 5 kips until cracking was observed. Once the loading reached 120-kips, loading progressed by increments of 10-

kips up to a maximum load of 150-kips. Figure 4-1 presents a visual diagram for the loading program of Series 1 beams.

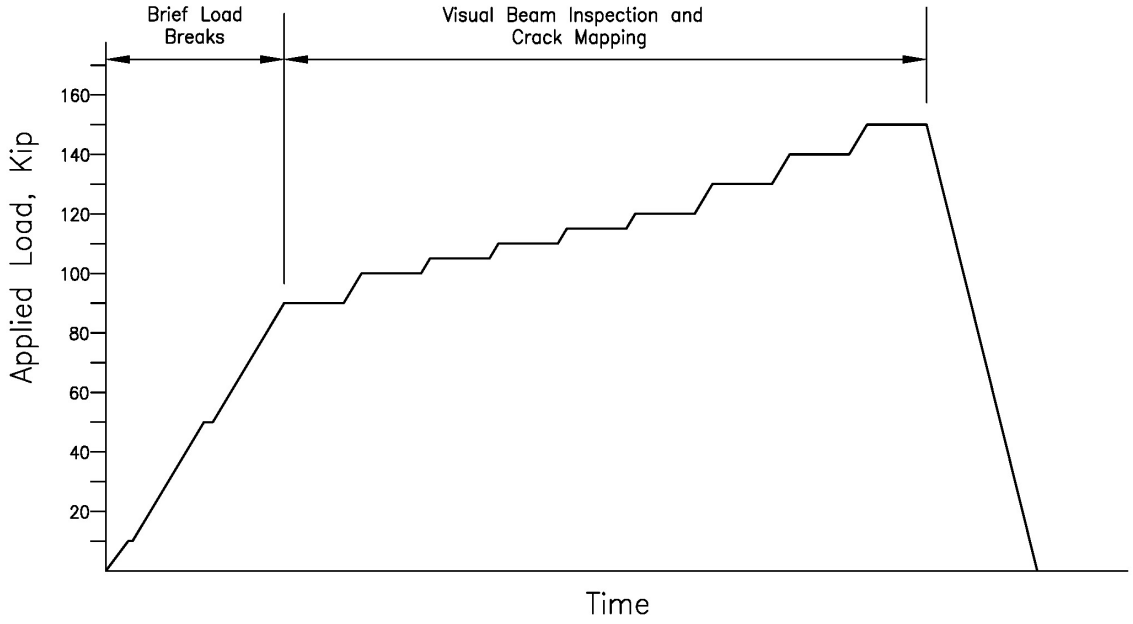

Figure 4-1 Series 1 Beam Loading Protocol

For typical static tests of Series 2 beams, loading began with brief pauses up to 130-kips. At this point, the beam was visually inspected for cracks. After this, loading progressed in smaller increments of 2 to 5-kips until cracking was observed. Once the loading reached 150-kips, the beam was inspected and then loaded to 160-kips. After inspection at 160-kips, the beam was loaded to its maximum value of 180-kips. At this point the beam was thoroughly inspected and all cracks were marked and measured. Figure 4-2 presents a visual diagram of the loading program for Series 2 beams.

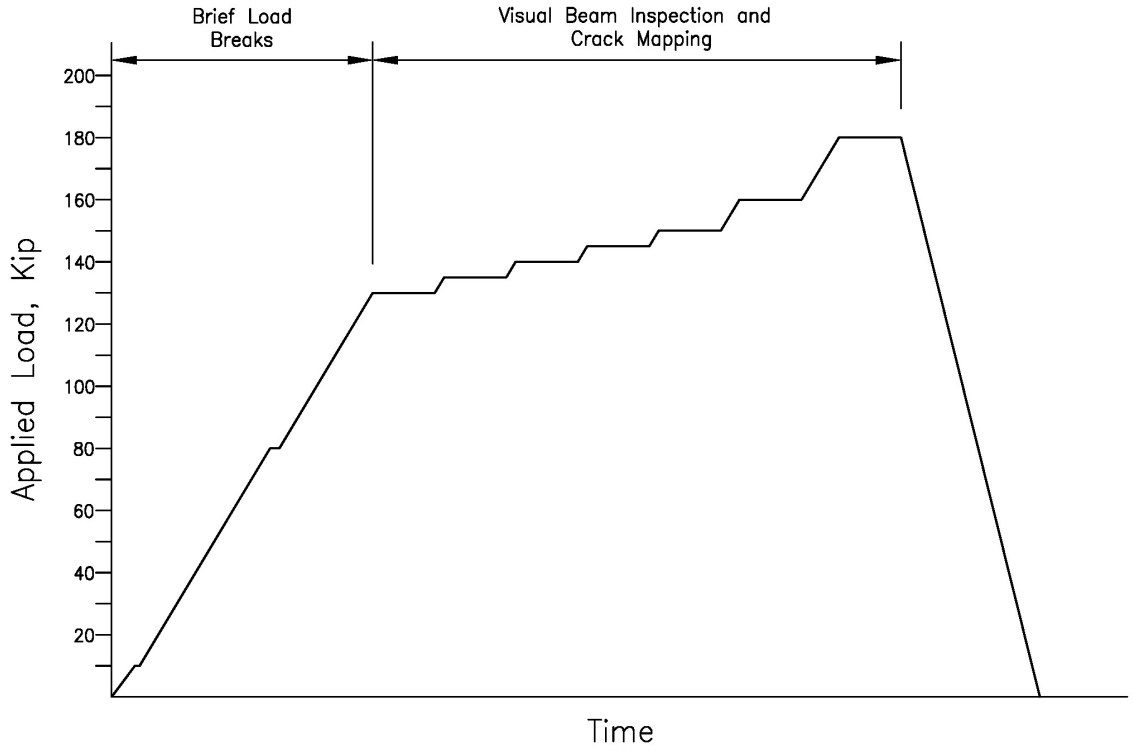

Figure 4-2 Series 2 Beam Loading Protocol

4.2.2 Test Setup

All forty-five Type-C beams were subjected to four-point loading. Figure 4-3 and Figure 4-4 display a schematic figure and a photograph of the Type-C beam test setup respectively.

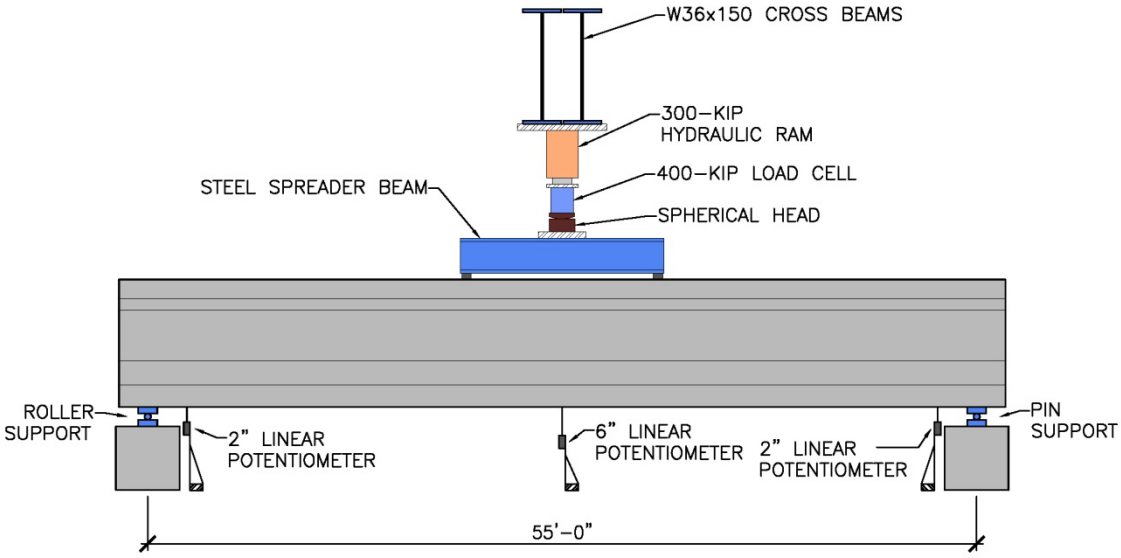

Figure 4-3 Type-C Beam Test Setup (Not to Scale)

Figure 4-4 Picture of a Type-C Beam Flexural Test Setup

A reaction frame of two steel columns and two coped wide flange beams was bolted to the strong floor at the midspan of the beam. Two inch thick steel plates were bolted across the top and bottom flanges of the coped wide flange beams to connect them together and provide stability. A single acting hydraulic ram was bolted to the steel plate below the coped wide flange beams. Below the ram, the following items were stacked on top of the beam:

- 400-kip capacity load cell
- 8-inch diameter steel spherical head and accompanying steel seat
- A combination of 2-inch, 1-inch or ¾-inch steel shim plates
- 64-inch long steel spreader beam
- Two 3 x14-inch Neoprene Bearing Pads

The neoprene bearing pads sat directly on the top surface of the beam and were placed 30 inches away from the beam centerline. The steel spreader beam was centered on the neoprene pads. Depending on the camber of the test specimen, either a 2" plate or a 1" plate was placed in the center of the spreader beam. The 8"diameter spherical head was placed on top of the steel plate and accounted for any slight eccentricities or non-level surfaces in the test setup. The load cell was placed directly on top of the spherical head followed by either a ¾" plate or a 1" plate; again, depending on the camber of the specimen. Great care was taken in aligning all of these pieces to ensure that the specimen was not loaded eccentrically. To apply load to the specimen, hydraulic fluid was transferred to the ram by a pneumatic pump. As the hydraulic fluid entered the ram, the piston pressed down onto the assembly below, loading the specimen. Figure 4-5 displays a close view of the constant moment region of a Type-C beam test.

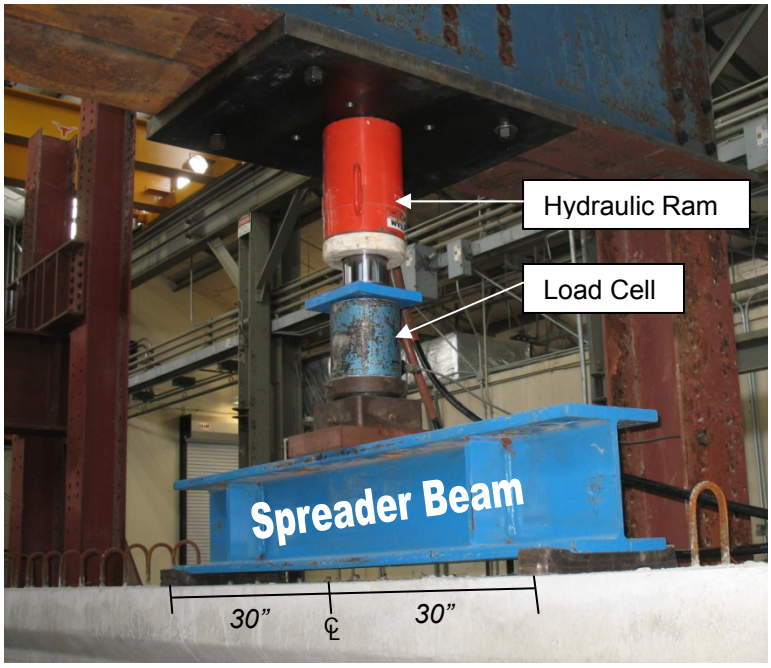

Figure 4-5 Midspan Region of a Type-C Beam Test

All Type-C beams were simply supported. At each end, a two inch thick steel rod was placed between two inch thick steel plates. To achieve a pin condition at one end of the beam, the rod was welded to the steel plate. The roller connection was free to displace at all times. To protect against the beam completely rolling off its support, steel tabs were welded on to the plates of the roller connection. It is important to note that the roller never came into contact with the tabs during a flexural test. Figure 4-6 displays these support conditions.

Figure 4-6 Type C-Beam Roller Support and Pin Support, respectively

In each test, the centerline distance of the pin and roller connections was 55-feet. This allowed for a 9-inch overhang at each end of the beam. A schematic figure and a photograph of the Type-C beam test setup is displayed in Figure 4-3 and Figure 4-4 respectively

4.2.3 Instrumentation and Data Acquisition

During all Type-C beam flexural tests, the following items were used to monitor and collect data:

- Two 6-inch linear potentiometers
- Two 2-inch linear potentiometers
- One 400-kip capacity Load Cell
- One Pressure Transducer

All of the devices listed above provide readings in voltages. These voltage readings were then converted to meaningful engineering data by using conversion factors. The output from all six devices was monitored and recorded for each test using computer software.

In all tests, beam deflection was measured by linear potentiometers in three places: at each end of the beam, and at midspan. At each end of the beam, one 2-inch linear potentiometer was placed approximately 6-inches away from the support and approximately 1-inch inside the bottom face of the beam. These linear potentiometers at the ends of the beam were used to ensure that the pin and roller supports did not deflect by unexpectedly large amounts and verify that the supports did not settle during a test. At midspan, two 6-inch linear potentiometers were placed on either side of the beam approximately 1-inch away from the edge of the bottom face. The average value of these two linear potentiometers was taken as the midspan deflection of the beam. All four linear potentiometers were carefully placed and plumbed before each test. Figure 4-7 displays a photograph of the two linear potentiometers located at midspan and Figure 4-8 displays a photograph of a linear potentiometer located at a support.

Figure 4-7 Linear Potentiometers Located at Midspan

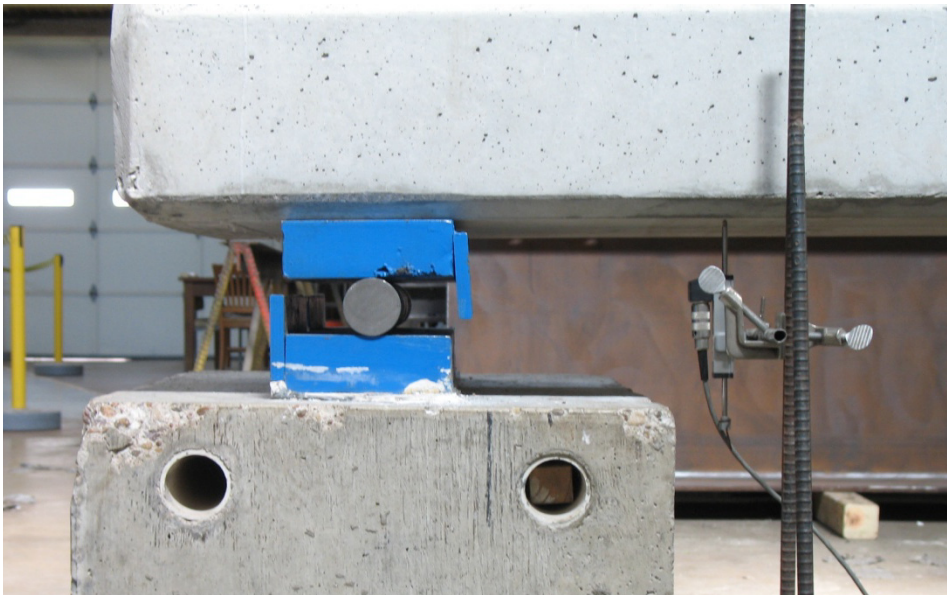

Figure 4-8 Linear Potentiometer Located at a Support (Type-C Beam)

The load applied during a test was measured using two devices. The load was explicitly measured using a 400-kip capacity load cell and verified using a pressure transducer. The pressure transducer converted the hydraulic pressure in the hydraulic

line into an equivalent applied load. The load cell, however, directly measured the applied load through internal strain gauges. It is for this reason that the load cell readings were taken as the actual load applied while the pressure transducer values were used to verify the load cell's accuracy.

When the beam was loaded in the range of its predicted cracking load, the load was maintained while the beam was visually inspected for cracks. Hand-held flashlights were used in an attempt to find the earliest crack possible. All visually observed cracks were marked on the beam and crack widths were measured using a crack comparator card. The largest crack width was recorded for each loading increment during the test. Figure 4-9 displays the use of crack comparator card to evaluate crack width.

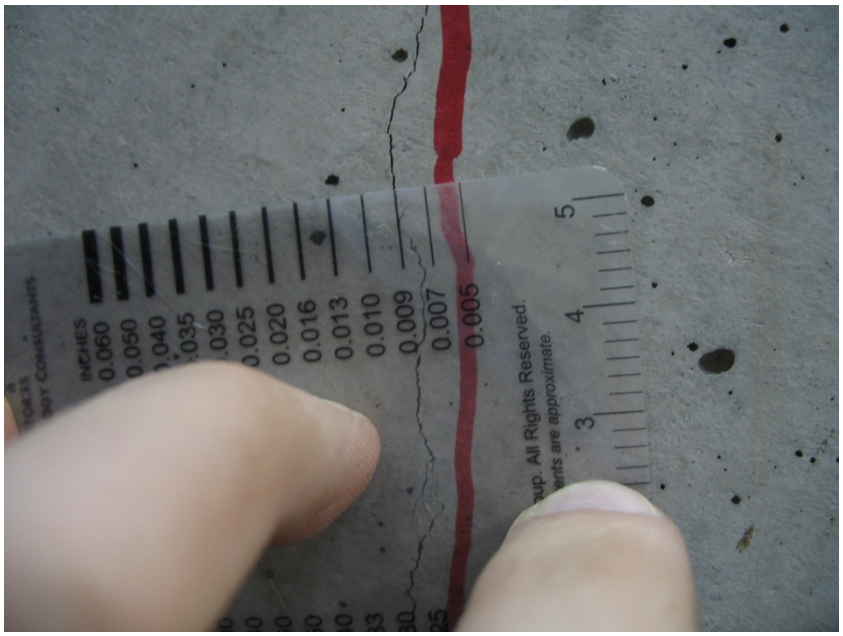

Figure 4-9 Crack Documentation using a Crack Comparator Card

Once the beams reached the maximum load, the beam was visually inspected, and then the load was completely removed from the beam. This concluded a flexural test of a Type-C girder.

4.3 TESTING OF FULL-SCALE 4B28 BOX BEAMS

Static flexural testing of ten TxDOT 4B28 box beams was performed to experimentally evaluate cracking load. The loading protocol, test setup, and instrumentation and data acquisition in these tests are described in the following sections.

4.3.1 Load Protocol

The box beams were initially loaded with brief breaks up to approximately 85-percent of their predicted cracking load. After visual inspection, the beams were loaded in increments of 5 kips up to visually observed cracking. Then, loading proceeded in increments of 10 kips up to an ultimate load approximately 20% above the observed cracking load (typically 200-220 kips). At each loading break, the beams were thoroughly inspected for cracks. Any observed cracks were marked and measured using a crack comparator card. Several photos were taken at each loading increment to document the crack propagation during the test. Figure 4-10 displays a visual representation of the loading protocol for the box beam tests.

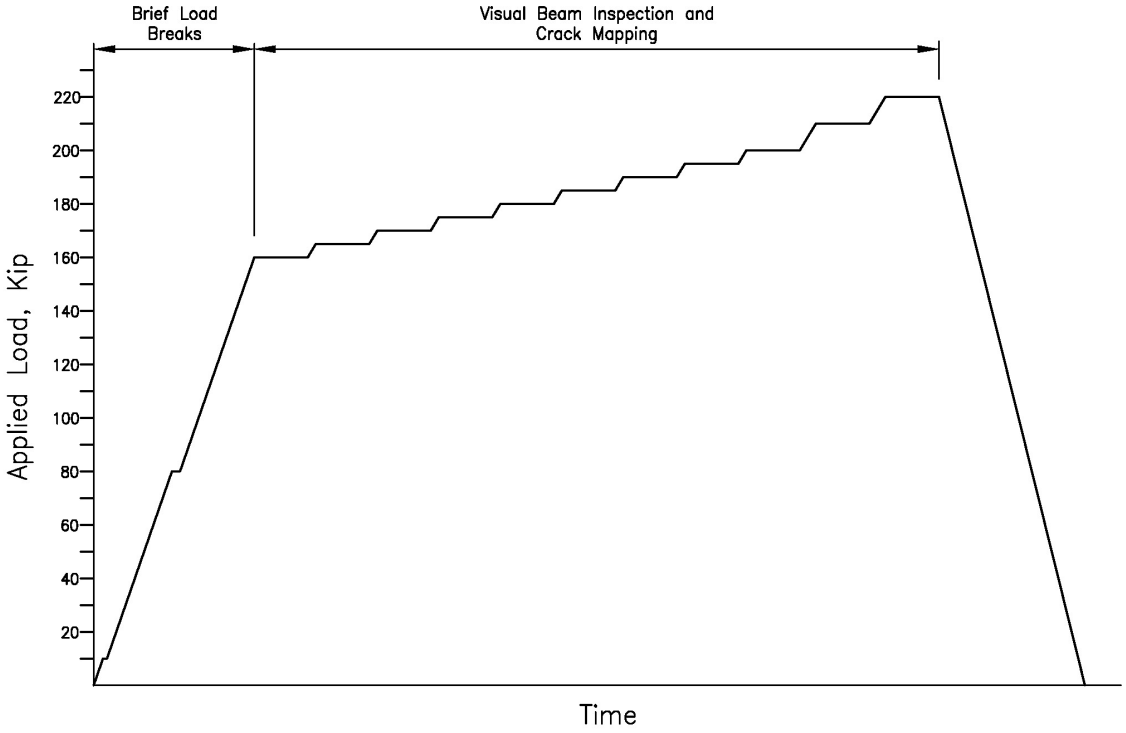

Figure 4-10 Box Beam Loading Protocol

4.3.2 Test Setup

The test setup used for the box beams was very similar to the test setup for the Type-C beams. All box beams were subjected to four point loading using the same reaction frame and hydraulic ram as described in section 4.2.2. The following items were stacked on top of the beam:

- 400-kip capacity load cell
- 8-inch Diameter steel spherical head and accompanying steel seat
- ¾-inch and 1-inch steel shim plates
- Three 64-inch long steel spreader beams oriented to create a 5-foot constant moment region at the center of the beam.
- Four 3 x10-inch Neoprene Bearing Pads

The four neoprene pads were centered under the webs of the beam and placed on top of the specimen. Each neoprene pad was 30-inches away from the center line of the

specimen, creating a 5-foot constant moment region during the test. The three blue beams were oriented as shown in Figure 4-11 to split the load applied by the ram and transfer it to the four neoprene pads. A ¾-inch thick plate was placed on top of the blue beams. The 8-inch diameter spherical head was placed on top of the steel plate and accounted for any slight eccentricities or non-level surfaces in the test setup. The load cell was placed directly on top of the spherical head followed by a 1-inch steel plate. As with the Type-C beams, these pieces were carefully aligned to ensure symmetric loading. To apply load to the specimen, hydraulic fluid was transferred to the ram by a pneumatic pump. As the hydraulic fluid entered the ram, the piston pressed down onto the assembly below, loading the specimen.

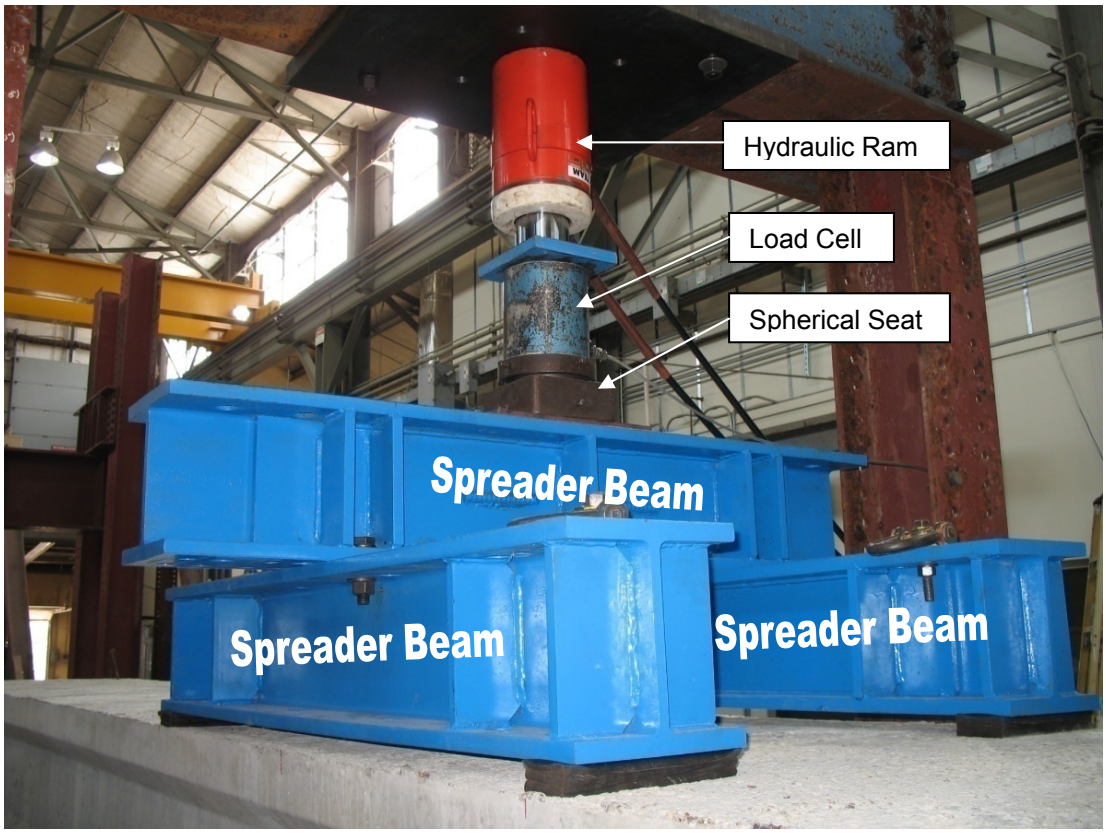

Figure 4-11 Box Beam Loading Apparatus

As with the Type-C beams, the box beams used simply supported conditions. In order to create these end conditions, a 2-inch thick steel rod was sandwiched between 2-

inch thick steel plates to create the pin and roller connections. For the pin connection, the rod was welded to the steel plate below, preventing any lateral translation. The roller connection was not welded, and could move freely. Pictures of the support conditions used in the box beam tests are displayed in Figure 4-12.

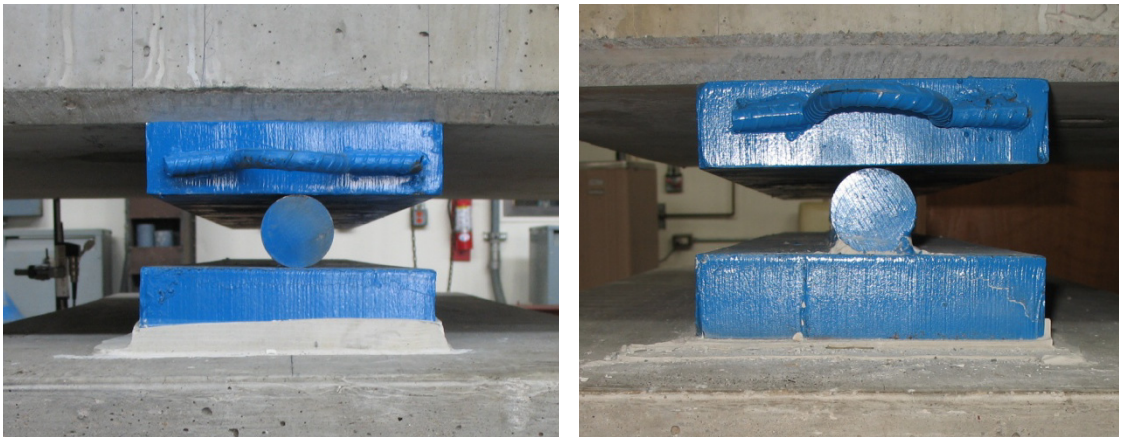

Figure 4-12 Box Beam Roller Support and Pin Support, respectively

After initial testing of the box beams, it was found that the soffit at the pinned end of the beam was not level. Therefore, the beam would not bear completely over the 48-inch long steel plate. To mitigate this problem, the 48-inch long steel plate on top of the pin connection was replaced with a 10-inch long steel plate. This allowed for complete bearing over the 10-inch plate. A photograph of the pinned end of the beam with the 10-inch top plate is displayed in Figure 4-13.

Figure 4-13 Pinned connection with 10-inch long top plate

For each box beam test, the beam was positioned such that the skewed end was part of the overhang beyond the roller support. This placement left a span of 36-feet between the well defined boundary conditions (pin and roller) for each box beam flexure test. A schematic drawing and picture of the test setup is displayed in Figure 4-14 and Figure 4-15 respectively

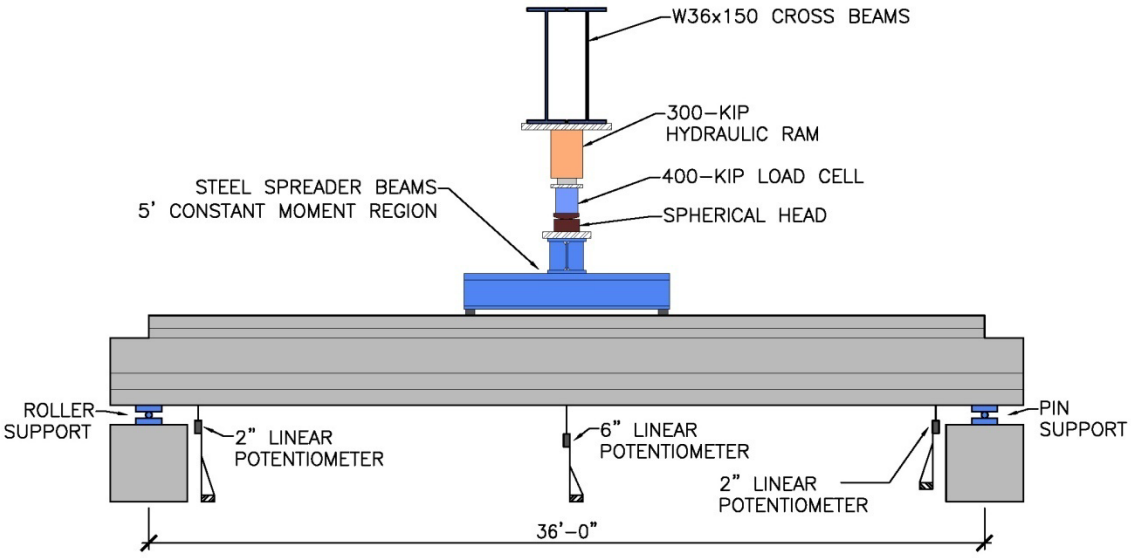

Figure 4-14 Box Beam Test Setup (Not to Scale)

Figure 4-15 Picture of Box Beam Flexural Test Setup

4.3.3 Instrumentation and Data Acquisition

The instrumentation used to monitor load, deflection, and support settlement during flexural testing of box beams was nearly identical to that of the Type-C beams. A thorough discussion of this instrumentation and the data acquisition process was presented in section 4.2.3.

Figure 4-16 displays the two 6-inch linear potentiometers located at midspan of the box beam specimen. As with the Type-C beam tests, additional 2-inch linear potentiometers were located at each support. Because the box beams were four feet wide, the 2-inch linear potentiometers were placed at the center of the bottom flange. Figure 4-17 displays a 2-inch linear potentiometer located near a support.

Figure 4-16 Linear Potentiometers Located at Midspan

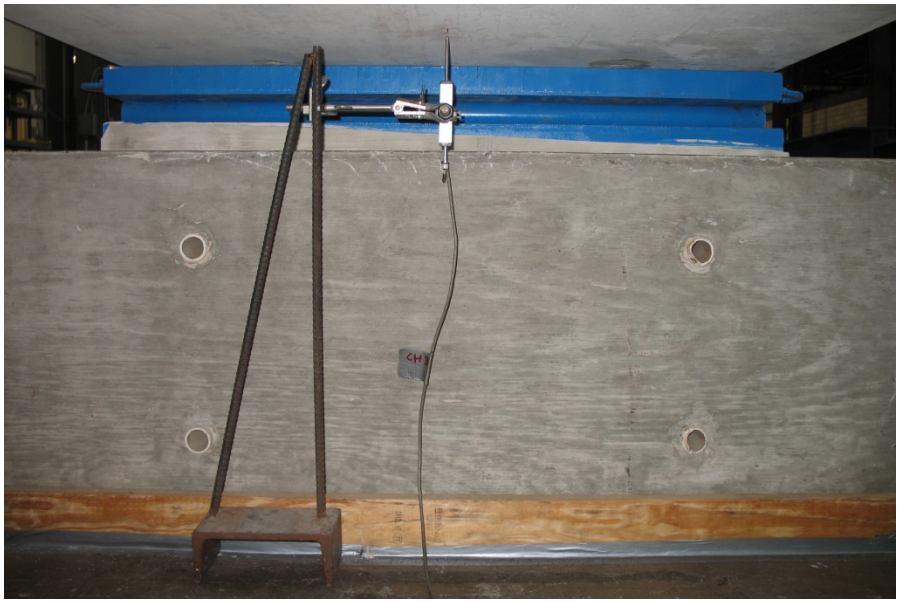

Figure 4-17 Linear Potentiometer Located at a Support (Box Beam)

4.4 SUMMARY

Part I of Phase II of TxDOT project 5197, reported herein, consisted of the flexural static testing of 45 Type-C beams and ten Box Beams. In the tests of the Type-C beams, the load was applied to create a 5-foot constant moment region in the middle of the beam. The load was applied up to approximately 30% above the beam's observed cracking load. During testing, applied load, midspan deflections, and support deflections were constantly monitored. For the tests of the box beams, the load was also applied to create a 5-foot constant moment region within the middle of the beam. The box beams were loaded up to approximately 20% above their observed cracking load. Applied load, midspan deflections and support deflections were monitored during testing.

In both the Type-C beam tests and the 4B28 box beam tests, loading was paused to visually inspect the beams and document crack formation. All visually observed cracks were marked and measured using a crack comparator card. Photographs were taken to document the crack growth during testing. The results of all static flexural testing are presented in Chapter 5.

CHAPTER 5
Analysis of Experimental Results

5.1 OVERVIEW

This chapter includes a presentation of the results and analysis from the full-scale flexural tests described in Chapter 4. The experimental research conducted under part 1 of phase II of project 5197 is presented in three sections:

- Type-C beam flexural test results and analysis
- 4B28 Box Beam flexural test results and analysis
- Experimental research on self consolidating concrete

The experimental results and analysis of the 45 Type-C beam flexural tests are presented in section 5.2. In each flexural test, measured cracking loads were compared to predicted cracking loads. The details of the procedure for measuring the cracking loads experimentally (Section 5.2.1) as well as the methods of predicting the cracking loads (Section 5.2.2) are presented. In order to predict the cracking loads, prestress losses were calculated with the NCHRP Report 496 method as well as the AASHTO-LRFD (2008) method as described in Chapter 2. Equations from both procedures used to calculate the predicted cracking load are presented. Finally, the data generated from this experimental research is compared to the prior flexural testing conducted by Birrcher and Bayrak (2007).

The test results and analysis of the 10 4B28 box beams are presented in Section 5.3. As with the Type-C beam specimens, the measured cracking loads were compared to predicted cracking loads for each box beam tested. The same methods (NCHRP 496 and AASHTO-LRFD 2008) were used to calculate prestress losses and predict cracking loads. The data from the box beam tests is then compared to the data from the Type-C beam tests along with the previous flexural testing by Birrcher and Bayrak (2007).

In addition to the results from the flexural tests, a discussion on the use of self consolidating concrete is presented in Section 5.4. Data from the five box beam specimens fabricated with SCC are presented and compared to those from the five box beam specimens fabricated with conventional concrete. The flexural behavior of beams made with these two types of concretes and observations made during beam fabrication and testing are also presented.

5.2 RESULTS OF TYPE-C BEAM TESTS

In this section, the methods used to measure and predict cracking loads in the 45 Type-C beam tests are presented. Section 5.2.1 describes the process of determining a specimen's cracking load and section 5.2.2 describes the two procedures (NCHRP 496 and AASHTO-LRFD 2008) used to calculate predicted cracking loads. For all 45 Type-C specimens, the accuracy of the predicted cracking load was determined based on the measured cracking load from the flexural tests. Finally for each Type-C beam, the accuracy of the specimen's predicted cracking load was plotted against the specimen's maximum compressive stress at release (measured at the critical section).

In order to identify each Type-C beam test specimen, a series of letters and numbers was used in the following format: LL-NN-N (Where L=letter and N = number). The first letter for each Type-C specimen was a C indicating that the specimen was a Type-C beam. The next letter was either A, B, C or D and represented the fabrication plant where the beams were produced. The next two numbers represented the target release strength for the beam (60, 65 or 70). Finally, the last number was used to identify a specific beam within a given casting. For example, fabricator A cast three beams with a target release strength of $0.70f'_{ci}$ on September 26, 2007. The three beams in that casting were designated CA-70-1, CA-70-2, and CA-70-3 respectively.

5.2.1 Measured Cracking Loads

In order to measure the cracking load of the test specimens, two primary methods were used: visual observations, and load deflection analysis. All visually observed

cracking was documented during loading breaks in flexural testing. At each load break, several research assistants using flashlights inspected the beam for any cracking. Effort was made to ensure a thorough visual inspection in order to catch any small flexural cracks during testing. The load at which the first crack was found was termed the visually observed cracking load.

In addition to visually observed cracking loads, an analysis of the load-deflection plot from the flexural tests was used to measure cracking loads. This analysis, as shown in Figure 5-1 and Figure 5-2, was a simple procedure that involved drawing two straight lines. The first line traced the initial linear-elastic portion of the load-deflection plot. The second straight line was traced along the portion of the load-deflection plot that indicated the significant departure from linearity. The intersection of these two lines provided the point at which the load deflection plot became non-linear. For each specimen, the load at the intersection of these two lines was taken as the measured cracking load.

The visually observed cracking loads were used to verify the measured cracking loads in this analysis. It is important to note that great effort was taken to ensure the most accurate cracking loads were taken from all 45 flexural tests. Figure 5-1 displays a sample load deflection plot of Series 1 specimen CA-60-3. Figure 5-2 includes a sample load deflection plot of Series 2 specimen CC-70-2. Both of these load deflection plots display the applied load measured by the load cell and the average deflection of the two 6-inch linear potentiometers located at midspan.

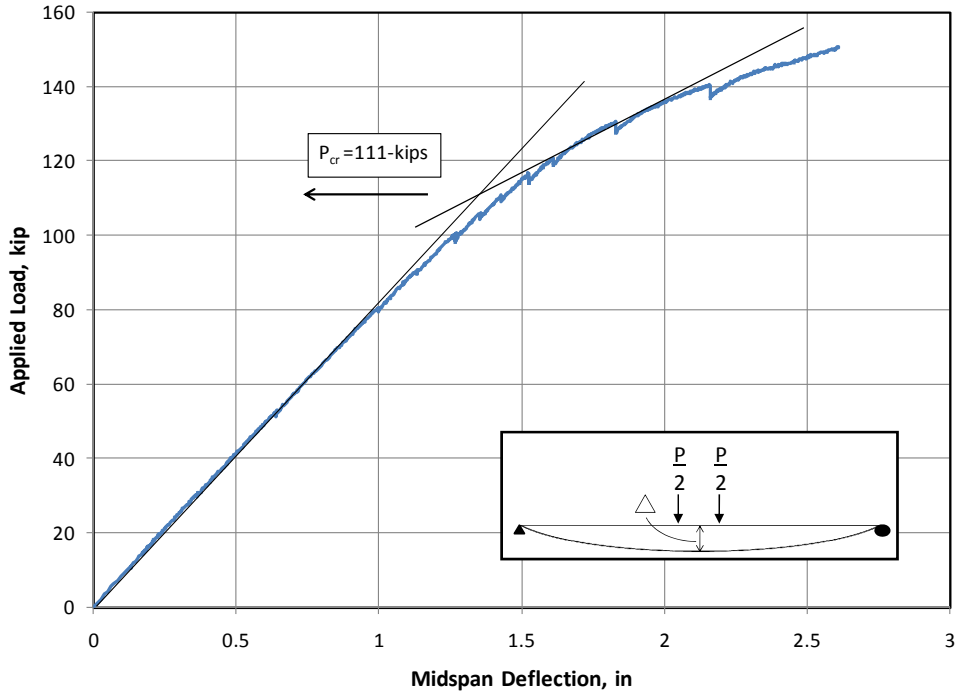

Figure 5-1 Applied Load versus Midspan Deflection for Specimen CA-60-3

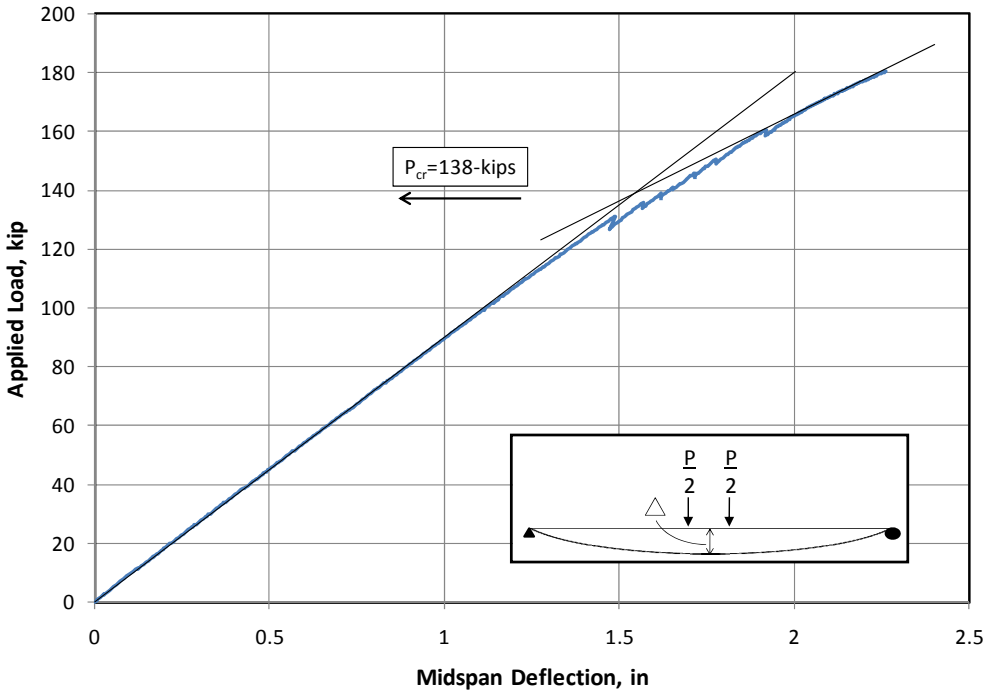

Figure 5-2 Applied Load versus Midspan Deflection for Specimen CC-70-2

During the Type-C beam tests, visually observed cracking loads were documented. These were used to verify the measured cracking loads obtained from the load-deflection plots. The first visually observed cracks occurred within the 5-foot constant moment region. The first cracks were located on the bottom flange of the specimen and progressed upward through the beam as the load was increased. All initial cracks were small and slowly progressed to a typical maximum crack width of 0.010-inches for Series 1 beams and 0.007-inches for Series 2 beams. Figure 5-3 and Figure 5-4 display the first visually observed crack for Series 1 Beam CA-60-1 and Series 2 Beam CD-65-5 respectively. In addition, Figure 5-5 displays a sketch of the typical crack patterns at the maximum applied load for Series 1 and Series 2 beams.

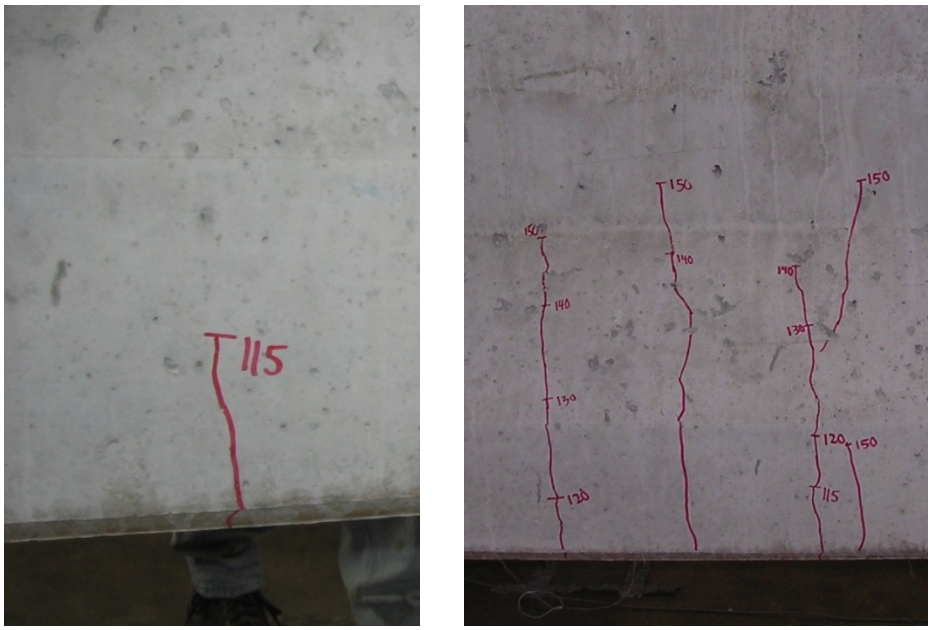

P = 115-kips P = 150-kips

Figure 5-3 Visually observed cracking load for Series 1 Beam CA-60-1

P = 147-kips P = 180-kips

Figure 5-4 Visually observed cracking load for Series 2 Beam CD-65-5

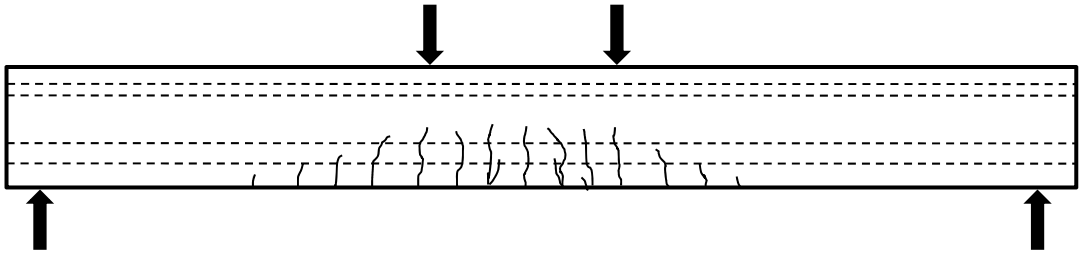

Figure 5-5 Typical crack pattern at maximum applied load for Type-C Beam tests

Measured cracking loads for all 45 Type-C beams were calculated by analyzing the load deflection plots and verified with the visually observed cracking loads. The measured cracking loads, maximum crack widths, and test dates for all Series 1 and Series 2 tests are displayed in Table 5-1 and Table 5-2 respectively.

Table 5-1 Measured Cracking Loads for Series 1 Type-C Beams

Fabricator	Beam Mark	Measured Cracking Load (kip)	Maximum Crack Width at Maximum Applied Load (in)	Date of Test
A	CA-70-3	107	0.007	11/1/2007
A	CA-70-2	110	0.007	11/15/2007
A	CA-70-1	108	0.009	11/27/2007
A	CA-60-1	111	0.010	11/29/2007
A	CA-60-2	112	0.009	12/4/2007
A	CA-60-3	111	0.010	12/12/2007
A	CA-65-1	110	0.010	12/18/2007
A	CA-65-2	107	0.010	1/4/2008
A	CA-65-3	113	0.010	1/8/2008
A	CA-65-4	110	0.010	1/10/2008
A	CA-65-5	111	0.010	1/15/2008
A	CA-65-6	109	0.010	1/17/2008
B	CB-60-1	130	0.007	6/19/2008
B	CB-60-2	126	0.007	6/23/2008
B	CB-60-3	120	0.007	6/24/2008
B	CB-70-1	118	0.007	6/25/2008
B	CB-70-2	121	0.007	6/26/2008
B	CB-70-3	118	0.009	6/27/2008
B	CB-70-4	110	0.009	7/1/2008
B	CB-70-5	118	0.007	7/2/2008
B	CB-70-6	112	0.009	7/7/2008

Table 5-2 Measured Cracking Loads for Series 2 Type-C Beams

Fabricator	Beam Mark	Measured Cracking Load (kip)	Maximum Crack Width at Maximum Applied Load (in)	Date of Test
C	CC-70-1	142	0.007	5/23/2008
C	CC-70-2	138	0.005	5/27/2008
C	CC-70-3	139	0.007	5/29/2008
C	CC-65-1	136	0.007	5/29/2008
C	CC-65-2	141	0.007	6/2/2008
C	CC-65-3	135	0.007	6/3/2008
C	CC-65-4	134	0.007	6/10/2008
C	CC-65-5	141	0.005	6/11/2008
C	CC-65-6	142	0.005	6/12/2008
C	CC-60-1	130	0.007	6/12/2008
C	CC-60-2	130	0.007	6/17/2008
C	CC-60-3	138	0.007	6/18/2008
D	CD-70-1	142	0.007	4/2/2008
D	CD-70-2	143	0.007	4/7/2008
D	CD-70-3	147	0.005	4/10/2008
D	CD-65-1	143	0.005	4/14/2008
D	CD-65-2	135	0.005	4/18/2008
D	CD-65-3	137	0.007	4/21/2008
D	CD-65-4	136	Hairline	4/24/2008
D	CD-65-5	148	0.005	4/29/2008
D	CD-65-6	143	0.005	5/1/008
D	CD-60-1	143	0.005	5/5/2008
D	CD-60-2	146	0.007	5/12/2008
D	CD-60-3	142	0.005	5/20/2008

5.2.2 Predicted Cracking Loads

In order to estimate cracking loads in an unbiased and consistent manner, two methods were used: the NCHRP Report 496 method and the AASHTO-LRFD (2008) method. The details of these prestress loss prediction methods were discussed in detail in Chapter 2. Both procedures use time-dependant equations to estimate prestress losses. For the purposes of this research, the following four prestress loss components were considered:

- Elastic Shortening
- Prestressing Strand Relaxation
- Creep of Concrete
- Shrinkage of Concrete

All loss components were calculated from the time of prestress transfer to the time of the flexural test. The loss equations given in the NCHRP 496 method and the AASHTO-LRFD (2008) method were used to generate an expected cracking moment for each beam. The simply supported conditions along with the applied loading pattern in the Type-C beam tests (discussed in Chapter 4) produce the shear force and bending moment diagrams shown in Figure 5-6. Based on the moment diagram and the calculated cracking moment, Equation 5-1 was used to calculate the expected cracking load for Type-C beam specimens.

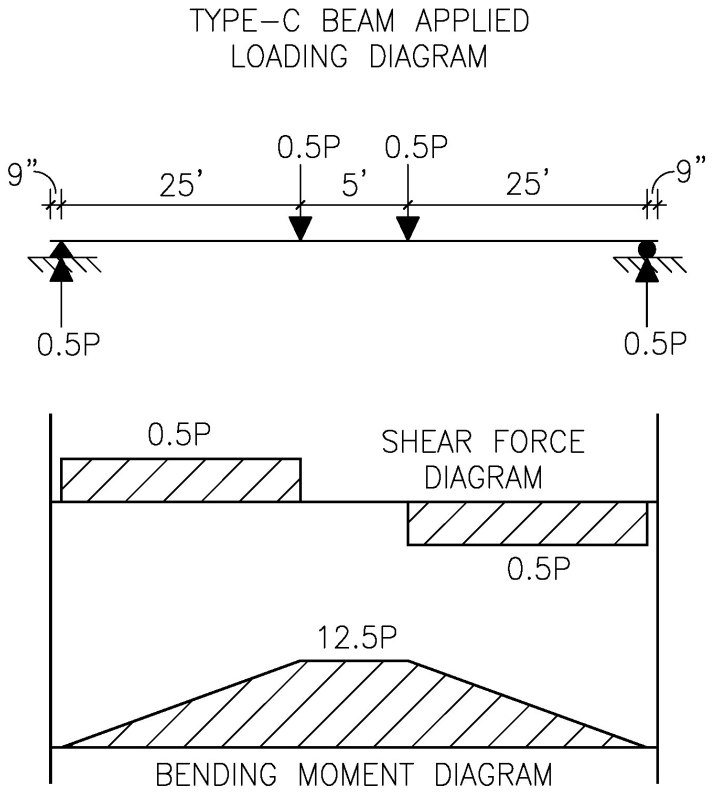

Figure 5-6 Type-C Beam Specimens: Applied Load, Shear Force, and Bending Moment Diagrams

$$P_{predicted} = \left(\frac{4}{L_c\text{-}5'}\right)(M_{cr}) - W_{app} \qquad \textbf{Equation 5-1}$$

where, L_c is the simply supported span length (55-feet for Type-C girders)

W_{app} is the total weight of the items stacked on top of the test specimen prior to loading. (W_{app} = 0.772 kips for Type-C Specimens)

M_{cr} is the predicted cracking moment accounting for prestress losses and member self weight (ft-k)

For all Type-C beam specimens, the measured load was compared to the predicted load using Equation 5-2. This comparison provided a consistent means of determining the accuracy of both the NCHRP 496 method and the AASHTO-LRFD (2008) method.

$$Accuracy = \left(\frac{P_{measured}-P_{predicted}}{P_{measured}}\right)(100) \qquad \textbf{Equation 5-2}$$

where, $P_{measured}$ is the cracking load determined from physical testing (kip)

$P_{predicted}$ is the cracking load determined from analysis (kip)

Using Equation 5-2, along with the NCHRP 496 prestress loss calculation procedure or the AASHTO-LRFD (2008) procedure, the accuracy of the predicted cracking loads were calculated in a consistent manner. Sections 5.2.2.1 and 5.2.2.2 discuss the use of the NCHRP 496 and the AASHTO-LRFD (2008) methods respectively.

5.2.2.1 NCHRP Report 496 Method

This section provides the equations and procedures used to calculate the cracking moment according to the NCHRP 496 procedure. The equations provided by the NCHRP 496 procedure were explicitly followed in determining the cracking moment for each of the 45 Type-C beams tested in flexure.

As mentioned in Chapter 2, both the NCHRP 496 and the AASHTO-LRFD (2008) material properties equations contain a K_1 factor to recognize the variation of local materials with respect to the national average. In order to accurately reflect the variation in local material properties from each of the five fabricators in this research, the K_1 factor was calculated empirically. The following steps were followed to calculate the K_1 factor for each of the four fabricators that produced Type-C girders:

1. Calculate the empirical modulus of elasticity using Equation 5-3

2. Back-calculate the apparent modulus of elasticity (Equation 5-4) by tracing the initial linear-elastic portion of the load deflection plot. Figure 5-7 displays a sample load deflection plot with the estimated linear elastic portion for specimen CB-70-1.
3. Calculate an average empirical modulus and the average apparent modulus for each fabricator.
4. For each fabricator, divide the average apparent modulus by the average empirical modulus to arrive at the K_1 value.

$$E_c = 33{,}000K_1K_2\left(0.140+\frac{f'_c}{1000}\right)^{1.5}\sqrt{f'_c} \qquad \textbf{Equation 5-3}$$

where, K_1 and K_2 are equal to unity (to reflect the national average empirical modulus)

$$\Delta_{mid} = \left(\frac{Pa}{24E_cI}\right)\left(3L^2-4a^2\right) \qquad \textbf{Equation 5-4}$$

where, P= applied concentrated load 2-½ feet away from midspan (kips)

L= simply supported span length of specimen (in)

a= distance from the support to a concentrated load (in)

E_c= modulus of elasticity (ksi)

I= moment of inertia of the cross section (in^4)

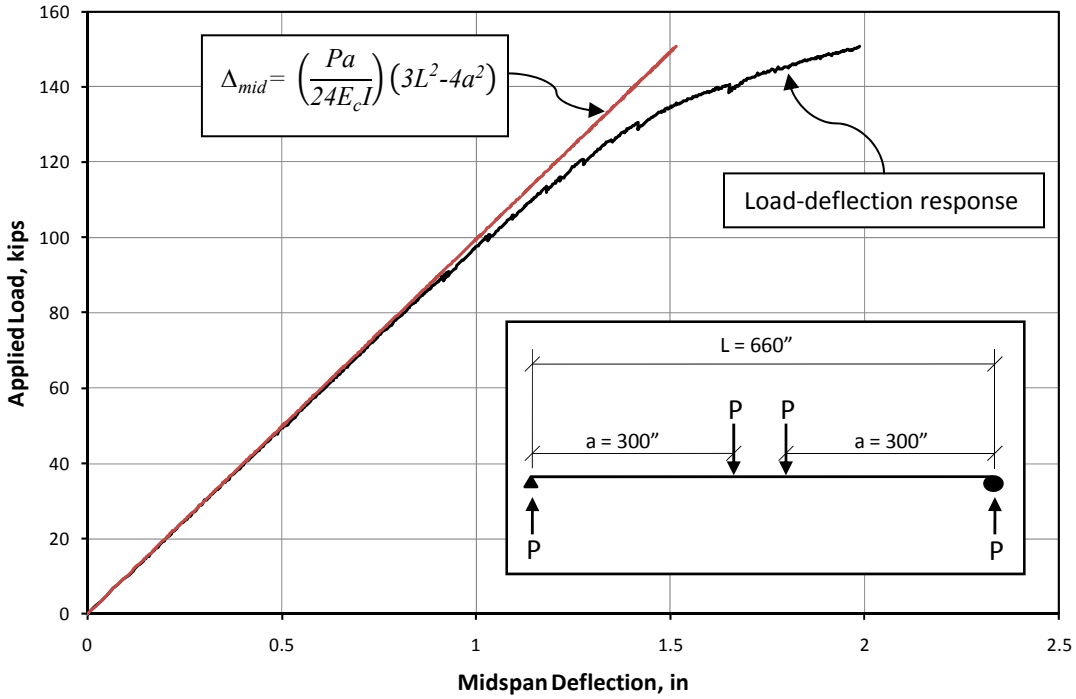

Figure 5-7 Estimated initial slope of load deflection plot to calculate the apparent modulus of elasticity for CB-70-1

Equation 5-3 is the NCHRP 496 equation for the modulus of elasticity and Equation 5-4 is derived from a linear elastic structural analysis of the flexural test setup. Dividing these two values provides a representation of local material properties relative to the national average. The process of calculating a K_1 factor was completed for each of the 45 Type-C beams tested in this study. These values are displayed in Table 5-3.

Table 5-3 Calculated K_1 values

Fabricator	Average K_1 Value
A	1.0
B	1.1
C	1.0
D	1.0

As shown in Table 5-3, the elastic moduli exhibited in the Type-C beam flexural tests was close to the national empirical moduli as calculated by Equation 5-3. In addition to the K_1 factor, the NCHRP 496 procedure uses a K_2 factor to represent an upper bound, lower bound, or average value. For purposes of this research, a K_2 value of 1.0 representing the average value was deemed appropriate. Once the K_1 and K_2 factors were incorporated into the material properties equations as shown in Chapter 2, the prestress loss equations of the NCHRP 496 method could be used accurately. In order to calculate the predicted cracking moment of the test specimens, Equation 5-5 through Equation 5-8 were used. First, Equation 5-5 was used to calculate the bottom-fiber stress of the specimen at prestress transfer. It is important to note that transformed section properties are used in Equation 5-5. Using transformed properties with the prestressing force just prior to release implicitly accounts for the loss component due to elastic shortening.

$$f_{cbi} = P_i\left(\frac{1}{A_{ti}} + \frac{e_{pti}y_{bti}}{I_{ti}}\right) - \frac{M_g y_{bti}}{I_{ti}} \qquad \textbf{Equation 5-5}$$

where,

P_i = Initial prestressing force immediately before transfer (kips)

A_{ti} = Area of the transformed section at prestress transfer (in^2)

e_{pti} = Eccentricty of the strands within the transformed cross section at prestress transfer (in)

y_{bti} = Distance from beam bottom fiber to centroid of the transformed section at prestress transfer (in)

I_{ti} = Moment of inertia of the transformed section at prestress transfer (in^4)

M_g = Self weight moment at midspan (in-k)

Once the bottom fiber stresses was computed, the next step was to calculate the reduction in prestressing force due to time dependant prestress losses. Equation 5-6 displays the equation that can be used to calculate the reduction in prestressing force due to shrinkage, creep, and relaxation losses. Elastic shortening is not included in this equation because it is implicitly accounted for in Equation 5-5.

$$\Delta P = \left(\Delta f_{pSR} + \Delta f_{pCR} + \Delta f_{pR}\right) * A_{ps} \qquad \textbf{Equation 5-6}$$

where, ΔP= Reduction of initial prestress force (kips)

Δf_{pSR}= Loss of prestress due to concrete shrinkage (ksi)

Δf_{pCR}= Loss of prestress due to concrete creep (ksi)

Δf_{pR}= Loss of prestress due to relaxation of strands (ksi)

A_{ps}= Area of prestressing strands (in^2)

Once the force reduction due to prestress loss is known, the change in bottom fiber stress due to this force reduction can be calculated. This calculation is shown in Equation 5-7.

$$\Delta f_{cb} = \left(\frac{\Delta P}{A_{tt}} + \frac{\Delta P e_{tt} y_{btt}}{I_{tt}}\right) \qquad \textbf{Equation 5-7}$$

where, Δf_{cb}= change in bottom fiber stress due to prestress losses (ksi)

ΔP= Loss of initial prestress force (kip)

A_{tt}= Area of the transformed section at the time of the flexural test (in^2)

e_{tt}= eccentricity of the strands in the transformed section at the time of the flexural test (in)

y_{btt}= distance from bottom fiber to centroid of transformed section at the time of flexural test (in)

I_{tt}= Moment of inertia of transformed section at time of flexural test (in^4)

Once the change in bottom fiber stress is known, the cracking moment can be calculated. As shown in Equation 5-8 the change in bottom fiber stress, Δf_{cb}, is subtracted from the bottom fiber stress at prestress transfer, f_{cbi}, and added to the modulus of rupture for concrete, f_r. The result gives the bottom fiber stress at which cracking will occur. Multiplying this stress by the moment of inertia of the transformed section and dividing by y_{btt} gives the predicted cracking moment.

$$M_{cr} = \frac{I_{tt}}{y_{btt}}\left(f_{cbi} - \Delta f_{cb} + f_r\right) \qquad \textbf{Equation 5-8}$$

where, M_{cr}=Predicted cracking moment (in-kip)

f_r=Tensile strength of concrete taken as $\frac{7.5}{1000}\sqrt{f'_c}$ (f'_c in psi, f_r in ksi)

I_{tt}, y_{btt}, f_{cbi}, Δf_{cb} are defined above

Upon calculating the predicted cracking moment from Equation 5-8, the predicted cracking load was computed using Equation 5-1. This procedure was completed for all 45 Type-C beam flexural tests. For each test, the accuracy of the cracking load prediction was computed using Equation 5-2. Finally for each beam, the accuracy measurement was plotted against the beam's maximum compressive stress at release (measured at the critical section).

As mentioned in Chapter 1, Phase I of project 5197 (Birrcher and Bayrak, 2007) involved the flexural testing of thirty six specimens. In the same process as the Type-C specimens, predicted cracking loads were calculated using NCHRP 496 prestress loss

equations. In order to make appropriate conclusions about the live load performance of prestressed girders stressed beyond the allowable limit, the data from Birrcher and Bayrak (2007) must be incorporated with the data generated by the Type-C beams. Combining the data from both phases of the project allows for a complete picture of the test results. The accuracy of cracking load calculations for the 45 Type-C beam specimens along with results from Birrcher and Bayrak (2007) are displayed graphically in Figure 5-8. It is important to note that the NCHRP 496 prestress loss equations were used to calculate predicted cracking loads in the data shown in Figure 5-8.

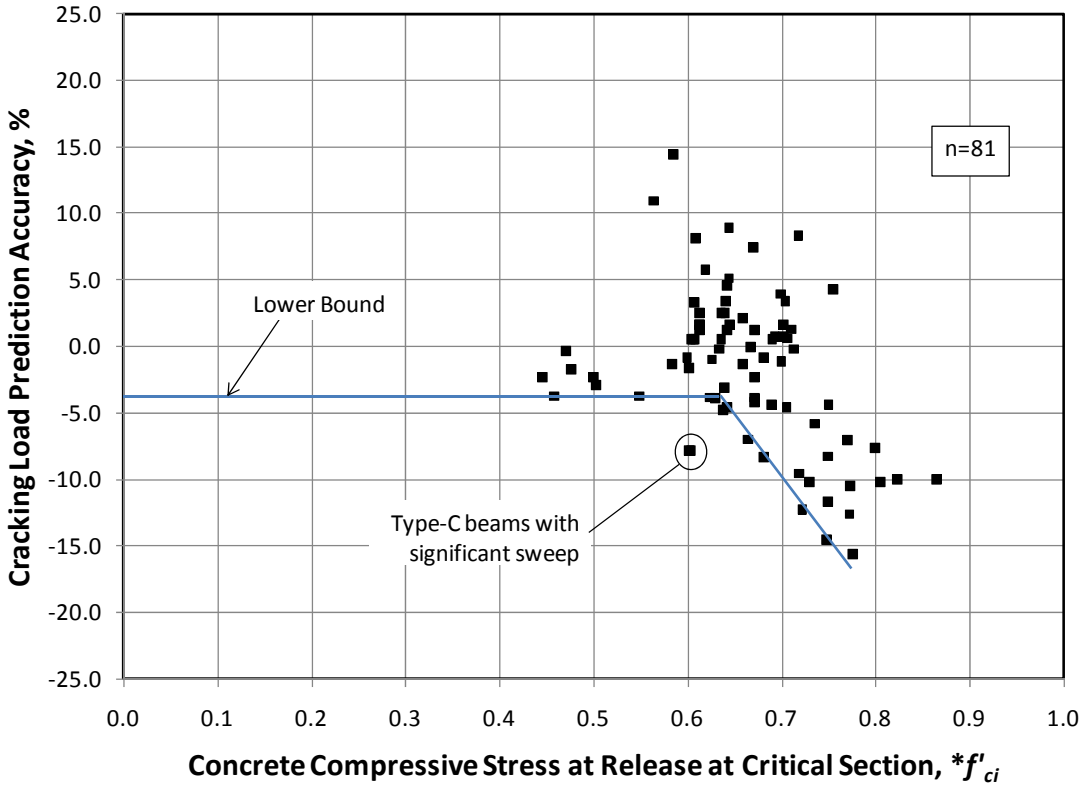

Figure 5-8 Comparison of measured and predicted cracking loads using NCHRP 496 losses

It is important to note that two Type-C beam test specimens (circled in Figure 5-8) exhibited significant sweep upon arrival to Ferguson Structural Engineering Lab. During the flexural tests of these two specimens, the East face of the beam specimens

cracked much earlier than the West face of the beam. As shown in Figure 5-8 these two beams exhibited a lower than expected cracking load due to premature cracking on the East face. Because of the nature of this premature cracking, the specimens were not considered to be representative of the behavior of typical Type-C beams.

As seen in Figure 5-8, there is a noticeable decline in accuracy as the concrete compressive stress at release increases. This decline in accuracy indicates that the test specimens subjected to higher levels of compressive stress at release exhibited flexural cracking earlier than predicted by the NCHRP 496 process. The data from Figure 5-8 was interpreted using the lower-bound line drawn with respect to all the data. In analyzing the test results displayed in Figure 5-8 it was assumed that a 5% error in predicted cracking load accuracy was acceptable and therefore used as the criteria for beams subjected to a maximum compressive stress at release greater than $0.60f'_{ci}$. Based on the lower bound line, the data suggests that a noticeable (greater than 5%) decrease in accuracy occurs at a maximum compressive stress at release of approximately $0.65f'_{ci}$.

5.2.2.2 AASHTO-LRFD 2008 Method

In addition to the NCHRP Report 496 method, the equations in the AASHTO-LRFD Interim 2008 specification were used to predict the cracking loads of the test specimens. This section details the AASHTO-LRFD (2008) procedure used to calculate the predicted cracking load for all 45 Type-C girders tested in this study.

As mentioned in Chapter 2, the AASHTO-LRFD (2008) method utilizes the same K_1 factor discussed in section 5.2.2.1. Unlike the NCHRP 496 method, the AASHTO-LRFD (2008) procedure only uses this K_1 factor for its modulus of elasticity equation. The absence of the K_1 factor in the shrinkage strain and creep coefficient equations make the AASHTO-LRFD (2008) procedure easier for designers to use, but less responsive to local materials. Therefore the K_1 factors shown in Table 5-3 were only incorporated into the AASHTO-LRFD (2008) modulus of elasticity calculation.

In order to determine the predicted cracking moment according to the AASHTO-LRFD (2008) method, an effective prestressing force and gross section properties were

used. Gross section properties aid the designer in simplicity, but cannot be used to implicitly account for elastic shortening. Therefore, in the AASHTO-LRFD (2008) method, a separate elastic shortening loss equation (see Chapter 2) was used. Equation 5-9 displays the equation used to calculate the effective prestressing force.

$$P_{eff} = \left(\Delta f_{pES} + \Delta f_{pSR} + \Delta f_{pCR} + \Delta f_{pR}\right)\left(A_{ps}\right) \qquad \textbf{Equation 5-9}$$

where, P_{eff}= Effective prestressing force (kips)

Δf_{pES}= Loss of prestress due to elastic shortening (ksi)

Δf_{pSR}= Loss of prestress due to concrete shrinkage (ksi)

Δf_{pCR}= Loss of prestress due to concrete creep (ksi)

Δf_{pR}= Loss of prestress due to strand relaxation (ksi)

A_{ps}= Area of prestressing strands (in^2)

Once the effective prestressing force was estimated, the predicted cracking moment was calculated. Equation 5-10, uses gross section properties along with the effective prestressing force to provide an estimated cracking moment.

$$M_{cr} = \left(\frac{I_g}{y_{bg}}\right)\left(\frac{P_{eff}}{A_g} + \frac{P_{eff} e_p y_{bg}}{I_g} - \frac{M_g y_{bg}}{I_g} + f_r\right) \qquad \textbf{Equation 5-10}$$

where, I_g= moment of inertia of the gross section (in^4)

y_{bg}=distance from the bottom fiber to the centroid of the gross section (in)

P_{eff}= Effective prestressing force (kips)

A_g= Area of gross section (in^2)

e_p= Eccentricity of prestressing strands (in)

M_g= Specimen self weight moment (in-kips)

f_r=Tensile strength of concrete taken as $\frac{7.5}{1000}\sqrt{f'_c}$ (f'_c in psi, f_r in ksi)

Once the predicted cracking moment was calculated, Equation 5-1 was used to determine the predicted cracking load of the specimen. After all the cracking loads were experimentally determined, Equation 5-2 was used to measure the accuracy of the AASHTO-LRFD (2008) predictions. This process was completed for all 45 Type-C beam test specimens in this study. As in section 5.2.2.1, the accuracy of the predicted cracking loads were plotted against the specimens' maximum compressive stress at release (measured at the critical section).

As with the data from section 5.2.2.1, the data from the Type-C beam tests was combined with the results from Birrcher and Bayrak (2007) in order to obtain comprehensive results and analyze the complete set of test data. The results of the 45 Type-C test specimens using the AASHTO-LRFD (2008) prestress loss equations are displayed along with the results from Birrcher and Bayrak (2007) in Figure 5-9.

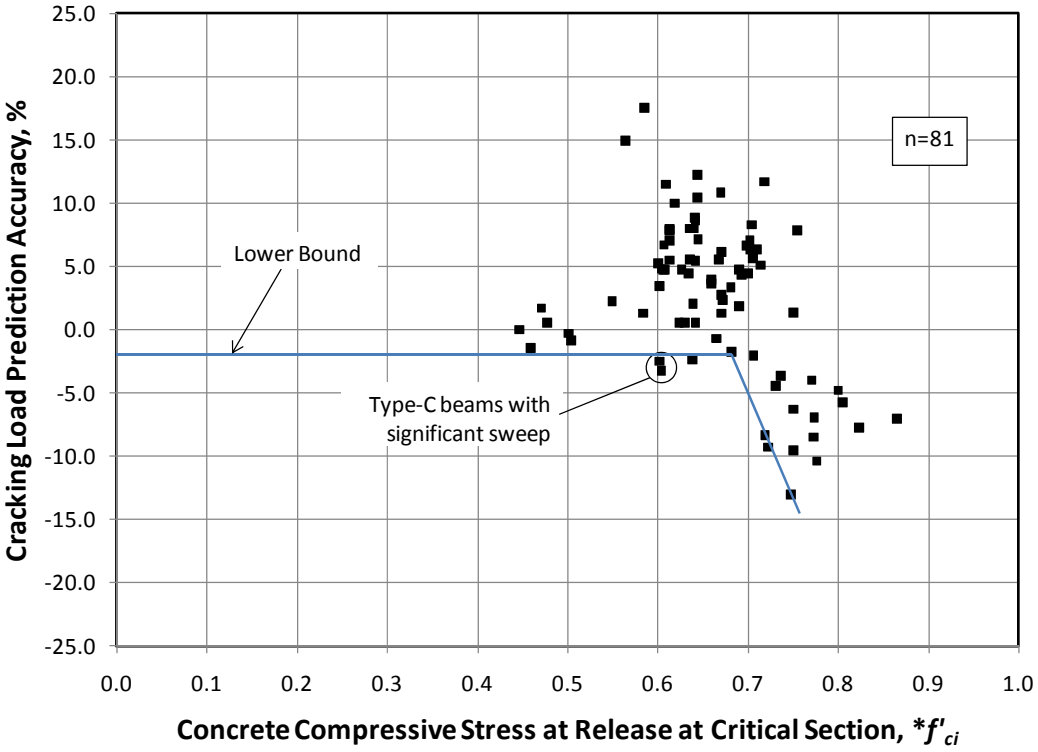

Figure 5-9 Comparison of measured and predicted cracking loads using AASHTO-LRFD 2008 losses

As with the NCHRP 496 plot (Figure 5-8) the two Type-C beams that exhibited significant sweep are circled in Figure 5-9. Because of the sweep, it was determined that these two specimens did not adequately represent typical Type-C beam behavior in flexure.

To analyze the test results shown in Figure 5-9, the lower bound line was again used. As with the NCHRP 496 plot, a 5% prediction error tolerance was deemed acceptable and used as the criteria to evaluate the test data. Based on this error tolerance, the data suggests that a substantial loss of prediction accuracy occurs when specimens are subjected to a maximum compressive stress at release greater than $0.7f'_{ci}$. Comparing this value with that obtained from the NCHRP plot ($0.65f'_{ci}$) suggests that the AASHTO-LRFD 2008 procedure would justify a higher allowable compressive stress at prestress transfer. It should be noted, however, that the use of gross section properties in the

AASHTO-LRFD (2008) prestress loss calculations creates a source of error. Using transformed section properties in the NCHRP 496 procedure was more responsive to individual test specimen geometry. This difference suggests that the NCHRP 496 procedure may be a more appropriate method to determine an acceptable allowable compressive stress at prestress transfer. A recommendation for increasing the maximum allowable compressive stress at prestress transfer is provided in Chapter 6. A table with the testing details for each of the 45 Type-C beams is included in Appendix C.

5.3 RESULTS OF BOX BEAM TESTS

In this section, the methods used to measure and predict cracking loads for the 10 4B28 box beam tests are presented. The purpose of investigating these box beams was to perform proof testing on an allowable limit that seemed appropriate based on the results from the Type-C beam testing. For this reason, four concrete mixture designs were used and all ten beams were targeted for a maximum compressive stress at release of $0.66f'_{ci}$. Additional information about the fabrication of these beams was presented in Chapter 3.

Section 5.3.1 includes a description of the procedure used to determine a box beam specimen's measured cracking load and Section 5.3.2 includes a summary of the two procedures (NCHRP 496 and AASHTO-LRFD 2008) used to calculate predicted cracking loads. As with the Type-C specimens, the accuracy of the predicted cracking load was determined based on the measured cracking load from the box beam flexural tests. Finally, the data from the box beam tests was plotted with the data from the Type-C beam tests and the data from Birrcher and Bayrak (2007).

In order to uniquely identify each box beam, a numbering system was used. This numbering system was in the following format: LL-NN (L=letter and N=number). The first two letters were "BB" standing for box-beam. The following two numbers indicated a specific box beam (01 through 10). The table containing all the detailed fabrication information about each individual box beam (presented in Chapter 3) is reproduced here for convenience.

Table 5-4 Box Beam Design Details

Beam Mark	Target Release Strength	Concrete Type	Coarse Aggregate Type	Skewed End Void Geometry
BB-01	4100 psi	Conventional	Limestone	30° Skew
BB-02	4100 psi	Conventional	Limestone	Square
BB-03	4100 psi	Conventional	Hard River Gravel	30° Skew
BB-04	4100 psi	Conventional	Hard River Gravel	Square
BB-05	4100 psi	Conventional	Hard River Gravel	Half Square/ Half Skew
BB-06	4100 psi	Self Consolidating	Limestone	30° Skew
BB-07	4100 psi	Self Consolidating	Limestone	Square
BB-08	4100 psi	Self Consolidating	Hard River Gravel	30° Skew
BB-09	4100 psi	Self Consolidating	Hard River Gravel	Square
BB-10	4100 psi	Self Consolidating	Hard River Gravel	Half Square/ Half Skew

In addition to experimentally measuring the cracking load of the box beam specimens, camber measurements and end region cracking due to prestress transfer were documented for each box beam. These items were monitored to determine if the four different mixture designs used to fabricate the beams as well as the maximum compressive stress at prestress transfer ($0.66f'_{ci}$) would have any impact on the overall quality of the beam. The results of the camber measurements indicated that beams fabricated with SCC contained higher cambers than those fabricated with conventional concrete. The results from the camber measurements are discussed further in section 5.4. No major concerns were noticed with the end region cracking and schematic diagrams documenting the observed cracks in the box beam end regions are presented in Appendix D.

5.3.1 Measured Cracking Loads

As with the Type-C beam specimens, both visually observed cracking loads and analysis of load-deflection plots were used to determine the measured cracking load. The visually observed cracking loads were determined during load breaks. As with the Type-C beams, researchers with flashlights inspected the beam at each loading break to identify

and mark cracks. The first observed flexural crack during flexural testing was defined as the visually observed cracking load.

In addition to visual observations, load deflection plots were analyzed to identify the cracking load in the same manner as the Type-C beam specimens. Two straight lines were drawn on the load deflection plot to target the cracking load of the specimen. The first line traced the linear elastic portion of the curve and the second line traced the portion of the curve exhibiting a significant departure from the initial tangent. Figure 5-10 displays the load deflection plot of specimen BB-03 fabricated with conventional concrete containing hard river gravel and Figure 5-11 displays the load deflection plot of specimen BB-10 fabricated with self consolidating concrete containing hard river gravel. Both of these plots display the applied load recorded by the load cell and the average deflection measured by the two 6-inch linear potentiometers located at midspan.

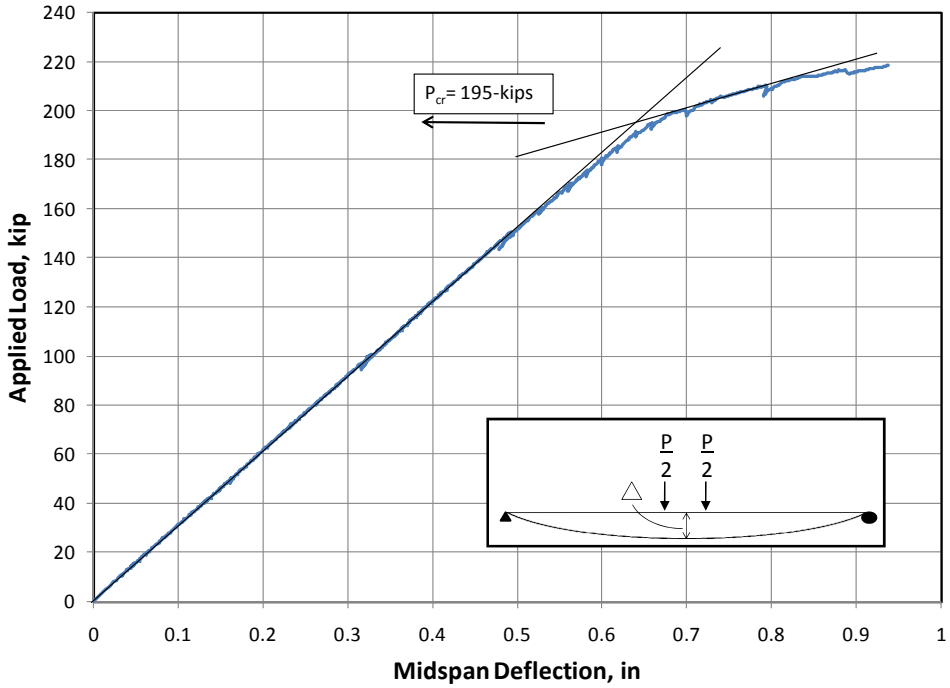

Figure 5-10 Applied Load versus Midspan Deflection for Specimen BB-03 (Conventional Concrete)

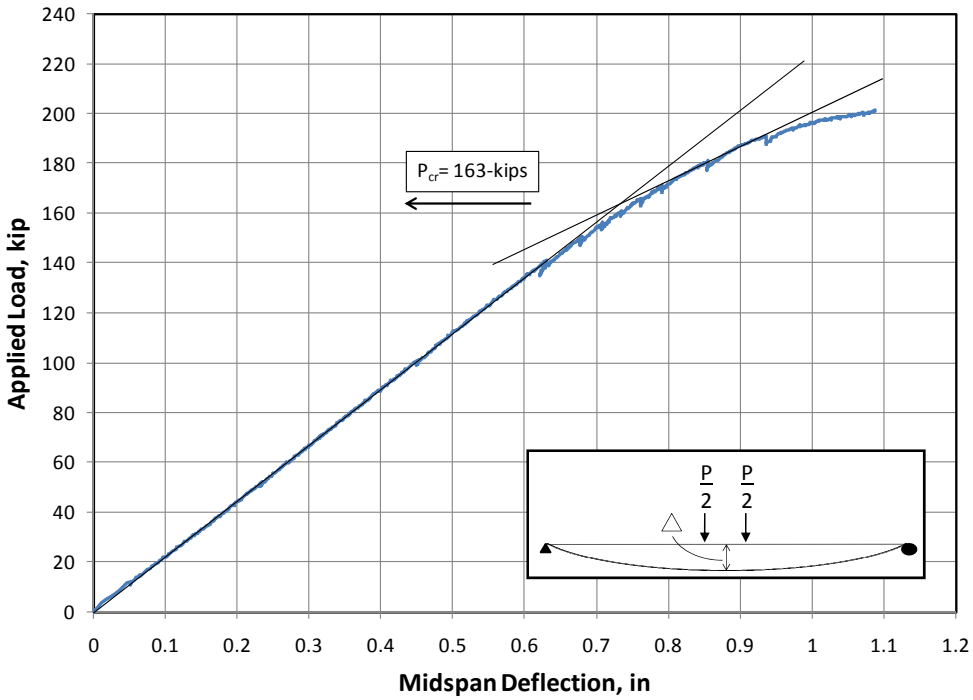

Figure 5-11 Applied Load versus Midspan Deflection for Specimen BB-10 (SCC)

It is interesting to note the differences between Figure 5-10 and Figure 5-11. Beam BB-03 fabricated with conventional concrete exhibited a much higher modulus of elasticity than beam BB-10. Additionally, beam BB-03 exhibited far less deflection at a load of 200-kips when compared with beam BB-10. These and other differences between self consolidating concrete and conventional concrete are discussed further in Section 5.4.

Visually observed cracking loads were recorded during all box beam flexural tests. As with the Type-C beams, these visually observed cracking loads were used to confirm the loads determined from the load-deflection analysis. The first visually observed cracks occurred on the bottom soffit of the beam in the 5-foot long constant moment region. With increasing load, all cracks propagated up through the bottom flange of the beam and into the web. Flexural testing was stopped once the visually observed cracks reached the mid-height of the web. The typical maximum recorded

crack width for the box beams was 0.09-inches. Figure 5-12 displays the visually observed cracks for specimen BB-10

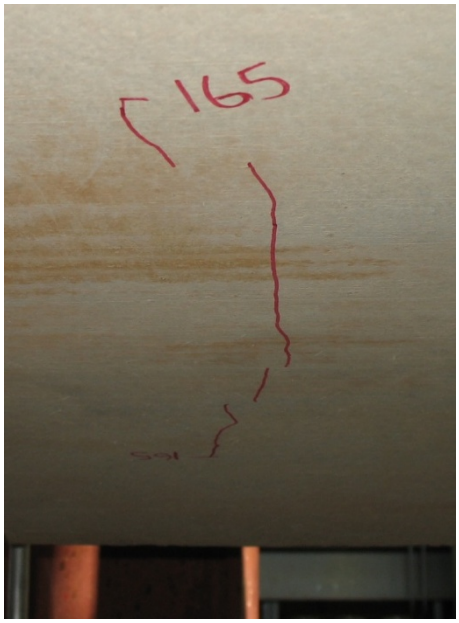

P = 165-kips
Photo of the beam soffit in the 5-foot constant moment region

P = 200-kips
Photo of the West side of the beam in the 5-foot constant moment region

Figure 5-12 Visually observed cracking load for specimen BB-10

As with the Type-C beam specimens, the measured cracking loads for all 10 box beams were carefully determined by analyzing the load deflection plots and verified with the visually observed cracking loads. Table 5-5 displays the measured cracking loads, maximum crack widths, and test dates for all 10 box beam specimens.

Table 5-5 Measured Cracking Loads for 4B28 Box Beam Specimens

Fabricator	Beam Mark	Measured Cracking Load (kip)	Maximum Crack Width at Maximum Applied Load (in)	Date of Test
E	BB-01	176	0.007	9/18/08
E	BB-02	178	0.009	9/18/08
E	BB-03	195	0.013	9/4/08
E	BB-04	196	0.010	8/19/08
E	BB-05	200	0.007	8/28/08
E	BB-06	162	0.010	10/2/08
E	BB-07	155	0.007	10/7/08
E	BB-08	161	0.009	9/24/08
E	BB-09	162	0.007	9/25/08
E	BB-10	163	0.009	9/30/08

5.3.2 Predicted Cracking Loads

As with the Type-C beam specimens, predicted cracking loads were determined based on the NCHRP Report 496 prestress loss equations and the AASHTO-LRFD 2008 prestress loss equations. These two procedures are outlined in sections 5.3.2.1 and 5.3.2.2 respectively. Both methods use time-dependant equations to estimate the amount of prestress loss in the specimens. As with the Type-C beams, all prestress losses were calculated from the time of fabrication to the time of the flexural test. The simply supported conditions along with the applied loading setup were used to produce the shear force and bending moment diagrams as shown in Figure 5-13. From these conditions, Equation 5-11 was developed to evaluate the predicted cracking load.

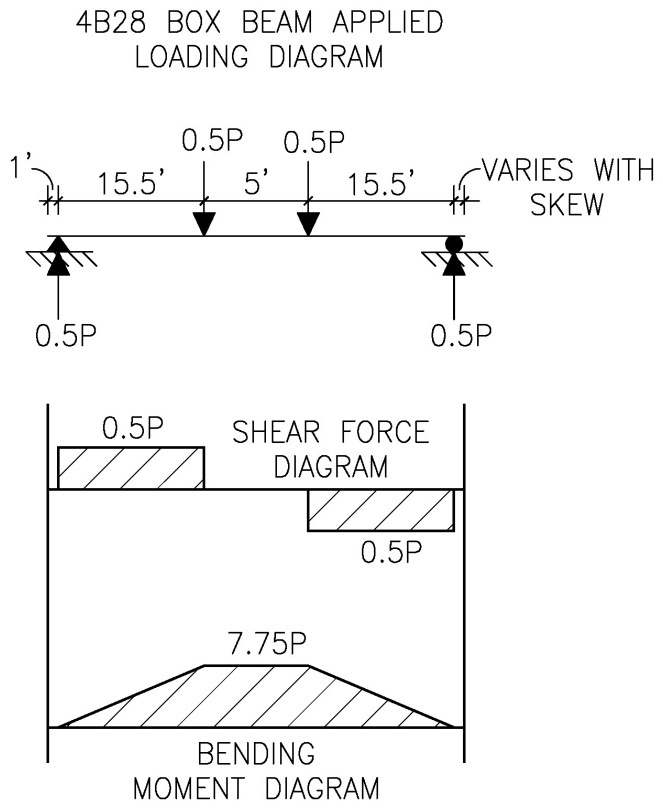

Figure 5-13 4B28 Box Beams: Applied Load, Shear Force, and Bending Moment Diagrams

$$P_{predicted} = \left(\frac{4}{L_c\text{-}5'}\right)(M_{cr}) - W_{app} \qquad \textbf{Equation 5-11}$$

where, L_c is the simply supported span length (36-feet for Box Beam Specimens)

W_{app} is the total weight of the items stacked on top of the test specimen prior to loading. (W_{app} = 1.972 kips for Box Beam Specimens)

M_{cr} is the predicted cracking moment accounting for prestress losses and member self weight (ft-k)

For all the box beam specimens, the predicted cracking load from Equation 5-11 was compared with the measured cracking loads using Equation 5-2. This accuracy calculation provided a consistent means of evaluating the predicted cracking loads from the NCHRP 496 prestress loss method and the AASHTO-LRFD (2008) prestress loss method. Section 5.3.2.1 and 5.3.2.2 include a discussion on the calculation of predicted cracking loads using NCHRP 496 prestress loss equations and AASHTO-LRFD (2008) prestress loss equations respectively.

5.3.2.1 NCHRP Report 496 Method

This section describes the process used to calculate predicted cracking loads for the 10 box beam specimens using the NCHRP 496 equations for calculating prestress losses.

In order to calculate material properties for the box beams using the NCHRP 496 method, an appropriate K_1 factor was needed to reflect the use of local materials with respect to the national average. As with the Type-C beams, the procedure described in section 5.2.2.1 to calculate the K_1 factor was used. Equation 5-3 was used to calculate the empirical modulus of elasticity and Equation 5-4 was used to back-calculate the apparent modulus of elasticity from the initial linear-elastic slope of the load deflection plot. Figure 5-14 displays a sample load deflection plot with the estimated linear elastic portion for specimen BB-05.

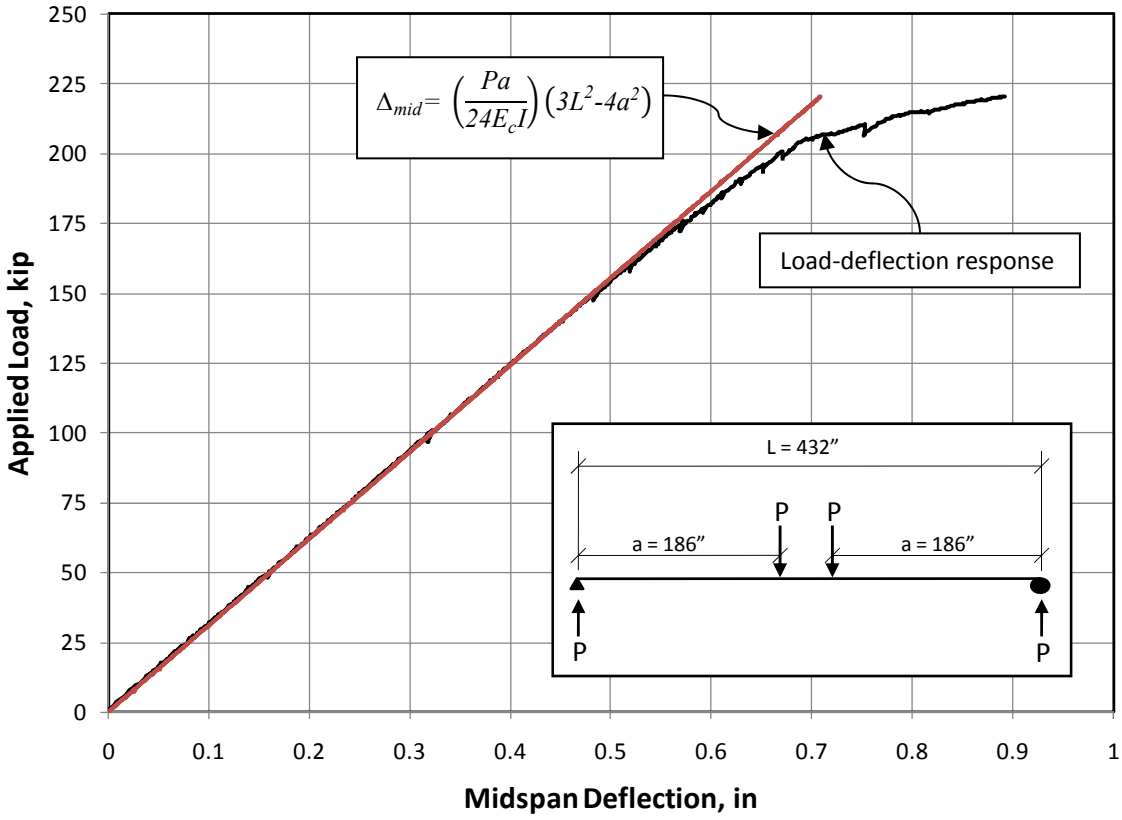

Figure 5-14 Estimated initial slope of load deflection plot to calculate the apparent modulus of elasticity for BB-05

Because four different concrete mixture designs were used to fabricate the 10 box beam specimens, four separate K_1 factors were calculated. Table 5-6 displays the concrete type, coarse aggregate type, and calculated K_1 factor for each of the 10 box beams.

Table 5-6 Calculated K_1 values for Box Beam test specimens

Beam Mark	K_1 Factor	Concrete Type	Coarse Aggregate Type
BB-01	0.9	Conventional	Limestone
BB-02			
BB-03	1.1	Conventional	Hard River Gravel
BB-04			
BB-05			
BB-06	0.8	Self Consolidating	Limestone
BB-07			
BB-08	0.9	Self Consolidating	Hard River Gravel
BB-09			
BB-10			

Using the calculated K_1 factors from Table 5-6, appropriate predicted cracking loads could be calculated. As described in section 5.2.2.1, Equation 5-5 through Equation 5-8 were used to calculated the predicted cracking moment. Using the predicted cracking moment, Equation 5-11 was used to calculate the predicted cracking load. This process was completed for all 10 box beam specimens.

Once predicted and measured cracking loads were established for all 10 box beams, the accuracy of each predicted cracking load was established for each specimen using Equation 5-2. For each box beam, the accuracy of the cracking load prediction was plotted against the specimen's maximum compressive stress at release (measured at the critical section). The data from the 10 box beam tests is plotted with the data from the 45 Type-C beams along with the data from Birrcher and Bayrak (2007) in Figure 5-15.

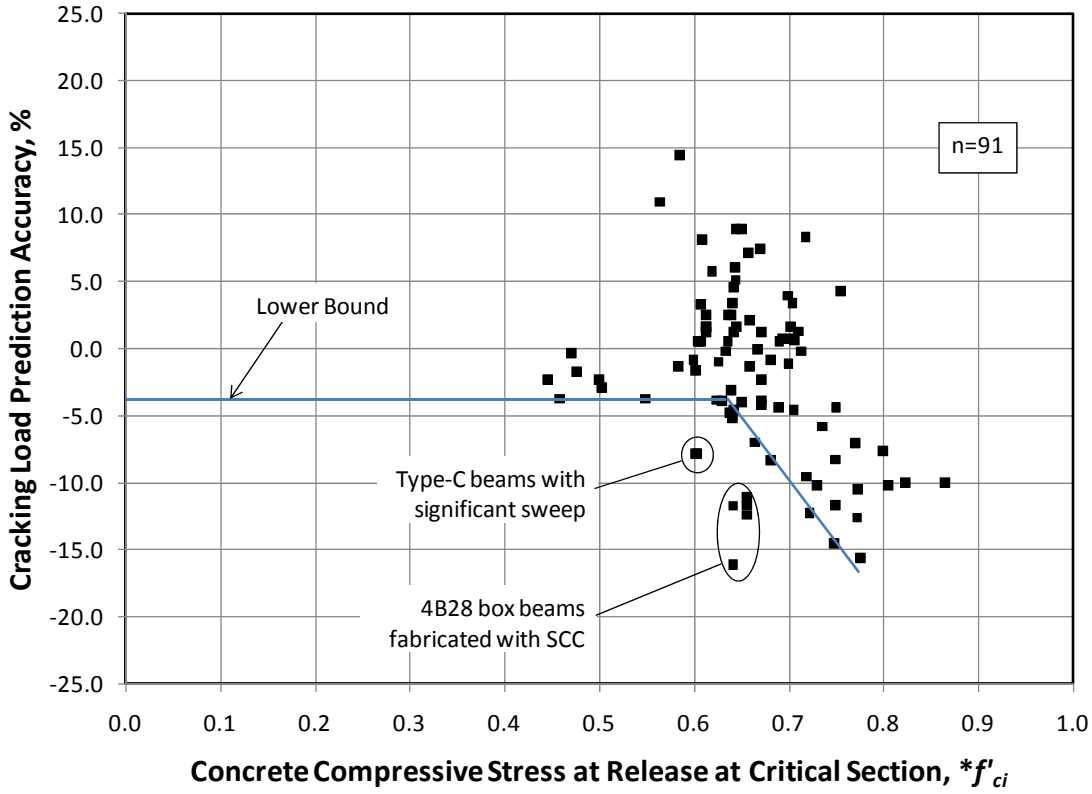

Figure 5-15 Comparison of measured and predicted cracking loads using NCHRP 496 losses

As previously mentioned, the data in Figure 5-15 shows a decrease in cracking load prediction accuracy as the compressive stress at release is increased. The two Type-C beams that exhibited significant sweep are circled, and the five box beams fabricated with self consolidating concrete are also circled. In addition, the lower bound line shown previously in Figure 5-8 is reproduced.

Of the 10 box beams tested, a range of results were observed. The five box beams fabricated with conventional concrete exhibited behavior similar to that of the Type-C beam specimens. The conventional beam data was very near or above the lower bound line and therefore did not indicate unconservative predictions of cracking loads. The box beams fabricated with SCC, however, exhibited substantial cracking at loads much lower than predicted by the NCHRP 496 method. The five points circled in Figure 5-15 are

clearly below the lower bound line and indicate a significant drop in the accuracy of cracking load estimates. Because of this unconservative result, further research is recommended to understand the behavior of SCC and its applications in prestressed concrete. More information about the observed behavior of the SCC beams is discussed in section 5.4.

If the beams fabricated with SCC are disregarded, the data still suggests that a substantial (greater than 5%) decrease in accuracy of cracking load predictions occurs at a maximum compressive stress at release of approximately $0.65f'_{ci}$.

5.3.2.2 AASHTO-LRFD 2008 Method

As with the Type-C beam specimens, the equations in the AASHTO-LRFD 2008 specification were used to predict box beam cracking loads. This section covers the AASHTO-LRFD (2008) procedure used to calculate the predicted cracking load for the 10 box beams tested in this study.

In order to calculate the modulus of elasticity using the AASHTO-LRFD (2008) specification, the K_1 factors shown in Table 5-6 were used. As previously mentioned, the K_1 factor was only used in the modulus of elasticity calculation and is not included in the equations for the shrinkage strain and creep coefficient calculations (as described in Chapter 2 and section 5.2.2.2).

As presented in section 5.2.2.2, Equation 5-9 and Equation 5-10 were used to calculate cracking moments. Using this cracking moment, the predicted cracking load was calculated using Equation 5-11. This process was utilized to calculate the predicted cracking load for all 10 box beams. The accuracy of the predicted cracking load was calculated using Equation 5-2. Figure 5-16 displays the results from the box beam tests using AASHTO-LRFD (2008) prestress loss equations as well as the Type-C beam data along with the data from Birrcher and Bayrak (2007).

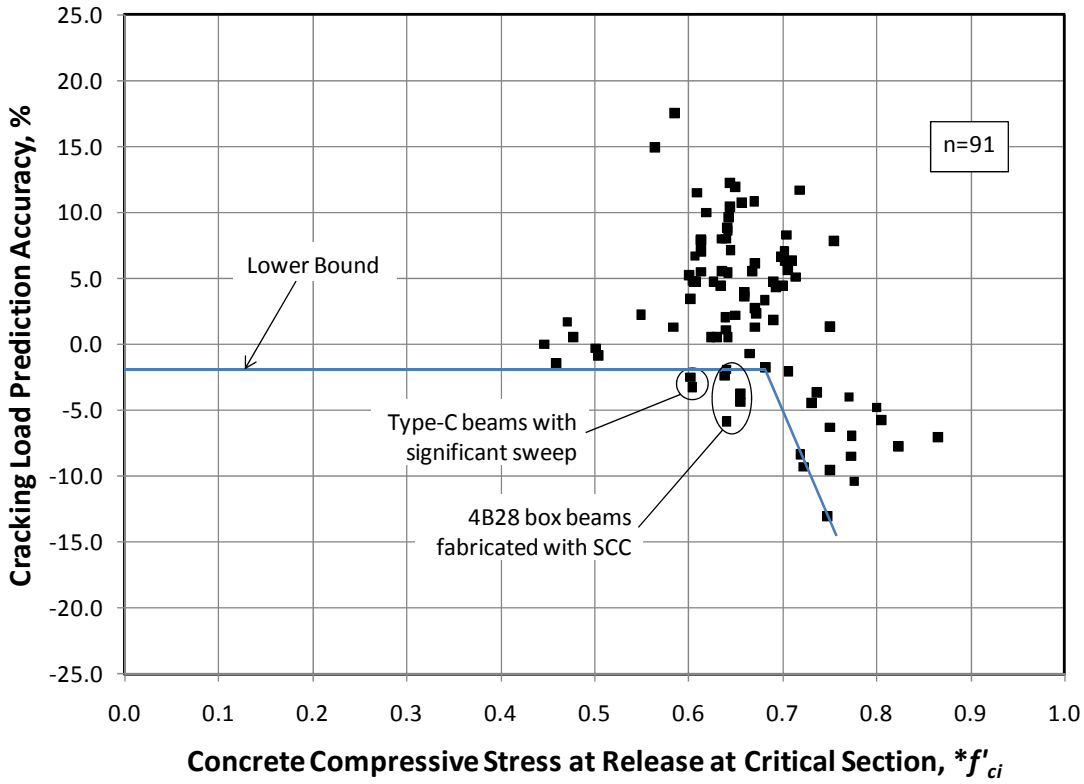

Figure 5-16 Comparison of measured and predicted cracking loads using AASHTO-LRFD 2008 losses

The data shown in Figure 5-16 exhibit lower cracking load prediction accuracy as the maximum compressive stress at release is increased. As with Figure 5-15, the two Type-C beams that exhibited significant sweep and the five box beams fabricated with SCC are circled. In addition, the lower bound line drawn in Figure 5-9 is reproduced.

As with the results calculated using NCHRP 496 prestress loss equations, the box beam data shown in Figure 5-16 exhibited a range of results. The five box beams fabricated with conventional concrete all lie above the lower bound line and did not display an unconservative error in predicted cracking load accuracy. Therefore, all five box beams fabricated with conventional concrete exhibited cracking at loads equal to or greater than predicted cracking loads. However, all five beams fabricated with SCC exhibited cracking at loads less than their predicted cracking load. This unconservative

result warrants further research into the behavior of prestressed concrete beams fabricated using SCC.

It is important to note that for the box beams fabricated with SCC, the cracking load prediction error using AASHTO-LRFD (2008) equations was smaller than the error using NCHRP 496 equations. Because the AASHTO-LRFD (2008) material properties equations for creep and shrinkage do not include the K_1 factor representing local material variability, the AASHTO-LRFD (2008) method predicted greater amounts of prestress loss for the SCC box beams than did the NCHRP 496 method. Because the AASHTO-LRFD (2008) method resulted in greater prestress losses, the AASHTO-LRFD (2008) procedure yielded smaller cracking loads than the NCHRP 496 method. This masked the unconservative nature of the cracking loads obtained for SCC beams when using the AASHTO-LRFD (2008) equations in comparison to the NCHRP 496 equations. Nevertheless, the five beams fabricated using SCC exhibited premature flexural cracking in relation to the five beams fabricated with conventional concrete.

Setting the five box beams fabricated with SCC aside, Figure 5-16, indicates that a substantial loss of prediction accuracy (greater than 5%) occurs when specimens are subjected to a maximum compressive stress at release greater than $0.7f'_{ci}$. It is important to note that the AASHTO-LRFD (2008) procedure uses the simplification of gross section properties along with the absence of the K_1 factor in material properties equations. As such, the NCHRP 496 equations provide a more appropriate measure to determine a new allowable compressive stress limit at prestress transfer. A recommendation for increasing the maximum allowable compressive stress at prestress transfer is provided in Chapter 6. A table displaying the details for each 4B28 box beam flexural test is provided in Appendix C.

5.4 OBSERVATIONS ON SELF CONSOLIDATING CONCRETE

In the fabrication of the 10 box beams tested in this research study, four different concrete mixture designs were utilized in an effort to gather comprehensive data. During the box beam testing, the five box beams fabricated with self consolidating concrete

exhibited significantly different behavior than the beams fabricated with conventional concrete. The following sections describe these differences and provide observations on the use of self consolidating concrete in prestressed concrete beams.

5.4.1 Fabrication of Box Beam Girders

During the fabrication of the box beams cast using SCC, honeycombs were observed on specimens BB-06 and BB-07. Figure 5-17 and Figure 5-18 display samples of the honeycombs from specimens BB-06 and BB-07 respectively.

Figure 5-17 Sample of honeycombing in box beam BB-06

Figure 5-18 Sample of honeycombing in box beam BB-07

It is important to note that during the fabrication of these two specimens, no external vibration was used to assist the consolidation of the concrete. The SCC mixture in both of these beams displayed unsatisfactory flow properties. In order to have an effective self consolidating concrete mixture, the concrete must be able to flow freely into the formwork leaving a smooth surface finish without serious defects. As evidenced by these two beams, SCC concrete may not always provide the smooth high quality finish required for prestressed concrete construction. In order to avoid this problem with the other three box beams fabricated using SCC (BB-08, BB-09, and BB-10) fabricator E decided to provide a very small amount of external vibration after the concrete was placed. While no honeycombing was noticed on those three specimens, external vibration of SCC defeats the primary purpose of a self consolidating mixture and ideally should not be necessary.

Since there was no exposed rebar in the honeycombed areas, these beams were repaired with grout according to TxDOT specifications. Figure 5-19 and Figure 5-20 show box beams BB-06 and BB-07 respectively after the grouting repair. Since the repaired regions were outside of the test region (i.e. the constant moment region) it is believed that the data obtained from test specimens BB-06 and BB-07 are reliable and representative.

Figure 5-19 Repaired Honeycombing of box beam BB-06

Figure 5-20 Repaired Honeycombing of box beam BB-07

5.4.2 Top Flange Cracking at Release

As mentioned in Chapter 3, the box beams were cast in two stages. Because the focus of the research was on the precompressed tensile zone, the concrete from the stage 1 casting was used to target the concrete release strength of 4100 psi. Due to the fact that on average, the stage 2 concrete was placed one hour after the stage 1 concrete, the tensile strength of the stage 2 concrete was lower at prestress transfer. Therefore, flexural tension cracking in the top flange was observed on all 10 box beam specimens. Although flexural tension cracking would not be desirable in prestressed beam fabrication, the observed cracking in the top flanges had no noticeable effect on the flexural performance of the box beams. Nevertheless, differences in the amount of flexural tension cracks in the top flanges were observed between beams fabricated with SCC mixtures and those fabricated with conventional concrete mixtures. Figure 5-21 displays a typical flexural tension crack observed in a beam containing conventional concrete with hard river gravel along with a typical flexural tension crack observed in an SCC beam containing hard river gravel coarse aggregate.

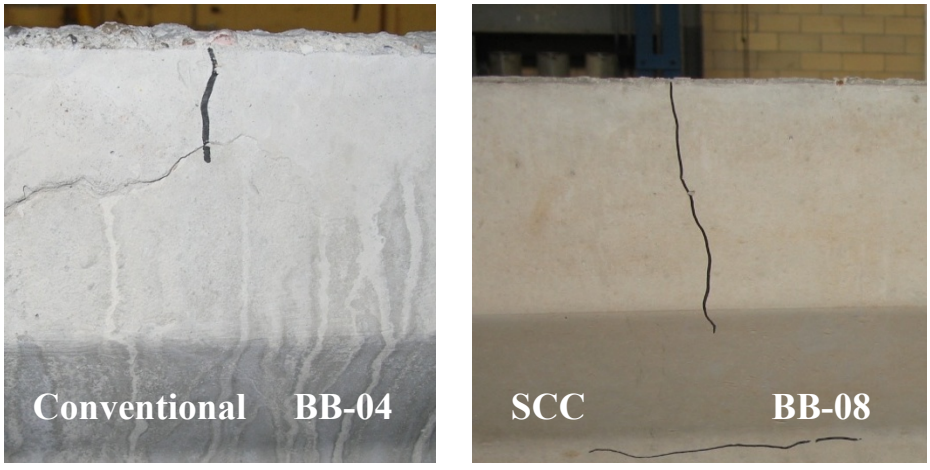

Figure 5-21 Typical flexural tension cracking in the top flange of test specimens

As shown in Figure 5-21, the SCC beam (BB-08) exhibited significantly longer tension cracks that beam BB-04. In addition, there were several more cracks along the length of box beam BB-08 within the top flange than there were for beam BB-04. The same phenomenon was observed in the concrete mixtures containing limestone. Figure

5-22 displays a typical top flange crack observed in a conventional concrete beam using limestone coarse aggregate along with a typical top flange crack from an SCC beam using limestone coarse aggregate.

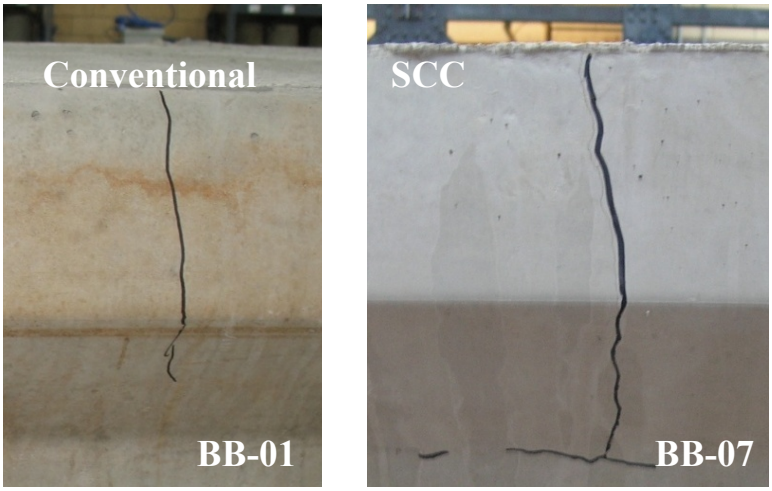

Figure 5-22 Typical flexural tension cracking in the top flange of test specimens

As with the mixtures using hard river gravel, the concrete mixtures with limestone exhibited similar behavior in regard to top flange cracking. It is important to note that for the beams fabricated with concrete mixtures using limestone, the observed difference in top flange cracking between conventional concrete mixtures and SCC mixtures was slight. In general, however, the beams fabricated with conventionally consolidating concrete mixtures exhibited less tensile cracking than those fabricated with SCC. This finding suggests that SCC may have a weaker tensile capacity than conventionally consolidating concrete. Therefore, the values typically used for design ($6\sqrt{f'_c}$. or $7.5\sqrt{f'_c}$) may not be adequate for prestressed elements fabricated with SCC.

5.4.3 Modulus of Elasiticty

After each box beam flexural test, load deflection plots were generated using the readings from the 400-kip load cell and the two 6-inch linear potentiometers located at midspan. From these load-deflection plots, an apparent modulus of elasticity could be

determined from the initial linear-elastic portion of the plot. Figure 5-23 displays the load deflection plots for all the box beams cast with concrete containing hard river gravel.

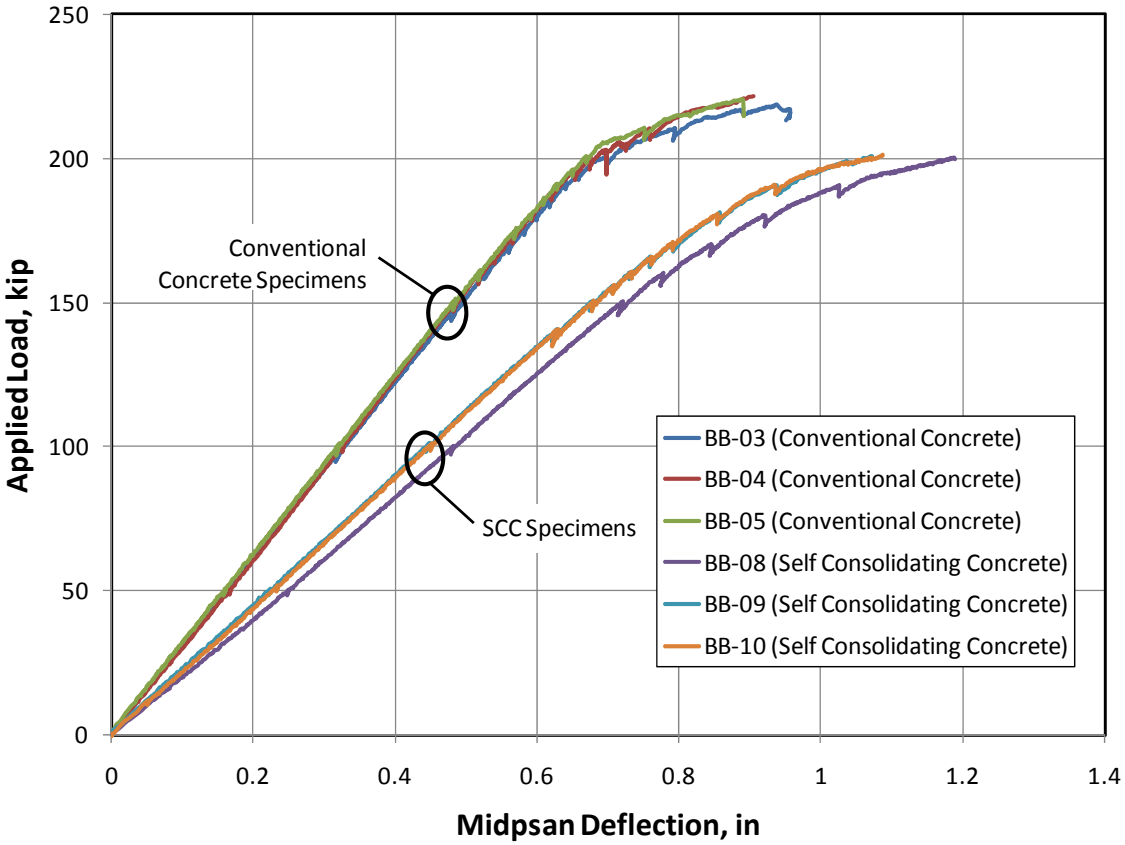

Figure 5-23 Load versus midspan deflection for box beams fabricated with concrete containing hard river gravel course aggregate

As shown in Figure 5-23, the beams fabricated using SCC were significantly less stiff and they displayed an increased amount of deflection than did those fabricated with conventional concrete. Since the moment of inertia of the cross section is the same for each box beam specimen, this difference in stiffness can be attributed directly to a difference in the modulus of elasticity. In short, the beams fabricated with SCC had a lower modulus of elasticity than the conventional concrete beams. This same trend was observed in the box beam specimens fabricated using limestone as the coarse aggregate.

Figure 5-24 displays the load deflection plots for all the box beams cast with concrete containing limestone.

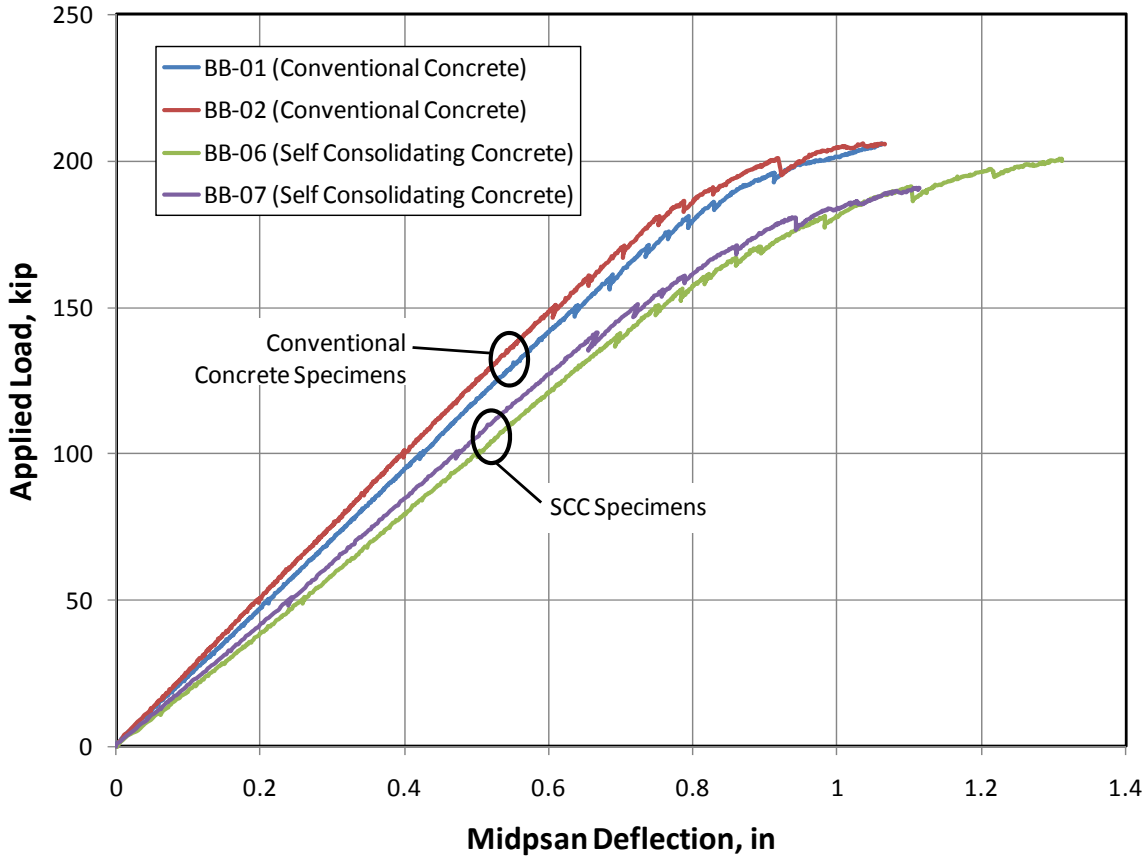

Figure 5-24 Load versus midspan deflection for box beams fabricated with concrete containing limestone coarse aggregate

Although less pronounced in Figure 5-24, the beams cast with SCC were more flexible (i.e. less stiff) and deflected more under comparable loads than the beams that were conventionally consolidated.

The trends observed in Figure 5-23 and Figure 5-24 suggest that SCC mixtures exhibit a smaller modulus of elasticity than do conventional concrete mixtures. This smaller modulus of elasticity leads to a decreased stiffness and increased deflections under live loading. These factors should be taken into account when using SCC. Further

research on the behavioral properties of specimens cast with SCC is recommended to ensure that accurate flexural response can be estimated.

5.4.4 Camber

Before every flexural test, the camber of the box beam specimen was measured. In order to measure camber, a tensioned string was held at each end of the box beam specimen. Once the string was taut and level, the distance between the top surface of the beam (at midspan) and the string was measured as the camber. Figure 5-25 displays the camber measurement for specimen BB-05.

Figure 5-25 Camber measurement at midspan for box beam BB-05 (West face)

This process was performed on both faces (East and West) of the beam and the average value was taken as the camber for the specimen. Each of these camber measurements was taken when the specimen was approximately 28-35 days old. Figure 5-26 displays the measured cambers in each of the 6 box beams fabricated with concrete containing hard river gravel coarse aggregate. Figure 5-27 displays the measured cambers in the 4 beams fabricated with concrete containing limestone coarse aggregate.

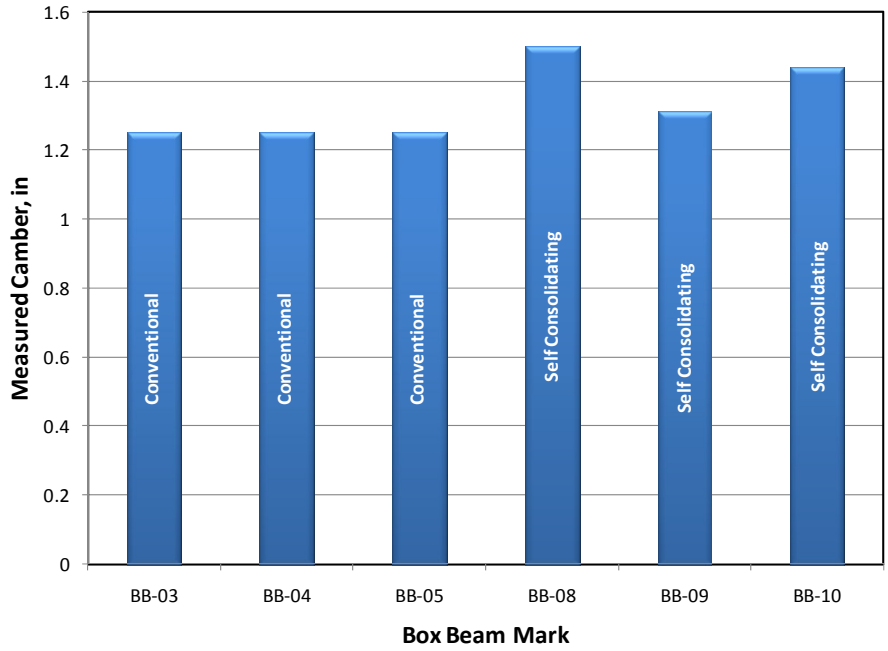

Figure 5-26 Measured Camber in box beams fabricated with concrete containing hard river gravel coarse aggregate

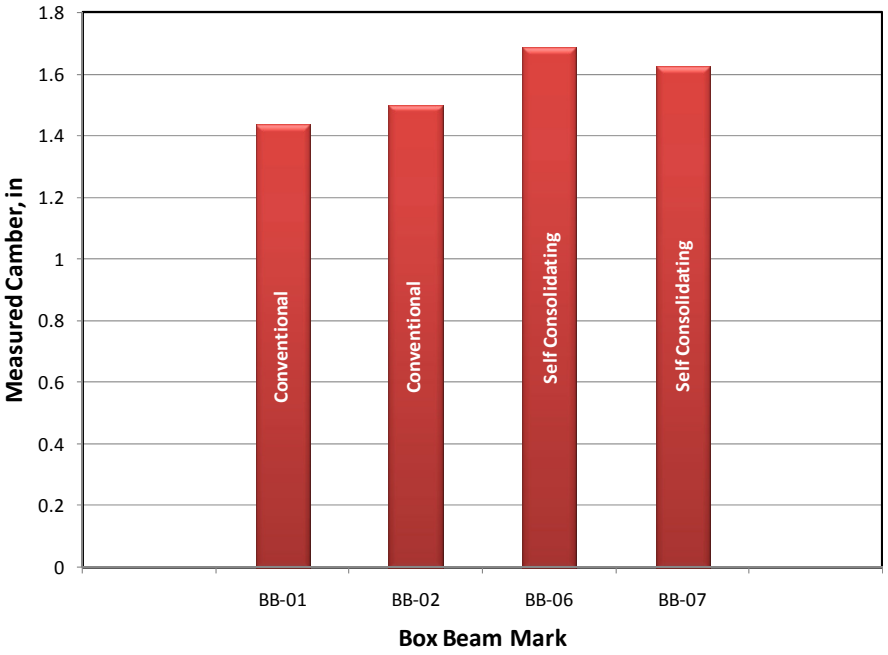

Figure 5-27 Measured camber in box beams fabricated with concrete containing limestone coarse aggregate

As evidenced by the measured cambers, the box beams fabricated with self consolidating concrete had slightly larger cambers. It is important to note that these differences in camber are small, but so are the absolute camber values. As a percentage, the differences can be considered more pronounced. This phenomenon may be attributed to the lower modulus of elasticity values observed in the load deflection plots. In effect, it can be anticipated that beams cast using SCC will exhibit higher 28-day cambers than beams cast with typical production conventional concrete.

5.4.5 Cracking Load

During all box beam flexural tests, several loading breaks were taken to visually observe the specimen, document cracks and measure crack widths. During these load breaks, several photos were taken to document the crack patterns and propagation of cracks through the beam specimens. As can be inferred from the load deflection plots (Figure 5-23 and Figure 5-24), the beams fabricated with SCC exhibited significant cracking and non-linear behavior at lower loads than did the beams fabricated with conventional concrete. In the flexural tests, this translated to the SCC beams with more severe cracking than conventional beams at a given load. Figure 5-28 displays the visually observed cracks of companion beams BB-04 (conventional) and BB-08 (SCC) at a load of 200-kips.

Figure 5-28 Visually observed cracks of beam BB-04 and BB-08 respectively at an applied load of 200-kips

As shown in Figure 5-28, the beam BB-08 fabricated with SCC exhibited substantially more cracking than did beam BB-04 fabricated with conventional concrete at an applied load of 200-kips. This same trend is observed in beams fabricated with concrete containing limestone coarse aggregate. Figure 5-29 displays the visually observed cracks of beam BB-01 (conventional) and BB-06 (SCC) at a load of 180-kips.

Figure 5-29 Visually observed cracks of beam BB-01 and BB-06 respectively at an applied load of 180-kips

As shown in both Figure 5-28 and Figure 5-29, the beams fabricated SCC exhibited higher amounts of cracking than the beams cast with conventional concrete at the same applied load. This observation is in agreement with the findings from the load deflection plots which indicated that the beams fabricated with SCC displayed larger deflections and a lower modulus of elasticity. Ultimately, it is believed that the box beams fabricated with SCC would be less serviceable and may experience more cracking from overloads than the beams cast with conventional concrete.

5.4.6 Summary of Observations on Self Consolidating Concrete

Prestressed concrete box beams fabricated with self consolidating concrete exhibited substantially different behavior than those fabricated with conventional concrete. The SCC mixtures in this study have has shown improper consolidation, increased amounts of top flange cracking at release, substantially lower modulus of elasticity (along with increased deflections under live loading), slightly higher cambers near 28-days, and lower than expected cracking loads. All of these factors present concerns about the implementation of SCC in prestressed concrete applications. Further research is recommended to examine these concerns with SCC concrete mixtures in future research projects.

5.5 SUMMARY

In this phase of TxDOT project 5197, 45 Type-C beams and 10 4B28 box beams were tested in flexure to experimentally determine their cracking load. The purpose of the testing was to determine the most appropriate maximum allowable compressive stress limit at prestress transfer for prestressed concrete beams. The chapter was presented in three main sections.

The results of the 45 Type-C beam tests were summarized in the section 5.2. Predicted cracking loads were calculated based on prestress loss equations from the NCHRP Report 496 and the AASHTO-LRFD (2008) specification. Measured cracking loads were determined by analyzing load-deflection plots and verified with visual

observations during the flexural tests. Based on these measured and predicted cracking loads, the accuracy of the predicted cracking loads was evaluated. Finally, each specimen's predicted cracking load was plotted against its maximum compressive stress at release. This plot was analyzed using a maximum acceptable error tolerance of 5%. Based on this criteria and the lower bound of the data, a value of $0.65f'_{ci}$ was found to be appropriate for the NCHRP 496 procedure and a value of $0.7f'_{ci}$ seemed appropriate for the AASHTO-LRFD (2008) procedure.

Next, the results of the 10 box beam tests were presented. In the same manner as the Type-C beam specimens, predicted and measured cracking loads were determined. Using the predicted and measured cracking loads, the predicted cracking load accuracy was computed. Then the data from the box beams was added to the data from the Type-C beam tests and the data from Birrcher and Bayrak (2007). It was observed that the box beams fabricated with conventional concrete fell within the scatter of the Type-C beams and the data from Birrcher and Bayrak (2007). However, the five box beams fabricated with self consolidating concrete exhibited lower cracking loads that were predicted unconservatively. Setting the data from the SCC box beams aside, the previous values of $0.65f'_{ci}$ for the NCHRP 496 method and $0.7f'_{ci}$ for the AASHTO-LRFD (2008) method were still acceptable limits for beams cast with conventional concrete.

Finally, observations regarding the use of self consolidating concrete were presented in section 5.4. Because the five beams fabricated with SCC behaved very differently than those fabricated with conventional concrete, several observations were made in regards to beam fabrication, top flange cracking at release, load-deflection analysis, camber measurements, and visually observed cracking. All of these observations indicated concern with the use of SCC in prestressed concrete beam construction.

A summary of this phase of TxDOT project 5197 along with the recommendations for the maximum allowable compressive stress at release are presented in Chapter 6.

CHAPTER 6
Summary, Conclusions, and Recommendations

6.1 SUMMARY OF EXPERIMENTAL PROGRAM

TxDOT Project 5197 was funded in order to investigate the feasibility of increasing the allowable compressive stress limit at prestress transfer. In phase I of this project, thirty-six specimens were tested to evaluate their live load performance (Birrcher and Bayrak, 2007). Based on the results from this testing, further research was recommended to investigate the behavior of different section types fabricated with several concrete mixture designs. The recommendation by Birrcher and Bayrak (2007) formed the basis for the research of Phase II of TxDOT project 5197.

The work in the current study (part 1 of phase II) involved the static flexural testing of 55 girders. 45 girders were TxDOT Type-C beams (40-inch deep I-beams) and 10 girders were TxDOT 4B28 box beams (28-inch deep by 48-inch wide box beams). In order to obtain a representative range of data, four different fabricators from the state of Texas produced the 45 Type-C beams using conventional concrete with either limestone or hard river gravel coarse aggregate. The maximum compressive stress at release for the Type-C beams ranged from $0.56f'_{ci}$ to $0.76f'_{ci}$. The 10 box beams were fabricated to perform proof-testing on a compressive stress limit that seemed adequate for the Type-C beams. For this purpose, all 10 box beams were targeted for a maximum compressive stress at prestress transfer of $0.66f'_{ci}$. The actual maximum compressive stress at release for the box beams ranged from $0.64f'_{ci}$ to $0.66f'_{ci}$. In order to gather comprehensive data, the box beams were fabricated with four different concrete mixture designs:

- Conventional Concrete containing hard river gravel coarse aggregate
- Conventional Concrete containing limestone coarse aggregate
- Self Consolidating Concrete containing hard river gravel coarse aggregate
- Self Consolidating Concrerte containing limestone coarse aggregate

With the use of several different concrete mixture designs along with different cross section shapes, a comprehensive set of data was evaluated in this research study.

In each static flexural test, an experimentally measured cracking load was determined using load deflection plots and visual observations. In addition to the measured cracking loads, predicted cracking loads were analytically determined for all 55 specimens using typical design calculations (P/A ± Mc/I) accounting for prestress losses. Two procedures were used to calculate prestress loss: The NCHRP Report 496 Detailed Prestress Loss Method (Tadros et al., 2003) and the AASHTO-LRFD Interim 2008 Refined Loss of Prestress Estimate (AASHTO, 2008). The accuracy of these predicted cracking loads were then compared to the maximum compressive stress at release for each of the 55 girders. The data from the 55 specimens of Phase II was added to the data from the 36 specimens of Phase I to arrive at a complete set of data from 91 beam specimens.

Because two separate methods were used to calculate prestress losses in the test specimens, the data was represented in two different ways. As mentioned in Chapter 5, the results calculated using the AASHTO-LRFD 2008 procedure indicated that a maximum compressive stress at release of $0.70f'_{ci}$ would be adequate. However, the results calculated using the NCHRP Report 496 procedure indicated that a maximum compressive stress of $0.70f'_{ci}$ would lead to premature cracking and a value of $0.65f'_{ci}$ would be an appropriate maximum limit for design.

To estimate elastic shortening loss, the AASHTO-LRFD (2008) procedure recommends the use of gross section properties along with an estimated force of 90-percent of the prestress force before transfer. This calculation explicitly accounts for the elastic shortening loss that a pretensioned element will undergo during prestress transfer. The NCHRP 496 method, however, involves the use transformed section properties. Calculating transformed section properties requires more computation, but implicitly accounts for prestress loss due elastic shortening. It is important to note that the AASHTO-LRFD Interim 2008 Bridge Design Specifications do not restrict the designer

from using transformed section properties. Section *C5.9.5.2.3a* of the AASHTO-LRFD Interim 2008 Specifications state:

> *When calculating concrete stresses using transformed section properties, the effects of losses and gains due to elastic deformations are implicitly accounted for and Δf_{pES} should not be included in the prestressing force applied to the transformed section at transfer (AASHTO, 2008).*

Therefore, if a designer chose to use transformed section properties in design, he or she would essentially be reverting back to the NCHRP 496 Method. Thus, developing conclusions and recommendations from the results derived using the NCHRP Report 496 was deemed appropriate and conservative. It is for these reasons that the conclusions and recommendations discussed in section 6.2 are generated from the results based on predicted cracking loads calculated using prestress losses from the NCHRP Report 496 procedure.

6.2 CONCLUSIONS AND RECOMMENDATIONS

After evaluating the live load performance of 91 specimens with different section types fabricated with different concrete mixture designs, several observations were made:

1) Specimens subjected to maximum compressive stresses greater than $0.65f'_{ci}$, exhibited premature cracking. The compressive stress imposed on these specimens at prestress transfer subjected the concrete in the pre-compressed tensile zone into the non-linear, inelastic range. This caused microcracking in the concrete that was not accounted for in prestress losses or standard design calculations of P/A ± Mc/I.
2) For the 91 specimens tested in TxDOT Project 5197, relaxing the allowable compressive stress at prestress transfer to $0.65f'_{ci}$ is justified. In general, premature cracking was not observed in specimens subjected to maximum compressive stresses of $0.65f'_{ci}$ or less. It is important to note that two Type-C beam specimens stressed below $0.65f'_{ci}$ did exhibit premature cracking but also contained significant sweep which impacted their flexural behavior. It was

determined that those two specimens did not represent typical behavior of Type-C beams.

3) For the five box beam specimens fabricated with self consolidating concrete, substantial premature cracking was observed. Based on the experimental data from these five box beam tests, the use of self consolidating concrete with a maximum compressive stress at release of $0.65f'_{ci}$ is not recommended.

Based on the conclusions listed above, it is recommended that the requirement concerning the allowable release stress in AASHTO-LRFD (2008) Bridge Design Specifications should be revised to read:

> "*Stresses in concrete immediately after prestress transfer (before time-dependent prestress losses): (a) Extreme fiber stress in compression except as permitted in (b) shall not exceed* $0.65f'_{ci}$. *(b) Extreme fiber stress in compression at ends of simply supported members shall not exceed* $0.70f'_{ci}$"

6.3 RECOMMENDATIONS FOR FUTURE WORK

In regards to the live load performance of beams fabricated with self consolidating concrete, additional testing should be performed. Based on the results of the five box beams fabricated at $0.65f'_{ci}$, further testing should be completed to determine an appropriate allowable compressive stress limit where satisfactory live load performance is achieved. Furthermore, an investigation to determine appropriate SCC mixture designs for prestressed applications should be completed. SCC mixture designs should be adjusted to ensure satisfactory material properties (workability, modulus of elasticity, tensile strength, etc.).

APPENDIX A

Additional Information for TxDOT Project 5197 Beams

Appendix A includes the following for the TxDOT Project 5197 pretensioned beams:

- Type-C Beams
    - Sample Series 1 Beam Shop Drawing
    - Sample Series 2 Beam Shop Drawing
    - Beam Fabrication Specifications
    - Series 1 Beam Stress Calculations at Prestress Release
    - Series 2 Beam Stress Calculations at Prestress Release
    - Prestress Losses / Cracking Load Calculations
        - NCHRP 496, and AASHTO LRFD Interim 2008
- 4B28 Box Beams
    - Sample Shop Drawing
    - Stress Calculations at Prestress Release
    - Prestress Losses / Cracking Load Calculations
        - NCHRP 496, and AASHTO-LRFD Interim 2008

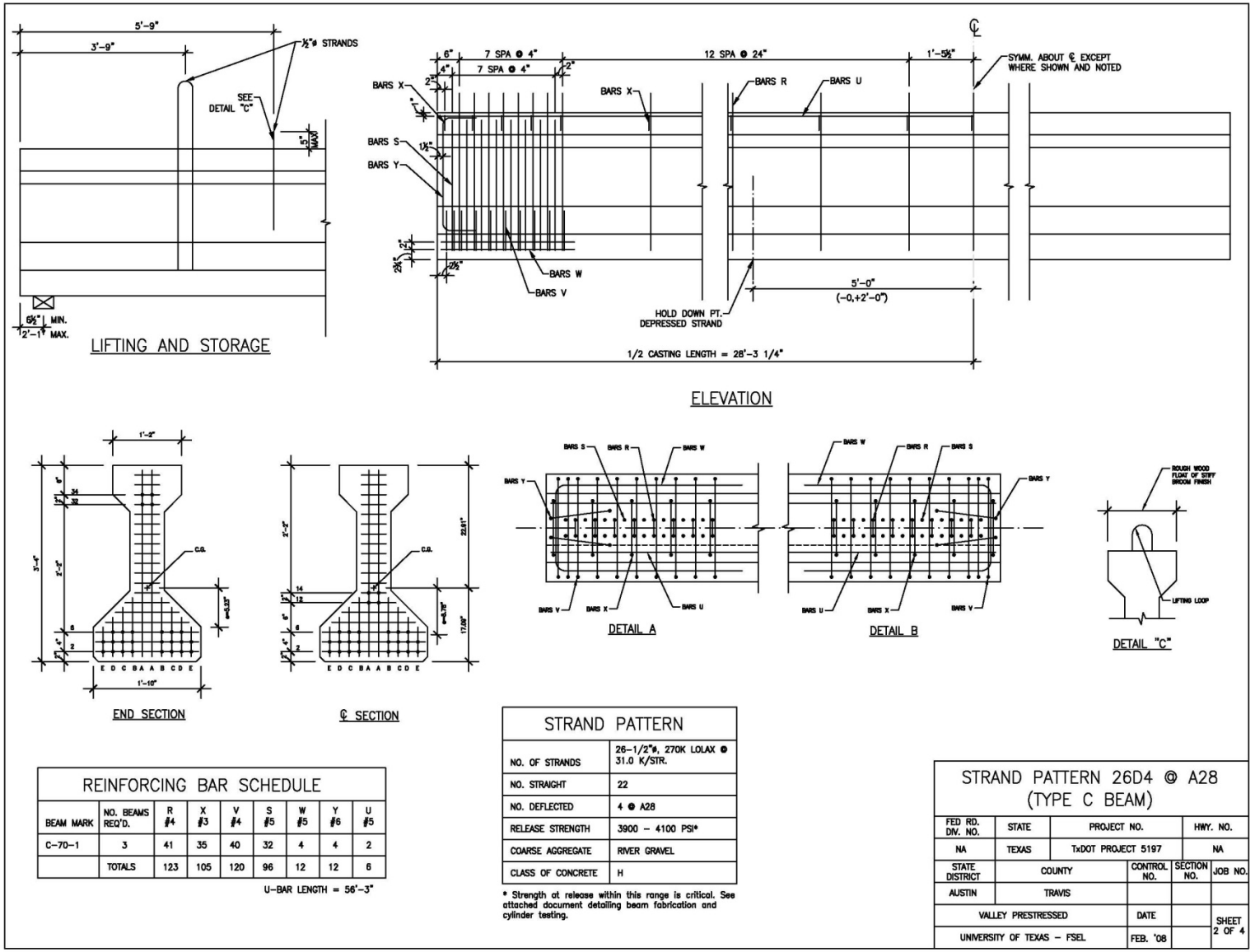

Figure A-1 Sample Shop Drawing for Series 1 Type-C Beam

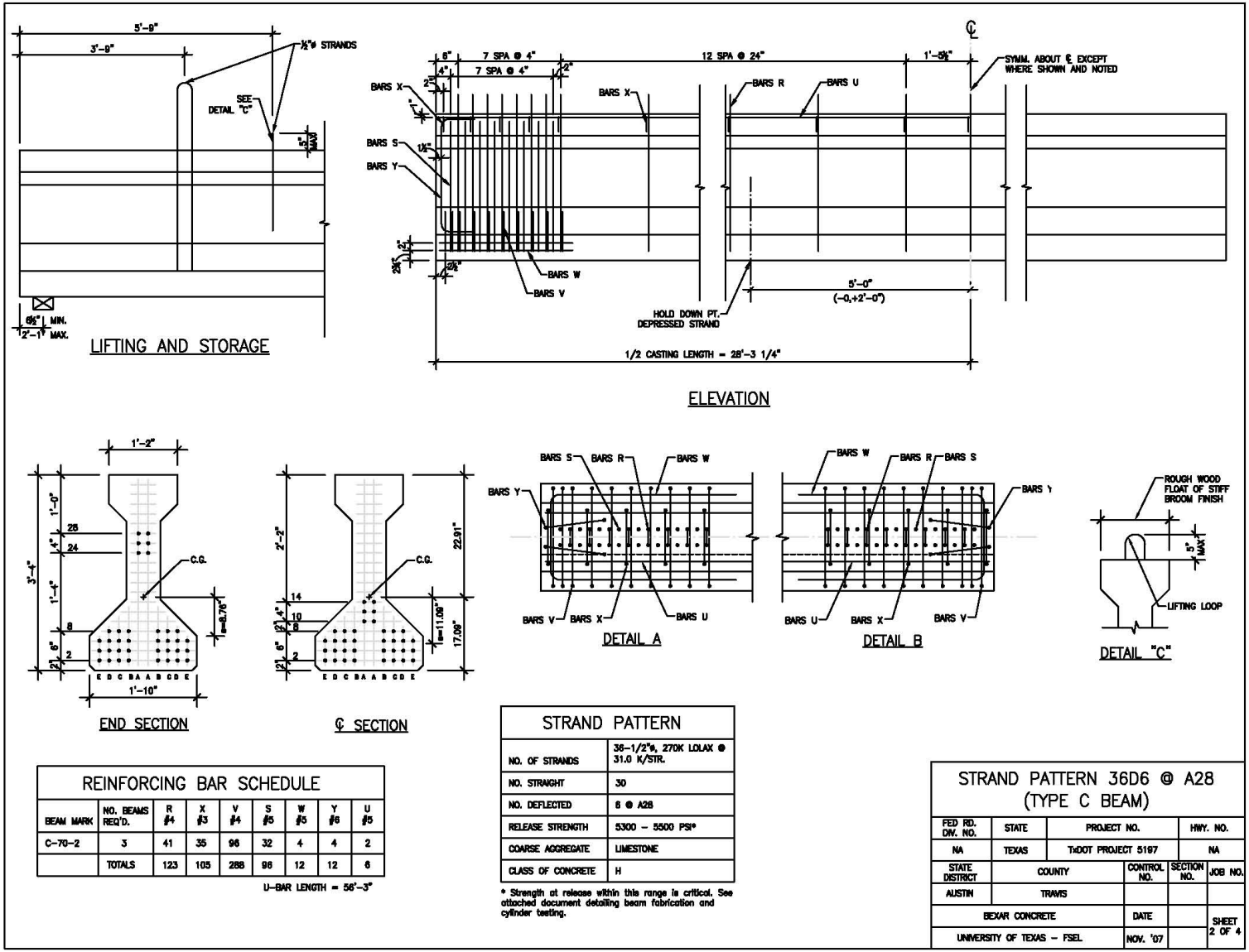

REINFORCING BAR SCHEDULE								
BEAM MARK	NO. BEAMS REQ'D.	R #4	X #3	V #4	S #5	W #5	Y #6	U #5
C-70-2	3	41	35	96	32	4	4	2
	TOTALS	123	105	288	96	12	12	6

U-BAR LENGTH = 56'-3"

STRAND PATTERN	
NO. OF STRANDS	36-1/2"ø, 270K LOLAX @ 31.0 K/STR.
NO. STRAIGHT	30
NO. DEFLECTED	6 @ A28
RELEASE STRENGTH	5300 - 5500 PSI*
COARSE AGGREGATE	LIMESTONE
CLASS OF CONCRETE	H

* Strength at release within this range is critical. See attached document detailing beam fabrication and cylinder testing.

STRAND PATTERN 36D6 @ A28 (TYPE C BEAM)				
FED RD. DIV. NO.	STATE	PROJECT NO.		HWY. NO.
NA	TEXAS	TxDOT PROJECT 5197		NA
STATE DISTRICT	COUNTY	CONTROL NO.	SECTION NO.	JOB NO.
AUSTIN	TRAVIS			
BEXAR CONCRETE		DATE		SHEET 2 OF 4
UNIVERSITY OF TEXAS - FSEL		NOV. '07		

Figure A-2 Sample Shop Drawing for Series 2 Type-C Beam

Project 5197 Extension

Beam Fabrication Specifications

1. Each fabricator will schedule a prefabrication meeting before fabricating any beams.

2. Each fabricator will submit a concrete mix design to be approved by TxDOT before beam fabrication. The approved mix design will be used to fabricate all 12 beams provided from each fabricator.

3. A ±2% prestressing force and elongation tolerance will be required for all fabricated beams.

4. Each fabricator will start by producing three (3) beams at 0.7f'c. This will be followed by six (6) beams at 0.65f'c and three (3) beams at 0.6f'c.

5. Twenty-four (24) cylinders shall be fabricated with each beam. Of the twenty-four (24), six (6) shall be shipped to the University of Texas with each beam. The remaining eighteen (18) cylinders shall be used to target the required release strength.

6. All cylinders shall be sure-cured.

7. All cylinders shall be marked with the corresponding beam mark (i.e. C70-1) and the date of casting.

8. Approximately six (6) hours after the beam is cast, two (2) cylinders shall be tested in compression every hour. As soon as the strength of the cylinders reaches within 1000-psi of the targeted strength at release, two (2) cylinders shall be tested every thirty (30) minutes or as needed to appropriately achieve the required release strength.

9. When the targeted strength is achieved, all prestressing force shall be transferred to the beam within fifteen (15) minutes.

10. After the beam has been released, two (2) cylinders will be tested in compression.

11. Each Fabricator will report the concrete strength immediately before and immediately after prestress transfer. The time at which the concrete strength was determined will also be reported.

12. Lifting Loops on each beam shall be located 5.75 feet from the end of the beam and be no higher than 5 inches from the top face of the beam. Additional lifting loops may be added if deemed necessary by the fabricator.

Stress Calculations at Prestress Release - Type C Beams

Beam Mark: CA-70-1
Series: Series 1

Material Properties		
Concrete	f'_{ci} (psi)	3929
	E_{ci} (ksi)	**3572**
	K_1	1.00
	K_2	1.00
Steel	E_{ps} (ksi)	29000
	f_{pi} (ksi)	202.5
	Strand Dia. (in)	0.5
	A_{ps_1} (in²/N)	0.153
	N_{total}	**26**

Section Properties	
	Type C
A_g (in²)	494.9
I_g (in⁴)	82602
y_b (in)	17.09
y_t (in)	22.91
e_{cl} (in)	**11.86**
e_{end} (in)	**8.78**
w_u (k/ft)	0.516
L (ft)	56.5

Elastic Shortening	
f_{cgp} (ksi)	**2.34**
n	**8.12**
ES (ksi)	**19.04**
f_{po} (ksi)	**183.46**
P_o (kips)	**730**

Strand Pattern			
Centerline		End	
Number	Height (in)	Number	Height (in)
8	at 2	8	at 2
8	at 4	8	at 4
6	at 6	6	at 6
2	at 12	2	at 32
2	at 14	2	at 34
C.G.	5.23	C.G.	8.31
Eccentricity	**11.86**	Eccentricity	**8.78**

Stress Calculations at Release

Section	x ft	x/L	P_o/A ksi	e in	$P_o e y_b/I$ ksi	$P_o e y_t/I$ ksi	M_g in-k	$M_g y_b/I$ ksi	$M_g y_t/I$ ksi
End	0.0	0.00	1.47	8.78	1.33	1.78	0	0.00	0.00
Transfer Length	2.5	0.04	1.47	9.11	1.38	1.84	417.96	0.09	0.12
	5.0	0.09	1.47	9.44	1.43	1.91	797.22	0.16	0.22
	10.0	0.18	1.47	10.11	1.53	2.05	1439.64	0.30	0.40
Hold Down	23.3	0.41	1.47	11.86	1.79	2.40	2393.4015	0.50	0.66
Critical	25.8	0.46	1.47	11.86	1.79	2.40	2451.4515	0.51	0.68
Midspan	28.3	0.50	1.47	11.86	1.79	2.40	2470.8015	0.51	0.69

Stress Calculations at Release

Section	Stress at Bottom Fiber ksi	% of f'ci	Stress at Top Fiber ksi	$*\sqrt{f'_c}$	LRFD Check
End	-2.80	71.3	0.30	4.83	OK
Transfer Length	-2.76	70.4	0.25	4.05	OK
	-2.74	69.6	0.22	3.44	OK
	-2.70	68.8	0.17	2.74	OK
Hold Down	-2.77	70.5	0.26	4.18	OK
Critical	-2.76	70.2	0.25	3.92	OK
Midspan	-2.75	70.1	0.24	3.84	OK

$$f_{top} = \frac{P_o}{A} - \frac{P_o e y_t}{I} + \frac{M_g y_t}{I}$$

$$f_{bot} = \frac{P_o}{A} + \frac{P_o e y_b}{I} - \frac{M_g y_b}{I}$$

$$E_c = 33000 K_1 K_2 \left(0.140 + \frac{f'_c}{1000}\right)^{1.5} \sqrt{f'_c}$$

$$f_{cgp} = 0.9 P_i \left(\frac{1}{A_g} + \frac{e_p^2}{I_g}\right) - \frac{M_g e_p}{I_g}$$

Figure A-3 Sample Stress Calculations at Prestress Release for beam CA-70-1 (Series 1)

Stress Calculations at Prestress Release - Type C Beams

Beam Mark:	CC-70-1
Series:	Series 2

Material Properties		
Concrete	f'_{ci} (psi)	5380
	E_{ci} (ksi)	4243
	K_1	1.00
	K_2	1.00
Steel	E_{ps} (ksi)	29000
	f_{pi} (ksi)	202.5
	Strand Dia. (in)	0.5
	A_{ps_1} (in²/N)	0.153
	N_{total}	36

Section Properties	
	Type C
A_g (in²)	494.9
I_g (in⁴)	82602
y_b (in)	17.09
y_t (in)	22.91
e_{cl} (in)	11.09
e_{end} (in)	8.76
w_u (k/ft)	0.516
L (ft)	56.5

Elastic Shortening	
f_{cgp} (ksi)	3.19
n	6.83
ES (ksi)	21.81
f_{po} (ksi)	180.69
P_o (kips)	995

Strand Pattern			
Centerline		End	
Number	Height (in)	Number	Height
8 at	2	8 at	2
8 at	4	8 at	4
8 at	6	8 at	6
6 at	8	6 at	8
2 at	10	2 at	24
2 at	12	2 at	26
2 at	14	2 at	28
at		at	
C.G.	6.00	C.G.	8.33
Eccentricity	11.09	Eccentricity	8.76

Stress Calculations at Release

Section	x	x/L	P_o/A	e	$P_o e y_b / I$	$P_o e y_t / I$	M_g	$M_g y_b / I$	$M_g y_t / I$
	ft		ksi	in	ksi	ksi	in-k	ksi	ksi
End	0.0	0.00	2.01	8.76	1.80	2.42	0	0.00	0.00
Transfer Length	2.5	0.04	2.01	9.01	1.85	2.49	417.96	0.09	0.12
	5.0	0.09	2.01	9.26	1.91	2.56	797.22	0.16	0.22
	10.0	0.18	2.01	9.76	2.01	2.69	1439.64	0.30	0.40
Hold Down	23.3	0.41	2.01	11.09	2.28	3.06	2393.40	0.50	0.66
Critical	25.8	0.46	2.01	11.09	2.28	3.06	2451.45	0.51	0.68
Midspan	28.3	0.50	2.01	11.09	2.28	3.06	2470.80	0.51	0.69

Stress Calculations at Release

Section	Stress at Bottom Fiber		Stress at Top Fiber		LRFD Check
	ksi	% of f'c	ksi	$*\sqrt{f'_c}$	
End	-3.81	-70.9	0.41	5.54	OK
Transfer Length	-3.78	-70.2	0.36	4.90	OK
	-3.75	-69.7	0.32	4.41	OK
	-3.72	-69.2	0.28	3.87	OK
Hold Down	-3.80	-70.6	0.39	5.27	OK
Critical	-3.79	-70.4	0.37	5.05	OK
Midspan	-3.78	-70.3	0.36	4.98	OK

$$f_{top} = \frac{P_o}{A} - \frac{P_o e y_t}{I} + \frac{M_g y_t}{I}$$

$$f_{bot} = \frac{P_o}{A} + \frac{P_o e y_b}{I} - \frac{M_g y_b}{I}$$

$$E_c = 33000 \; K_1 K_2 \left(0.140 + \frac{f'_c}{1000} \right)^{1.5} \sqrt{f'_c}$$

$$f_{cgp} = 0.9 P_i \left(\frac{1}{A_g} + \frac{e_p^2}{I_g} \right) - \frac{M_g e_p}{I_g}$$

Figure A-4 Sample Stress Calculations at Prestress Release for beam CC-70-1 (Series 2)

Loss of Prestress/Cracking Load Calculations - Series 1 Beam

Method: NCHRP Report 496

	Date		
Cast:	3/14/08	t_i(days)	1
Release:	3/15/08	t_t(days)	73
Test:	5/27/08		

INPUT

Section Properties

Section at Midspan

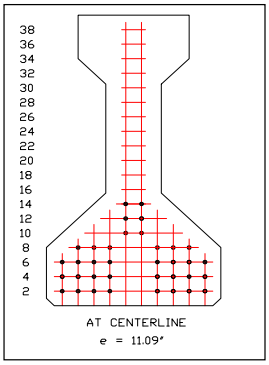

Term	At Release Gross	At Release Net	At Release Transform	At Static Test Gross	At Static Test Net	At Static Test Transform
A (in²)	494.9	492.97	530.70	494.9	491.5	516.2
y_b (in)	17.09	17.37	16.56	17.09	17.31	16.77
I (in⁴)	82602	83487	88096	82602	82851	85900
A_s (in²)	0.612	0	0	0.612	0	0
y_s (in)	38.75	38.75	38.75	38.75	38.75	38.75
A_{ps_1} (in²/N)	0.153	0	0	0.153	0	0
N	36	36	36	36	36	36
A_{ps} (in²)	5.508	0	0	5.508	0	0
e_p (in)	11.09	11.37	10.56	11.09	11.31	10.77
y_p (in)	6.00	6.00	6.00	6.00	6.00	6.00
E_c (ksi)	4234	4234	4234	6458	6458	6458
E_{ps} (ksi)	29000	29000	29000	28883	28883	28883
n	6.85	6.85	6.85	4.47	4.47	4.47

Strand Pattern

Centerline Number		Height (in)
8	at	2
8	at	4
8	at	6
6	at	8
2	at	10
2	at	12
2	at	14
C.G.		6.00

Material Properties

Equations

$$f_r = 7.5 * \sqrt{f'_{c_28}}$$

$$E_c = 33000\, K_1 K_2 \left(0.140 + \frac{f'_c}{1000}\right)^{1.5} \sqrt{f'_c}$$

Concrete		Steel		Additional	
K_1	1.0	f_{pi} (ksi)	202.5	L (ft)	56.45833
K_2	1.0	A_{ps} (in²)	5.508	Span(ft)	55
f'_{ci} (ksi)	5.36	f_{py} (ksi)	243	H (%)	70
f'_{c_t} (ksi)	11.1	f_{pu} (ksi)	270	V (in³)	335294.8
				SA (in²)	85220.5
f_{r_t} (ksi)	0.790	P_i (kips)	1115.4	V/SA (in)	3.9
Mes. f_{r_t} (ksi)	0				
E_{ci} (ksi)	4234	$\Delta\varepsilon_p$=	0.00698276		
E_{c_t} (ksi)	6458	$\Delta\varepsilon_p.\Delta\varepsilon_{p_ES}$=	0.00622262		
w (pcf)	150				
w (plf)	516				
M_{g_span} (in-k)	2341.4				
M_{g_max} (in-k)	2467.2				

Figure A-5 Prestress Loss/Cracking Load Calculations according to the NCHRP 496 procedure for Specimen CC-70-2, page 1 of 3

OUTPUT

Elastic Shortening:

Equations	Summary	
	f_{cgp}=	3.22 ksi
	Δf_{pES}=	**22.0 ksi**
	Prestressing Force	
$\Delta f_{pES} = n_i f_{cgp}$	Initial (f_{pi})	202.5 ksi
	After ES (f_{po})	180.46 ksi

Relaxation:

Equations	Stress	
$\Delta f_{pR} = \phi_i L_i K_{it}$	K_{it}=	0.79
$\phi_i = 1 - \frac{3\left(\Delta f_{pSR} + \Delta f_{pCR}\right)}{f_{po}}$	φ_i=	0.65
	L_i=	1.43
$L_i = \frac{f_{po}}{45}\left(\frac{f_{po}}{f_{py}} - 0.55\right)\log\left(\frac{24t_t + 1}{24t_i + 1}\right)$	**Δf_{pR}=**	**0.7 ksi**
	E_{pst}=	28883 ksi

Shrinkage:

Equations	Strain		Equations	Stress	
$\varepsilon_{sh} = 480 * 10^{-6}\gamma_{sh} K_1 K_2$	e_{sh}=	0.000231	$\Delta f_{pSR} = \varepsilon_{sh} E_{ps} K_{it}$	K_{it}=	0.79
$\gamma_{sh} = k_{td} k_s k_{hs} k_f$	K_1=	1		ρ_n=	0.01
	K_2=	1	$K_{it} = \frac{1}{1 + n_i \rho_n \alpha_n (1 + \chi\psi_{ult})}$	α_n=	1.76
$k_{td} = \frac{t}{61 - 4f'_{ci} + t}$				n_i=	6.85
	γ_{sh}=	0.48		ψ_{ult}=	1.41
$k_{hs} = 2.00 - 0.0143\ H$	k_{td}=	0.65	$\rho_n = \frac{A_{ps}}{A_n}$	χ=	0.7
	k_{hs}=	1.00			
$k_s = \frac{1064 - 94\left(V/S\right)}{735}$	k_s=	0.94	$\alpha_n = \left(1 + \frac{A_n e_{pn}^{\ 2}}{I_n}\right)$	**Δf_{pSR}=**	**5.3 ksi**
	k_f=	0.79			
$k_f = \frac{5}{1 + f'_{ci}}$			$n_i = \frac{E_{ps}}{E_{ci}}$		

Creep:

Equations	Quantitiy	At Test	At Ultimate	Equations	Stress	
$\psi(t, t_i) = 1.90\gamma_{cr} K_1 K_2$	γ_{cr}=	0.48	0.74	$\Delta f_{pCR} = n_i f_{cgp} \psi_t K_{it}$	K_{it}=	0.79
$\gamma_{cr} = k_{td} k_{ta} k_s k_{hc} k_f$	k_{td}=	0.65	1.00		ρ_n=	0.01
	k_{ta}=	1.00	1.00	$K_{it} = \frac{1}{1 + n_i \rho_n \alpha_n (1 + \chi\psi_{ult})}$	α_n=	1.76
$k_{td} = \frac{t}{61 - 4f'_{ci} + t}$	k_s=	0.94	0.94		n_i=	6.85
	k_{hc}=	1.00	1.00		ψ_{ult}=	1.41
$k_{hc} = 1.56 - 0.008\ H$	k_f=	0.79	0.79		ψ_i=	0.91
	K_1=	1	1	$\rho_n = \frac{A_{ps}}{A_n}$	χ=	0.7
$k_s = \frac{1064 - 94\left(V/S\right)}{735}$	K_2=	1	1			
	ψ_t=	0.91	1.41	$\alpha_n = \left(1 + \frac{A_n e_{pn}^{\ 2}}{I_n}\right)$	**Δf_{pCR}=**	**15.9 ksi**
$k_f = \frac{5}{1 + f'_{ci}}$						
$k_{ta} = t_i^{-0.118}$				$n_i = \frac{E_{ps}}{E_{ci}}$		

Total Losses:

Elastic Shortening (ES)	**Δf_{pES}=**	**22.0 ksi**
Shrinkage	**Δf_{pSR}=**	**5.3 ksi**
Creep	**Δf_{pCR}=**	**15.9 ksi**
Relaxation	**Δf_{pR}=**	**0.7 ksi**
Total	**Δf_{pT}=**	**44.0 ksi**
Total-ES	**Δf_{pT}-Δf_{pES}=**	**21.9 ksi**

Figure A-6 Prestress Loss/Cracking Load Calculations according to the NCHRP 496 procedure for Specimen CC-70-2, page 2 of 3

Cracking Load:

Equations

$$f_{cbi} = P_i\left(\frac{1}{A_{ti}} + \frac{e_{pti}\, y_{bti}}{I_{ti}}\right) - \frac{M_g\, y_{bti}}{I_{ti}}$$

$$\Delta P = \left(\Delta f_{pT} - \Delta f_{pES}\right) * A_{ps}$$

$$\Delta f_{cb} = \frac{\Delta P}{A_{tt}} + \frac{\Delta P e_{ptt}\, y_{btt}}{I_{tt}}$$

$$M_{cr} = \frac{I_{tt}}{y_{btt}}\left(f_{cbi} - \Delta f_{cb} + f_r\right)$$

f_{cbi}=	3.85 ksi
ΔP=	120.69 kips
Δf_{cb}=	0.49 ksi

Predicted Values

M_{cr}=	**21288.11 in-kips**
P_{cr}=	**137.9 kips**

Figure A-7 Prestress Loss/Cracking Load Calculations according to the NCHRP 496 procedure for Specimen CC-70-2, page 3 of 3

Loss of Prestress/Cracking Load Calculations - Series 1 Beam

Method: AASHTO LRFD

	Date		
Cast:	3/14/08	t_i(days)	1
Release:	3/15/08	t_i(days)	73
Test:	5/27/08		

INPUT

Section Properties

Section at Midspan

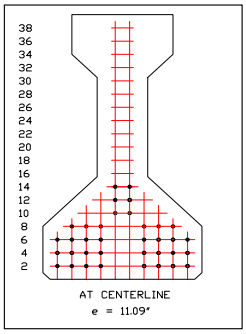

Term	At Release Gross	At Release Net	At Release Transform	At Static Test Gross	At Static Test Net	At Static Test Transform
A (in²)	494.9	492.78	528.77	494.9	491.5	516.4
y_b (in)	17.09	17.36	16.59	17.09	17.31	16.76
I (in^4)	82602	83403	87807	82602	82862	85936
A_s (in^2)	0.612	0	0	0.612	0	0
y_s (in)	38.75	38.75	38.75	38.75	38.75	38.75
A_{ps_1} (in^2/N)	0.153	0	0	0.153	0	0
N	36	36	36	36	36	36
A_{ps} (in^2)	5.508	0	0	5.508	0	0
e_p (in)	11.09	11.36	10.59	11.09	11.31	10.76
y_p (in)	6.00	6.00	6.00	6.00	6.00	6.00
E_c (ksi)	4438	4438	4438	6387	6387	6387
E_{ps} (ksi)	29000	29000	29000	28809	28809	28809
n	6.53	6.53	6.53	4.51	4.51	4.51

Strand Pattern

Centerline Number		Height (in)
8	at	2
8	at	4
8	at	6
6	at	8
2	at	10
2	at	12
2	at	14
C.G.		6.00

Material Properties

Equations

$$E_c = 33{,}000 K_1 w_c^{1.5} \sqrt{f'_c}$$

Concrete		Steel		Additional	
K_1	1.0	f_{pi} (ksi)	202.5	L (ft)	56.45833333
		A_{ps} (in^2)	5.508	L span (ft)	55
f'ci (ksi)	5.36	f_{py} (ksi)	243	H (%)	70
f'c_t (ksi)	11.1	f_{pu} (ksi)	270	V (in^3)	335294.75
				SA (in^2)	85220.5
f_{r_t} (ksi)	0.790	P_i (kips)	1115.4	V/SA (in)	3.9
Measured fr_t (ksi)	0				
E_{ci} (ksi)	4438	$\Delta\varepsilon_p$=	0.00698		
E_{c_t} (ksi)	6387	$\Delta\varepsilon_p$,$\Delta\varepsilon_{p_ES}$=	0.00626		
w (pcf)	150				
w (plf)	516				
M_{g_span} (in-k)	2341.4				
M_{g_max} (in-k)	2467.2				

Figure A-8 Prestress Loss/Cracking Load Calculations according to the AASHTO-LRFD Interim 2008 procedure for Specimen CC-70-2, page 1 of 3

OUTPUT

Elastic Shortening:

Equations	Summary	
$f_{cgp} = 0.9{*}P_i\left(\frac{1}{A_g} + \frac{e_{pg}^2}{I_g}\right) - \frac{M_{g_max} e_{pg}}{I_g}$	0.9* P_i=	1003.83 k
	f_{cgp}=	3.19 ksi
	Δf_{pES}=	**20.9 ksi**
$\Delta f_{pES} = \frac{E_p}{E_{ct}} f_{cgp}$	Prestressing Force	
	Initial (f_{pi})	202.5 ksi
	After ES (f_{pt})	181.65 ksi

Relaxation:

Equations	Stress	
$\Delta f_{pR} = \frac{f_{pt}}{K_L}\left(\frac{f_{pt}}{f_{py}} - 0.55\right)$	f_{py}=	243.00
	f_{pt}=	181.65
	K_L=	30.00
	Δf_{pR}=	**1.2 ksi**
	E_{psi}=	28809 ksi

Shrinkage:

Equations	Strain		Equations	Stress	
$\varepsilon_{sh} = k_s k_{hs} k_f k_{td} 0.48{*}10^{-3}$	e_{sh}=	0.000249628	$K_{it} = \frac{1}{1 + \frac{E_p}{E_{ci}}\frac{A_{ps}}{A_g}\left(1 + \frac{A_g e_{pg}^2}{I_g}\right)\left[1 + 0.7\psi_b(t_f, t_i)\right]}$	K_{it}=	0.79
$k_{hs} = (2.00 - .014H)$	k_{td}=	0.65			
$k_s = 1.45 - 0.13(V/S)$	k_{hs}=	1.02			
	k_s=	1.00			
$k_f = \frac{5}{1 + f'_{ci}}$	k_f=	0.79			
			$\Delta f_{pSR} = \varepsilon_{sh} E_p K_{it}$	**Δf_{pSR}=**	**5.8 ksi**
$k_{td} = \left(\frac{t}{61 - 4f'_{ci} + t}\right)$					

Creep:

Equations	Quantitiy	At Test	At Ultimate	Equations	Stress	
$\psi_b(t_f, t_i) = 1.9 k_s k_{hc} k_f k_{td} t_i^{-0.118}$	k_{td}=	0.65	1.00			
	k_s=	1.00	1.00		K_{it}=	0.79
$k_{hc} = 1.56 - 0.008H$	k_{hc}=	1.00	1.00		$\Psi_b(t_f,t_i)$=	0.97
	k_f=	0.79	0.79			
$k_s = 1.45 - 0.13(V/S)$	$\Psi_b(t,t_i)$=	0.97	1.49			
$k_f = \frac{5}{1 + f'_{ci}}$				$\Delta f_{pCR} = \frac{E_p}{E_{ci}} f_{cgp} \psi_b(t_t, t_i) K_{it}$	**Δf_{pCR}=**	**16.1 ksi**
$k_{td} = \left(\frac{t}{61 - 4f'_{ci} + t}\right)$						

Total Losses:

Elastic Shortening (ES)	**Δf_{pES}=**	**20.9 ksi**
Shrinkage	**Δf_{pSR}=**	**5.8 ksi**
Creep	**Δf_{pCR}=**	**16.1 ksi**
Relaxation	**Δf_{pR}=**	**1.2 ksi**
Total	**Δf_{pT}=**	**43.9 ksi**
Total-ES	**Δf_{pT}-Δf_{pES}=**	**23.0 ksi**

Figure A-9 Prestress Loss/Cracking Load Calculations according to the AASHTO-LRFD Interim 2008 procedure for Specimen CC-70-2, page 2 of 3

Cracking Load:

Equations

$$M_{cr} = \frac{I_g}{y_{bg}}\left(\frac{P_{eff}}{A_g} + \frac{P_{eff}\, e_{cl}\, y_{bg}}{I_g} - \frac{M_{g_test}\, y_{bg}}{I_g} + f_r\right)$$

f_{eff}=	158.64 ksi
P_{eff}=	873.80 kips

Predicted Values

M_{cr}=	**19702 in-k**
P_{cr}=	**131.3 kips**

Figure A-10 Prestress Loss/Cracking Load Calculations according to the AASHTO-LRFD Interim 2008 procedure for Specimen CC-70-2, page 3 of 3

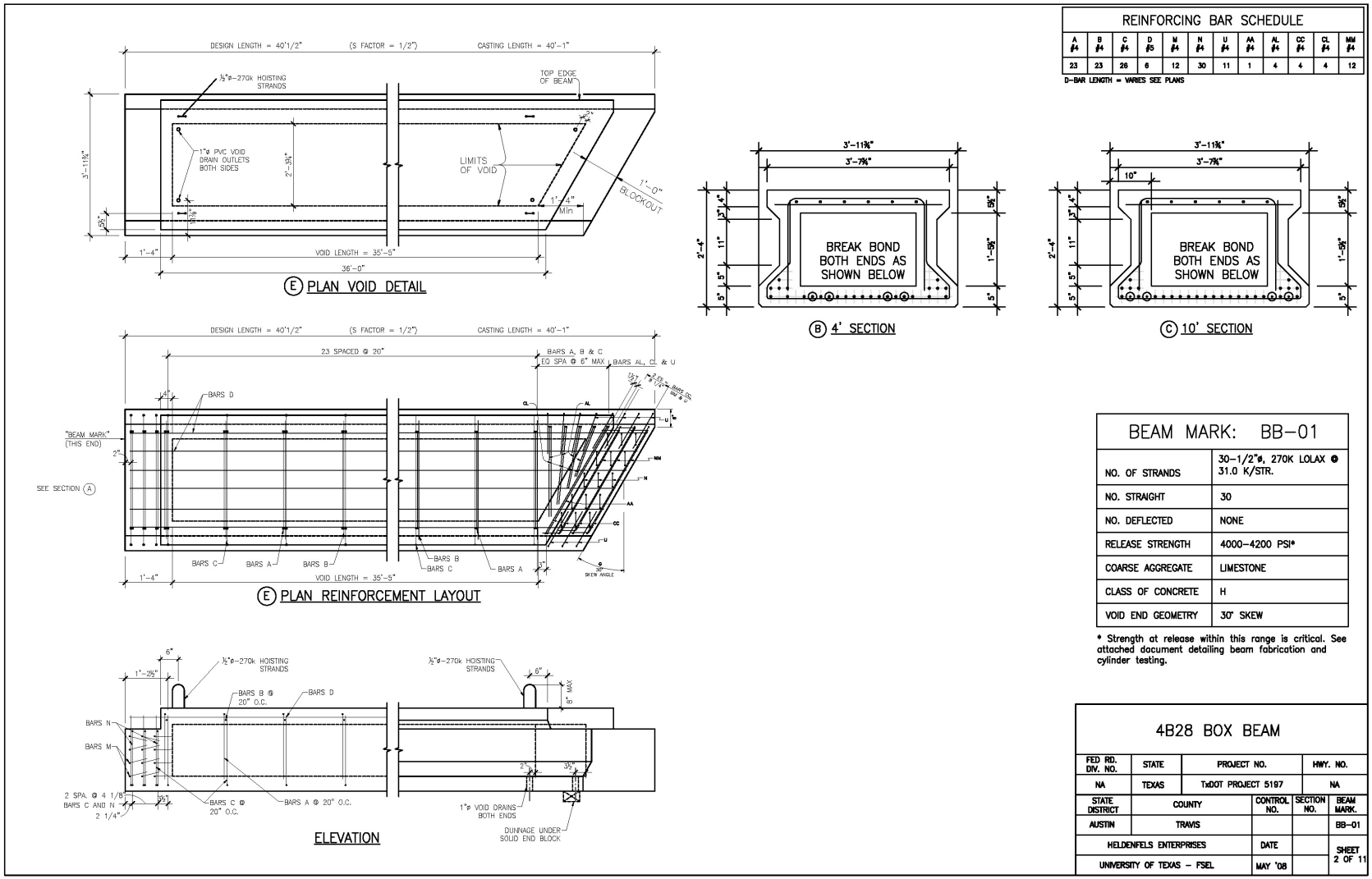

Figure A-11 Sample Box Beam Shop Drawing for specimen BB-01

Stress Calculations at Prestress Release - Box Beams

Beam Mark: BB-01
Series: Box

Material Properties		
Concrete	f'_{ci} (psi)	4140
	E_{ci} (ksi)	**3307**
	K_1	0.90
	K_2	1.00
Steel	E_{ps} (ksi)	29000
	f_{pi} (ksi)	202.5
	Strand Dia. (in)	0.5
	A_{ps_1} (in²/N)	0.153
	N_{total}	**30**

Section Properties	4B28
A_g (in²)	678.8
I_g (in⁴)	68745
y_b (in)	13.62
y_t (in)	14.38
e_{cl} (in)	**10.45**
e_{end} (in)	**10.45**
w_u (k/ft)	0.707
L (ft)	39

Elastic Shortening	
f_{cgp} (ksi)	**2.32**
n	**8.77**
ES (ksi)	**20.32**
f_{po} (ksi)	**182.18**
P_o (kips)	**836**

Strand Pattern			
Centerline		End	
Number	Height (in)	Number	Height (in)
22 at	2.5	22 at	2.5
6 at	4.5	6 at	4.5
2 at	6.5	2 at	6.5
C.G.	3.17	C.G.	3.17
Eccentricity	**10.45**	Eccentricity	**10.45**

Debonding Pattern				
		New Value		
Number	Distance (ft)	C.G.	Eccentricty	P_o (kips)
4	10	3.27	10.35	725
4	4	3.41	10.21	613

Stress Calculations at Release

Section	x ft	x/L	P_o	P_o/A ksi	e in	$P_o e y_b/I$ ksi	$P_o e y_t/I$ ksi	M_g in-k	$M_g y_b/I$ ksi	$M_g y_t/I$ ksi
End	0.0	0.00	613	0.90	10.21	1.24	1.31	0	0.00	0.00
Transfer Length	2.5	0.06	613	0.90	10.21	1.24	1.31	387.1	0.08	0.08
4	4.0	0.10	613	0.90	10.21	1.24	1.31	593.9	0.12	0.12
4.01	4.0	0.10	725	1.07	10.35	1.49	1.57	595.2	0.12	0.12
6	6.0	0.15	725	1.07	10.35	1.49	1.57	839.9	0.17	0.18
8	8.0	0.21	725	1.07	10.35	1.49	1.57	1052.0	0.21	0.22
10	10.0	0.26	725	1.07	10.35	1.49	1.57	1230.2	0.24	0.26
10.01	10.0	0.26	836	1.23	10.45	1.73	1.83	1231.0	0.24	0.26
12	12.0	0.31	836	1.23	10.45	1.73	1.83	1374.4	0.27	0.29
14	14.0	0.36	836	1.23	10.45	1.73	1.83	1484.7	0.29	0.31
14.5	14.5	0.37	836	1.23	10.45	1.73	1.83	1507.0	0.30	0.32
Critical	17.0	0.44	836	1.23	10.45	1.73	1.83	1586.5	0.31	0.33
Midspan	19.5	0.50	836	1.23	10.45	1.73	1.83	1613.0	0.32	0.34

Stress Calculations at Release

Section	Stress at Bottom Fiber ksi	% of f'ci	Stress at Top Fiber ksi	$*\sqrt{f'_c}$	LRFD Check
End	-2.14	51.8	0.41	6.31	OK
Transfer Length	-2.07	49.9	0.33	5.06	OK
4	-2.03	48.9	0.28	4.38	OK
4.01	-2.44	58.8	0.38	5.86	OK
6	-2.39	57.7	0.33	5.06	OK
8	-2.35	56.7	0.28	4.37	OK
10	-2.31	55.8	0.24	3.79	OK
10.01	-2.72	65.7	0.34	5.27	OK
12	-2.69	65.0	0.31	4.80	OK
14	-2.67	64.5	0.29	4.45	OK
14.5	-2.67	64.4	0.28	4.37	OK
Critical	-2.65	64.0	0.26	4.11	OK
Midspan	-2.64	63.9	0.26	4.03	OK

$$f_{top} = \frac{P_o}{A} - \frac{P_o e y_t}{I} + \frac{M_g y_t}{I}$$

$$f_{bot} = \frac{P_o}{A} + \frac{P_o e y_b}{I} - \frac{M_g y_b}{I}$$

$$E_c = 33000 \; K_1 K_2 \left(0.140 + \frac{f'_c}{1000} \right)^{1.5} \sqrt{f'_c}$$

$$f_{cgp} = 0.9 P_i \left(\frac{1}{A_g} + \frac{e_p^2}{I_g} \right) - \frac{M_g e_p}{I_g}$$

Figure A-12 Sample Stress Calculations at Prestress Release for beam BB-01

Loss of Prestress/Cracking Load Calculations - Box Beam

Method: NCHRP Report 496

	Date		
Cast:	8/21/08	t_i(days)	1
Release:	8/21/08	t_t(days)	28
Test:	9/18/08		

INPUT

Section Properties								Strand Pattern	
		At Release			At Static Test			Centerline	
	Term	Gross	Net	Transform	Gross	Net	Transform	Number	Height (in)
	A (in²)	678.8	688.66	728.91	678.8	681.5	704.1	22 at	2.5
	y_b (in)	13.62	13.95	13.35	13.62	13.82	13.48	6 at	4.5
	I (in⁴)	68745	70236	74805	68745	69276	71812	2 at	6.5
	A_s (in²)	1.86	0	0	1.86	0	0	at	
	y_s (in)	26	26	26	26	26	26	at	
	A_{ps_1} (in²/N)	0.153	0	0	0.153	0	0	at	
	N	30	30	30	30	30	30	at	
	A_{ps} (in²)	4.59	0	0	4.59	0	0	C.G.	3.17
	e_p (in)	10.45	10.78	10.19	10.45	10.66	10.31		
	y_p (in)	3.17	3.17	3.17	3.17	3.17	3.17		
	E_c (ksi)	3307	3307	3307	5876	5876	5876		
	E_{ps} (ksi)	29000	29000	29000	28884	28884	28884		
	n	8.77	8.77	8.77	4.92	4.92	4.92		

Material Properties						
Equations	Concrete		Steel		Additional	
	K_1	0.9	f_{pi} (ksi)	202.5	Length (ft)	39
	K_2	1.0	A_{ps} (in²)	4.59	Span (ft)	36
	f'ci (ksi)	4.14	f_{py} (ksi)	243	L (ft)	39.00
	f'c_t (ksi)	11.3	f_{pu} (ksi)	270	H (%)	70
$f_r = 7.5 * \sqrt{f'_{c_28}}$					V (in³)	317678.4
	f_{r_t} (ksi)	0.797	P_i (kips)	929.5	SA (in²)	72131.63
					V/SA (in)	4.4
	Eci (ksi)	3307	$\Delta\varepsilon_p$=	0.00698276		
$E_c = 33000\, K_1 K_2 \left(0.140 + \frac{f'_c}{1000}\right)^{1.5} \sqrt{f'_c}$	E_{c_t} (ksi)	5876	$\Delta\varepsilon_p$.$\Delta\varepsilon_{p_ES}$=	0.00627365		
	w (pcf)	150				
	w (plf)	707				
	M_{g_span} (in-k)	1374.408				
	M_{g_max} (in-k)	1613.021				

Figure A-13 Prestress Loss/Cracking Load Calculations according to the NCHRP 496 procedure for Specimen BB-01, page 1 of 3

OUTPUT

Elastic Shortening:

Equations	Summary	
$\Delta f_{pES} = n_i f_{cgp}$	f_{cgp}=	2.35 ksi
	Δf_{pES}=	**20.6 ksi**
	Prestressing Force	
	Initial (f_{pi})	202.5 ksi
	After ES (f_{po})	181.94 ksi

Relaxation:

Equations	Stress	
$\Delta f_{pR} = \phi_i L_i K_{it}$	K_{it}=	0.80
$\phi_i = 1 - \frac{3(\Delta f_{pSR} + \Delta f_{pCR})}{f_{po}}$	φ_i=	0.79
	L_i=	1.15
$L_i = \frac{f_{po}}{45}\left(\frac{f_{po}}{f_{py}} - 0.55\right)\log\left(\frac{24t_i + 1}{24t_i + 1}\right)$	**Δf_{pR}=**	**0.7 ksi**
	E_{pst}=	28884 ksi

Shrinkage:

Equations	Strain		Equations	Stress	
$\varepsilon_{sh} = 480 * 10^{-6} \gamma_{sh} K_1 K_2$	e_{sh}=	0.000144	$\Delta f_{pSR} = \varepsilon_{sh} E_{ps} K_{it}$	K_{it}=	0.80
$\gamma_{sh} = k_{td} k_s k_{hs} k_f$	K_1=	0.9	$K_{it} = \frac{1}{1 + n_i \rho_n \alpha_n (1 + \chi \psi_{ult})}$	ρ_n=	0.01
$k_{td} = \frac{t}{61 - 4f'_{ci} + t}$	K_2=	1		α_n=	2.14
			$\rho_n = \frac{A_{ps}}{A_n}$	n_i=	8.77
$k_{hs} = 2.00 - 0.0143\ H$	γ_{sh}=	0.33		ψ_{ult}=	1.47
$k_s = \frac{1064 - 94\left(V/S\right)}{735}$	k_{td}=	0.39	$\alpha_n = \left(1 + \frac{A_n e_{pn}^2}{I_n}\right)$	χ=	0.7
	k_{hs}=	1.00			
$k_f = \frac{5}{1 + f'_{ci}}$	k_s=	0.88	$n_i = \frac{E_{ps}}{E_{ci}}$	**Δf_{pSR}=**	**3.3 ksi**
	k_f=	0.97			

Creep:

Equations	Quantitiy	At Test	At Ultimate	Equations	Stress	
$\psi(t, t_i) = 1.90 \gamma_{cr} K_1 K_2$	γ_{cr}=	0.33	0.86	$\Delta f_{pCR} = n_i f_{cgp} \psi_t K_{it}$	K_{it}=	0.80
$\gamma_{cr} = k_{td} k_{la} k_s k_{hc} k_f$	k_{td}=	0.39	1.00		ρ_n=	0.01
$k_{td} = \frac{t}{61 - 4f'_{ci} + t}$	k_{la}=	1.00	1.00	$K_{it} = \frac{1}{1 + n_i \rho_n \alpha_n (1 + \chi \psi_{ult})}$	α_n=	2.14
	k_s=	0.88	0.88		n_i=	8.77
$k_{hc} = 1.56 - 0.008\ H$	k_{hc}=	1.00	1.00	$\rho_n = \frac{A_{ps}}{A_n}$	ψ_{ult}=	1.47
$k_s = \frac{1064 - 94\left(V/S\right)}{735}$	k_f=	0.97	0.97		ψ_t=	0.57
$k_f = \frac{5}{1 + f'_{ci}}$	K_1=	0.9	0.9	$\alpha_n = \left(1 + \frac{A_n e_{pn}^2}{I_n}\right)$	χ=	0.7
$k_{la} = t_i^{-0.118}$	K_2=	1	1		**Δf_{pCR}=**	**9.3 ksi**
	ψ_t=	0.57	1.47	$n_i = \frac{E_{ps}}{E_{ci}}$		

Total Losses:

Elastic Shortening (ES)	**Δf_{pES}=**	**20.6 ksi**
Shrinkage	**Δf_{pSR}=**	**3.3 ksi**
Creep	**Δf_{pCR}=**	**9.3 ksi**
Relaxation	**Δf_{pR}=**	**0.7 ksi**
Total	**Δf_{pT}=**	**33.9 ksi**
Total-ES	**Δf_{pT}-Δf_{pES}=**	**13.4 ksi**

Figure A-14 Prestress Loss/Cracking Load Calculations according to the NCHRP 496 procedure for Specimen BB-01, page 2 of 3

Cracking Load:

Equations

$$f_{cbi} = P_i\left(\frac{1}{A_{ti}} + \frac{e_{pti}\, y_{bti}}{I_{ti}}\right) - \frac{M_g\, y_{bti}}{I_{ti}}$$

$$\Delta P = \left(\Delta f_{pT} - \Delta f_{pES}\right) * A_{ps}$$

$$\Delta f_{cb} = \frac{\Delta P}{A_{tt}} + \frac{\Delta P e_{ptt}\, y_{btt}}{I_{tt}}$$

$$M_{cr} = \frac{I_{tt}}{y_{btt}}\left(f_{cbi} - \Delta f_{cb} + f_r\right)$$

f_{cbi}=	2.68 ksi
ΔP=	61.37 kips
Δf_{cb}=	0.21 ksi

Predicted Values

M_{cr}=	**17412.62 in-kips**
P_{cr}=	**187.2 kips**

Figure A-15 Prestress Loss/Cracking Load Calculations according to the NCHRP 496 procedure for Specimen BB-01, page 3 of 3

Loss of Prestress/Cracking Load Calculations - Box Beam

Method: AASHTO LRFD

	Date		
Cast:	8/21/08	t_i(days)	1
Release:	8/21/08	t_i(days)	28
Test:	9/18/08		

INPUT

Section Properties								Strand Pattern	
		At Release			At Static Test			Centerline	
	Term	Gross	Net	Transform	Gross	Net	Transform	Number	Height (in)
	A (in²)	678.8	687.71	725.63	678.8	681.6	704.4	22 at	2.5
	y_b (in)	13.62	13.93	13.37	13.62	13.82	13.48	6 at	4.5
	I (in^4)	68745	70113	74411	68745	69289	71851	2 at	6.5
	A_s (in^2)	1.86	0	0	1.86	0	0	at	
	y_s (in)	26	26	26	26	26	26	at	
	A_{ps_1} (in²/N)	0.153	0	0	0.153	0	0	at	
	N	30	30	30	30	30	30	at	
	A_{ps} (in^2)	4.59	0	0	4.59	0	0	C.G.	3.17
	e_p (in)	10.45	10.77	10.20	10.45	10.66	10.31		
	y_p (in)	3.17	3.17	3.17	3.17	3.17	3.17		
	E_c (ksi)	3511	3511	3511	5800	5800	5800		
	E_{ps} (ksi)	29000	29000	29000	28802	28802	28802		
	n	8.26	8.26	8.26	4.97	4.97	4.97		

Material Properties						
Equations	Concrete		Steel		Additional	
$E_c = 33{,}000 K_1 w_c^{1.5} \sqrt{f'_c}$	K_1	0.9	f_{pi} (ksi)	202.5	L (ft)	39
			A_{ps} (in^2)	4.59	L span (ft)	36
	f'_{ci} (ksi)	4.14	f_{py} (ksi)	243	H (%)	70
	f'_{c_t} (ksi)	11.3	f_{pu} (ksi)	270	V (in^3)	317678.4
					SA (in^2)	72131.63116
	f_{r_t} (ksi)	0.797	P_i (kips)	929.5	V/SA (in)	4.4
	E_{ct} (ksi)	3511	$\Delta\varepsilon_p$=	0.00698		
	E_{c_t} (ksi)	5800	$\Delta\varepsilon_p$,$\Delta\varepsilon_{p_ES}$=	0.00632		
	w (pcf)	150				
	w (plf)	707				
	M_{g_span} (in-k)	1374.408				
	M_{g_max} (in-k)	1613.0				

Figure A-16 Prestress Loss/Cracking Load Calculations according to the AASHTO-LRFD Interim 2008 procedure for Specimen BB-01, page 1 of 3

OUTPUT

Elastic Shortening:

Equations	Summary	
$f_{cgp} = 0.9{*}P_i\left(\frac{1}{A_g} + \frac{e_{pg}^{\ 2}}{I_g}\right) - \frac{M_{g_max} e_{pg}}{I_g}$	0.9* P_i=	836.53 k
	f_{cgp}=	2.32 ksi
	Δf_{pES}=	**19.1 ksi**
$\Delta f_{pES} = \frac{E_p}{E_{ct}} f_{cgp}$	Prestressing Force	
	Initial (f_{pi})	202.5 ksi
	After ES (f_{pt})	183.36 ksi

Relaxation:

Equations	Stress	
$\Delta f_{pR} = \frac{f_{pt}}{K_L}\left(\frac{f_{pt}}{f_{py}} - 0.55\right)$	f_{py}=	243.00
	f_{pt}=	183.36
	K_L=	30.00
	Δf_{pR}=	**1.3 ksi**
	E_{psi}=	28802 ksi

Shrinkage:

Equations	Strain		Equations	Stress	
$\varepsilon_{sh} = k_s k_{hs} k_f k_{td} 0.48{*}10^{-3}$	e_{sh}=	0.000184089	$K_{it} = \frac{1}{1 + \frac{E_p}{E_{ci}}\frac{A_{ps}}{A_g}\left(1 + \frac{A_g e_{pg}^{\ 2}}{I_g}\right)\left[1 + 0.7\psi_b(t_f, t_i)\right]}$	K_{it}=	0.79
$k_{hs} = (2.00 - .014H)$	k_{td}=	0.39			
$k_s = 1.45 - 0.13(V/S)$	k_{hs}=	1.02			
	k_s=	1.00			
$k_f = \frac{5}{1 + f'_{ci}}$	k_f=	0.97			
			$\Delta f_{pSR} = \varepsilon_{sh} E_p K_{it}$	**Δf_{pSR}=**	**4.2 ksi**
$k_{td} = \left(\frac{t}{61 - 4f'_{ci} + t}\right)$					

Creep:

Equations	Quantitiy	At Test	At Ultimate	Equations	Stress	
$\psi_b(t_f, t_i) = 1.9 k_s k_{hc} k_f k_{td} t_i^{-0.118}$	k_{td}=	0.39	1.00			
	k_s=	1.00	1.00		K_{it}=	0.79
$k_{hc} = 1.56 - 0.008H$	k_{hc}=	1.00	1.00		$\Psi_b(t_f,t_i)$=	0.71
	k_f=	0.97	0.97			
$k_s = 1.45 - 0.13(V/S)$	$\Psi_b(t,t_i)$=	0.71	1.85			
$k_f = \frac{5}{1 + f'_{ci}}$						
				$\Delta f_{pCR} = \frac{E_p}{E_{ci}} f_{cgp} \psi_b(t_t, t_i) K_{it}$	**Δf_{pCR}=**	**10.8 ksi**
$k_{td} = \left(\frac{t}{61 - 4f'_{ci} + t}\right)$						

Total Losses:

Elastic Shortening (ES)	**Δf_{pES}=**	**19.1 ksi**
Shrinkage	**Δf_{pSR}=**	**4.2 ksi**
Creep	**Δf_{pCR}=**	**10.8 ksi**
Relaxation	**Δf_{pR}=**	**1.3 ksi**
Total	**Δf_{pT}=**	**35.4 ksi**
Total-ES	**Δf_{pT}-Δf_{pES}=**	**16.3 ksi**

Figure A-17 Prestress Loss/Cracking Load Calculations according to the AASHTO-LRFD Interim 2008 procedure for Specimen BB-01, page 2 of 3

Cracking Load:

Equations

$$M_{cr} = \frac{I_g}{y_{bg}}\left(\frac{P_{eff}}{A_g} + \frac{P_{eff} e_{cl} y_{bg}}{I_g} - \frac{M_{g_test} y_{bg}}{I_g} + f_r\right)$$

$$P_{cr} = \frac{2M_{cr}}{\frac{L}{2} - \frac{5(12)}{2}}$$

f_{eff}=	167.10 ksi
P_{eff}=	766.99 kips

Predicted Values

M_{cr}=	**16370 in-k**
P_{cr}=	**176.0 kips**

Figure A-18 Prestress Loss/Cracking Load Calculations according to the AASHTO-LRFD Interim 2008 procedure for Specimen BB-01, page 3 of 3

APPENDIX B

Concrete Batch Tickets from Type-C Beam and 4B28 Box Beam Fabrication

Appendix B contains the information from the batch tickets used to fabricate all 55 girders in this research. The batch tickets provide the detailed proportions if all concrete mixture materials accounting for moisture content. The following list outlines the order of batch tickets presented in this appendix:

- Fabricator A (3 castings)
- Fabricator B (2 castings)
- Fabricator C (3 castings)
- Fabricator D (4 castings)
- Fabricator E (4 castings)

Fabricator A Batch Tickets:

Material Sources			
Fine Aggregate	TXI-Green Pit	**Cement**	Alamo Type III
Coarse Aggregate	Hanson-Ogden	**Retarding Admixture**	Sika Plastiment
Water	San Marcos Water Co	**High Range Water Reducer**	Sika Viscocrete 2100

Fabricator A: Casting #1

Date: *9/26/07* ***w/cm ratio:*** *0.368*

Batch Size: *4 yards* ***Mix Design:*** *21P- ATH6.0*

Material Description	Actual Mix		Target Value	
Fine Aggregate	6066	lbs	6107	lbs
Coarse Aggregate	7213	lbs	7213	lbs
Water	656	lbs	660	lbs
Cement	2240	lbs	2256	lbs
Retarding Admixture	68	oz	68	oz
High Range Water Reducer	161	oz	160	oz

Fabricator A: Casting #1

Date: *9/26/07* ***w/cm ratio:*** *0.373*

Batch Size: *4 yards* ***Mix Design:*** *21P- ATH6.0*

Material Description	Actual Mix		Target Value	
Fine Aggregate	6090	lbs	6143	lbs
Coarse Aggregate	7227	lbs	7220	lbs
Water	624	lbs	627	lbs
Cement	2241	lbs	2256	lbs
Retarding Admixture	68	oz	68	oz
High Range Water Reducer	161	oz	160	oz

Fabricator A: Casting #1

Date: *9/26/07* ***w/cm ratio:*** *0.373*

Batch Size: *4 yards* ***Mix Design:*** *21P- ATH6.0*

Material Description	Actual Mix		Target Value	
Fine Aggregate	6188	lbs	6143	lbs
Coarse Aggregate	7221	lbs	7220	lbs
Water	621	lbs	624	lbs
Cement	2237	lbs	2256	lbs
Retarding Admixture	68	oz	68	oz
High Range Water Reducer	161	oz	160	oz

Fabricator A: Casting #1

Date: *9/26/07* ***w/cm ratio:*** *0.369*

Batch Size: *4 yards* ***Mix Design:*** *21P- ATH6.0*

Material Description	Actual Mix		Target Value	
Fine Aggregate	6103	lbs	6143	lbs
Coarse Aggregate	7213	lbs	7220	lbs
Water	614	lbs	617	lbs
Cement	2234	lbs	2256	lbs
Retarding Admixture	68	oz	68	oz
High Range Water Reducer	162	oz	160	oz

Fabricator A: Casting #1

Date: *9/26/07* ***w/cm ratio:*** *0.369*

Batch Size: *4 yards* ***Mix Design:*** *21P- ATH6.0*

Material Description	Actual Mix		Target Value	
Fine Aggregate	6164	lbs	6143	lbs
Coarse Aggregate	7209	lbs	7220	lbs
Water	613	lbs	615	lbs
Cement	2237	lbs	2256	lbs
Retarding Admixture	68	oz	68	oz
High Range Water Reducer	161	oz	160	oz

Fabricator A: Casting #1

Date: *9/26/07* ***w/cm ratio:*** *0.365*

Batch Size: *4 yards* ***Mix Design:*** *21P- ATH6.0*

Material Description	Actual Mix		Target Value	
Fine Aggregate	6194	lbs	6143	lbs
Coarse Aggregate	7215	lbs	7220	lbs
Water	609	lbs	614	lbs
Cement	2254	lbs	2256	lbs
Retarding Admixture	68	oz	68	oz
High Range Water Reducer	161	oz	160	oz

Fabricator A: Casting #2

Date: *10/03/07* ***w/cm ratio:*** *0.355*

Batch Size: *4 yards* ***Mix Design:*** *21P- ATH6.0*

Material Description	Actual Mix		Target Value	
Fine Aggregate	6169	lbs	6213	lbs
Coarse Aggregate	7236	lbs	7241	lbs
Water	495	lbs	493	lbs
Cement	2241	lbs	2256	lbs
Retarding Admixture	68	oz	68	oz
High Range Water Reducer	161	oz	160	oz

Fabricator A: Casting #2

Date: *10/03/07* ***w/cm ratio:*** *0.358*

Batch Size: *4 yards* ***Mix Design:*** *21P- ATH6.0*

Material Description	Actual Mix		Target Value	
Fine Aggregate	6227	lbs	6255	lbs
Coarse Aggregate	7236	lbs	7241	lbs
Water	459	lbs	460	lbs
Cement	2244	lbs	2256	lbs
Retarding Admixture	68	oz	68	oz
High Range Water Reducer	161	oz	160	oz

Fabricator A: Casting #2

Date: *10/03/07* ***w/cm ratio:*** *0.357*

Batch Size: *4 yards* ***Mix Design:*** *21P- ATH6.0*

Material Description	Actual Mix		Target Value	
Fine Aggregate	6200	lbs	6227	lbs
Coarse Aggregate	7237	lbs	7241	lbs
Water	485	lbs	488	lbs
Cement	2244	lbs	2256	lbs
Retarding Admixture	68	oz	68	oz
High Range Water Reducer	161	oz	160	oz

Fabricator A: Casting #2

Date: *10/03/07* ***w/cm ratio:*** *0.354*

Batch Size: *4 yards* ***Mix Design:*** *21P- ATH6.0*

Material Description	Actual Mix		Target Value	
Fine Aggregate	6231	lbs	6245	lbs
Coarse Aggregate	7239	lbs	7241	lbs
Water	469	lbs	473	lbs
Cement	2268	lbs	2256	lbs
Retarding Admixture	68	oz	68	oz
High Range Water Reducer	162	oz	160	oz

Fabricator A: Casting #2

Date: *10/03/07* ***w/cm ratio:*** *0.356*

Batch Size: *4 yards* ***Mix Design:*** *21P- ATH6.0*

Material Description	Actual Mix		Target Value	
Fine Aggregate	6215	lbs	6263	lbs
Coarse Aggregate	7239	lbs	7241	lbs
Water	453	lbs	457	lbs
Cement	2259	lbs	2256	lbs
Retarding Admixture	68	oz	68	oz
High Range Water Reducer	161	oz	160	oz

Fabricator A: Casting #2

Date: *10/03/07* ***w/cm ratio:*** *0.357*

Batch Size: *4 yards* ***Mix Design:*** *21P- ATH6.0*

Material Description	Actual Mix		Target Value	
Fine Aggregate	6242	lbs	6293	lbs
Coarse Aggregate	7237	lbs	7241	lbs
Water	418	lbs	421	lbs
Cement	2239	lbs	2256	lbs
Retarding Admixture	68	oz	68	oz
High Range Water Reducer	161	oz	160	oz

Fabricator A: Casting #2

Date: *10/03/07* ***w/cm ratio:*** *0.352*

Batch Size: *4 yards* ***Mix Design:*** *21P- ATH6.0*

Material Description	Actual Mix		Target Value	
Fine Aggregate	6217	lbs	6244	lbs
Coarse Aggregate	7242	lbs	7241	lbs
Water	465	lbs	468	lbs
Cement	2267	lbs	2256	lbs
Retarding Admixture	68	oz	68	oz
High Range Water Reducer	161	oz	160	oz

Fabricator A: Casting #2

Date: *10/03/07* ***w/cm ratio:*** *0.351*

Batch Size: *4 yards* ***Mix Design:*** *21P- ATH6.0*

Material Description	Actual Mix		Target Value	
Fine Aggregate	6201	lbs	6243	lbs
Coarse Aggregate	7250	lbs	7241	lbs
Water	467	lbs	470	lbs
Cement	2275	lbs	2256	lbs
Retarding Admixture	68	oz	68	oz
High Range Water Reducer	161	oz	160	oz

Fabricator A: Casting #2

Date: *10/03/07* ***w/cm ratio:*** *0.358*

Batch Size: *4 yards* ***Mix Design:*** *21P- ATH6.0*

Material Description	Actual Mix		Target Value	
Fine Aggregate	6243	lbs	6236	lbs
Coarse Aggregate	7240	lbs	7241	lbs
Water	477	lbs	478	lbs
Cement	2244	lbs	2256	lbs
Retarding Admixture	68	oz	68	oz
High Range Water Reducer	162	oz	160	oz

Fabricator A: Casting #2

Date: *10/03/07* ***w/cm ratio:*** *0.354*

Batch Size: *4 yards* ***Mix Design:*** *21P- ATH6.0*

Material Description	Actual Mix		Target Value	
Fine Aggregate	6210	lbs	6227	lbs
Coarse Aggregate	7234	lbs	7241	lbs
Water	485	lbs	488	lbs
Cement	2264	lbs	2256	lbs
Retarding Admixture	68	oz	68	oz
High Range Water Reducer	161	oz	160	oz

Fabricator A: Casting #2

Date: *10/03/07* ***w/cm ratio:*** *0.351*

Batch Size: *4 yards* ***Mix Design:*** *21P- ATH6.0*

Material Description	Actual Mix		Target Value	
Fine Aggregate	6216	lbs	6227	lbs
Coarse Aggregate	7240	lbs	7241	lbs
Water	483	lbs	488	lbs
Cement	2276	lbs	2256	lbs
Retarding Admixture	68	oz	68	oz
High Range Water Reducer	161	oz	160	oz

Fabricator A: Casting #2

Date: *10/03/07* ***w/cm ratio:*** *0.362*

Batch Size: *4 yards* ***Mix Design:*** *21P- ATH6.0*

Material Description	Actual Mix		Target Value	
Fine Aggregate	6191	lbs	6226	lbs
Coarse Aggregate	7237	lbs	7241	lbs
Water	494	lbs	493	lbs
Cement	2236	lbs	2256	lbs
Retarding Admixture	68	oz	68	oz
High Range Water Reducer	161	oz	160	oz

Fabricator A: Casting #3

Date: *10/09/07* ***w/cm ratio:*** *0.357*

Batch Size: *4 yards* ***Mix Design:*** *21P- ATH6.0*

Material Description	Actual Mix		Target Value	
Fine Aggregate	6110	lbs	6167	lbs
Coarse Aggregate	7262	lbs	7256	lbs
Water	540	lbs	541	lbs
Cement	2269	lbs	2256	lbs
Retarding Admixture	68	oz	68	oz
High Range Water Reducer	161	oz	160	oz

Fabricator A: Casting #3

Date: *10/09/07* ***w/cm ratio:*** *0.357*

Batch Size: *4 yards* ***Mix Design:*** *21P- ATH6.0*

Material Description	Actual Mix		Target Value	
Fine Aggregate	6101	lbs	6143	lbs
Coarse Aggregate	7243	lbs	7241	lbs
Water	577	lbs	579	lbs
Cement	2266	lbs	2256	lbs
Retarding Admixture	68	oz	68	oz
High Range Water Reducer	161	oz	160	oz

Fabricator A: Casting #3

Date: *10/09/07* ***w/cm ratio:*** *0.363*

Batch Size: *4 yards* ***Mix Design:*** *21P- ATH6.0*

Material Description	Actual Mix		Target Value	
Fine Aggregate	6137	lbs	6143	lbs
Coarse Aggregate	7248	lbs	7241	lbs
Water	590	lbs	594	lbs
Cement	2273	lbs	2256	lbs
Retarding Admixture	68	oz	68	oz
High Range Water Reducer	161	oz	160	oz

Fabricator A: Casting #3

Date: *10/09/07* ***w/cm ratio:*** *0.361*

Batch Size: *4 yards* ***Mix Design:*** *21P- ATH6.0*

Material Description	Actual Mix		Target Value	
Fine Aggregate	6112	lbs	6143	lbs
Coarse Aggregate	7245	lbs	7241	lbs
Water	578	lbs	578	lbs
Cement	2247	lbs	2256	lbs
Retarding Admixture	68	oz	68	oz
High Range Water Reducer	161	oz	160	oz

Fabricator A: Casting #3

Date: *10/09/07* ***w/cm ratio:*** *0.363*

Batch Size: *4 yards* ***Mix Design:*** *21P- ATH6.0*

Material Description	Actual Mix		Target Value	
Fine Aggregate	6117	lbs	6143	lbs
Coarse Aggregate	7258	lbs	7241	lbs
Water	592	lbs	595	lbs
Cement	2271	lbs	2256	lbs
Retarding Admixture	68	oz	68	oz
High Range Water Reducer	161	oz	160	oz

Fabricator A: Casting #3

Date: *10/09/07* ***w/cm ratio:*** *0.364*

Batch Size: *4 yards* ***Mix Design:*** *21P- ATH6.0*

Material Description	Actual Mix		Target Value	
Fine Aggregate	6093	lbs	6143	lbs
Coarse Aggregate	7241	lbs	7241	lbs
Water	595	lbs	596	lbs
Cement	2273	lbs	2256	lbs
Retarding Admixture	68	oz	68	oz
High Range Water Reducer	162	oz	160	oz

Fabricator A: Casting #3

Date: *10/09/07* ***w/cm ratio:*** *0.369*

Batch Size: *4 yards* ***Mix Design:*** *21P- ATH6.0*

Material Description	Actual Mix		Target Value	
Fine Aggregate	6147	lbs	6143	lbs
Coarse Aggregate	7240	lbs	7241	lbs
Water	591	lbs	594	lbs
Cement	2237	lbs	2256	lbs
Retarding Admixture	68	oz	68	oz
High Range Water Reducer	161	oz	160	oz

Fabricator A: Casting #3

Date: *10/09/07* ***w/cm ratio:*** *0.369*

Batch Size: *4 yards* ***Mix Design:*** *21P- ATH6.0*

Material Description	Actual Mix		Target Value	
Fine Aggregate	6083	lbs	6143	lbs
Coarse Aggregate	7239	lbs	7241	lbs
Water	596	lbs	596	lbs
Cement	2246	lbs	2256	lbs
Retarding Admixture	68	oz	68	oz
High Range Water Reducer	161	oz	160	oz

Fabricator A: Casting #3

Date: *10/09/07* ***w/cm ratio:*** *0.362*

Batch Size: *4 yards* ***Mix Design:*** *21P- ATH6.0*

Material Description	Actual Mix		Target Value	
Fine Aggregate	6085	lbs	6143	lbs
Coarse Aggregate	7236	lbs	7241	lbs
Water	579	lbs	579	lbs
Cement	2243	lbs	2256	lbs
Retarding Admixture	68	oz	68	oz
High Range Water Reducer	161	oz	160	oz

Fabricator A: Casting #3

Date: *10/09/07* ***w/cm ratio:*** *0.370*

Batch Size: *4 yards* ***Mix Design:*** *21P- ATH6.0*

Material Description	Actual Mix		Target Value	
Fine Aggregate	6149	lbs	6143	lbs
Coarse Aggregate	7177	lbs	7241	lbs
Water	595	lbs	595	lbs
Cement	2240	lbs	2256	lbs
Retarding Admixture	68	oz	68	oz
High Range Water Reducer	161	oz	160	oz

Fabricator A: Casting #3

Date: *10/09/07* ***w/cm ratio:*** *0.365*

Batch Size: *4 yards* ***Mix Design:*** *21P- ATH6.0*

Material Description	Actual Mix		Target Value	
Fine Aggregate	6142	lbs	6143	lbs
Coarse Aggregate	7241	lbs	7241	lbs
Water	591	lbs	594	lbs
Cement	2262	lbs	2256	lbs
Retarding Admixture	68	oz	68	oz
High Range Water Reducer	161	oz	160	oz

Fabricator A: Casting #3

Date: *10/09/07* ***w/cm ratio:*** *0.355*

Batch Size: *4 yards* ***Mix Design:*** *21P- ATH6.0*

Material Description	Actual Mix		Target Value	
Fine Aggregate	6146	lbs	6143	lbs
Coarse Aggregate	7178	lbs	7241	lbs
Water	592	lbs	595	lbs
Cement	2245	lbs	2256	lbs
Retarding Admixture	68	oz	68	oz
High Range Water Reducer	161	oz	160	oz

Fabricator B Batch Tickets:

Material Sources			
Fine Aggregate	Arena	**Cement**	Alamo Type III 1a
Coarse Aggregate	Eagle Lake	**Retarding Admixture**	Plastiment
Water	Well Water	**High Range Water Reducer**	Sika 2100
Class F Fly Ash	Headwaters Jewitt, TX		

Fabricator B: Casting #1

Date: *4/23/08* ***w/cm ratio:*** *0.27*

Batch Size: *3.5 yards* ***Mix Design:*** *437-2.08*

Material Description	Actual Mix		Target Value	
Fine Aggregate	4380	lbs	4377	lbs
Coarse Aggregate	6360	lbs	6381	lbs
Water	452	lbs	454	lbs
Cement	2285	lbs	2303	lbs
Class F Fly Ash	575	lbs	N/A	lbs
Retarding Admixture	15	oz	14	oz
High Range Water Reducer	185	oz	186	oz

Fabricator B: Casting #1

Date: *4/23/08* ***w/cm ratio:*** *0.27*

Batch Size: *3.5 yards* ***Mix Design:*** *437-2.08*

Material Description	Actual Mix		Target Value	
Fine Aggregate	4400	lbs	4377	lbs
Coarse Aggregate	6340	lbs	6381	lbs
Water	454	lbs	454	lbs
Cement	2285	lbs	2303	lbs
Class F Fly Ash	575	lbs	578	lbs
Retarding Admixture	15	oz	14	oz
High Range Water Reducer	185	oz	186	oz

Fabricator B: Casting #1

Date: *4/23/08* ***w/cm ratio:*** *0.27*

Batch Size: *3.5 yards* ***Mix Design:*** *437-2.08*

Material Description	Actual Mix		Target Value	
Fine Aggregate	4340	lbs	4377	lbs
Coarse Aggregate	6320	lbs	6381	lbs
Water	452	lbs	454	lbs
Cement	2280	lbs	2303	lbs
Class F Fly Ash	580	lbs	578	lbs
Retarding Admixture	15	oz	14	oz
High Range Water Reducer	185	oz	186	oz

Fabricator B: Casting #1

Date: *4/23/08* ***w/cm ratio:*** *0.27*

Batch Size: *3.5 yards* ***Mix Design:*** *437-2.08*

Material Description	Actual Mix		Target Value	
Fine Aggregate	4360	lbs	4377	lbs
Coarse Aggregate	6320	lbs	6381	lbs
Water	452	lbs	454	lbs
Cement	2285	lbs	2303	lbs
Class F Fly Ash	585	lbs	587	lbs
Retarding Admixture	14	oz	14	oz
High Range Water Reducer	185	oz	186	oz

Fabricator B: Casting #1

Date: *4/23/08* ***w/cm ratio:*** *0.27*

Batch Size: *3.5 yards* ***Mix Design:*** *437-2.08*

Material Description	Actual Mix		Target Value	
Fine Aggregate	4380	lbs	4377	lbs
Coarse Aggregate	6340	lbs	6381	lbs
Water	456	lbs	454	lbs
Cement	2300	lbs	2303	lbs
Class F Fly Ash	585	lbs	578	lbs
Retarding Admixture	14	oz	14	oz
High Range Water Reducer	185	oz	186	oz

Fabricator B: Casting #1

Date: *4/23/08* ***w/cm ratio:*** *0.27*

Batch Size: *3.5 yards* ***Mix Design:*** *437-2.08*

Material Description	Actual Mix		Target Value	
Fine Aggregate	4340	lbs	4377	lbs
Coarse Aggregate	6320	lbs	6381	lbs
Water	454	lbs	454	lbs
Cement	2300	lbs	2303	lbs
Class F Fly Ash	585	lbs	578	lbs
Retarding Admixture	15	oz	14	oz
High Range Water Reducer	185	oz	186	oz

Fabricator B: Casting #1

Date: *4/23/08* ***w/cm ratio:*** *0.27*

Batch Size: *3.5 yards* ***Mix Design:*** *437-2.08*

Material Description	Actual Mix		Target Value	
Fine Aggregate	4340	lbs	4377	lbs
Coarse Aggregate	6320	lbs	6381	lbs
Water	456	lbs	454	lbs
Cement	2305	lbs	2303	lbs
Class F Fly Ash	580	lbs	578	lbs
Retarding Admixture	14	oz	14	oz
High Range Water Reducer	200	oz	200	oz

Fabricator B: Casting #1

Date: *4/23/08* ***w/cm ratio:*** *0.27*

Batch Size: *3.5 yards* ***Mix Design:*** *437-2.08*

Material Description	Actual Mix		Target Value	
Fine Aggregate	4360	lbs	4377	lbs
Coarse Aggregate	6340	lbs	6381	lbs
Water	452	lbs	454	lbs
Cement	2295	lbs	2303	lbs
Class F Fly Ash	585	lbs	578	lbs
Retarding Admixture	14	oz	14	oz
High Range Water Reducer	200	oz	200	oz

Fabricator B: Casting #1

Date: *4/23/08* ***w/cm ratio:*** *0.27*

Batch Size: *3.5 yards* ***Mix Design:*** *437-2.08*

Material Description	Actual Mix		Target Value	
Fine Aggregate	4360	lbs	4377	lbs
Coarse Aggregate	6320	lbs	6381	lbs
Water	454	lbs	454	lbs
Cement	2300	lbs	2303	lbs
Class F Fly Ash	580	lbs	578	lbs
Retarding Admixture	15	oz	14	oz
High Range Water Reducer	200	oz	200	oz

Fabricator B: Casting #1

Date: *4/23/08* ***w/cm ratio:*** *0.27*

Batch Size: *3.5 yards* ***Mix Design:*** *437-2.08*

Material Description	Actual Mix		Target Value	
Fine Aggregate	4340	lbs	4377	lbs
Coarse Aggregate	6340	lbs	6381	lbs
Water	454	lbs	454	lbs
Cement	2305	lbs	2303	lbs
Class F Fly Ash	585	lbs	578	lbs
Retarding Admixture	15	oz	14	oz
High Range Water Reducer	200	oz	200	oz

Fabricator B: Casting #1				
Date: *4/23/08*	***w/cm ratio:*** *0.27*			
Batch Size: *3.5 yards*	***Mix Design:*** *437-2.08*			
Material Description	**Actual Mix**		**Target Value**	
Fine Aggregate	4340	lbs	4377	lbs
Coarse Aggregate	6360	lbs	6381	lbs
Water	454	lbs	454	lbs
Cement	2300	lbs	2303	lbs
Class F Fly Ash	585	lbs	578	lbs
Retarding Admixture	14	oz	14	oz
High Range Water Reducer	200	oz	200	oz

Fabricator B: Casting #1				
Date: *4/23/08*	***w/cm ratio:*** *0.27*			
Batch Size: *3.5 yards*	***Mix Design:*** *437-2.08*			
Material Description	**Actual Mix**		**Target Value**	
Fine Aggregate	4360	lbs	4377	lbs
Coarse Aggregate	6340	lbs	6381	lbs
Water	454	lbs	454	lbs
Cement	2300	lbs	2303	lbs
Class F Fly Ash	575	lbs	578	lbs
Retarding Admixture	15	oz	14	oz
High Range Water Reducer	200	oz	200	oz

Fabricator B: Casting #1				
Date: *4/23/08*	***w/cm ratio:*** *0.27*			
Batch Size: *3.5 yards*	***Mix Design:*** *437-2.08*			
Material Description	**Actual Mix**		**Target Value**	
Fine Aggregate	4360	lbs	4377	lbs
Coarse Aggregate	6340	lbs	6381	lbs
Water	452	lbs	454	lbs
Cement	2300	lbs	2303	lbs
Class F Fly Ash	585	lbs	578	lbs
Retarding Admixture	15	oz	14	oz
High Range Water Reducer	200	oz	200	oz

Fabricator B: Casting #2				
Date: *5/6/08*	***w/cm ratio:*** *0.27*			
Batch Size: *3.5 yards*	***Mix Design:*** *437-2.08*			
Material Description	**Actual Mix**		**Target Value**	
Fine Aggregate	4280	lbs	4323	lbs
Coarse Aggregate	6340	lbs	6375	lbs
Water	512	lbs	514	lbs
Cement	2290	lbs	2303	lbs
Class F Fly Ash	585	lbs	578	lbs
Retarding Admixture	14	oz	14	oz
High Range Water Reducer	200	oz	202	oz

Fabricator B: Casting #2				
Date: *5/6/08*	***w/cm ratio:*** *0.27*			
Batch Size: *3.5 yards*	***Mix Design:*** *437-2.08*			
Material Description	**Actual Mix**		**Target Value**	
Fine Aggregate	4280	lbs	4323	lbs
Coarse Aggregate	6320	lbs	6375	lbs
Water	512	lbs	514	lbs
Cement	2310	lbs	2303	lbs
Class F Fly Ash	575	lbs	578	lbs
Retarding Admixture	14	oz	14	oz
High Range Water Reducer	200	oz	202	oz

Fabricator B: Casting #2				
Date: *5/6/08*	***w/cm ratio:*** *0.27*			
Batch Size: *3.5 yards*	***Mix Design:*** *437-2.08*			
Material Description	**Actual Mix**		**Target Value**	
Fine Aggregate	4300	lbs	4323	lbs
Coarse Aggregate	6340	lbs	6375	lbs
Water	514	lbs	514	lbs
Cement	2285	lbs	2303	lbs
Class F Fly Ash	580	lbs	578	lbs
Retarding Admixture	14	oz	14	oz
High Range Water Reducer	200	oz	202	oz

Fabricator B: Casting #2

Date: *5/6/08* ***w/cm ratio:*** *0.27*

Batch Size: *3.5 yards* ***Mix Design:*** *437-2.08*

Material Description	Actual Mix		Target Value	
Fine Aggregate	4280	lbs	4323	lbs
Coarse Aggregate	6320	lbs	6375	lbs
Water	512	lbs	514	lbs
Cement	2285	lbs	2303	lbs
Class F Fly Ash	575	lbs	578	lbs
Retarding Admixture	14	oz	14	oz
High Range Water Reducer	200	oz	202	oz

Fabricator B: Casting #2

Date: *5/6/08* ***w/cm ratio:*** *0.27*

Batch Size: *3.5 yards* ***Mix Design:*** *437-2.08*

Material Description	Actual Mix		Target Value	
Fine Aggregate	4280	lbs	4323	lbs
Coarse Aggregate	6320	lbs	6375	lbs
Water	514	lbs	514	lbs
Cement	2290	lbs	2303	lbs
Class F Fly Ash	580	lbs	578	lbs
Retarding Admixture	14	oz	14	oz
High Range Water Reducer	200	oz	202	oz

Fabricator B: Casting #2

Date: *5/6/08* ***w/cm ratio:*** *0.27*

Batch Size: *3.5 yards* ***Mix Design:*** *437-2.08*

Material Description	Actual Mix		Target Value	
Fine Aggregate	4280	lbs	4323	lbs
Coarse Aggregate	6320	lbs	6375	lbs
Water	512	lbs	514	lbs
Cement	2280	lbs	2303	lbs
Class F Fly Ash	580	lbs	578	lbs
Retarding Admixture	15	oz	14	oz
High Range Water Reducer	200	oz	202	oz

Fabricator B: Casting #2

Date: *5/6/08* ***w/cm ratio:*** *0.27*

Batch Size: *3.5 yards* ***Mix Design:*** *437-2.08*

Material Description	Actual Mix		Target Value	
Fine Aggregate	4280	lbs	4323	lbs
Coarse Aggregate	6340	lbs	6375	lbs
Water	512	lbs	514	lbs
Cement	2335	lbs	2303	lbs
Class F Fly Ash	580	lbs	578	lbs
Retarding Admixture	15	oz	14	oz
High Range Water Reducer	185	oz	189	oz

Fabricator B: Casting #2

Date: *5/6/08* ***w/cm ratio:*** *0.27*

Batch Size: *3.5 yards* ***Mix Design:*** *437-2.08*

Material Description	Actual Mix		Target Value	
Fine Aggregate	4280	lbs	4323	lbs
Coarse Aggregate	6320	lbs	6375	lbs
Water	514	lbs	514	lbs
Cement	2300	lbs	2303	lbs
Class F Fly Ash	580	lbs	578	lbs
Retarding Admixture	14	oz	14	oz
High Range Water Reducer	185	oz	189	oz

Fabricator B: Casting #2

Date: *5/6/08* ***w/cm ratio:*** *0.27*

Batch Size: *3.5 yards* ***Mix Design:*** *437-2.08*

Material Description	Actual Mix		Target Value	
Fine Aggregate	4280	lbs	4323	lbs
Coarse Aggregate	6360	lbs	6375	lbs
Water	516	lbs	514	lbs
Cement	2320	lbs	2303	lbs
Class F Fly Ash	575	lbs	578	lbs
Retarding Admixture	15	oz	14	oz
High Range Water Reducer	185	oz	189	oz

Fabricator B: Casting #2

Date: *5/6/08* ***w/cm ratio:*** *0.27*

Batch Size: *3.5 yards* ***Mix Design:*** *437-2.08*

Material Description	Actual Mix		Target Value	
Fine Aggregate	4280	lbs	4323	lbs
Coarse Aggregate	6360	lbs	6375	lbs
Water	514	lbs	514	lbs
Cement	2295	lbs	2303	lbs
Class F Fly Ash	575	lbs	578	lbs
Retarding Admixture	14	oz	14	oz
High Range Water Reducer	185	oz	189	oz

Fabricator B: Casting #2

Date: *5/6/08* ***w/cm ratio:*** *0.27*

Batch Size: *3.5 yards* ***Mix Design:*** *437-2.08*

Material Description	Actual Mix		Target Value	
Fine Aggregate	4280	lbs	4323	lbs
Coarse Aggregate	6320	lbs	6375	lbs
Water	516	lbs	514	lbs
Cement	2285	lbs	2303	lbs
Class F Fly Ash	575	lbs	578	lbs
Retarding Admixture	14	oz	14	oz
High Range Water Reducer	185	oz	189	oz

Fabricator B: Casting #2

Date: *5/6/08* ***w/cm ratio:*** *0.27*

Batch Size: *3.5 yards* ***Mix Design:*** *437-2.08*

Material Description	Actual Mix		Target Value	
Fine Aggregate	4280	lbs	4323	lbs
Coarse Aggregate	6340	lbs	6375	lbs
Water	512	lbs	514	lbs
Cement	2295	lbs	2303	lbs
Class F Fly Ash	580	lbs	578	lbs
Retarding Admixture	14	oz	14	oz
High Range Water Reducer	185	oz	189	oz

Fabricator B: Casting #2

Date: *5/6/08* ***w/cm ratio:*** *0.27*

Batch Size: *3.5 yards* ***Mix Design:*** *437-2.08*

Material Description	Actual Mix		Target Value	
Fine Aggregate	4280	lbs	4323	lbs
Coarse Aggregate	6320	lbs	6375	lbs
Water	512	lbs	514	lbs
Cement	2335	lbs	2303	lbs
Class F Fly Ash	575	lbs	578	lbs
Retarding Admixture	14	oz	14	oz
High Range Water Reducer	185	oz	189	oz

Fabricator B: Casting #2

Date: *5/6/08* ***w/cm ratio:*** *0.27*

Batch Size: *3.5 yards* ***Mix Design:*** *437-2.08*

Material Description	Actual Mix		Target Value	
Fine Aggregate	4280	lbs	4323	lbs
Coarse Aggregate	6320	lbs	6375	lbs
Water	514	lbs	514	lbs
Cement	2300	lbs	2303	lbs
Class F Fly Ash	575	lbs	578	lbs
Retarding Admixture	15	oz	14	oz
High Range Water Reducer	185	oz	189	oz

Fabricator B: Casting #2

Date: *5/6/08* ***w/cm ratio:*** *0.27*

Batch Size: *3.5 yards* ***Mix Design:*** *437-2.08*

Material Description	Actual Mix		Target Value	
Fine Aggregate	4280	lbs	4323	lbs
Coarse Aggregate	6340	lbs	6375	lbs
Water	512	lbs	514	lbs
Cement	2310	lbs	2303	lbs
Class F Fly Ash	580	lbs	578	lbs
Retarding Admixture	14	oz	14	oz
High Range Water Reducer	185	oz	189	oz

Fabricator C Batch Tickets:

Material Sources			
Fine Aggregate	River Sand Multisources	**Cement**	Capital Type III
Coarse Aggregate	Vulcan 1604 Grade 5	**Retarding Admixture**	Sika Plastiment
Water	BCW Well	**High Range Water Reducer**	Sika 2100

Fabricator C: Casting #1

Date: *3/14/08* ***w/cm ratio:*** *0.37*

Batch Size: *4 yards* ***Mix Design:*** *7S2100C*

Material Description	Actual Mix		Target Value	
Fine Aggregate	5500	lbs	5500	lbs
Coarse Aggregate	7240	lbs	7299	lbs
Water	618.0	lbs	616.4	lbs
Cement	2644	lbs	2632	lbs
Retarding Admixture	91	oz	92	oz
High Range Water Reducer	172	oz	172	oz

Fabricator C: Casting #1

Date: *3/14/08* ***w/cm ratio:*** *0.37*

Batch Size: *4 yards* ***Mix Design:*** *7S2100C*

Material Description	Actual Mix		Target Value	
Fine Aggregate	5480	lbs	5500	lbs
Coarse Aggregate	7340	lbs	7299	lbs
Water	616.0	lbs	616.4	lbs
Cement	2624	lbs	2632	lbs
Retarding Admixture	92	oz	92	oz
High Range Water Reducer	172	oz	172	oz

Fabricator C: Casting #1

Date: *3/14/08* ***w/cm ratio:*** *0.37*

Batch Size: *4 yards* ***Mix Design:*** *7S2100C*

Material Description	Actual Mix		Target Value	
Fine Aggregate	5500	lbs	5500	lbs
Coarse Aggregate	7300	lbs	7299	lbs
Water	614.0	lbs	616.4	lbs
Cement	2616	lbs	2632	lbs
Retarding Admixture	93	oz	92	oz
High Range Water Reducer	172	oz	172	oz

Fabricator C: Casting #1

Date: *3/14/08* ***w/cm ratio:*** *0.37*

Batch Size: *4 yards* ***Mix Design:*** *7S2100C*

Material Description	Actual Mix		Target Value	
Fine Aggregate	5500	lbs	5500	lbs
Coarse Aggregate	7320	lbs	7299	lbs
Water	616.0	lbs	616.4	lbs
Cement	2636	lbs	2632	lbs
Retarding Admixture	92	oz	92	oz
High Range Water Reducer	172	oz	172	oz

Fabricator C: Casting #1

Date: *3/14/08* ***w/cm ratio:*** *0.37*

Batch Size: *4 yards* ***Mix Design:*** *7S2100C*

Material Description	Actual Mix		Target Value	
Fine Aggregate	5500	lbs	5500	lbs
Coarse Aggregate	7320	lbs	7299	lbs
Water	614.0	lbs	616.4	lbs
Cement	2636	lbs	2632	lbs
Retarding Admixture	92	oz	92	oz
High Range Water Reducer	172	oz	172	oz

Fabricator C: Casting #1

Date: *3/14/08* ***w/cm ratio:*** *0.37*

Batch Size: *4 yards* ***Mix Design:*** *7S2100C*

Material Description	Actual Mix		Target Value	
Fine Aggregate	5520	lbs	5500	lbs
Coarse Aggregate	7280	lbs	7285	lbs
Water	632.0	lbs	631.1	lbs
Cement	2648	lbs	2632	lbs
Retarding Admixture	81	oz	80	oz
High Range Water Reducer	172	oz	172	oz

Fabricator C: Casting #1

Date: *3/14/08* ***w/cm ratio:*** *0.37*

Batch Size: *4 yards* ***Mix Design:*** *7S2100C*

Material Description	Actual Mix		Target Value	
Fine Aggregate	5520	lbs	5500	lbs
Coarse Aggregate	7280	lbs	7285	lbs
Water	630.0	lbs	631.1	lbs
Cement	2644	lbs	2632	lbs
Retarding Admixture	80	oz	80	oz
High Range Water Reducer	172	oz	172	oz

Fabricator C: Casting #1

Date: *3/14/08* ***w/cm ratio:*** *0.37*

Batch Size: *4 yards* ***Mix Design:*** *7S2100C*

Material Description	Actual Mix		Target Value	
Fine Aggregate	5480	lbs	5500	lbs
Coarse Aggregate	7240	lbs	7285	lbs
Water	632.0	lbs	631.1	lbs
Cement	2652	lbs	2632	lbs
Retarding Admixture	80	oz	80	oz
High Range Water Reducer	172	oz	172	oz

Fabricator C: Casting #2

Date: *3/26/08* ***w/cm ratio:*** *0.37*

Batch Size: *4 yards* ***Mix Design:*** *7S2100C*

Material Description	Actual Mix		Target Value	
Fine Aggregate	5460	lbs	5495	lbs
Coarse Aggregate	7260	lbs	7292	lbs
Water	632.0	lbs	629.3	lbs
Cement	2608	lbs	2632	lbs
Retarding Admixture	81	oz	80	oz
High Range Water Reducer	172	oz	172	oz

Fabricator C: Casting #2

Date: *3/26/08* ***w/cm ratio:*** *0.37*

Batch Size: *4 yards* ***Mix Design:*** *7S2100C*

Material Description	Actual Mix		Target Value	
Fine Aggregate	5520	lbs	5495	lbs
Coarse Aggregate	7300	lbs	7292	lbs
Water	632.0	lbs	629.3	lbs
Cement	2612	lbs	2632	lbs
Retarding Admixture	80	oz	80	oz
High Range Water Reducer	172	oz	172	oz

Fabricator C: Casting #2

Date: *3/26/08* ***w/cm ratio:*** *0.37*

Batch Size: *4 yards* ***Mix Design:*** *7S2100C*

Material Description	Actual Mix		Target Value	
Fine Aggregate	5500	lbs	5495	lbs
Coarse Aggregate	7300	lbs	7292	lbs
Water	630.0	lbs	629.3	lbs
Cement	2632	lbs	2632	lbs
Retarding Admixture	80	oz	80	oz
High Range Water Reducer	172	oz	172	oz

Fabricator C: Casting #2

Date: *3/26/08* ***w/cm ratio:*** *0.37*

Batch Size: *4 yards* ***Mix Design:*** *7S2100C*

Material Description	Actual Mix		Target Value	
Fine Aggregate	5500	lbs	5495	lbs
Coarse Aggregate	7300	lbs	7292	lbs
Water	632.0	lbs	629.3	lbs
Cement	2624	lbs	2632	lbs
Retarding Admixture	80	oz	80	oz
High Range Water Reducer	172	oz	172	oz

Fabricator C: Casting #2

Date: *3/26/08* ***w/cm ratio:*** *0.37*

Batch Size: *4 yards* ***Mix Design:*** *7S2100C*

Material Description	Actual Mix		Target Value	
Fine Aggregate	5500	lbs	5495	lbs
Coarse Aggregate	7300	lbs	7292	lbs
Water	622.0	lbs	629.3	lbs
Cement	2616	lbs	2632	lbs
Retarding Admixture	80	oz	80	oz
High Range Water Reducer	172	oz	172	oz

Fabricator C: Casting #2

Date: *3/26/08* ***w/cm ratio:*** *0.37*

Batch Size: *4 yards* ***Mix Design:*** *7S2100C*

Material Description	Actual Mix		Target Value	
Fine Aggregate	5480	lbs	5495	lbs
Coarse Aggregate	7280	lbs	7292	lbs
Water	630.0	lbs	629.3	lbs
Cement	2612	lbs	2632	lbs
Retarding Admixture	81	oz	80	oz
High Range Water Reducer	172	oz	172	oz

Fabricator C: Casting #2

Date: *3/26/08* ***w/cm ratio:*** *0.37*

Batch Size: *4 yards* ***Mix Design:*** *7S2100C*

Material Description	Actual Mix		Target Value	
Fine Aggregate	5540	lbs	5495	lbs
Coarse Aggregate	7260	lbs	7292	lbs
Water	628.0	lbs	629.3	lbs
Cement	2612	lbs	2632	lbs
Retarding Admixture	79	oz	80	oz
High Range Water Reducer	172	oz	172	oz

Fabricator C: Casting #3

Date: *4/1/08* ***w/cm ratio:*** *0.37*

Batch Size: *4 yards* ***Mix Design:*** *7S2100C*

Material Description	Actual Mix		Target Value	
Fine Aggregate	5500	lbs	5490	lbs
Coarse Aggregate	7260	lbs	7285	lbs
Water	644.0	lbs	641.8	lbs
Cement	2632	lbs	2632	lbs
Retarding Admixture	80	oz	80	oz
High Range Water Reducer	172	oz	172	oz

Fabricator C: Casting #3

Date: *4/1/08* ***w/cm ratio:*** *0.37*

Batch Size: *4 yards* ***Mix Design:*** *7S2100C*

Material Description	Actual Mix		Target Value	
Fine Aggregate	5500	lbs	5490	lbs
Coarse Aggregate	7280	lbs	7285	lbs
Water	2656	lbs	641.8	lbs
Cement	642.0	lbs	2632	lbs
Retarding Admixture	79	oz	80	oz
High Range Water Reducer	171	oz	172	oz

Fabricator C: Casting #3

Date: *4/1/08* ***w/cm ratio:*** *0.37*

Batch Size: *4 yards* ***Mix Design:*** *7S2100C*

Material Description	Actual Mix		Target Value	
Fine Aggregate	5500	lbs	5490	lbs
Coarse Aggregate	7300	lbs	7285	lbs
Water	642.0	lbs	641.8	lbs
Cement	2644	lbs	2632	lbs
Retarding Admixture	81	oz	80	oz
High Range Water Reducer	172	oz	172	oz

Fabricator C: Casting #3

Date: *4/1/08* ***w/cm ratio:*** *0.37*

Batch Size: *4 yards* ***Mix Design:*** *7S2100C*

Material Description	Actual Mix		Target Value	
Fine Aggregate	5480	lbs	5490	lbs
Coarse Aggregate	7280	lbs	7285	lbs
Water	640.0	lbs	641.8	lbs
Cement	2628	lbs	2632	lbs
Retarding Admixture	80	oz	80	oz
High Range Water Reducer	172	oz	172	oz

Fabricator C: Casting #3

Date: *4/1/08* ***w/cm ratio:*** *0.37*

Batch Size: *4 yards* ***Mix Design:*** *7S2100C*

Material Description	Actual Mix		Target Value	
Fine Aggregate	5500	lbs	5490	lbs
Coarse Aggregate	7260	lbs	7285	lbs
Water	646.0	lbs	641.8	lbs
Cement	2616	lbs	2632	lbs
Retarding Admixture	81	oz	80	oz
High Range Water Reducer	172	oz	172	oz

Fabricator C: Casting #3

Date: *4/1/08* ***w/cm ratio:*** *0.37*

Batch Size: *4 yards* ***Mix Design:*** *7S2100C*

Material Description	Actual Mix		Target Value	
Fine Aggregate	5500	lbs	5490	lbs
Coarse Aggregate	7260	lbs	7285	lbs
Water	644.0	lbs	641.8	lbs
Cement	2644	lbs	2632	lbs
Retarding Admixture	79	oz	80	oz
High Range Water Reducer	172	oz	172	oz

Fabricator C: Casting #3

Date: *4/1/08* ***w/cm ratio:*** *0.37*

Batch Size: *4 yards* ***Mix Design:*** *7S2100C*

Material Description	Actual Mix		Target Value	
Fine Aggregate	5520	lbs	5490	lbs
Coarse Aggregate	7300	lbs	7285	lbs
Water	644.0	lbs	641.8	lbs
Cement	2632	lbs	2632	lbs
Retarding Admixture	81	oz	80	oz
High Range Water Reducer	172	oz	172	oz

Fabricator C: Casting #3				
***Date:** 4/1/08*		***w/cm ratio:** 0.37*		
***Batch Size:** 4 yards*		***Mix Design:** 7S2100C*		
Material Description	**Actual Mix**		**Target Value**	
Fine Aggregate	5500	lbs	5490	lbs
Coarse Aggregate	7280	lbs	7285	lbs
Water	644.0	lbs	641.8	lbs
Cement	2624	lbs	2632	lbs
Retarding Admixture	80	oz	80	oz
High Range Water Reducer	172	oz	172	oz

Fabricator C: Casting #3				
***Date:** 4/1/08*		***w/cm ratio:** 0.37*		
***Batch Size:** 4 yards*		***Mix Design:** 7S2100C*		
Material Description	**Actual Mix**		**Target Value**	
Fine Aggregate	5500	lbs	5490	lbs
Coarse Aggregate	7280	lbs	7285	lbs
Water	640.0	lbs	641.8	lbs
Cement	2640	lbs	2632	lbs
Retarding Admixture	79	oz	80	oz
High Range Water Reducer	172	oz	172	oz

Fabricator C: Casting #3				
***Date:** 4/1/08*		***w/cm ratio:** 0.37*		
***Batch Size:** 4 yards*		***Mix Design:** 7S2100C*		
Material Description	**Actual Mix**		**Target Value**	
Fine Aggregate	5500	lbs	5490	lbs
Coarse Aggregate	7280	lbs	7285	lbs
Water	646.0	lbs	641.8	lbs
Cement	2644	lbs	2632	lbs
Retarding Admixture	79	oz	80	oz
High Range Water Reducer	172	oz	172	oz

Fabricator D Batch Tickets:

Material Sources			
Fine Aggregate	Fordyce Murphy	**Cement**	Alamo Type III
Coarse Aggregate	Fordyce Murphy	**Retarding Admixture**	Pozzolith 300R
Water	City of Victoria	**High Range Water Reducer**	Rheobuild 1000

Fabricator D: Casting #1

Date: *3/4/08* ***w/cm ratio:*** *0.334*

Batch Size: *3.75 yards* ***Mix Design:*** *PT-SWR-SS*

Material Description	Actual Mix		Target Value	
Fine Aggregate	5060	lbs	5009	lbs
Coarse Aggregate	7470	lbs	7466	lbs
Water	60.0	lbs	60.8	lbs
Cement	2313	lbs	2291	lbs
Retarding Admixture	69.0	oz	68.6	oz
High Range Water Reducer	616	oz	619	oz

Fabricator D: Casting #1

Date: *3/4/08* ***w/cm ratio:*** *0.334*

Batch Size: *3.75 yards* ***Mix Design:*** *PT-SWR-SS*

Material Description	Actual Mix		Target Value	
Fine Aggregate	5030	lbs	5028	lbs
Coarse Aggregate	7450	lbs	7466	lbs
Water	58.0	lbs	58.5	lbs
Cement	2284	lbs	2291	lbs
Retarding Admixture	68.0	oz	68.6	oz
High Range Water Reducer	620	oz	619	oz

Fabricator D: Casting #1

Date: *3/4/08* ***w/cm ratio:*** *0.334*

Batch Size: *3.75 yards* ***Mix Design:*** *PT-SWR-SS*

Material Description	Actual Mix		Target Value	
Fine Aggregate	5010	lbs	5009	lbs
Coarse Aggregate	7470	lbs	7466	lbs
Water	61.0	lbs	60.8	lbs
Cement	2280	lbs	2291	lbs
Retarding Admixture	68.0	oz	68.6	oz
High Range Water Reducer		oz	619	oz

Fabricator D: Casting #1

Date: *3/4/08* ***w/cm ratio:*** *0.334*

Batch Size: *3.75 yards* ***Mix Design:*** *PT-SWR-SS*

Material Description	Actual Mix		Target Value	
Fine Aggregate	5070	lbs	5028	lbs
Coarse Aggregate	7460	lbs	7466	lbs
Water	59.0	lbs	58.5	lbs
Cement	2280	lbs	2291	lbs
Retarding Admixture	68.0	oz	68.6	oz
High Range Water Reducer	620	oz	619	oz

Fabricator D: Casting #1

Date: *3/4/08* ***w/cm ratio:*** *0.334*

Batch Size: *3.75 yards* ***Mix Design:*** *PT-SWR-SS*

Material Description	Actual Mix		Target Value	
Fine Aggregate	5010	lbs	5028	lbs
Coarse Aggregate	7430	lbs	7466	lbs
Water	58.0	lbs	58.5	lbs
Cement	2304	lbs	2291	lbs
Retarding Admixture	68.0	oz	68.6	oz
High Range Water Reducer	620	oz	619	oz

Fabricator D: Casting #1

Date: *3/4/08* ***w/cm ratio:*** *0.334*

Batch Size: *3.75 yards* ***Mix Design:*** *PT-SWR-SS*

Material Description	Actual Mix		Target Value	
Fine Aggregate	5030	lbs	5028	lbs
Coarse Aggregate	7460	lbs	7466	lbs
Water	58.0	lbs	58.5	lbs
Cement	2282	lbs	2291	lbs
Retarding Admixture	69.0	oz	68.6	oz
High Range Water Reducer	620	oz	619	oz

Fabricator D: Casting #1

Date: *3/4/08* ***w/cm ratio:*** *0.334*

Batch Size: *3.75 yards* ***Mix Design:*** *PT-SWR-SS*

Material Description	Actual Mix		Target Value	
Fine Aggregate	1000	lbs	1006	lbs
Coarse Aggregate	1490	lbs	1493	lbs
Water	12.0	lbs	11.7	lbs
Cement	454	lbs	458	lbs
Retarding Admixture	13.0	oz	13.7	oz
High Range Water Reducer	124	oz	124	oz

Fabricator D: Casting #2

Date: *3/7/08* ***w/cm ratio:*** *0.334*

Batch Size: *3.75 yards* ***Mix Design:*** *PT-SWR-SS*

Material Description	Actual Mix		Target Value	
Fine Aggregate	4980	lbs	4981	lbs
Coarse Aggregate	7510	lbs	7541	lbs
Water	55.0	lbs	55.3	lbs
Cement	2288	lbs	2291	lbs
Retarding Admixture	68.0	oz	68.6	oz
High Range Water Reducer	616	oz	619	oz

Fabricator D: Casting #2

Date: *3/7/08* ***w/cm ratio:*** *0.334*

Batch Size: *3.75 yards* ***Mix Design:*** *PT-SWR-SS*

Material Description	Actual Mix		Target Value	
Fine Aggregate	5120	lbs	5123	lbs
Coarse Aggregate	7560	lbs	7541	lbs
Water	38.0	lbs	38.2	lbs
Cement	2276	lbs	2291	lbs
Retarding Admixture	68.0	oz	68.6	oz
High Range Water Reducer	616	oz	619	oz

Fabricator D: Casting #2

Date: *3/7/08* ***w/cm ratio:*** *0.334*

Batch Size: *3.75 yards* ***Mix Design:*** *PT-SWR-SS*

Material Description	Actual Mix		Target Value	
Fine Aggregate	5770	lbs	5515	lbs
Coarse Aggregate	8040	lbs	8044	lbs
Water	35.0	lbs	34.7	lbs
Cement	2442	lbs	2444	lbs
Retarding Admixture	73.0	oz	73.2	oz
High Range Water Reducer	660	oz	660	oz

Fabricator D: Casting #2

Date: *3/7/08* ***w/cm ratio:*** *0.334*

Batch Size: *3.75 yards* ***Mix Design:*** *PT-SWR-SS*

Material Description	Actual Mix		Target Value	
Fine Aggregate	5490	lbs	5515	lbs
Coarse Aggregate	8020	lbs	8044	lbs
Water	35.0	lbs	34.7	lbs
Cement	2445	lbs	2444	lbs
Retarding Admixture	73.0	oz	73.2	oz
High Range Water Reducer	660	oz	660	oz

Fabricator D: Casting #2

Date: *3/7/08* ***w/cm ratio:*** *0.334*

Batch Size: *3.75 yards* ***Mix Design:*** *PT-SWR-SS*

Material Description	Actual Mix		Target Value	
Fine Aggregate	4980	lbs	4981	lbs
Coarse Aggregate	7530	lbs	7541	lbs
Water	55.0	lbs	55.3	lbs
Cement	2274	lbs	2291	lbs
Retarding Admixture	69.0	oz	68.6	oz
High Range Water Reducer	620	oz	619	oz

Fabricator D: Casting #2

Date: *3/7/08* ***w/cm ratio:*** *0.334*

Batch Size: *3.75 yards* ***Mix Design:*** *PT-SWR-SS*

Material Description	Actual Mix		Target Value	
Fine Aggregate	4990	lbs	4981	lbs
Coarse Aggregate	7520	lbs	7541	lbs
Water	54.0	lbs	55.3	lbs
Cement	2288	lbs	2291	lbs
Retarding Admixture	69.0	oz	68.6	oz
High Range Water Reducer	620	oz	619	oz

*****Batch tickets for castings 3 and 4 were not available*****

Fabricator E Batch Tickets:

Castings 1,3,and 4 Material Sources			
Manufactured Fine Aggregate	Hanson	**Type III Cement**	Alamo Type III
Natural Fine Aggregate	TXI Green Pit	**Class F Fly Ash**	Headwaters Jewitt, TX
Limestone Coarse Aggregate	Hanson-Ogden Quarry	**Retarding Admixture**	Sika Plastiment
River Gravel Coarse Aggregate	TXI River Gravel	**High Range Water Reducer**	Sika Viscocrete 4100
Water	San Marcos Water Co.		

Casting 2 Material Sources			
Fine Aggregate	Wrights FM 3088	**Class F Fly Ash**	Headwaters Jewitt, TX
Coarse Aggregate	Wrights Realitos	**Retarding Admixture**	Sika Plastiment
Type I/II Cement	Alamo Type I/II LA	**High Range Water Reducer**	Sika Viscocrete 2100
Water	City of Corpus Christi		

Casting	Concrete Type	Coarse Aggregate Type	Date
1	Conventional	Limestone	8/21/08
2	Conventional	River Gravel	7/22/08
3	SCC	Limestone	8/25/08
4	SCC	River Gravel	8/26/08

Fabricator E: Casting #1

Date: *8/21/08* ***w/cm ratio:*** *0.295*

Batch Size: *2.5 yards* ***Mix Design:****8.5-25-4100*

Material Description	Actual Mix		Target Value	
Fine Aggregate	3000	lbs	2993	lbs
Coarse Aggregate	4640	lbs	4624	lbs
Water	425	lbs	405	lbs
Cement	1490	lbs	1498	lbs
Class F Fly Ash	495	lbs	500	lbs
Retarding Admixture	45	oz	45	oz
High Range Water Reducer	66	oz	65	oz

Fabricator E: Casting #1

Date: *8/21/08* ***w/cm ratio:*** *0.295*

Batch Size: *3 yards* ***Mix Design:****8.5-25-4100*

Material Description	Actual Mix		Target Value	
Fine Aggregate	3580	lbs	3592	lbs
Coarse Aggregate	5540	lbs	5550	lbs
Water	490	lbs	486	lbs
Cement	1785	lbs	1797	lbs
Class F Fly Ash	605	lbs	600	lbs
Retarding Admixture	55	oz	54	oz
High Range Water Reducer	78	oz	78	oz

Fabricator E: Casting #1

Date: *8/21/08* ***w/cm ratio:*** *0.292*

Batch Size: *3 yards* ***Mix Design:****8.5-25-4100*

Material Description	Actual Mix		Target Value	
Fine Aggregate	3560	lbs	3592	lbs
Coarse Aggregate	5520	lbs	5517	lbs
Water	525	lbs	520	lbs
Cement	1795	lbs	1797	lbs
Class F Fly Ash	610	lbs	600	lbs
Retarding Admixture	54	oz	54	oz
High Range Water Reducer	78	oz	78	oz

Fabricator E: Casting #1

Date: *8/21/08* ***w/cm ratio:*** *0.294*

Batch Size: *3 yards* ***Mix Design:****8.5-25-4100*

Material Description	Actual Mix		Target Value	
Fine Aggregate	3560	lbs	3592	lbs
Coarse Aggregate	5500	lbs	5518	lbs
Water	520	lbs	519	lbs
Cement	1780	lbs	1797	lbs
Class F Fly Ash	615	lbs	600	lbs
Retarding Admixture	54	oz	54	oz
High Range Water Reducer	78	oz	78	oz

Fabricator E: Casting #1				
Date: *8/21/08*		***w/cm ratio:*** *0.295*		
Batch Size: *3 yards*		***Mix Design:****8.5-25-4100*		
Material Description	**Actual Mix**		**Target Value**	
Fine Aggregate	3580	lbs	3592	lbs
Coarse Aggregate	5520	lbs	5519	lbs
Water	515	lbs	516	lbs
Cement	1785	lbs	1797	lbs
Class F Fly Ash	595	lbs	600	lbs
Retarding Admixture	54	oz	54	oz
High Range Water Reducer	78	oz	78	oz

Fabricator E: Casting #1				
Date: *8/21/08*		***w/cm ratio:*** *0.292*		
Batch Size: *2.5 yards*		***Mix Design:****8.5-25-4100*		
Material Description	**Actual Mix**		**Target Value**	
Fine Aggregate	2980	lbs	2993	lbs
Coarse Aggregate	4600	lbs	4599	lbs
Water	435	lbs	431	lbs
Cement	1495	lbs	1498	lbs
Class F Fly Ash	515	lbs	500	lbs
Retarding Admixture	45	oz	45	oz
High Range Water Reducer	66	oz	65	oz

Fabricator E: Casting #2				
Date: *7/22/08*		***w/cm ratio:*** *0.273*		
Batch Size: *2.8 yards*		***Mix Design:*** *22.06*		
Material Description	**Actual Mix**		**Target Value**	
Fine Aggregate	3037	lbs	3036	lbs
Coarse Aggregate	5456	lbs	5449	lbs
Water	450	lbs	450	lbs
Cement	1833	lbs	1842	lbs
Class F Fly Ash	491	lbs	462	lbs
Retarding Admixture	45	oz	45	oz
High Range Water Reducer	148	oz	148	oz

Fabricator E: Casting #2				
Date: *7/22/08*		***w/cm ratio:*** *0.273*		
Batch Size: *2.8 yards*		***Mix Design:*** *22.06*		
Material Description	**Actual Mix**		**Target Value**	
Fine Aggregate	3043	lbs	3047	lbs
Coarse Aggregate	5445	lbs	5449	lbs
Water	467	lbs	468	lbs
Cement	1835	lbs	1842	lbs
Class F Fly Ash	456	lbs	462	lbs
Retarding Admixture	45	oz	45	oz
High Range Water Reducer	148	oz	148	oz

Fabricator E: Casting #2				
Date: *7/22/08*		***w/cm ratio:*** *0.273*		
Batch Size: *3 yards*		***Mix Design:*** *22.06*		
Material Description	**Actual Mix**		**Target Value**	
Fine Aggregate	3289	lbs	3276	lbs
Coarse Aggregate	5832	lbs	5827	lbs
Water	493	lbs	488	lbs
Cement	1979	lbs	1974	lbs
Class F Fly Ash	505	lbs	495	lbs
Retarding Admixture	48	oz	48	oz
High Range Water Reducer	165	oz	165	oz

Fabricator E: Casting #2				
Date: *7/22/08*		***w/cm ratio:*** *0.273*		
Batch Size: *3.5 yards*		***Mix Design:*** *22.06*		
Material Description	**Actual Mix**		**Target Value**	
Fine Aggregate	3826	lbs	3825	lbs
Coarse Aggregate	6803	lbs	6805	lbs
Water	561	lbs	560	lbs
Cement	2302	lbs	2303	lbs
Class F Fly Ash	585	lbs	578	lbs
Retarding Admixture	56	oz	56	oz
High Range Water Reducer	193	oz	193	oz

Fabricator E: Casting #2				
Date: *7/22/08*	***w/cm ratio:*** *0.273*			
Batch Size: *3.5 yards*	***Mix Design:*** *22.06*			
Material Description	**Actual Mix**		**Target Value**	
Fine Aggregate	3820	lbs	3829	lbs
Coarse Aggregate	6794	lbs	6798	lbs
Water	564	lbs	564	lbs
Cement	2310	lbs	2303	lbs
Class F Fly Ash	567	lbs	578	lbs
Retarding Admixture	56	oz	56	oz
High Range Water Reducer	193	oz	193	oz

Fabricator E: Casting #2				
Date: *7/22/08*	***w/cm ratio:*** *0.273*			
Batch Size: *3.5 yards*	***Mix Design:*** *22.06*			
Material Description	**Actual Mix**		**Target Value**	
Fine Aggregate	3828	lbs	3832	lbs
Coarse Aggregate	6823	lbs	6811	lbs
Water	547	lbs	547	lbs
Cement	2315	lbs	2303	lbs
Class F Fly Ash	576	lbs	578	lbs
Retarding Admixture	56	oz	56	oz
High Range Water Reducer	193	oz	193	oz

Fabricator E: Casting #2				
Date: *7/22/08*	***w/cm ratio:*** *0.273*			
Batch Size: *3.5 yards*	***Mix Design:*** *22.06*			
Material Description	**Actual Mix**		**Target Value**	
Fine Aggregate	3851	lbs	3835	lbs
Coarse Aggregate	6799	lbs	6805	lbs
Water	551	lbs	550	lbs
Cement	2303	lbs	2303	lbs
Class F Fly Ash	573	lbs	578	lbs
Retarding Admixture	56	oz	56	oz
High Range Water Reducer	193	oz	193	oz

Fabricator E: Casting #2				
Date: *7/22/08*	***w/cm ratio:*** *0.273*			
Batch Size: *2.2 yards*	***Mix Design:*** *22.06*			
Material Description	**Actual Mix**		**Target Value**	
Fine Aggregate	2406	lbs	2412	lbs
Coarse Aggregate	4276	lbs	4277	lbs
Water	345	lbs	345	lbs
Cement	1436	lbs	1448	lbs
Class F Fly Ash	367	lbs	363	lbs
Retarding Admixture	36	oz	35	oz
High Range Water Reducer	121	oz	121	oz

Fabricator E: Casting #3				
Date: *8/25/08*	***w/cm ratio:*** *0.354*			
Batch Size: *2.5 yards*	***Mix Design:*** *SCC7.5UT*			
Material Description	**Actual Mix**		**Target Value**	
Fine Aggregate	3880	lbs	3890	lbs
Coarse Aggregate	3860	lbs	3851	lbs
Water	470	lbs	467	lbs
Cement	1350	lbs	1363	lbs
Class F Fly Ash	350	lbs	340	lbs
Retarding Admixture	26	oz	26	oz
High Range Water Reducer	96	oz	95	oz

Fabricator E: Casting #3				
Date: *8/25/08*	***w/cm ratio:*** *0.356*			
Batch Size: *3 yards*	***Mix Design:*** *SCC7.5UT*			
Material Description	**Actual Mix**		**Target Value**	
Fine Aggregate	4640	lbs	4653	lbs
Coarse Aggregate	4620	lbs	4624	lbs
Water	580	lbs	578	lbs
Cement	1630	lbs	1635	lbs
Class F Fly Ash	410	lbs	408	lbs
Retarding Admixture	31	oz	31	oz
High Range Water Reducer	114	oz	114	oz

Fabricator E: Casting #3				
Date: *8/25/08*		***w/cm ratio:*** *0.355*		
Batch Size: *3 yards*		***Mix Design:*** *SCC7.5UT*		
Material Description	**Actual Mix**		**Target Value**	
Fine Aggregate	4640	lbs	4653	lbs
Coarse Aggregate	4620	lbs	4625	lbs
Water	570	lbs	566	lbs
Cement	1620	lbs	1635	lbs
Class F Fly Ash	405	lbs	408	lbs
Retarding Admixture	31	oz	31	oz
High Range Water Reducer	114	oz	114	oz

Fabricator E: Casting #3				
Date: *8/25/08*		***w/cm ratio:*** *0.346*		
Batch Size: *3 yards*		***Mix Design:*** *SCC7.5UT*		
Material Description	**Actual Mix**		**Target Value**	
Fine Aggregate	4660	lbs	4650	lbs
Coarse Aggregate	4620	lbs	4624	lbs
Water	560	lbs	559	lbs
Cement	1635	lbs	1635	lbs
Class F Fly Ash	405	lbs	408	lbs
Retarding Admixture	31	oz	31	oz
High Range Water Reducer	114	oz	114	oz

Fabricator E: Casting #3				
Date: *8/25/08*		***w/cm ratio:*** *0.336*		
Batch Size: *3 yards*		***Mix Design:*** *SCC7.5UT*		
Material Description	**Actual Mix**		**Target Value**	
Fine Aggregate	4640	lbs	4650	lbs
Coarse Aggregate	4620	lbs	4623	lbs
Water	555	lbs	561	lbs
Cement	1630	lbs	1635	lbs
Class F Fly Ash	450	lbs	408	lbs
Retarding Admixture	31	oz	31	oz
High Range Water Reducer	114	oz	114	oz

Fabricator E: Casting #3				
Date: *8/25/08*		***w/cm ratio:*** *0.347*		
Batch Size: *1.5 yards*		***Mix Design:*** *SCC7.5UT*		
Material Description	**Actual Mix**		**Target Value**	
Fine Aggregate	2320	lbs	2325	lbs
Coarse Aggregate	2300	lbs	2313	lbs
Water	285	lbs	279	lbs
Cement	825	lbs	818	lbs
Class F Fly Ash	200	lbs	204	lbs
Retarding Admixture	15	oz	15	oz
High Range Water Reducer	58	oz	57	oz

Fabricator E: Casting #4				
Date: *8/26/08*		***w/cm ratio:*** *0.354*		
Batch Size: *2.5 yards*		***Mix Design:*** *SCC7.45S*		
Material Description	**Actual Mix**		**Target Value**	
Fine Aggregate	3820	lbs	3857	lbs
Coarse Aggregate	3780	lbs	3770	lbs
Water	475	lbs	474	lbs
Cement	1390	lbs	1400	lbs
Class F Fly Ash	345	lbs	350	lbs
Retarding Admixture	26	oz	26	oz
High Range Water Reducer	108	oz	105	oz

Fabricator E: Casting #4				
Date: *8/26/08*		***w/cm ratio:*** *0.357*		
Batch Size: *2.5 yards*		***Mix Design:*** *SCC7.45S*		
Material Description	**Actual Mix**		**Target Value**	
Fine Aggregate	3860	lbs	3857	lbs
Coarse Aggregate	3780	lbs	3777	lbs
Water	485	lbs	482	lbs
Cement	1415	lbs	1400	lbs
Class F Fly Ash	355	lbs	350	lbs
Retarding Admixture	26	oz	26	oz
High Range Water Reducer	106	oz	105	oz

Fabricator E: Casting #4				
Date: *8/26/08*		***w/cm ratio:*** *0.362*		
Batch Size: *3 yards*		***Mix Design:*** *SCC7.45S*		
Material Description	**Actual Mix**		**Target Value**	
Fine Aggregate	4640	lbs	4627	lbs
Coarse Aggregate	4520	lbs	4532	lbs
Water	585	lbs	582	lbs
Cement	1670	lbs	1680	lbs
Class F Fly Ash	415	lbs	420	lbs
Retarding Admixture	33	oz	32	oz
High Range Water Reducer	130	oz	131	oz

Fabricator E: Casting #4				
Date: *8/26/08*		***w/cm ratio:*** *0.356*		
Batch Size: *4 yards*		***Mix Design:*** *SCC7.45S*		
Material Description	**Actual Mix**		**Target Value**	
Fine Aggregate	6140	lbs	6175	lbs
Coarse Aggregate	6040	lbs	6044	lbs
Water	765	lbs	768	lbs
Cement	2220	lbs	2240	lbs
Class F Fly Ash	585	lbs	560	lbs
Retarding Admixture	42	oz	42	oz
High Range Water Reducer	174	oz	174	oz

Fabricator E: Casting #4				
Date: *8/26/08*		***w/cm ratio:*** *0.354*		
Batch Size: *4 yards*		***Mix Design:*** *SCC7.45S*		
Material Description	**Actual Mix**		**Target Value**	
Fine Aggregate	6120	lbs	6169	lbs
Coarse Aggregate	6040	lbs	6042	lbs
Water	770	lbs	777	lbs
Cement	2225	lbs	2240	lbs
Class F Fly Ash	590	lbs	560	lbs
Retarding Admixture	42	oz	42	oz
High Range Water Reducer	174	oz	174	oz

Fabricator E: Casting #4				
Date: *8/26/08*		***w/cm ratio:*** *0.357*		
Batch Size: *4 yards*		***Mix Design:*** *SCC7.45S*		
Material Description	**Actual Mix**		**Target Value**	
Fine Aggregate	6160	lbs	6175	lbs
Coarse Aggregate	6040	lbs	6040	lbs
Water	765	lbs	772	lbs
Cement	2235	lbs	2240	lbs
Class F Fly Ash	560	lbs	560	lbs
Retarding Admixture	43	oz	42	oz
High Range Water Reducer	174	oz	174	oz

Fabricator E: Casting #4				
Date: *8/26/08*		***w/cm ratio:*** *0.359*		
Batch Size: *3.5 yards*		***Mix Design:*** *SCC7.45S*		
Material Description	**Actual Mix**		**Target Value**	
Fine Aggregate	5360	lbs	5392	lbs
Coarse Aggregate	5280	lbs	5283	lbs
Water	685	lbs	689	lbs
Cement	1945	lbs	1960	lbs
Class F Fly Ash	485	lbs	490	lbs
Retarding Admixture	37	oz	37	oz
High Range Water Reducer	154	oz	152	oz

APPENDIX C

Static Flexural Test Specimen Information

Appendix C contains the detailed testing information for each of the 55 girders tested in flexure. The table in this appendix presents the specimen identification information, fabrication and test dates, maximum compressive stresses at prestress transfer, measured cracking loads, predicted cracking loads, and predicted cracking load accuracies using both the NCHRP 496 prestress loss procedure and the AASHTO-LRFD (2008) prestress loss procedure.

Specimen Information

Test	Mark	Precaster	Precaster Mark	Series	Design Release Strength	Coarse Aggregate	Date of Cast	Date of Release	Date of Test	Actual Release Strength, psi	Bottom Fiber Compressive Stress at Release (*f'ci) Critical Section Hold Down	Critical Section	Transfer Length	Concrete Strength at Test Strength, psi	Cracking Load: Predicted Cracking Load NCHRP Method	NCHRP with Dead Loads	AASHTO-LRFD Method	AASHTO-LRFD with DL	Measured P_{cr} kips	NCHRP Error (%)	AASHTO-LRFD Error (%)
1	CA-70-3	A	A1	1	4000	Limestone	9/26/2007	9/26/2007	11/1/2007	3940	0.703	0.700	0.702	10200	109	108.228	103	102.228	107	-1.15	4.46
2	CA-70-2	A	A2	1	4000	Limestone	9/26/2007	9/26/2007	11/15/2007	3930	0.705	0.702	0.703	10550	109	108.228	103	102.228	110	1.61	7.07
3	CA-70-1	A	A3	1	4000	Limestone	9/26/2007	9/26/2007	11/27/2007	3930	0.705	0.702	0.704	10800	108	107.228	102	101.228	108	0.71	6.27
4	CA-60-1	A	A6	1	4700	Limestone	10/3/2007	10/4/2007	11/29/2007	4540	0.616	0.613	0.614	10500	110	109.228	104	103.228	111	1.60	7.00
5	CA-60-2	A	A4	1	4700	Limestone	10/3/2007	10/4/2007	12/4/2007	4540	0.616	0.613	0.614	10700	110	109.228	104	103.228	112	2.48	7.83
6	CA-60-3	A	A5	1	4700	Limestone	10/3/2007	10/4/2007	12/12/2007	4540	0.616	0.613	0.614	11050	110	109.228	103	102.228	111	1.60	7.90
7	CA-65-1	A	A3	1	4300	Limestone	10/9/2007	10/10/2007	12/18/2007	4370	0.638	0.636	0.636	10200	108	107.228	102	101.228	110	2.52	7.97
8	CA-65-2	A	A6	1	4300	Limestone	10/9/2007	10/10/2007	1/4/2008	4380	0.637	0.634	0.635	11150	108	107.228	103	102.228	107	-0.21	4.46
9	CA-65-3	A	A4	1	4300	Limestone	10/9/2007	10/10/2007	1/8/2008	4310	0.647	0.644	0.645	11400	108	107.228	102	101.228	113	5.11	10.42
10	CA-65-4	A	A5	1	4300	Limestone	10/9/2007	10/10/2007	1/10/2008	4340	0.641	0.640	0.641	11500	108	107.228	102	101.228	110	2.52	7.97
11	CA-65-5	A	A2	1	4300	Limestone	10/9/2007	10/10/2007	1/15/2008	4330	0.644	0.641	0.642	11800	108	107.228	102	101.228	111	3.40	8.80
12	CA-65-6	A	A1	1	4300	Limestone	10/9/2007	10/10/2007	1/17/2008	4300	0.648	0.645	0.646	11900	108	107.228	102	101.228	109	1.63	7.13
13	CD-70-1	D	D1	2	5400	River Gravel	3/4/2008	3/5/2008	4/2/2008	5580	0.683	0.681	0.679	11000	144	143.228	138	137.228	142	-0.86	3.36
14	CD-70-2	D	D2	2	5400	River Gravel	3/4/2008	3/5/2008	4/7/2008	5500	0.692	0.690	0.688	11600	143	142.228	137	136.228	143	0.54	4.74
15	CD-70-3	D	D3	2	5400	River Gravel	3/4/2008	3/5/2008	4/10/2008	5420	0.701	0.699	0.698	12000	142	141.228	138	137.228	147	3.93	6.65
16	CD-65-1	D	D1	2	5850	River Gravel	3/7/2008	3/8/2008	4/14/2008	5670	0.673	0.671	0.669	9600	142	141.228	135	134.228	143	1.24	6.13
17	CD-65-2	D	D2	2	5850	River Gravel	3/7/2008	3/8/2008	4/18/2008	5670	0.673	0.671	0.669	9600	141	140.228	134	133.228	135	-3.87	1.31
18	CD-65-3	D	D3	2	5850	River Gravel	3/7/2008	3/8/2008	4/21/2008	5670	0.673	0.671	0.669	9600	141	140.228	134	133.228	137	-2.36	2.75
19	CD-65-4	D	D1	2	5850	River Gravel	3/14/2008	3/15/2008	4/24/2008	5940	0.644	0.642	0.640	10700	143	142.228	136	135.228	136	-4.58	0.57
20	CD-65-5	D	D2	2	5850	River Gravel	3/14/2008	3/15/2008	4/29/2008	5940	0.644	0.642	0.640	11200	142	141.228	136	135.228	148	4.58	8.63
21	CD-65-6	D	D3	2	5850	River Gravel	3/14/2008	3/15/2008	5/1/2008	5940	0.644	0.642	0.640	11400	142	141.228	136	135.228	143	1.24	5.43
22	CD-60-1	D	D1	2	6400	River Gravel	3/12/2008	3/13/2008	5/5/2008	6320	0.608	0.606	0.604	11700	143	142.228	137	136.228	143	0.54	4.74
23	CD-60-2	D	D2	2	6400	River Gravel	3/12/2008	3/13/2008	5/12/2008	6310	0.609	0.607	0.605	12000	142	141.228	137	136.228	146	3.27	6.69
24	CD-60-3	D	D3	2	6400	River Gravel	3/12/2008	3/13/2008	5/20/2008	6300	0.610	0.608	0.606	12400	142	141.228	136	135.228	142	0.54	4.77
25	CC-70-1	C	A4	2	5400	Limestone	3/14/2008	3/15/2008	5/23/2008	5380	0.706	0.704	0.702	10700	138	137.228	131	130.228	142	3.36	8.29
26	CC-70-2	C	A5	2	5400	Limestone	3/14/2008	3/15/2008	5/27/2008	5360	0.709	0.706	0.705	11100	138	137.228	131	130.228	138	0.56	5.63
27	CC-70-3	C	A6	2	5400	Limestone	3/14/2008	3/15/2008	5/29/2008	5330	0.712	0.710	0.709	11300	138	137.228	131	130.228	139	1.27	6.31
28	CC-65-1	C	A6	2	5850	Limestone	3/26/2008	3/27/2008	5/29/2008	5970	0.641	0.639	0.637	11050	141	140.228	134	133.228	136	-3.11	2.04
29	CC-65-2	C	A3	2	5850	Limestone	3/26/2008	3/27/2008	6/2/2008	6000	0.638	0.636	0.634	11180	141	140.228	134	133.228	141	0.55	5.51
30	CC-65-3	C	A2	2	5850	Limestone	3/26/2008	3/27/2008	6/3/2008	6130	0.626	0.624	0.622	11200	141	140.228	135	134.228	135	-3.87	0.57
31	CC-65-4	C	A5	2	5850	Limestone	3/26/2008	3/27/2008	6/10/2008	6070	0.631	0.630	0.628	11450	140	139.228	134	133.228	134	-3.90	0.58
32	CC-65-5	C	A4	2	5850	Limestone	3/26/2008	3/27/2008	6/11/2008	6350	0.606	0.604	0.602	11480	141	140.228	135	134.228	141	0.55	4.80
33	CC-65-6	C	A1	2	5850	Limestone	3/26/2008	3/27/2008	6/12/2008	6250	0.615	0.613	0.611	11500	141	140.228	135	134.228	142	1.25	5.47
34	CC-60-1	C	A6	2	6400	Limestone	4/1/2008	4/2/2008	6/12/2008	6350	0.606	0.604	0.602	10750	141	140.228	135	134.228	130	-7.87	-3.25
35	CC-60-2	C	A4	2	6400	Limestone	4/1/2008	4/2/2008	6/17/2008	6370	0.604	0.602	0.600	10800	141	140.228	134	133.228	130	-7.87	-2.48
36	CC-60-3	C	A5	2	6400	Limestone	4/1/2008	4/2/2008	6/18/2008	6370	0.604	0.602	0.600	10800	141	140.228	134	133.228	138	-1.61	3.46
37	CB-60-1	B	L5	1	5850	River Gravel	4/23/2008	4/23/2008	6/19/2008	4820	0.588	0.585	0.585	12300	112	111.228	108	107.228	130	14.44	17.52
38	CB-60-2	B	L4	1	5850	River Gravel	4/23/2008	4/23/2008	6/23/2008	5010	0.567	0.564	0.564	12700	113	112.228	108	107.228	126	10.93	14.90
39	CB-60-3	B	L6	1	5850	River Gravel	4/23/2008	4/23/2008	6/24/2008	4620	0.612	0.609	0.609	12800	111	110.228	107	106.228	120	8.14	11.48
40	CB-70-1	B	G1	1	5400	River Gravel	5/6/2008	5/6/2008	6/25/2008	4540	0.622	0.619	0.619	12100	112	111.228	107	106.228	118	5.74	9.98
41	CB-70-2	B	G2	1	5400	River Gravel	5/6/2008	5/6/2008	6/26/2008	4360	0.646	0.644	0.644	12140	111	110.228	107	106.228	121	8.90	12.21
42	CB-70-3	B	G3	1	5400	River Gravel	5/6/2008	5/6/2008	6/27/2008	4180	0.673	0.670	0.670	12200	110	109.228	106	105.228	118	7.43	10.82
43	CB-70-4	B	G4	1	5400	River Gravel	5/6/2008	5/6/2008	7/1/2008	4030	0.696	0.693	0.694	12430	110	109.228	106	105.228	110	0.70	4.34
44	CB-70-5	B	G5	1	5400	River Gravel	5/6/2008	5/6/2008	7/2/2008	3880	0.721	0.718	0.719	12500	109	108.228	105	104.228	118	8.28	11.67
45	CB-70-6	B	G6	1	5400	River Gravel	5/6/2008	5/6/2008	7/7/2008	3680	0.758	0.755	0.756	12800	108	107.228	104	103.228	112	4.26	7.83
46	BB-01	E	D2	Box	4100	Limestone	8/21/2008	8/21/2008	9/18/2008	4140		0.640		11300	187	185.028	176	174.028	176	-5.13	1.12
47	BB-02	E	D1	Box	4100	Limestone	8/21/2008	8/21/2008	9/18/2008	4070		0.650		11300	187	185.028	176	174.028	178	-3.95	2.23
48	BB-03	E	M1	Box	4100	River Gravel	7/22/2008	7/22/2008	9/4/2008	4120		0.657		11160	183	181.028	176	174.028	195	7.17	10.75
49	BB-04	E	M3	Box	4100	River Gravel	7/22/2008	7/22/2008	8/19/2008	4220		0.643		10672	186	184.028	179	177.028	196	6.11	9.68
50	BB-05	E	M2	Box	4100	River Gravel	7/22/2008	7/22/2008	8/28/2008	4170		0.650		10900	184	182.028	178	176.028	200	8.99	11.99
51	BB-06	E	D2	Box	4100	Limestone	8/25/2008	8/26/2008	10/2/2008	4060		0.641		9530	183	181.028	167	165.028	162	-11.75	-1.87
52	BB-07	E	D1	Box	4100	Limestone	8/25/2008	8/26/2008	10/7/2008	4060		0.641		9575	182	180.028	166	164.028	155	-16.15	-5.82
53	BB-08	E	D3	Box	4100	River Gravel	8/26/2008	8/27/2008	9/24/2008	4040		0.655		8730	183	181.028	170	168.028	161	-12.44	-4.37
54	BB-09	E	D2	Box	4100	River Gravel	8/26/2008	8/27/2008	9/25/2008	4040		0.655		8900	183	181.028	170	168.028	162	-11.75	-3.72
55	BB-10	E	D1	Box	4100	River Gravel	8/26/2008	8/27/2008	9/30/2008	4040		0.655		9730	183	181.028	171	169.028	163	-11.06	-3.70

Figure C-1 Static Flexural Test Information

APPENDIX D

Bursting Cracks in 4B28 Box Beam Specimens

Cracks forming due to bursting, spalling, and splitting stresses in the end regions of the 4B28 box beams were monitored during this phase of TxDOT Project 5197. The observed cracks were termed "bursting cracks." All cracks were marked on the beam and crack widths were measured using a crack comparator card. The observed crack widths in the box beams did not exceed 0.007-inches. Anything smaller than 0.005-inches was termed hairline. Both sides of each end of the beam were inspected and photographed totaling 40 photographs in all (10 specimens x four sides from each specimen). The crack maps for each end of the beam are presented in this appendix.

After inspecting all 10 box beams for bursting cracks, several observations were made. First, the most common bursting crack occurred at the re-entrant corner of the blockout at each end of the box beam. This bursting crack was the largest, widest, and most consistent crack among all 10 specimens. Secondly, the coarse aggregate type (limestone or hard river gravel) used in specimen fabrication did not appear to affect the number, length, or width of the bursting cracks. Finally, the use of conventional concrete or SCC mixture designs did not appear to effect the number, length or width of the bursting cracks.

The following pages present the crack maps for the bursting cracks in the box beams. All observed cracks wider than "hairline" are noted on the crack maps. For convenience, Figure D-1 provides a lettering key for the crack maps that follow.

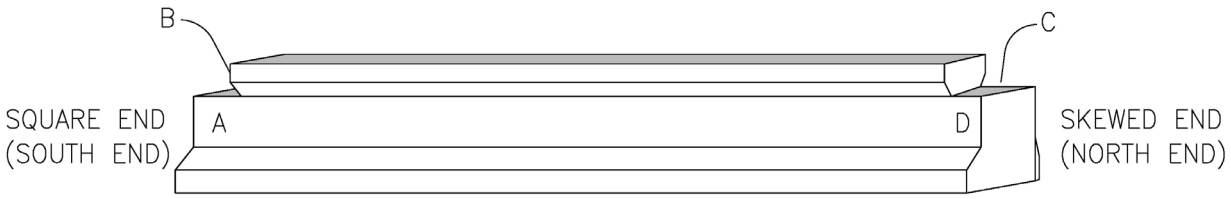

Figure D-1 Bursting crack map key for box beams

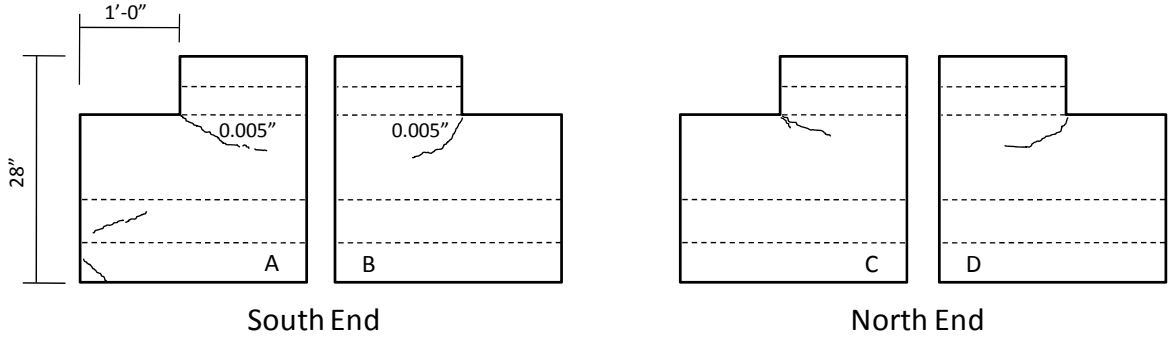

Specimen BB-01

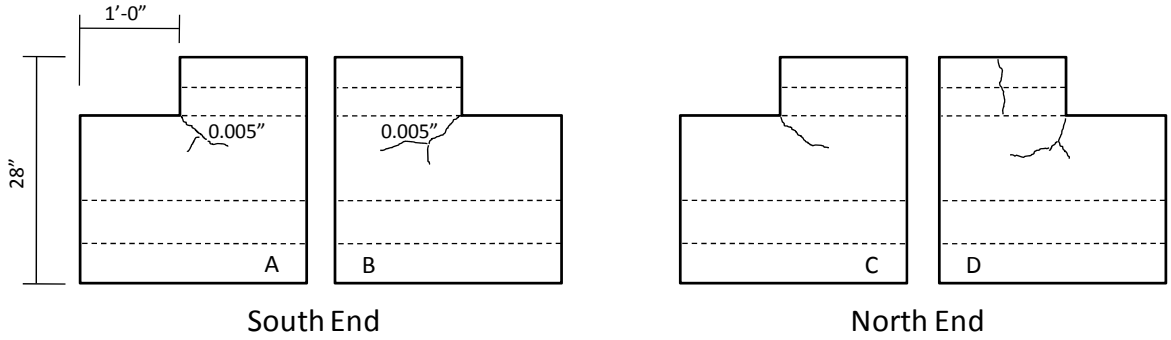

Specimen BB-02

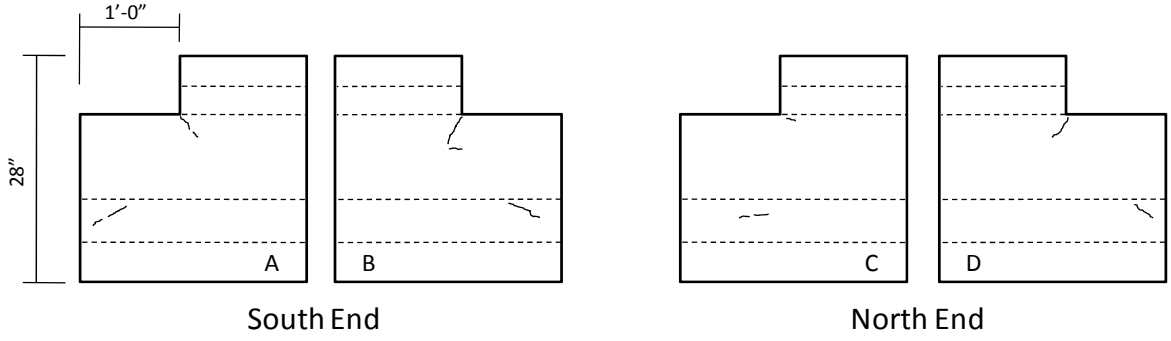

Specimen BB-03

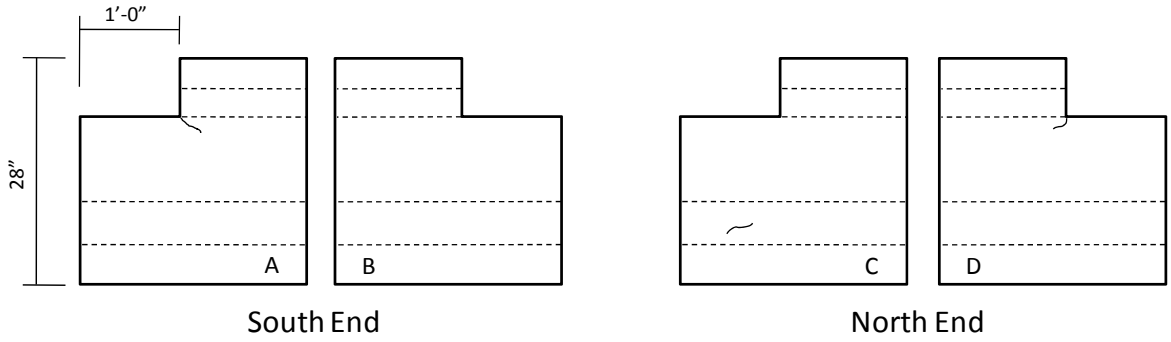

Specimen BB-04

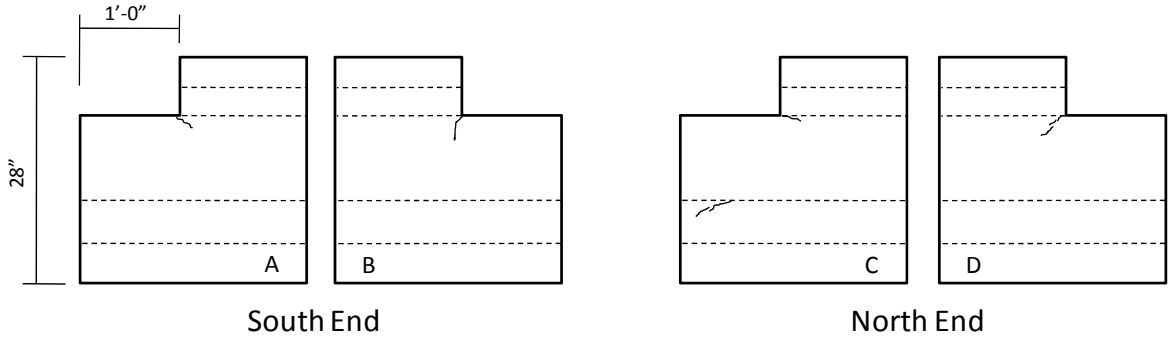

Specimen BB-05

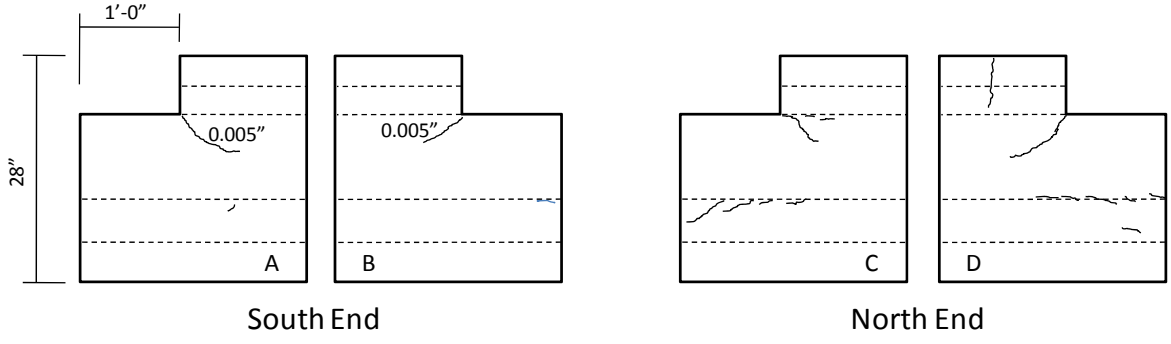

Specimen BB-06

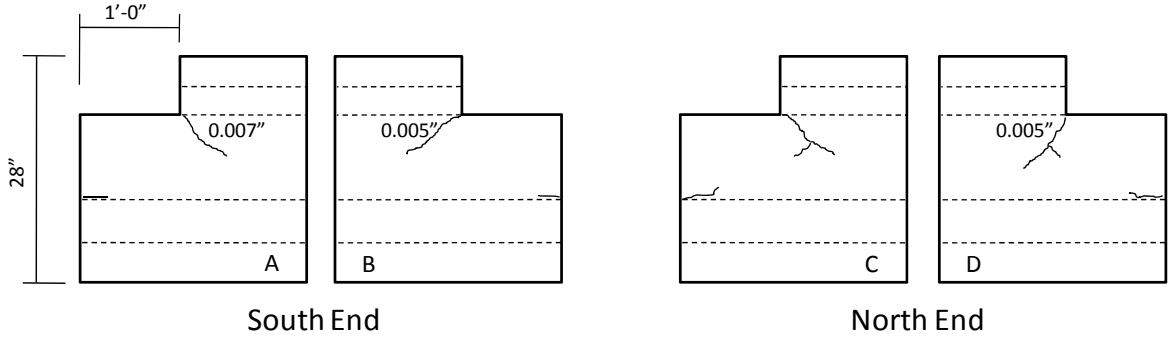

Specimen BB-07

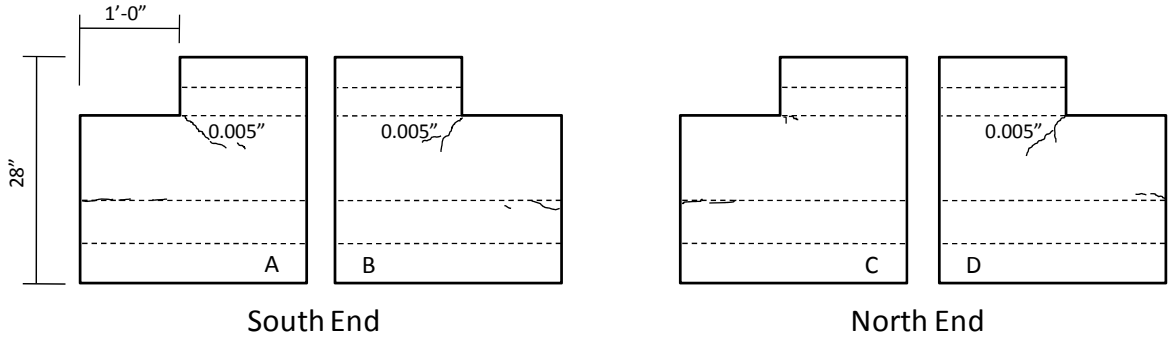

Specimen BB-08

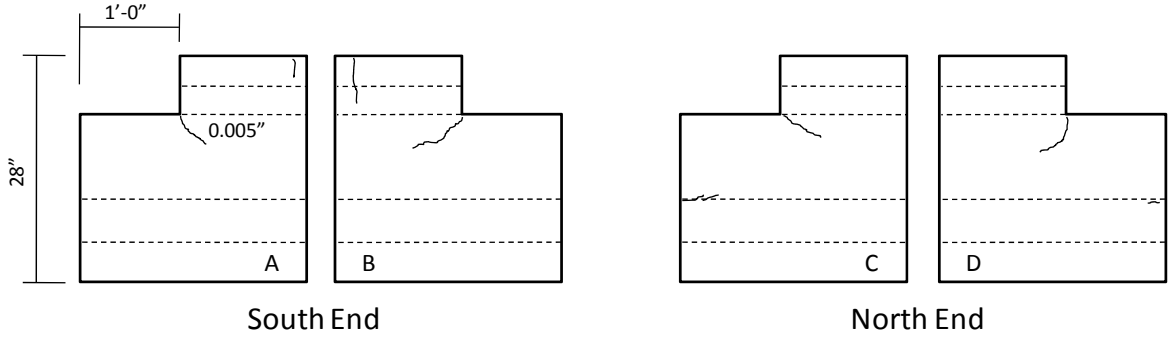

Specimen BB-09

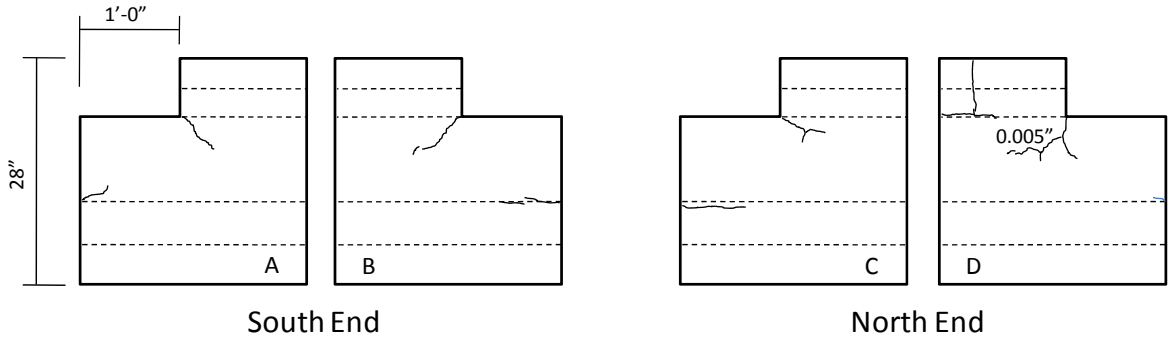

Specimen BB-10

BIBLIOGRAPHY

1. AASHTO, *Standard Specifications for Highway Bridges*, 8th Edition, American Association of State Highway and Transportation Officials, Washington, D.C., 1961

2. AASHTO, *LRFD Bridge Design Specifications*, Interim 2005 Edition, American Association of State Highway and Transportation Officials, Washington, D.C., 2005.

3. AASHTO, *LRFD Bridge Design Specifications*, 4th Edition, American Association of State Highway and Transportation Officials, Washington, D.C., 2007.

4. AASHTO, *LRFD Bridge Design Specifications*, Interim 2008 Edition, American Association of State Highway and Transportation Officials, Washington, D.C., 2008.

5. ACI Committee 318, *Building Code Requirements for Reinforced Concrete (ACI 318-63*), American Concrete Institute, Detroit, MI, 1963.

6. ACI Committee 318, *Building Code Requirements for Reinforced Concrete (ACI 318-08*), American Concrete Institute, Farmington Hills, MI, 2008.

7. ACI-ASCE Joint Committee 323, "Tentative Recommendations for Prestressed Concrete," *Journal of the American Concrete Institute–Proceedings*, Vol. 54, January 1958, pp. 545-578.

8. ACI-ASCE Joint Committee 323, "Tentative Recommendations for Prestressed Concrete – Committee Closure," *Journal of the American Concrete Institute–Proceedings*, Vol. 54, Part 2, December 1958, pp. 1291-1299.

9. Birrcher, D. B., and Bayrak, O.,"Effects of Increasing the Allowable Compressive Stress at Release of Prestressed Concrete Girders," Research Report 0-5197-1, Center for Transportation Research, The University of Texas at Austin, March 2007, 206 pp.

10. Birrcher D. B., "Effects of Increasing the Allowable Compressive Stress at Release of Prestressed Concrete Girders," MS Thesis, The University of Texas at Austin, December 2006, 286 pp.

11. Bonen, D., and Shah, S. P., "Fresh and hardened properties of self-consolidating concrete," *Progress in Structural Engineering and Materials*, Vol. 7, No. 1, January/March 2005, pp. 14-26.

12. Burgueño, R., and Bendert, D. A., "Structural Behavior and Field-Monitoring of SCC Prestressed Box Beams for Demonstration Bridge," *ACI Special Publications Series SP-247: Self Consolidating Concrete for Precast Applications*, October 2007, pp. 67-76.

13. Castro, A., Kreger, M. E., Bayrak, O., Breen, J. E., and Wood, S. L., "Allowable Design Release Stresses for Pretensioned Concrete Beams," Research Report 0-4086-2, Center for Transportation Research, The University of Texas at Austin, August 2004, 142 pp.

14. Collins, M. P. and Mitchell, D., *Prestressed Concrete Structures*, Response Publications, Toronto and Montreal, Canada, 1997.

15. D'Ambrosia, M. D., Lange, and Brinks, A. J., "Mechanical Performance of Self-Consolidating Concrete at Early Age," *Young Researchers' Forum – Proceedings from the International Conference*, 2005, pp. 83-94.

16. D'Arcy, T. J., "Good Performance – The Engineer's Quest," *Journal of the Precast / Prestressed Concrete Institute*, Vol. 50, July-August 2005, p. 15.

17. D'Arcy, T. J., Nasser, G. D., and Ghosh, S. K., "Building Code Provisions for Precast/Prestressed Concrete: A Brief History," *Journal of the Precast / Prestressed Concrete Institute*, Vol. 48, No. 6, November-December 2003, pp.116-124.

18. Delibes Liniers, A., "Microcracking of concrete under compression and its influence on tensile strength," *Materials and Structures*, Vol. 20, No. 116, pp. 111-116.

19. Dolan, C. W., and Krohn, J. J., "A Case for Increasing the Allowable Compressive Release Stress for Prestressed Concrete," *Journal of the Precast / Prestressed Concrete Institute*, Vol. 52, No. 1, January-February 2007, pp. 2-5.

20. Erickson, E.L., "The Bureau of Public Roads 'Criteria for Prestressed Concrete Bridges,'" *Proceedings World Conference on Prestressed Concrete*, San Francisco, CA, July 1957, pp. A9-1-A9-8.

21. Gettu, R., Aguado, A., and Oliveira, O. F., "Damage in High-Strength Concrete Due to Monotonic and Cyclic Compression–A Study Based on Splitting Tensile Strength," *ACI Materials Journal*, Vol. 93, No. 6, November-December 1996, pp. 519-523.

22. Gross, S. P., Yost, J. R., and Gaynor, E., "Experimental Study of Prestress Land and Camber in High-Strength SCC Beams," *ACI Special Publications Series SP-247: Self Consolidating Concrete for Precast Applications*, October 2007, pp. 77-91.

23. Hale, W. M. and Russell, B. W., "Effect of Allowable Compressive Stress at Release on Prestress Losses and on the Performance of Precast, Prestressed Concrete Girders," *Journal of the Precast / Prestressed Concrete Institute*, Vol. 51, No. 2, March-April 2006, pp. 14-25.

24. Hawkins, N.M., *Impact of Research on Prestressed Concrete Specimens*, ACI SP-72-7, American Concrete Institute, Detroit, MI, 1981, pp. 163-176.

25. Heckmann, C. P., "Effects of Increasing the Allowable Compressive Stress at Release on the Shear Strength of Prestressed Concrete Girders" MS Thesis, The University of Texas at Austin, August 2008, 175 pp.

26. Hsu, T.T.C., Slate, F.O., Sturman, G.M., and Winter, G., "Microcracking of Plain Concrete and the Shape of the Stress-Strain Curve," *Journal of the American Concrete Institute–Proceedings*, Vol. 60, No. 2, February 1963, pp. 209-223.

27. Huo, X., and Tadros, M., "Allowable Compressive Strength of Concrete at Prestress Release," Open Forum Problems and Solutions, *Journal of the Precast / Prestressed Concrete Institute*, Vol. 42, No. 1, January-February 1997, pp. 95-99.

28. Kerekes, F. and Reid, H. B., "Fifty Years of Development in Building Code Requirements for Reinforced Concrete," *Journal of the American Concrete Institute–Proceedings*, Vol. 50, No. 6, February, 1954, pp. 441-470.

29. Khan A., Cook W., and Mitchell, D., "Early Age Compressive Stress-Strain Properties of Low-, Medium, and High-Strength Concretes," *ACI Materials Journal*, Vol. 92, No. 6, November-December 1995, pp. 617-624.

30. Khayat, K. H., Assaad, J., Daczka, J., "Comparison of Field-Oriented Test Methods to Assess Dynamic Stability of Self-Consolidating Concrete," *ACI Materials Journal*, Vol. 101, No. 2, March-April 2004, p. 172.

31. Kreger, M. E., and Bayrak, O., "Project 0-4086: Allowable Design Release Stresses for Pretensioned Concrete Beams," Project Summary Report 0-4086-S, Center for Transportation Research, The University of Texas at Austin, July 2005, 4 pp.

32. Lin, T. Y., "Tentative Recommendations for Prestressed Concrete," *Journal of the American Concrete Institute–Proceedings*, Vol. 54, Part 2, September 1958, pp. 1232-1233.

33. MacGregor, J. G., and Wight, J. K., *Reinforced Concrete Mechanics and Design*, Fourth Edition, Prentice Hall, New Jersey, 2005.

34. Naito, C. J., Parent, G., and Brunn, G. "Performance of Bulb-Tee Girders Made with Self-Consolidating Concrete," *Journal of the Precast / Prestressed Concrete Institute*, Vol. 51, No. 6, November-December 2006, pp. 2-15.

35. Ngab, A. S., Nilson, A. H., and Slate, F. O., "Shrinkage and Creep of High Strength Concrete," *Journal of the American Concrete Institute–Proceedings*, Vol. 78, No. 4, July-August 1981, pp. 255-261

36. Ngab, A. S., Slate, F. O., and Nilson, A. H., "Microcracking and Time-Dependent Strains in High Strength Concrete," *Journal of the American Concrete Institute–Proceedings*, Vol. 78, No. 4, July-August 1981, pp. 262-268.

37. Noppakunwijai P., Tadros, M.K., Ma, Z., and Mast, R.F., "Strength Design of Pretensioned Flexural Concrete Members at Prestress Transfer," *Journal of the Precast / Prestressed Concrete Institute*, Vol. 46, No. 1, January-February 2001, pp. 34-52.

38. Ozyildirim, C., and Davis, R. T., "Bulb-T Beams with Self-Consolidating Concrete on Route 33 in Virginia," *Transportation Research Record: Journal of the Transportation Research Board*, No. 2020, Washington D.C. 2007, pp. 76-82.

39. Ozyildirim, C., and Lane, S. D., "Evaluation of Self-Consolidating Concrete," VTRC 03-R13, Virginia Transportation Research Council, Charlottesville, VA, June 2003.

40. Ozyildirim, C., "Virginia Department of Transportation Early Experience with Self-Consolidating Concrete," *Transportation Research Record: Journal of the Transportation Research Board*, No. 1914, Washington D.C. 2005, pp. 81-84.

41. PCI Self-Consolidating Concrete FAST Team, "Interim Guidelines for the Use of Self-Consolidating Concrete in PCI Member Plants," *Jouranl of the Precast / Prestressed Concrete Institute*, Vol. 48, No. 3, May-June 2003, pp.14-19.

42. PCI Technical Activities Council and PCI Committee on Building Code, "PCI Standard Design Practice," *Journal of the Precast / Prestressed Concrete Institute*, Vol. 41, No. 4, July-August 1996, pp. 31-43.

43. PCI Technical Activities Council and PCI Committee on Building Code, "PCI Standard Design Practice," *Journal of the Precast / Prestressed Concrete Institute*, Vol. 42, No. 2, March-April 1997, pp. 43-51.

44. PCI Technical Activities Council and PCI Committee on Building Code, "PCI Standard Design Practice," *Journal of the Precast / Prestressed Concrete Institute*, Vol. 48, No. 1, January-February 2003.

45. PCI, *PCI Design Handbook*, Sixth Edition, Precast/Prestressed Concrete Institute, Chicago, IL, 2004.

46. Raths, D. C., and Nasser, G. D., "Historical Overview of the PCI Journal and Its Contributions to the Precast/Prestressed Concrete Industry," *Journal of the Precast / Prestressed Concrete Institute*, Vol. 52, No.1, January-February 2007, pp. 32-51.

47. Richart, F.E., Brandtzaeg, A., and Brown, R.L., "The Failure of Plain and Spirally Reinforced Concrete in Compression," Bulletin No. 190, University of Illinois Engineering Experiment Station, Urbana, Ill., April 1929, pp. 1-74.

48. Ruiz, E. D., Station, B. W., Do, N. H., and Hale, W. M., "Prestress Losses in Beams Cast with Self-Consolidating Concrete," *ACI Special Publications Series SP-247: Self Consolidating Concrete for Precast Applications*, October 2007, pp. 93-104.

49. Russell, B. W. and Pang, J. P., "Investigation of Allowable Compressive Stresses for High Strength, Prestressed Concrete," *Proceedings of the PCI/FHWA Intl. Symposium on High Performance Concrete*, New Orleans, LA, October 1997, pp. 554-565.

50. Smadi, M. M., Slate, F. O., and Nilson, A. H., "High-, Medium-, and Low-Strength Concretes Subject to Sustained Overloads–Strains, Strengths, and Failure Mechanisms," *ACI Materials Journal*, Vol. 82, No. 5, September-October 1985, pp. 657-664.

51. Smadi, M. M., Slate, F. O., and Nilson, A. H., "Shrinkage and Creep of High-, Medium-, and Low-Strength Concretes, Including Overloads," *ACI Materials Journal*, Vol. 84, No. 3, May-June 1987, pp. 224-234.

52. Tadros, M. K., Al-Omaishi, N., Seguirant, S. J., and Gallt, J. G., "Prestress Losses in Pretensioned High-Strength Concrete Bridge Girders," NCHRP Report 496, Transportation Research Board, Washington, D. C., 2003.

53. Thorenfeldt, E., Tomaszewicz, A., and Jensen, J. J., "Mechanical Properties of High-Strength Concrete and Application in Design," *Proceedings of the Symposium "Utilization of High Strength Concrete*," Stavanger, Norway, June 1987, Tapir, Trondheim, pp. 149-159.

54. Texas Department of Transportation, www.dot.state.tx.us, Bridge Division Standard Drawings, 2007.

55. Winter, G., "Development of a National Building Code for Reinforced Concrete 1908-1977," *Concrete International*, Vol. 4, No. 12, December 1982, pp. 27-37.

VITA

Brian Allen Schnittker was born in Dallas, Texas, on December 27, 1984, the son of Patty Tallant Schnittker and Douglas Allen Schnittker. After graduating from Plano West Senior High School in Plano, TX, he attended the University of Texas at Austin. He received his Bachelor of Science in Architectural Engineering in May of 2007. In June of 2007, he began his study in the Graduate School at the University of Texas at Austin, working as a research assistant at the Phil M. Ferguson Structural Engineering Laboratory.

Permanent address: 6401 Glenhollow Dr.
Plano, TX 75093

This thesis was typed by the author.